# TOUGHENED EPOXY NANOCOMPOSITES BASED ON SURFACE ENGINEERED NANOFILLERS

*A Thesis submitted*

*in partial fulfillment for the Degree of*

**Doctor of Philosophy**

*by*

**RANEESH KONNOLA**

**Department of Chemistry**

**INDIAN INSTITUTE OF SPACE SCIENCE AND TECHNOLOGY**

**THIRUVANANTHAPURAM**

**MAY, 2016**

*To my beloved father, mother, brother, sister, wife and friends…..*

# CERTIFICATE

This is to certify that the thesis entitled **Toughened Epoxy Nanocomposites based on Surface Engineered Nanofillers** submitted by **Raneesh Konnola** to the Indian Institute of Space Science and Technology, Thiruvananthapuram, in partial fulfillment for the award of the degree of **Doctor of Philosophy** is a *bona fide* record of research work carried out by him under my supervision. The contents of this thesis, in full or in parts, have not been submitted to any other Institution or University for the award of any degree or diploma.

**Prof. Kuruvilla Joseph**
Supervisor
Dean (SA) and Senior Professor
Department of Chemistry

Thiruvananthapuram
May, 2016

Counter signature of the HOD with seal

# DECLARATION

I declare that this thesis entitled **Toughened Epoxy Nanocomposites based on Surface Engineered Nanofillers** submitted in partial fulfillment of the degree of **Doctor of Philosophy** is a record of original work carried out by me under the supervision of Prof. Kuruvilla Joseph, and has not formed the basis for the award of any other degree or diploma, in this or any other Institution or University. In keeping with the ethical practice in reporting scientific information, due acknowledgements have been made wherever the finding of others have been cited.

Raneesh Konnola

SC11D001

Thiruvananthapuram-695 547

May, 2016

# ACKNOWLEDGEMENTS

First and foremost, I would like to take this opportunity to express my gratitude to my beloved mentor and guide Dr. Kuruvilla Joseph, Professor and Dean (Student Activities), Department of Chemistry, IIST for his excellent guidance, effective inspiration, constant encouragement, invaluable insights and endless patience in directing and designing the work. My work has been moulded under his excellent supervision, critical acumen, constant encouragement and inspiring discussions. His positive spirit, persistent work ethic and never-give-up attitude is the fuel and dynamic motivation that drives me to complete this work. It is an honor to have worked with and learned from him.

I owe my sincere thanks to Dr. K. S. Dasgupta, Director, IIST for the research facilities provided to me during the tenure of my research work. It is my pleasure to extend my deep gratitude to Dr. Nirmala R James, Head of the Department of Chemistry for her continuous support and encouragement during my stay. Financial assistance from IIST is greatly appreciated.

The lively discussions with one of my doctoral committee member Dr. C. P. Reghunadhan Nair, VSSC was of great inspiration and sharpened my views. My other doctoral committee members, Prof. Sabu Thomas, Dr. Vijayamohanan K Pillai, Dr. K Prabhakaran, and Dr. Raju K George have all been instrumental in the realization of this research work. I wish to express my sense of gratitude to all of them. I extend my heartfelt thanks to Dr. Srinivasan Sampath, Professor, IISc Bangalore and Dr. Jyotishkumar, Inspire Faculty, Cochin University, Kerala, for their valuable academic help. I also thank all the faculty members of the Department of chemistry, IIST for their valuable guidance which enabled the successful completion of the research work.

I extend my sincere thanks to SAIF, IIT Madras, Amrita Centre for Nanoscience, Cochin, National Institute for Interdisciplinary Science & Technology (NIIST), Thiruvananthapuram, M.G University, Kottayam and CESS Akkulam for kindly providing access to characterize my samples.

This work would not have been possible without the unstinting support extended to me by my colleagues. My deep gratitude and sincere thanks are due to my dear friends, Narasimman Rajaram, Arun Prasad Kumar, Rohith M, Mohammed Mukthar Ali, Sujith Vijayan, Rakesh, Manjunatha Ganiga, Praveen Wilson, Meegle S Mathew, Reshma, Aswathy, Sarah Titus, Jalaja, Sarika and Devi Renuka. I also wish to express my appreciation to all the staffs in Department of Chemistry IIST, especially to Mr. Dileep Kumar, Mr. Loveson Albert and Mr. Sreekumaran Nair for helping me in every possible way. I would also like to extend my sincere thanks to Mr. S B M Guruvayurappan, VSSC for his wholehearted cooperation and support during mechanical studies. I would like to thank sincerely Dr. Saritha A for her effort to correct my thesis. I am grateful to the Librarian and staff members of IIST Library for their help during my research programme.

My heartfelt thanks to my wife Najiya KPP for her unconditional love, care, affection, motivation, encouragement and support which empowered me during the preparation of this thesis. Finally, I express my deep sense of gratitude to my beloved parents, my brother and sister whose prayers, affection, encouragement, inspiration and support smoothly paved my path towards the successful completion of this research work.

Raneesh Konnola

# ABSTRACT

Epoxy resin is an important thermosetting matrix with good stiffness, thermal resistance, chemical resistance and long pot life period. On the other hand, cured epoxies are highly brittle, which limits their utility in many composite applications. The incorporation of nanofillers into epoxy matrix is gaining significant interest in the structural composite application, where strength, stiffness, durability, lightweight, design, and process flexibility are required such as in aerospace and automobile industry. The inherent brittle nature of the epoxy matrix can be improved by the incorporation of nanofillers in the matrix. The realization of nanofiller reinforced epoxies with high toughness requires a homogeneous dispersion and strong interfacial interaction between the nanofiller and the polymer matrix. Generally nanoparticles have a tendency for agglomeration because of the weak van der Waals force of attraction. Surface modifications of nanofillers are an effective way to improve interfacial interaction between the nanofillers and the epoxy matrix, which in turn leads to better filler dispersion, and enhanced mechanical performance in the nanocomposites. The main objective of this research work is to study the influence of geometry and surface modification of nanofiller on the morphology, mechanical, thermal and viscoelastic properties of the epoxy composite system. We focus our work to develop epoxy systems with high toughness as well as mechanical strength.

Glycidyl polyhedral oligomeric silsesquioxane (POSS) was used as a crosslinking agent to prepare a new organic–inorganic hybrid material from carboxyl terminated poly(acrylonitrile-co-butadiene) (CTBN). Differential Scanning Calorimetry (DSC) at different heating rates in the presence and absence of catalyst, triphenyl phosphine (TPP), was conducted to investigate the curing kinetics. The curing mechanism of POSS-CTBN system followed an autocatalytic model.

A novel hybrid epoxy nanocomposite has prepared using CTBN as modifier, glycidyl POSS as nanofiller and diaminodiphenyl sulfone (DDS) as curing agent. We have carried out a comparison of the properties of the hybrid systems with POSS/epoxy nanocomposites and CTBN/epoxy blends. Fracture toughness measurement showed 59 % improvement in $K_{IC}$ for 2.5 phr POSS/epoxy composites as compared to neat epoxy, whereas only 38 % improvement was observed for hybrid composite. A decrease in toughness for the hybrid composite was observed due to the occurrence of high crosslink density created by octa-functional POSS particles near rubber particles which might have reduced the rubber particle size and this in turn, causes the toughening capability of soft rubber particles.

The surface of multi-walled carbon nanotubes (MWCNTs) were modified by grafting with CTBN and hydroxyl terminated poly(ethersulfone) (PES). Incorporation of PES and CTBN grafted MWCNTs in epoxy matrix composites imparted tremendous improvement in fracture toughness when compared to pristine and acid modified MWCNT/epoxy composites (125 % improvement for 0.3 wt% MWNCT-g-PES and 119 % improvement for 0.3 wt% MWNCT-g-CTBN compared to neat epoxy) in addition to the improvement in mechanical characteristics. The mechanism

of fracture behavior revealed that crack deflection, pullout of nanotubes, debonding of MWCNTs and bridging mechanism were responsible for the improvement in fracture toughness of the composites.

The effect of surface modification of graphite oxide (GO) on the thermo-mechanical properties of epoxy composites was investigated. CTBN grafted GO and polyethylenimine (PEI) grafted GO were successfully synthesized. Partial reduction of GO was observed during functionalisation with CTBN and PEI. The mechanical properties of the epoxy system showed an excellent improvement by the addition of polymer functionalized GOs. The surface morphology revealed improved interfacial bonding between the filler/matrix. Therefore, polymer functionalized GO modified composites were able to carry higher level of loading during fracture. The viscoelastic properties also showed drastic improvement in modulus and $T_g$. This improvement in $T_g$ is due to the hindered polymer chain mobility near the filler/matrix interface. The improvement in modulus and $T_g$ was further confirmed by the quantitative analysis of the constrained region.

$TiO_2$-derived nanowires were prepared by a simple hydrothermal synthesis using commercial $TiO_2$ powder. The $TiO_2$(B)-NWs showed the highest mechanical properties and analogous thermal properties compared to $TiO_2$ nanoparticle. The optimum properties of this system are attributed to the particle shape or particle dimension that has been described by the aspect ratio wherein the elongated filler shows the highest aspect ratio hence improving the bonding between resin and filler. $TiO_2$/epoxy composite showed little effect on fracture toughness, but $TiO_2$ nanowires increased toughness significantly. The $TiO_2$(B)-NWs incorporated into the epoxy matrix effectively disrupted the development of crack growth and prevented crack propagation.

# TABLE OF CONTENTS

# LIST OF TABLES

# LIST OF FIGURES

# ABBREVIATIONS

| | |
|---|---|
| APS | Aminated poly(styrene) |
| ATBN | Amine terminated butadiene acrylonitrile copolymer |
| ATPDMS | Amine-terminated polydimethylsiloxane |
| BCP | Block Copolymer |
| CIPS | Crystallization-Induced Phase-Separation |
| CNT | Carbon Nanotube |
| CNF | Carbon Nanofiber |
| MWCNT-COOH | Carboxyl Functionalized Multi-walled Carbon Nanotube |
| GCTBN | Carboxyl Terminated poly(acrylonitrile-co-butadiene) Grafted Graphite Oxide |
| MWCNT-g-CTBN | Carboxyl Terminated poly(acrylonitrile-co-butadiene) Grafted Multi-walled Carbon Nanotube |
| CTBN | Carboxyl Terminated poly(acrylonitrile-co-butadiene) Rubber |
| CTPEHA | Carboxyl Terminated poly(2-ethyl hexyl acylate) |
| CSR | Core Shell Rubber Particles |
| DPSO | Dendritic polysiloxane |
| DDM | 4,4-diaminodiphenylmethane |
| DDS | 4,4’-Diaminodiphenylsulfone |

| | |
|---|---|
| DETA | Diethylenetetramine |
| DSC | Differential Scanning Calorimeter |
| DGEBA | Diglycidyl Ether of Bisphenol-A |
| DMDES | Dimethyldiethoxylsilane |
| DMA | Dynamic Mechanical Analyzer |
| EHBPES | Epoxide-terminated hyperbranched polyether sulfone |
| EHTPB | Epoxidized hydroxy-terminated polybutadiene |
| EPN | Epoxy Phenol Novolac resins |
| ECN | Epoxy Cresol Novolac resins |
| ETPB | Epoxy terminated polybutadiene |
| FTIR | Fourier Transform Infrared Spectroscopy |
| GO | Graphite Oxide |
| GPTMS | 3-glycidoxypropyl trimethoxysilane |
| HRTEM | High Resolution Transmission Electron Microscopy |
| MWCNT-OH | Hydroxyl Functionalized Multi-walled Carbon Nanotube |
| HTPB | Hydroxyl Terminated polybutadiene |
| PEEKTOH | Hydroxyl Terminated poly (ether ether ketone) |
| MWCNT-g-PES | Hydroxyl Terminated poly(ether sulfone) Grafted Multi-walled Carbon Nanotube |

| | |
|---|---|
| HBP | Hyperbranched Polymer |
| HBPEE | Hyperbranched polyether-epoxy ended |
| HBPI | Hyperbranched polyimide |
| HBPU | Hyperbranched polyurethane |
| IPN | Interpenetrating Polymer Network |
| LCP | Liquid Crystalline Polymer |
| MPDA | Metaphenylenediamine |
| MMT | Montmorillonite |
| MWCNT | Multi-Walled Carbon Nanotube |
| NMR | Nuclear Magnetic Resonance Spectroscopy |
| PBAE | Poly(bisphenol A-co-epichlorohydrin) |
| PBT | Poly(butylene terephthalate) |
| PC | Polycarbonate |
| PEO | Poly(ethylene oxide) |
| PEP | Poly(ethylene-*alt*-propylene) |
| PES | Poly(ether sulfone) |
| PESEK | Poly(ether sulfone ether ketone) |
| PEI | Polyethylenimine |
| GOPEI | Polyethylenimine Grafted Graphite Oxide |

| | |
|---|---|
| PMMA | Poly(methy1 methacrylate) |
| PNC | Polymer Nanocomposite |
| POSS | Polyhedral Oligomeric Silsesquioxane |
| PPO | Poly(phenylene oxide) |
| PSF | Polysulfone |
| PVC | Poly(vinylene chloride) |
| RIPS | Reaction-Induced Phase-Separation |
| SBS | Poly (styrene-block-butadiene-block-styrene) |
| SEM | Scanning Electron Microscopy |
| sPS | Syndiotactic polystyrene |
| SWCNT | Single-Walled Carbon Nanotube |
| TGDDM | Tetraglycidyl-4,4'-diaminodiphenylmethane |
| TRGO | Thermally Reduced Graphene Oxide |
| TGA | Thermogravimetric Analyzer |
| $TiO_2$(B)-NW | Titanium Dioxide Nanowire |
| TOM | Transmission Optical Microscope |
| TETA | Triethyleneteramine |
| TGAP | Triglycidyl-p-aminophenol |
| TPP | Triphenylphosphine |

| | |
|---|---|
| UTM | Universal Testing Machine |
| XRD | X-Ray Diffractometer |
| XPS | X-Ray Photoelectron Spectroscopy |

# NOTATIONS

| | |
|---|---|
| Ea | Apparent activation energy |
| $f_c$ | Carboxyl functionality in CTBN |
| a | Crack length |
| $f(\alpha)$ | Differential conversion function |
| $W$ | Energy loss fraction |
| $f_e$ | Epoxy functionality in DGEBA |
| $\alpha$ | Extent of conversion |
| $\chi_{gel}$ | Extent of reaction at the gel point |
| $G_{IC}$ | Fracture energy |
| B | Fracture test specimen thickness |
| W | Fracture test specimen width |
| $T_g$ | Glass transition temperature |
| β | Heating rate |
| $Ti$ | Initial decomposition temperature |
| L | Load at crack initiation |
| $G''$ | Loss modulus |
| A | Pre-exponential factor |
| n | Pseudo-plasticity index |
| φ | Shape factor |
| γ | Shear rate |
| τ | Shear stress |
| $G'$ | Storage modulus |

| | |
|---|---|
| $K_{IC}$ | Stress intensity factor |
| $T$ | Temperature |
| $t$ | Time |
| $t_{gel}$ | Time of gelation |
| $\eta$ | Viscosity |
| $C_r$ | Volume fraction of the constrained region |
| $\upsilon_f$ | Volume fraction of the filler |
| R | Universal gas constant |
| E | Young's modulus of the composite |
| $E_m$ | Young's modulus of the epoxy matrix |
| $E_f$ | Young's modulus of the filler |

# CHAPTER 1

# INTRODUCTION

*The aim of this chapter is to introduce and provide the state-of-the-art literature survey on the toughening of epoxy using different toughening modifiers. This chapter introduces the motivation and objectives of the research work. At the end of the chapter, the organization of the whole thesis and a brief introduction of each chapter is provided.*

## 1.1. Polymer Nanocomposites

Polymer nanocomposites (PNCs) are a new class of composites, for which at least one dimension of the dispersed particles, are in the nanometer range (Koo, 2006). Nowadays, development of polymer nanocomposites became an efficient strategy to improve the properties of polymers to the level where potential of these materials exceed the ones of conventional composites. Compared to conventional materials, nanocomposites offer useful new and interesting properties due to which it has received much interest in the scientific community. The necessary loadings of nanofillers in the polymer matrices are usually lower than those of their microfiller counterparts (typically 10–40 vol% for microfillers). As a result, nano material incorporated polymer matrices grant huge advantage when compared to microfilled ones. Besides, many inherent properties of polymers such as flexibility, strength, optical transparency, and good processability will be maintained after nanofiller addition. As far as mechanical properties are concerned, the changes in stiffness and strength depend mainly on the degree of interaction between the reinforcing filler and the polymer matrix. It has been established that incorporation of small amount of nanofiller into the polymer matrix can significantly improve the thermo-mechanical, optical and electrical properties without affecting its processability, density and appearance. Because of the unique nanostructure and interesting properties, addition of carbon base nano fillers, such as carbon nanotubes (CNTs) and graphene can improve mechanical and electrical properties as well as thermal conductivities of polymer composites (Ruiz-Pérez et al., 2008). Because of these reasons, the fabrication and applications of polymer nanocomposites have become essential part in the industrial as well as academic research community. These nanocomposites are now find application in all kinds of fields including small commodity articles, automotive, electronics, packaging materials, and highly strategic fields like defense, aerospace and marine industries. Commercialization of nanocomposite technology started with the realisation by the researchers from Toyota Central Research

Laboratory, Tokyo that incorporation of as little as four percent by weight of a layered and nanostructured silicate clay into a polyamide 6 polymer matrix produced a composite material with improved mechanical and barrier properties as well as improved thermal resistance.

Nature has long ago demonstrated the usage of nanocomposites. For example, nacre (available in abalone shell) is composed of 99 vol% aragonite ($CaCO_3$) and 1 vol% biopolymer. Nacre is 2 times harder and 1000 times tougher than its main component aragonite. Such a remarkable enhancement in properties due to the presence of only 1 vol% of biopolymer is the result of a highly controlled structure, which nature produces by a process called biomineralisation (process by which nature produces minerals, often to harden or stiffen the existing tissues). Thus nanocomposite technology is an attempt by man to mimic nature.

Two critical issues have to be rectified inorder to fully realize the mechanical and electrical property improvement in nanocomposites. The primary factor is the dispersion of nanomaterials inside the polymer matrix and the other is the interfacial interaction between the nanomaterial and the matrix. Because of the large surface area, surface energy and strong van der Waals force of attraction, nanofillers are very difficult to disperse in a polymer matrix. A large number of processing techniques have been tried to disperse nanofillers in polymer matrix which include high speed shear mixing and sonication resulting in improved properties of nanocomposites. Strategic sectors such as aerospace and marine fields which needs high strength, toughened, heat resistant and lightweight materials are the biggest markets for polymer nanocomposites (Koo, 2006). Aerospace composites that have the required properties are already being developed. However, these composites are still in their infancy, and problems related to manufacturing such as dispersion, alignment, load transfer between filler and matrix have to be improved before they can be widely used in structural elements. Consequently, a fundamental understanding of the

reinforcing mechanism between the nanofiller and matrix is needed for both the manufacture and application of nano-composite materials.

## 1.2. Nanofillers

Nanofillers can be defined as fillers having average particle size in the range 1 to 100 nanometer (Rao et al., 2006). As the dimension of filler gets smaller, the surface area (per volume of filler) available for interaction with the matrix increases and hence a remarkable improvement in reinforcement efficiency can be achieved. It is now well established that the incorporation of a small percentage of nanofillers in a polymer matrix may markedly enhance its mechanical strength. When comparing with micron size fillers, the nano size filler particles are able to occupy substantially large number of sites in the polymer matrix. This intimate contact can influence the inherent properties of the polymer matrix such as its chain entanglements, its morphology and even its crystallinity. The concentration of the nanofiller for getting optimal properties in the polymer composites is dependent on its particle size and shape, dispersion behavior and interfacial bonding interaction between the filler and polymer matrix. The range of properties where nano-sized fillers are expected to yield improvements over neat polymers is wide, improved mechanical strength, electrical conductivity and toughness properties can be cited as examples.

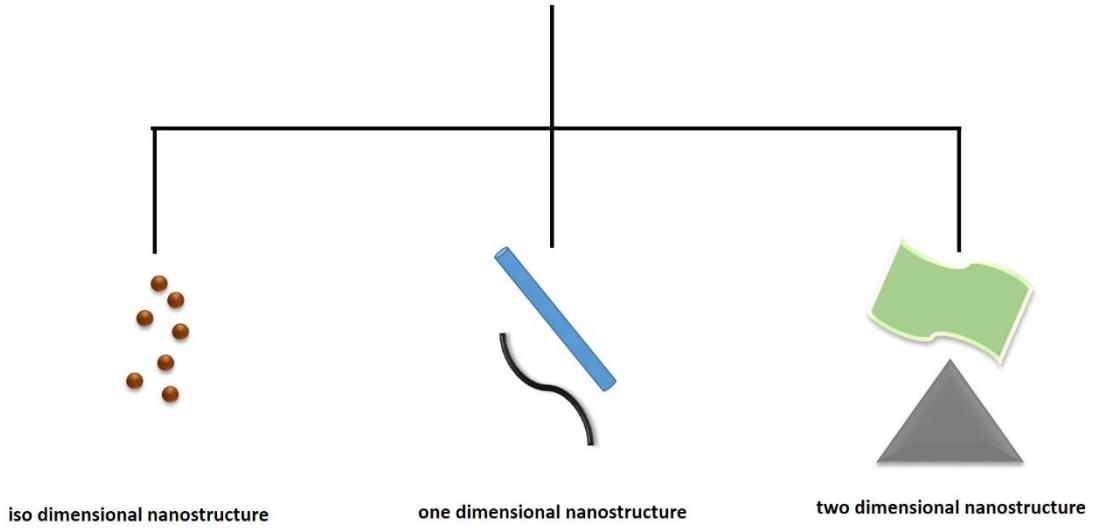


Figure 1.1: Classification of nanostructures

By knowing how many dimensions of the dispersed particles are in the nanometer range, one can distinguish nanostructures into three types (Figure 1.1). When the three dimensions are in the order of nanometers, we are dealing with **iso dimensional nanostructures** like silica obtained by in-situ sol gel methods. In addition to silica, various nano particles like titanium dioxide, zinc oxide, calcium carbonate, ceramic oxides etc. are also used to reinforce various polymer matrices. If two of the dimensions are reduced to nano range and the other one is large, the resulting structure is a **one dimensional nanostructure**. One dimensional nanostructures includes nanowires, nanorods, nanotubes etc. whose lateral dimensions fall in the range of 1 to 100 nm. One dimensional nanostructures play a unique role in the growing research areas of nanoscience with outstanding mechanical, electrical and optical properties being shown by the material due to the quantum confinement of electrons in two-dimension. Various metal oxide nanowires, carbon nanofibers, cellulose whiskers, and carbon nanotubes belongs to one dimensional nanostructures. If any one of the dimension is reduced to nano range while the two dimensions are large, the resulting structure is a **two-dimensional nanostructures**. Because of the low dimensional characteristics different from the bulk properties, synthesis of two dimensional nanofillers have become a focal area in

nanomaterials research. Graphene and nanoclays are examples of two dimensional nanofillers. Interestingly, carbon nanostructures exist in all the three forms (Figure 1.2).

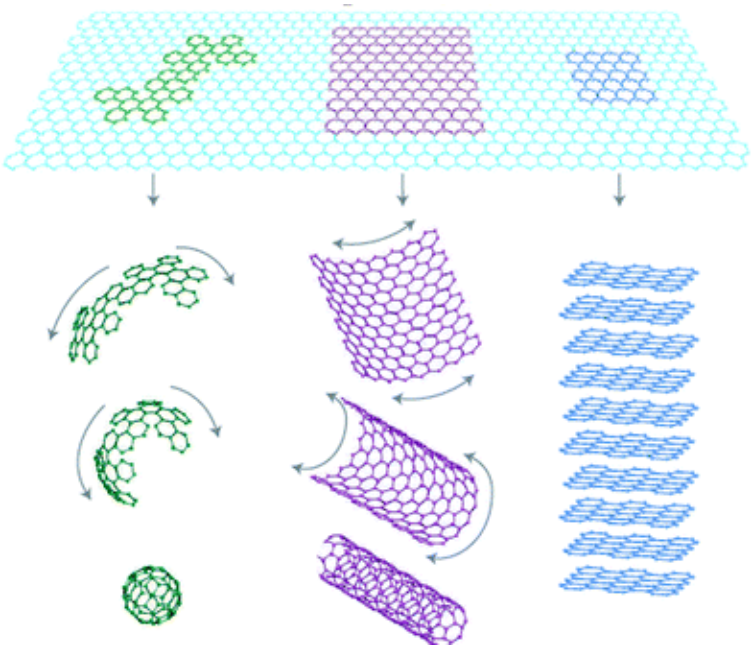

Figure 1.2: Formation of different carbon nanostructures from graphene layer (Geim et. al., 2010)

A humble detail of the commonly used nanofillers in polymer nanocomposites is presented in the forthcoming paras.

## 1.2.1. Carbon nanotube

Carbon nanotubes are long, thin cylinders of carbon, discovered by Sumio Iijima in 1991 (Iijima, 1991). Because of its outstanding tensile strength, very high thermal conductivity (higher than purest diamond) and electrical conductivity (greater than copper), it is often known as the "wonder material". Elemental carbon can form amazing structures in its $sp^2$ hybridization. Carbon can build closed and open cage

structures with honeycomb arrangement of carbon atoms. CNTs are one-dimensional nanostructures consisting of single or multiple sheets of graphene wrapped into a cylinder (Figure 1.3). CNTs are of two types – single walled carbon nanotube (SWCNT) and multi-walled carbon nanotube (MWCNT). SWCNTs are single sheets of graphene wrapped up into the form of a cylinder. MWCNTs consists concentric arrays of single walled nanotubes nested together. Depending on the diameter and number of concentric shells in the MWCNT, the interlayer spacing for MWCNTs ranges from 0.342 to 0.375 nm (Gogotsi and Presser, 2013). The increase in intershell spacing with decreased nanotube diameter is due to the increased repulsive force as a result of the high curvature. CNTs are quite non-reactive due to the absence of dangling bonds in the hexagonal arrangement of carbon atoms, and the fullerene like tips of the CNT are more reactive than the CNT sidewalls. CNTs exhibits excellent electrical, mechanical and structural properties.

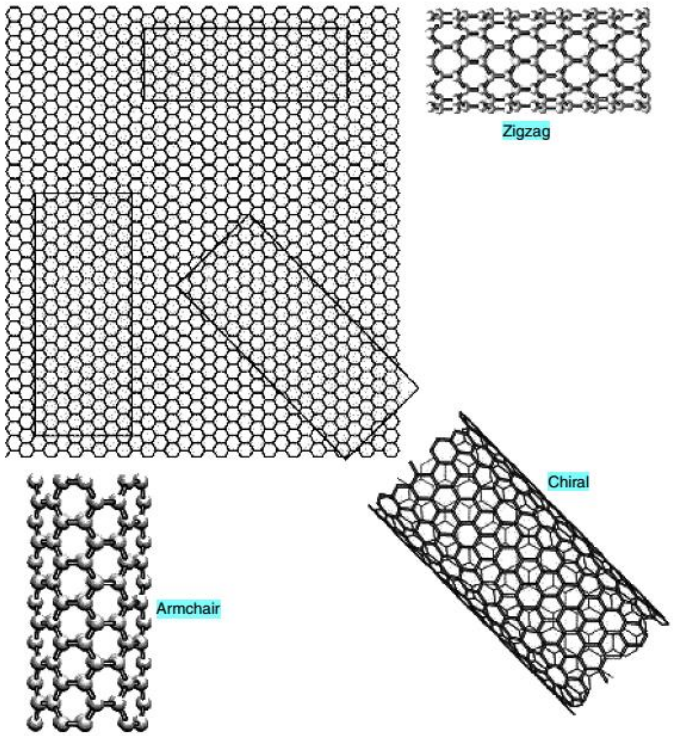


Figure 1.3: Different chiral structures of carbon nanotube (Gogotsi & Presser, 2013)

Carbon nanotubes are large macromolecules which are distinctive for their size, shape, and outstanding physical properties. They can be considered as a hexagonal lattice of carbon atoms rolled into the form of a cylinder. A pair of indices (n,m) represents how the graphene sheets are wrapped up to form a carbon nanotube and are referred as chiral vectors. Depending on the chiral vectors (n,m) carbon nanotube can be classified as arm chair (n=m and chiral angle = 30º), zigzag (n=0, m=0 and chiral angle = 0º) and chiral (n ≠ m and chiral angle = 0º). The chirality of nanotubes has significant impact on its transport properties, particularly the electronic properties. The nanotubes can be metallic or semiconducting depending on their structural parameters.

The diameter, length, and chirality of the CNTs plays a key role in exhibiting a wide range of structural, thermal and electronic properties in nanotubes. The diameter $d$ and the chiral angle $\theta$ of the CNT can be given as

$$d = 0.783\sqrt{n^2 + nm + m^2}\,A^{\circ} \tag{1.1}$$

$$\theta = \sin^{-1}\left[\frac{\sqrt{3}m}{2(n^2 + nm + m^2)}\right] \tag{1.2}$$

The intriguing structures of the CNT and the outstanding properties have sparked much excitement in the recent years and enormous research has been carried out in this area. The quasi-one dimensional structure and graphitic arrangement of the carbon atoms in the shells leads to the amazing electronic and mechanical properties in CNTs. The physical properties of CNTs are still being explored. Due to the one-dimensional electronic structure, ballistic conduction of electrons occurs in CNTs resulting in high conductivity. CNTs have current densities of $10^9$ – $10^{10}$A/cm$^2$ and the resistance is stable upto 250ºC. CNTs are brittle at low temperature. At low temperatures CNTs behaves as superconductors. CNTs possess high axial strength

and stiffness due to the carbon-carbon $sp^2$ bonding. CNTs possess ultra-high Youngs modulus of ~1 TPa and tensile strength in the range of 11-63 GPa and are promising materials as nanofillers in high-performance polymer matrix composites (Moniruzzaman and Winey, 2006). The very high Young's modulus and tensile strength of the CNTs makes them suitable for composite materials with enhanced mechanical properties (Schadler et al., 1998).

### 1.2.2. Graphene

Graphene is the first two-dimensional atomic crystal of carbon; is also referred as zero resistance wonder material (Figure 1.4). The revolutionary discovery of graphene has added a new dimension of research in the fields of physics, chemistry, biotechnology, and materials science (Geim and Novoselov, 2007). It is a promising material for various applications due to its fascinating properties such as exceptionally high thermal conductivity, charge carrier mobility, surface area, Young's modulus, fracture strength etc. The unique features of graphene have attracted tremendous interest both in academics and industry. Graphene sheets consist of two-dimensional honeycomb lattice of $sp^2$ bonded carbon atoms. Graphene is the basic building block of all graphitic materials; it can be wrapped up to form zero dimensional fullerene, rolled into one dimensional nanotubes and stacked upto form three dimensional graphite. Graphene is known as the strongest material present today as it possesses Young's modulus of 1 TPa and ultimate strength of 130 GPa. Graphene has stimulated enormous research among the scientific community. Graphene exhibits a wide variety of excellent properties like quantum Hall effect, 2D Dirac Fermions, high value of aspect ratio, high surface area, high optical transmittance, Young's modulus, fracture toughness, electron mobility and thermal conductivity (Rao et al., 2009). Because of its excellent electrical properties, graphene can be used in making solar cells, super capacitors, sensors, batteries etc. The incorporation of graphene into polymer nanocomposites can enhance the properties of polymer nanocomposites to a great extend (Stankovich et al., 2006). The

superior properties of graphene are associated with its single-layer. But the preparation of single-layer graphene is difficult at room temperature. The major challenge with graphene is its tendency to restack to form graphite, as a result of its high surface energy and strong van der Waals force of attraction (Loh et al., 2010). Enormous researches are being carried out to functionalize graphene and to improve the dispersion and interaction of graphene in the polymer matrix. On incorporating graphene into host material, the properties such as electrical conductivity, elastic modulus, tensile strength and thermal stability are enhanced to a greater extent. The property enhancement occurs at even low loading of the filler due to large interfacial area and high aspect ratio. Due to the larger surface area of the graphene sheets, the contact area of the graphene with polymer matrix is higher and so it maximizes the stress transfer from polymer to graphene nanosheets. Chemical modification of graphene improves the compatibility, dispersion and interfacial interaction of nano-fillers in polymer matrix. Graphene can also take part in certain classes of reactions including cyclo-additions, click reactions, and carbine insertion reactions (Loh et al., 2010). However, reactions on the surfaces of graphene hamper its planar structure. The destruction of the $sp^2$ structure leads to the formation of defects and loss of electrical conductivity.

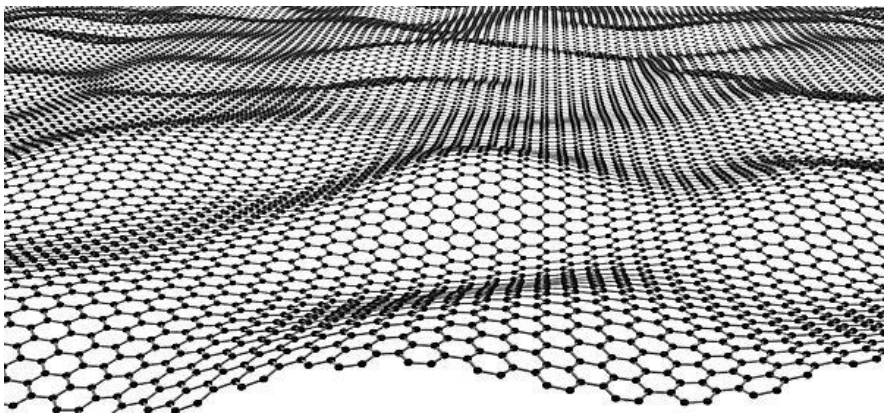

Figure 1.4: Structure of graphene

### 1.2.3. Graphene oxide

Graphene oxide is produced by the exfoliation of graphite oxide (GO) (Figure 1.5). Graphene oxide has attracted great attention as it is easy to produce, low cost, and highly efficient in improving the properties of polymers. There are different methods for production of graphene oxide from natural graphite; the modified Hummers method is very fruitful in preparing graphene oxide (Hummers Jr and Offeman, 1958). The interlayer distance between the graphene oxide sheets is around 6 to 12 Å. The stirring and sonication of graphite oxide can lead to the complete exfoliation to produce aqueous colloidal suspension of graphene oxide. With a great deal of epoxy, hydroxyl, and carboxyl functional groups on its basal planes, graphene oxide can be stably dispersed in water, these functional groups also make it more compatible with organic polymers. Graphene oxide is a non-stoichiometric material because the density of oxygen groups cannot be precisely controlled, which means that functionalization chemistry based on coupling chemistry to the oxygenated groups will inevitably lead to non-stoichiometric functionalization (Loh et al., 2010). Reduction process of graphene oxide can partially restore the outstanding properties of graphene. The exfoliated sheets of graphene oxide can be chemically, electrochemically, or thermally reduced into graphene. Chemical reduction has been performed with several reducing agents including hydrazine or sodium borohydrate (Dreyer et al., 2010). During this reduction process, the graphene oxide becomes less hydrophilic and increases its tendency to agglomerate irreversibly in aqueous media, thus precipitating in the form of black aggregates. Direct thermal treatment provides another way to reduce graphene oxide sheets. Functionalization of graphene oxide can result in chemically modified graphenes which could then potentially become much more adaptable for a lot of applications. Graphene oxide and surface modified graphene oxide were used as building blocks for new polymer composites to obtain high performance composite materials (Zhu et al., 2010). The presence of various oxygen functional groups in graphene oxide can lead to strong interfacial interactions

between graphene oxide and the polymer and hence use of graphene oxide as a reinforcing filler is advantageous in terms of mechanical property improvement.

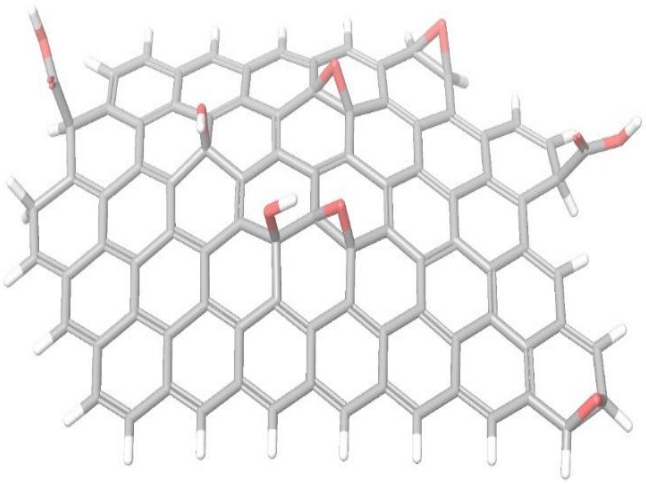

Figure 1.5: Structure of graphene oxide

## 1.2.4. Polyhedral oligomeric silsesquioxane (POSS)

Polyhedral oligomeric silsesquioxanes (POSS) can be considered as a nano form of silica. POSS-based hybrid nano materials have received gradually increased attention due to their unique structure of POSS (Konnola et al., 2016). The most common form of POSS ($Si_8O_{12}R_8$) is comprised of a cubic cage with eight silicon atoms in the corner and twelve oxygen atoms on the edge with each of the silicon atoms carrying a functional group (R) (Hartmann-Thompson, 2011) (Figure 1.6). The diameter of a fully extended POSS molecule can vary from one to several nanometers, depending on the structure of the substituent. Unlike traditional organic compounds, POSS derivatives are nonvolatile, odorless and environmentally friendly materials. POSS have both the properties of the inorganic materials (i.e., thermal chemical, radiation and oxidative stability, high modulus,) and the organic polymers (i.e., processibility, solubility, ductility, ease of manipulation using conventional

chemical techniques, low toxicity, and potential to tailor the structure by varying R to achieve the desired properties). The inner inorganic silicon and oxygen core surrounded by organic substituents renders high reactivity and compatibility to POSS molecules which make them attractive as additive for altering the properties of a variety of polymer matrices (Kuo and Chang, 2011). The incorporation of POSS into the polymer enhances the mechanical, thermal, oxidative, dielectric properties and reduces the flammability of polymers. POSS could be incorporated into polymers via blending, copolymerization or some other chemical approaches. POSS nanostructures also have significant promise for use in catalyst supports and biomedical applications, such as scaffolds for drug delivery, imaging reagents, and combinatorial drug development.

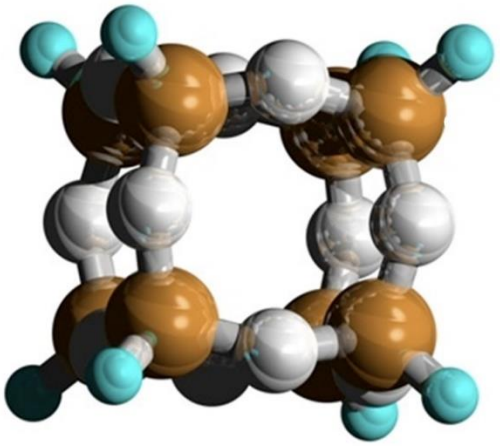

Figure 1.6: Structure of polyhedral oligomeric silsesquioxane

## 1.2.5. Titanium dioxide

$TiO_2$ belongs to the family of transition metal oxides (Figure 1.7). There are mainly four commonly known polymorphs of $TiO_2$ occurring naturally which includes anatase, rutile, brookite and $TiO_2$(B). Besides these naturally occurring polymorphs, additional high-pressure forms have been reported – $TiO_2$ (II) with the $\alpha$-$PbO_2$ structure, $TiO_2$ (H) with hollandite, baddelleyite with $ZrO_2$, Cotunnite with

$PdCl_2$. The surface properties of $TiO_2$ can be tailored and has been the interest of research community. The complex $TiO_2$ surface holds an important role in a wide variety of applications. The step edges, oxygen vacancies, line deficiencies, foreign cations, crystallographic shear planes and the surface planes of $TiO_2$ adds to the complex surface features of $TiO_2$ and plays a vital role in a wide variety of applications. Due to the improved surface wettability property of titania nanoparticles, it is useful in many photochemical applications such as antifogging and self-cleaning coatings. Because of its non-toxicity, high dispersibility and corrosion protective as well as UV absorbing nature, it is widely used in paint industry. $TiO_2$ is having excellent optical transmittance in the visible and near-infrared region and therefore it is used in antireflective coatings, metal mirrors with enhanced reflection, and filters. Because of its high chemical and thermal stability, low cost and nontoxicity, $TiO_2$ can act as a semiconductor photo catalyst for the decomposition of a great variety of organic pollutants. $TiO_2$ is widely used as a filler in polymer composites of polyethylene, polystyrene, ABS, PVC etc. due to their improved physical and mechanical properties induced by $TiO_2$ while without loss of inherent polymer properties like ease of processing, light weight and flexible nature. Traditionally, the polymer composites were reinforced with micron-sized $TiO_2$. Recently, processing techniques like sonication, high shear mixing etc. have been developed to allow the size of $TiO_2$ to go down to nanoscale. Experiments have shown that nanoscale reinforcement brings new electrical, optical, physiochemical properties, which lead to new material properties and correspondingly extended applications.

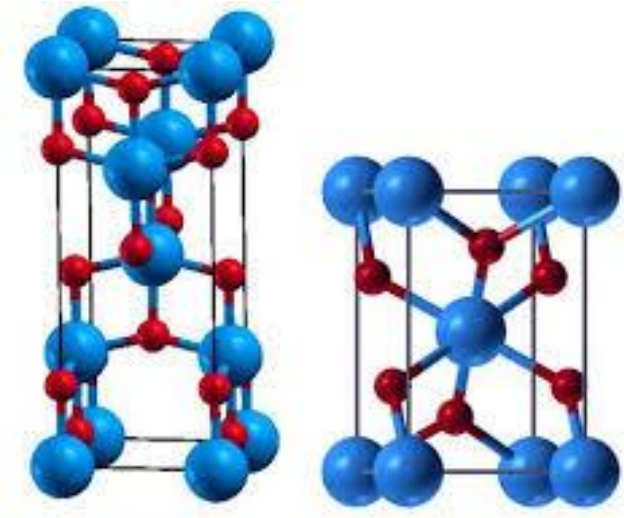

Figure 1.7: General chemical structures of anatase and rutile forms of $TiO_2$ nanoparticles

## 1.2.6 Nanoclay

Clays are one group of nano fillers which is widely used to make polymer nanocomposites. Clays belong to the family of layered silicates. Layered silicates consist of regular stacks of aluminosilicate layers with high aspect ratio and large surface area. They are easily available and usually cheap compared to other nanofillers. Those members of the clay family that can be exfoliated of polymer chains or monomers and distributed as individual layers within the polymer matrix are suitable to be used in nanocomposite fabrication. These individual clay layers cause dramatic improvements in polymer properties due to their high aspect ratio and large surface area.

Each layer in a clay contains two outer tetrahedral sheets of Si with a central octahedral sheet of Al or Mg. The tetrahedral and octahedral sheets are fused together by the sharing of oxygen atoms. Unshared oxygen atoms are present in hydroxyl form. Clays are classified into different types based on the condensation ratio of silica to alumina sheet:

(1) 1:1 type: It consists of one octahedral sheet of alumina sheet and one tetrahedral sheet condensed in 1:1 ratio. This is known as kaolin group of clays.

(2) 2:1 type: It consists of one octahedral sheet of alumina sandwiched in between two tetrahedral sheets of Si. These are known as phyllosilicates (Figure 1.8). Stacking of these layers create a Vander Waals gap between the layers. Isomorphic substitution of $Al^{3+}$ with $Fe^{2+}$, $Mg^{2+}$ in the octahedron sheet and / or $Si^{4+}$ with $Al^{3+}$ in the tetrahedron sheets gives each layer an overall negative charge. This charge is balanced by metal cations like $Na^{+}$, $Ca^{2+}$ residing in the inter layer. Smectite clays result by this substitution. Smectite clays are a favourite filler in nanocomposites due to the high aspect ratio (10 - 1000) and large surface area of the thus intercalated/exfoliated layers (this makes the total interface area of the layers and matrix much greater than conventional nanocomposites). Clay minerals usually belong to the nanoplatelet filler particles in polymer composite technology. Montmorillonite, hectorite and saponite are some well-known smectite clays used in polymer nanocomposites. Montmorillonite (MMT) has the widest acceptability for use in polymer nanocomposites because of its ease availability, well known intercalation/exfoliation chemistry, high surface area and high surface reactivity.

Clay layers are hydrophilic in nature. This along with the face to face stacking of layers in the agglomerated tactoids makes them incompatible with polymers in general. This incompatibility and weak interfacial interactions hinders the exfoliation and preparation of dispersed stable nanocomposite with improved properties. Modification of clay layers with hydrophobic agents is necessary in order to render the clay layers more compatible with polymer chains. Hence it is necessary that an alteration be done in the clay polarity to make it hydrophobic. This is achieved by ion exchange with primary, secondary, tertiary or quaternary alkyl ammonium cations or phosphonium cations which contain a variety of substituents. The alkyl ammonium cations lower the surface energy of the inorganic reinforcement, improve the wetting characteristics of the polymer matrix, and result in larger interlayer spacing (swelling). Additionally, the alkyl ammonium cations can provide functional groups

that react with the polymer matrix or, in some cases, can initiate the polymerization of monomers to form the polymer in-situ.

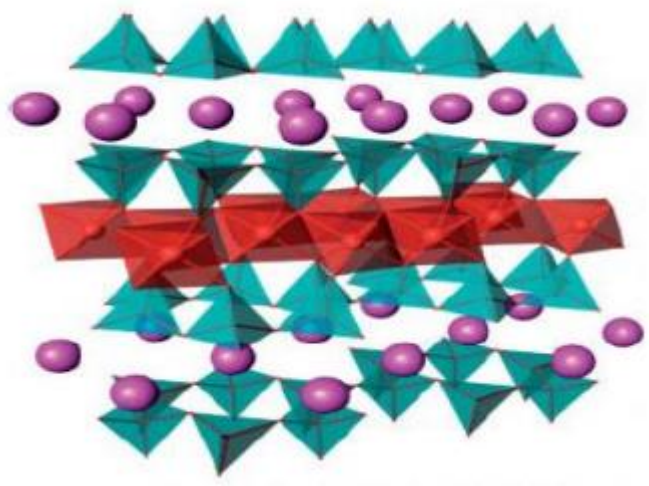

Figure 1.8: The general chemical structure of phyllosilicates (Saritha, 2012)

## 1.3. Epoxy Resins

Epoxy resins are one important class of thermosetting resin materials characterized by two or more oxirane rings (epoxy groups) in their structure. In an epoxy resin, the epoxy group is commonly situated at one or both ends of a chain molecule, but it may sometimes be located internally or in a cyclic structure. The epoxy group is shown in Figure 1.9.

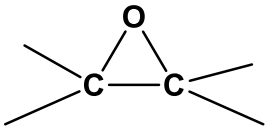


Figure 1.9: Structure of epoxide group

Epoxy resins in the uncured state are liquids or low melting point solids. Like other thermosets they also form a network on curing with a variety of crosslinking agents such as amines, anhydrides, thiols etc. By adding suitable crosslinking agents, the resins can be made to cure at room temperature or at elevated temperature.

Some of the salient features of epoxy resins over the other thermosets are:

- Minimum pressure is needed for fabrication of products normally used for thermosetting resins
- Cured epoxy resins possess excellent tensile strength; outstanding moisture, chemical, and corrosion resistance; good thermal, adhesive, and electrical properties.
- Low shrinkage upon cure and hence there is lower residual stress in the cured product than that encountered in the vinyl polymerization used to cure unsaturated polyester resins.
- Ability to be processed under a variety of conditions
- Ability to accept wide range of fillers and pigments
- Use of a wide range of temperatures by judicious selection of curing agents enables good control over the degree of crosslinking
- No volatile products of the curing reaction to cause undesired bubble or void formation.

Most common epoxy resins are produced from a reaction between epichlorohydrin and bisphenol-A, and was first synthesized in the late 1930s by Dr. Pierre Castan of Switzerland and Dr. S.O. Greenlee of United States (Mark, 2013). Epoxies form one of the major groups of thermosetting plastics in use today. Western Europe and the USA each had about 40% of the market and Japan a little over 10%. This situation has not greatly changed since then; but by the late 2010s the world market for epoxide resins had risen to about 1000 000 tons per year. The production of epoxies in India is less than 2000 tons (Mark, 2013).

Depending on the molecular weight, epoxy resins are available in various physical forms ranging from low viscosity liquids to tack free solids. The non-epoxy part of the molecule may be aliphatic, cycloaliphatic or highly aromatic hydrocarbon or it may be non-hydrocarbon and possibly polar. By the judicious selection of a curing agent and appropriate modifiers, epoxy resins can be specifically tailored to fit to a variety of applications from coatings to military and aerospace applications.

Epoxy resins can be broadly classified into glycidyl epoxy, and non-glycidyl epoxy resins. Glycidyl epoxies are synthesized by utilizing the condensation reaction between epichlorohydrin and an appropriate diamine, dibasic acid or a dihydroxy compound. Whereas, non-glycidyl epoxies are synthesized by peroxidation of olefinic double bond. One of the most commonly used epoxy resins are diglycidyl ethers of bisphenol A (DGEBA) and is synthesized by reacting bisphenol-A with epichlorohydrin in the presence of a basic catalyst, where the degree of polymerization $n$ is nearly zero ($n \sim 0.2$). Bisphenol-A is prepared from 2 $M$ of phenol and 1 $M$ of acetone (Figure 1.10). Since both phenol and acetone are available and the bisphenol-A is easy to manufacture, this intermediate is comparatively inexpensive. This is one of the reasons why it has been the preferred dihydric phenol employed in epoxide resin manufacture (Brydson, 1999).

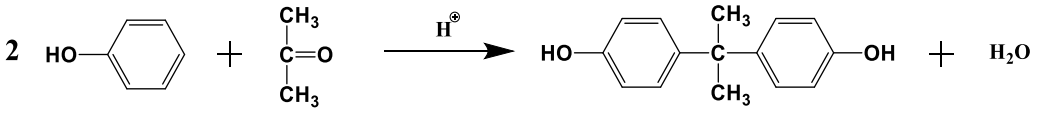


Figure 1.10: Preparation of bisphenol-A from phenol and acetone

Epichlorohydrin, or 3-chloro-1,2-epoxy propane (Boiling point 115◦C), is more commonly prepared from propylene by chlorination to allyl chloride, followed by treatment with hypochlorous acid (Figure 1.11). This yields glycerol dichlorohydrin, which is dehydrochlorinated by sodium hydroxide or calcium hydroxide.

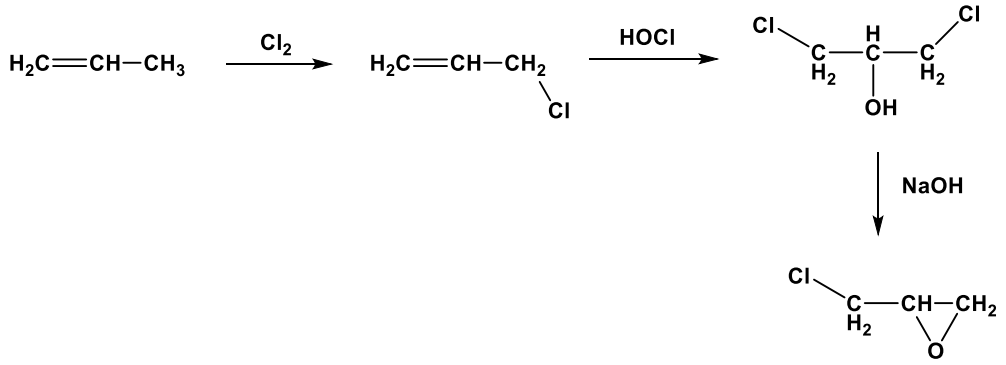


Figure 1.11: Preparation of epichlorohydrin from propylene

Epichlorohydrin and bisphenol-A are used as the precursors to prepare bisphenol-A based liquid epoxy resins by a two-step reaction. The first step is the base-catalyzed reaction of bisphenol-A and epichlorohydrin to yield a chlorohydrin. Dehydrohalogenation of the chlorohydrin intermediate with a stoichiometric amount of base gives the glycidyl ether (Figure 1.12).

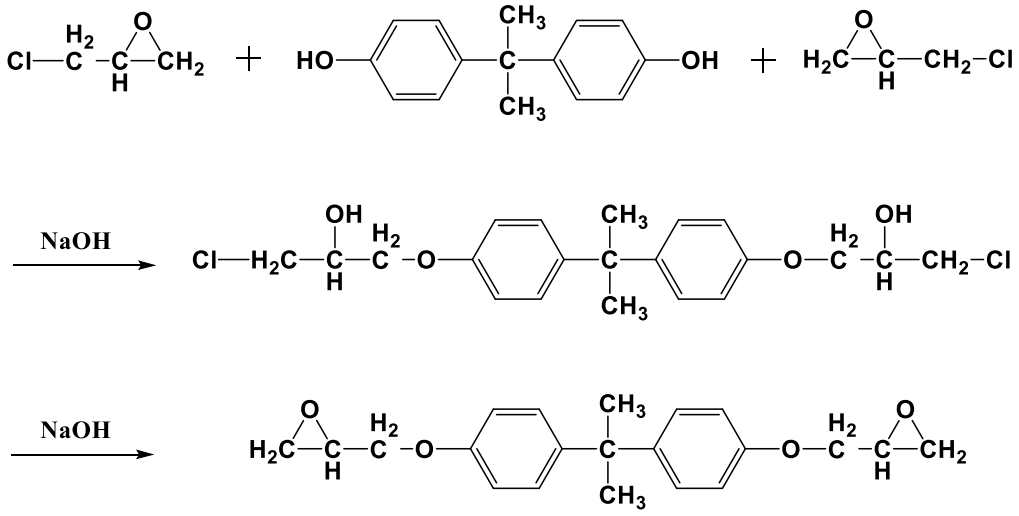


Figure 1.12: Preparation of DGEBA from epichlorohydrin and bisphenol-A

The epoxy resins (DGEBA) are prepared using different molar ratios of epichlorohydrin to bisphenol-A to afford different molecular weight products. The diglycidyl ether has a molecular weight of 340. Average molecular weights of the commercial liquid glycidyl ether resins are in the range 340-400 and it is therefore obvious that these materials are composed largely of the diglycidyl ether. Figure 1.13 represents the chemical structure of DGEBA. By the reduction of the excess of epichlorohydrin and reacting under strongly basic conditions, high molecular weight resins can be synthesized. Depending on molecular weight, the polymer is a viscous liquid or a brittle high melting solid. Other hydroxyl containing compounds such resorcinol, glycols and glycerol can replace bisphenol-A. No epoxides, other than epichlorohydrin are available at attractive prices.

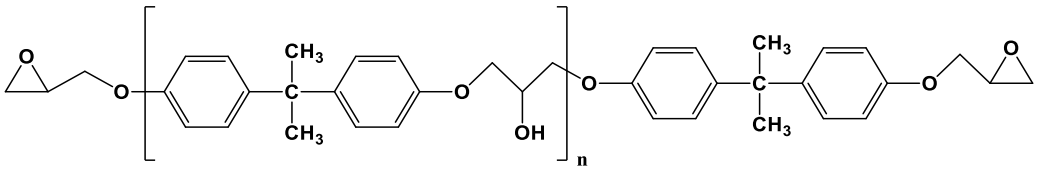


Figure 1.13: Chemical structure of diglycidyl ether of bisphenol-A (DGEBA)

Approximately 75% of the epoxy resins currently used worldwide are derived from DGEBA. This market dominance of bisphenol-A based epoxy resins is a result of a combination of their relatively low cost and adequate-to-superior performance\ in many applications. DGEBA resins are used in filament winding, pultrusion, vacuum impregnating, contact moulding and for manufacture of prepregs from glass and carbon fibers. They can be cured with a wide range of curing agents both at ambient and elevated temperatures

Multifunctional epoxy resins such as epoxy phenol novolac resins (EPN) and epoxy cresol novolac resins (ECN) have also attained commercial importance. In these resins the range in the value of *n* is in between 0.2 and 3. A wide variety of novolac resins based on a range of phenols including resorcinol, cresols, t-butyl

phenols, and catechol are used to synthesize epoxy novolac resins. The functionality of the epoxy novolac resins can be increased by increasing the molecular weight of the navolac. High functionality of phenolic resins results in high crosslink density and better thermal and chemical resistance than bisphenol-A resins. Because of these, epoxy novolac resins find applications in high temperature adhesives, chemical resistant filament wound pipes and structural laminates. Triglycidyl-p-aminophenol (TGAP) and tetraglycidyl-4,4'-diaminodiphenylmethane (TGDDM) are some of the multifunctional glycidyl amine resins, which gained commercial importance (Figure 1.14). TGDDM is used as binders in graphite reinforced composite structures which are used for military applications (Goodman, 1999).

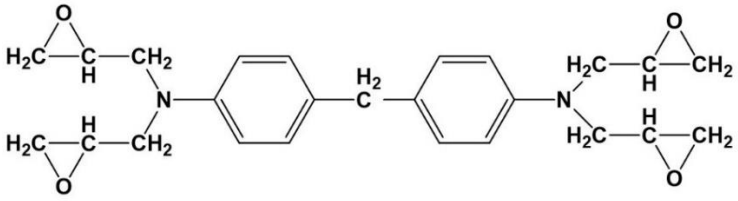

TGDDM

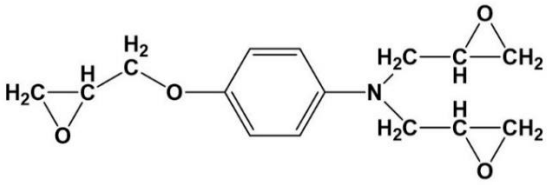

TGAP

Figure 1.14: Chemical structures of triglycidyl-p-aminophenol (TGAP) and tetraglycidyl-4,4'-diaminodiphenylmethane (TGDDM)

## 1.3.1. Curing of epoxy resin system

Due to the presence of highly strained three membered ring structure of epoxide group, epoxy resins are highly reactive and it can react with both nucleophilic and electrophilic reagents. Hence, a wide variety of organic compounds

having active hydrogen atoms can be used as curing agents. The chemical nature and the amount used of curing agents or hardeners play an important role in determining thermo-mechanical properties of the cured networks. A wide range of properties can be demonstrated and materials can be developed for extreme applications using the same resin, by judicious selection of curing agents. The time taken from the initial mixing of the resin and curing agents to the point when the viscosity of the mixture has become so high is called “pot life” of the system. This time is therefore the practical working life of the mixture, during which the material must be applied to the matter of concern. The most commonly used curing agents are aliphatic, primary and secondary amines, aromatic primary and secondary amines, polyamidoamines and acid anhydrides (Harper, 2000). Cure of epoxy resins normally occurs without the formation of any by-products. Proper selection of an epoxy resin, curing agent and its right formulation are essential to achieve desirable properties. Sometimes catalysts, accelerators, etc. are added to facilitate the curing process and fillers, diluents, plasticizers, and tougheners are added to improve the final properties of the products. A variety of techniques such as differential scanning calorimetry (DSC), thermal scanning rheometry, Raman spectroscopy and Fourier transform infrared spectroscopy (FTIR) have been used to monitor the curing reaction of epoxy resins.

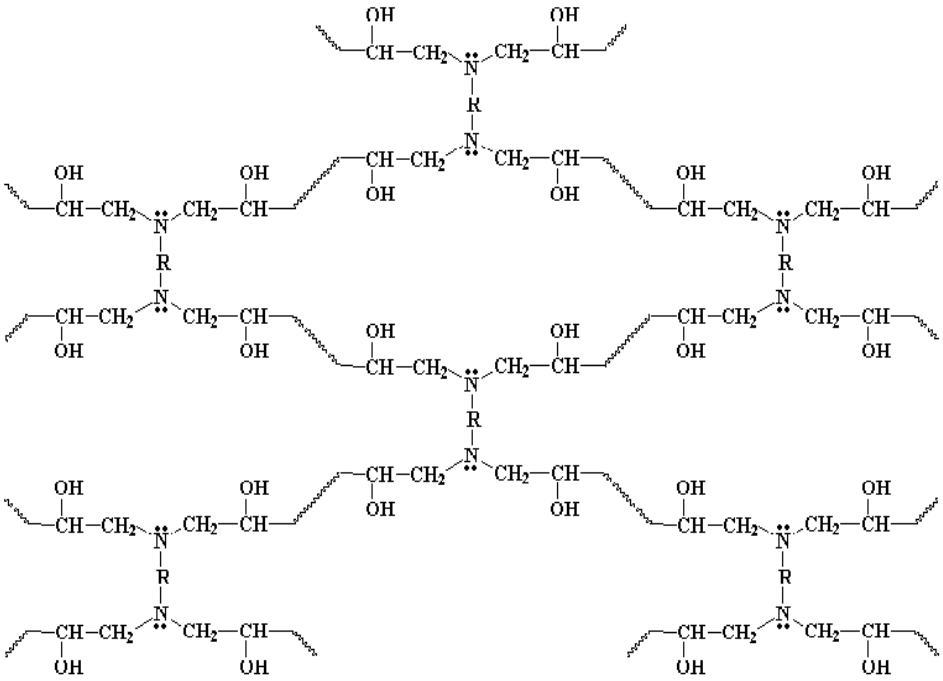

Figure 1.15: Cross-linked chemical structure of epoxy resin with an amine (Mark, 2013)

## 1.3.2. Curing agents used in epoxy systems

Two types of curing agent may also be distinguished, catalytic systems and polyfunctional cross-linking agents that link the epoxide resin molecules together. Some systems used may involve both the catalytic and cross-linking systems.

### 1.3.2.1. Catalytic curing agents

The catalytic curing agents are a group of compounds that promote epoxy reactions without being consumed in the process. These chemicals act as initiator for epoxy homopolymerization, as a supplemental curing agent with polyamines or polyamides or as accelerators along with anhydrides. Catalytic curing agents are having high temperature resistance capacity and are having long pot lives. Hence these are mainly used as accelerators for other curing agents. benzyldimethylamine

(BDMA), 2,4,6-tris(diniethylaminomethy1phenol) and borontrifluoride monoethylamine are examples for catalytic curing agents. Another rapidly growing method is photoinitiated cationic cure. The catalysts include aryldiazonium, diaryliodonium and onium salts of group Vl A elements.

### 1.3.2.2. Co-reactive cure

These curatives can act as a co-monomer in the polymerization process. Aliphatic and aromatic amines, acid anhydrides, isocyanates, mercaptanes and carboxylic acids etc. are examples of some of the widely used co-reactive curing agents.

*Primary and secondary amines*

Crosslinking of epoxide resins with amine curing agents occur either by a catalytic mechanism or by bridging across epoxy molecules. In general the primary and secondary amines act as reactive curing agents whilst the tertiary amines are catalytic. The functionality of an amine is determined from the number of amine hydrogen atoms present on the molecule. A primary amine group will react with two epoxy groups while a secondary amine will react with only one epoxy group. The loading of the curing agent in epoxy resin becomes optimal when the number of moles in epoxy groups is equal to that of active hydrogen. (Harper, 2000). Reactions of a primary amine with an oxirane group or an epoxy resin are shown in the following Figure 1.16.

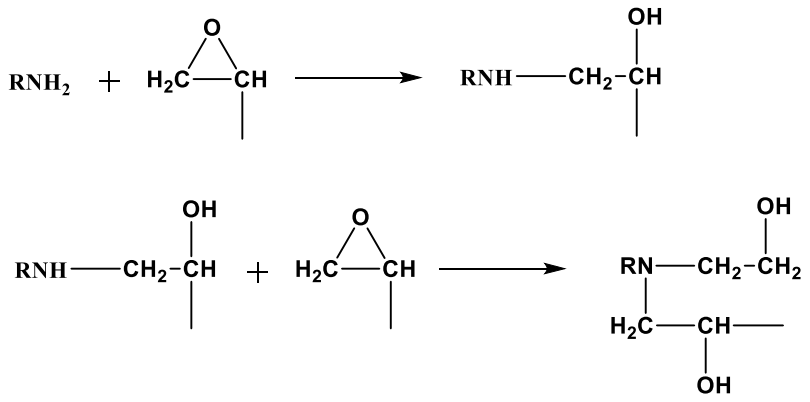

Figure 1.16: Mechanism of curing reaction between amine and epoxide

Reaction of primary amine with epoxy gives a secondary amine and secondary hydroxyl group. This secondary amine reacts with an epoxide ring to give a tertiary amine and two secondary hydroxyl groups. The tendency of the etherification reaction to take place depends on the temperature and the basicity of the diamine and increases with the initial epoxy/amine ratio. A tertiary amine group, which has no active hydrogen will act as a catalyst to accelerate epoxy reactions. The reactivity of the amine increases with its nucleophilic character: aliphatic > cycloaliphatic > aromatic.

*Aliphatic amines*

Aliphatic amine are highly reactive and it rapidly reacts with epoxy resin. It is a room-temperature curing agent and has a short pot life (usable time). Although both materials are widely used in small castings and in laminates because of their high reactivity, they have the disadvantage of high volatility, pungency and being skin sensitizers. It is thus seen that as a class the primarily aliphatic amines provide fast-curing hardeners for use at room temperatures. Some of the most common amines used are diethylenetetramine (DETA, functionality=5), triethyleneteramine (TETA, functionality=6), hexamethylenediamine (HMD, functionality=4) etc. They are highly reactive due to the unhindered polyfunctional nature and give cross-linked

networks due to the short chain distances between active sites. Molecular structures of some of the aliphatic amine hardeners are given in Figure 1.17.

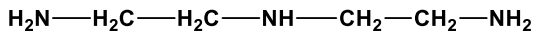

**Diethylenetriamine (DETA)**

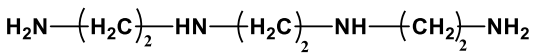

**Triethylenetetramine (TETA)**

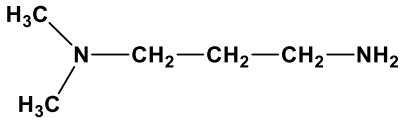

**Dimethylaminopropylamine**

Figure 1.17: Chemical structures of commonly used aliphatic amine curing agents

*Aromatic amine*

Because of the steric hindrance by the aromatic ring, basicity of aromatic amines are weaker than aliphatic amines. Therefore epoxy resins will cure slowly at room temperature when aromatic amines are used as curing agents. B**y** incorporating the rigid benzene ring structure into the cross-linked network, products are obtained with significantly higher heat distortion temperatures than are obtainable with the aliphatic amines. They have longer pot-lives and usually require elevated temperature cures. Aromatic amines are usually solid at room temperature. These hardeners are routinely melted at elevated temperatures and blended with warmed resins to improve solubility. Use of aromatic amines in epoxy provide excellent heat resistance, good mechanical properties, electrical properties and excellent chemical resistance to solvents (Mark, 2013). MDA or 4,4-diaminodiphenylmethane (DDM), 4,4-diaminodiphenyl sulfone (DDS), and MPDA are the principal commercial aromatic amines. DDS is the standard curing agent used with a multifunctional amine epoxy

for high performance aerospace and military composite application. In DDS, sulfone group being an electron withdrawing group decreased the basicity of the diamine. DDS was least reactive because the electron transfer from $–NH_2$ to $–SO_2$ is the easiest for para substitution. High *Tg* epoxy matrices can be made by using an aromatic curing agent such as DDM, DDS, DETDA. The advantage of DETDA over others is that it is a liquid and offers better processability. The *Tg* can be further increased by using a higher functionality resin. Thermally stable high performance resins are required for use in composite structures for aerospace applications. Molecular structures of some of the aromatic amine hardeners are given in Figure 1.18.

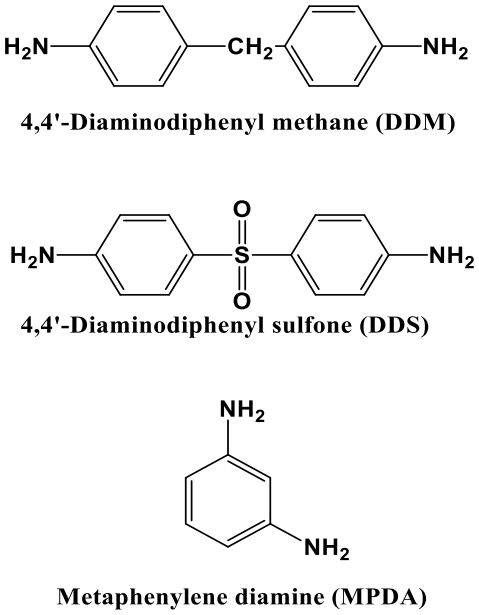


Figure 1.18: Chemical structures of commonly used aromatic amine curing agents

*Polyamides*

Polyamides are one of the largest volume epoxy curing agents used. They are prepared by the reaction of dimerized and trimerized vegetable-oil fatty acids with polyamines, and contain reactive primary and secondary amines in its molecules. They are dimerized or polymerized fatty acids that have been co-reacted with various

aliphatic amines such as ethylenediamine, DETA, TETA, tetraethylenepentamine (TEPA). Polyamide amine reacts with bisphenol-A-type epoxy resin to cure at or below normal temperature with moderate heat generation. They are user-friendly systems since tolerance on mix ratio is very broad and have a long pot life (Goodman, 1999). Due to the presence of high hydrocarbon moiety in its molecules, the cured product will be a highly plasticized rigid thermosetting polymer having high tensile, compression, and bending strengths and excellent shock resistance. Polyamides are extremely versatile curing agents. The polyamides react with the epoxide group through the amine functionality in the polyamide backbone. The unreacted amide NH groups in the backbone provide good intercoat adhesion and the fatty acid structures provide good moisture resistance and mechanical properties. They are inexpensive, less toxic to handle; give no blushing; exhibit readily workable pot lives; and cure under mild conditions. Polyamides are mainly used in coating and adhesive formulations, mostly in industrial maintenance and civil engineering applications. Disadvantages of polyamides include slower cure speeds and darker color than polyamine-cured epoxies. Polyamide-cured epoxies lose structural strength rapidly with increasing temperature. The high viscosity of polyamides limits their uses primarily to low solids coatings, which have been losing ground to higher solid coatings.

*Mercaptans*

The mercaptan group of curing agents include polysulfide and polymercaptan compounds which contain terminal thiols. Mercaptans also can be employed for cross-linking epoxies. When compared to the epoxy-amine reaction, epoxy mercaptan reaction is faster especially at low temperatures. The reaction is accelerated by primary and secondary amines (Figure 1.19).

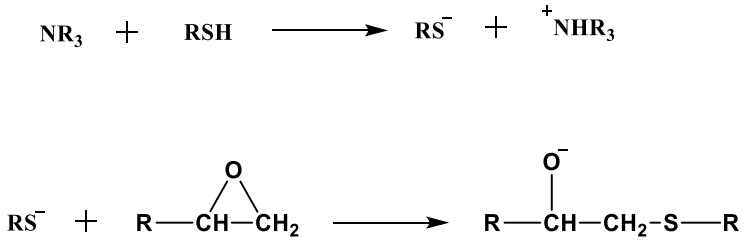

Figure 1.19: Mechanism of curing reaction between mercaptan and epoxide (Mark, 2013)

*Isocyanates*

Epoxy groups react with isocyanates or with hydroxyl groups to produce oxazolidone structures or a urethane linkage respectively, which are shown in Figure 1.20. The main advantages of using isocyanate curing agent are fast curing at low temperature, good flexibility and solvent resistance. Moisture sensitivity and toxicity limit its application to power coatings and maintenance coatings (Mark, 2013).

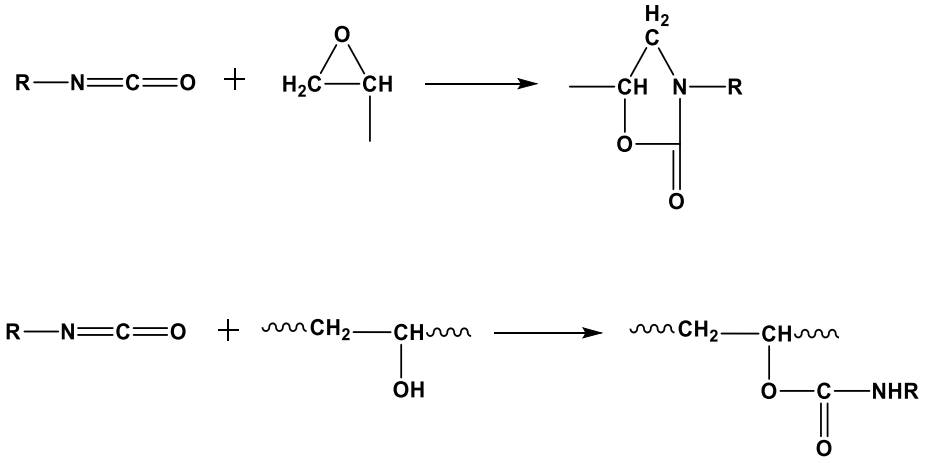

Figure 1.20: Mechanism of curing reaction between isocyanate and epoxide

*Carboxylic acids*

Carboxylic acids react with epoxy groups to form ß-hydroxy propyl ester, which, in turn, reacts with another carboxylic acid to yield a diester. The hydroxyl ester can also undergo polymerization by the reaction of secondary hydroxyl group with the epoxy. The possible reactions are summarized in Figure 1.21 (Mark, 2013).

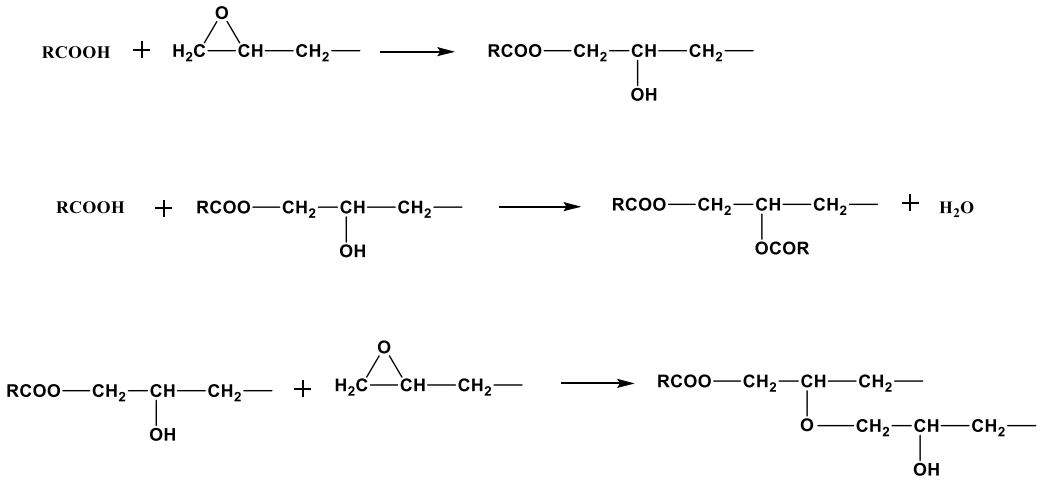

Figure 1.21: Mechanism of curing reaction between carboxylic acid and epoxide (Mark, 2013)

*Anhydrides*

Due to the low viscosity, long pot life, low exothermic heats of reaction, epoxy-anhydride systems can be used in large scale applications. Normally anhydrides are preferred to acids since the latter release more water on curing leading to foaming and dimensional instability of the product. There are large variety of structurally different anhydrides that can be used as epoxy curing agents. The most important commercial anhydrides are based on a cycloaliphatic structure. To improve the degree of cross-linking, anhydride hardeners with higher functionalities such as pyromellitic dianhydride and trimellitic anhydride have been used (Jyotishkumar, 2010).

The curing reaction of acid anhydride and epoxy monomer proceed via chain-wise polymerization. The initiation of reaction is done by a Lewis base. The mechanism of the reaction is given in Figure 1.22. In initiation step, a tertiary amine opens the ring of an epoxy monomer giving rise to a quaternary nitrogen cation and an active anion. The anion attacks the anhydride group to give carboxylate anion as active site. This ester is considered as the initiator of the polymerization reaction. This initiator attacks the epoxy ring to give alkoxide which again attacks an anhydride. Propagation occurs through the alternating copolymerisation of epoxy and acid anhydride groups (Ratna, 2009).

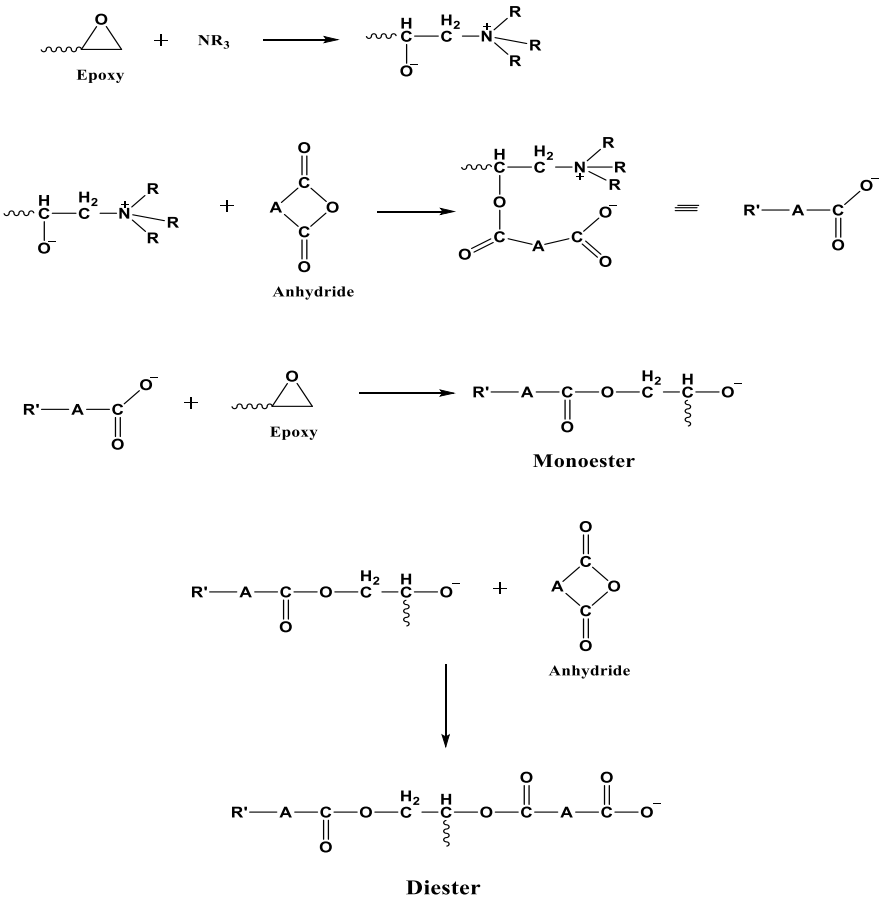


Figure 1.22: Mechanism of curing of epoxy using an anhydride (Ratna, 2009)

Epoxy resins cured with anhydrides have excellent properties with better outdoor weathering resistance. Some of the anhydride cured resins have high heat distortion temperature and excellent retention of strength at high temperature. These systems have low viscosity and long pot life. They exhibit good mechanical and electrical properties. Epoxy-anhydride systems have better thermal stabilities than similar amine-cured systems. Anhydrides are the principal curing agents for cycloaliphatic resins. Molecular structures of some of the anhydride hardeners are given in Figure 1.23.

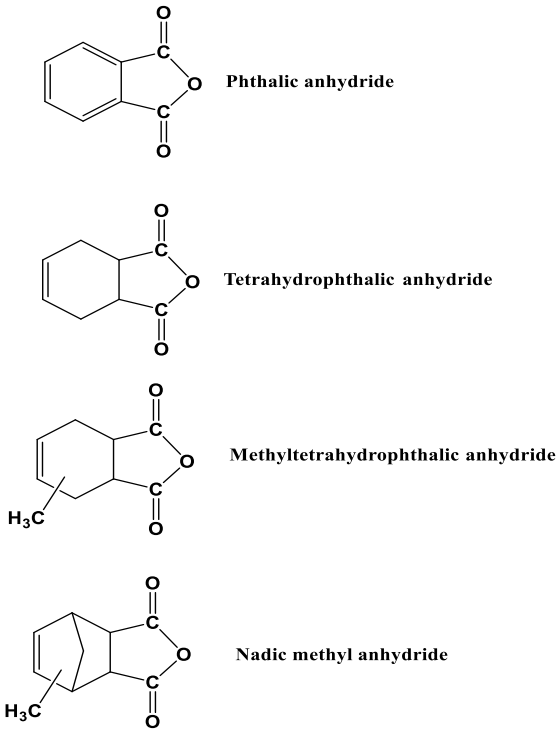


Figure 1.23: Chemical structures of commonly used anhydride curing agents

The number of hardening agents used commercially is very large and the final choice will depend on the relative importance of economics, ease of handling, pot life, cure rates, and the mechanical, chemical, thermal and electrical properties of the

cured products. Since these will differ from application to application, it is understandable that such a wide range of material is employed.

## 1.3.3. Toughening of epoxy resin

Epoxy polymers are considered to be the most important classes of thermosetting polymers. They are used extensively as high performance composite materials, due to their outstanding mechanical and thermal properties such as high modulus and tensile strength, low creep, high glass transition temperature, high thermal stability, and moisture resistance. However, like other thermoset resins, the crosslinking character of epoxies lead to highly undesirable property of brittleness with poor resistance to crack initiation and growth. The inherent brittle nature of epoxy resin necessitates toughening for many structural applications. To address this issue, resin formulators have developed technology that permits some thermosets to be toughened by the addition of a second phase. Different kinds of modifiers have been used to improve the toughness or ductility of cured epoxy resins; a) elastomer modifiers b) engineering thermoplastic modifiers c) inorganic particles d) core shell rubber particles e) hyperbranched polymers e) polyorganic siloxane modifiers and f) nanofillers.

### 1.3.3.1. Toughening of epoxy using liquid rubber

One of the most well-known methods is to incorporate various amounts of a reactive rubber into the epoxy matrix. When the curing reactions of epoxy and a liquid rubber proceed under controlled sets of conditions, phase separation occurs between the epoxy matrix and rubber particles. Preliminary studies on rubber modified epoxies reported only modest increases in fracture toughness; however, as the technology developed, more significant increases in toughness were obtained. The use of rubber modification of epoxy resins has been known and documented since 1960s. Traditional toughness modifiers such as carboxyl terminated butadiene

acrylonitrile copolymer rubbers (CTBN) have been widely used to improve toughness since the frontier work by McGary and Sultan (Sultan et al., 1971; Sultan and McGarry, 1973). Most of the studies reported in the literature have used CTBN for toughening. The role of matrix ductility on the toughenability and toughening mechanism of CTBN modified, DGEBA based epoxies is investigated by Pearson and coworkers (Pearson and Yee, 1989). Fracture toughness values for the neat epoxies are found to be almost independent of the monomer molecular weight of the epoxide resin used. However, the fracture toughness of the elastomer-modified epoxies is found to be very dependent upon the epoxide monomer molecular weight. Thomas et al. (2004) studied the potential of an anhydride system as a reactive curing for CTBN modified epoxy system. The incorporation of the elastomer of about 15 wt % showed better toughened properties. The fracture toughness is found to be increased from 0.7 for virgin epoxy to 1.9 $MPa.m^{1/2}$ for the modified one. Akbari et al. (2013) studied the toughening of dicyandiamide-cured DGEBA with liquid CTBN copolymer by varying the composition of CTBN from 0 to 25 phr using Monuron as accelerator. The maximum toughness was achieved at optimum concentration of 15 phr of CTBN (1.5 $MPa.m^{1/2}$) and it more or less remained constant for higher CTBN content. Chonkaew et al. (2012) investigated the tribological and mechanical properties of the CTBN-modified epoxy resins and to characterize the wear mechanisms. Impact resistance increased whereas the storage modulus and the hardness decreased when the CTBN rubber was introduced to the epoxy network. The coefficient of friction of the CTBN-modified epoxy was lower than that of the neat epoxy. Zhao et al. (2013) employed carboxylic nitrile-butadiene nano-rubber (NR) particles to improve the tensile strength and fracture toughness at 77 K of diglycidyl ether of bisphenol-F epoxy using diethyl toluene diamine as curing agent. It was shown that the cryogenic tensile strength and fracture toughness are simultaneously enhanced by the addition of NR. Zhou and Xu (2014) in their new method, epoxy composites with different grades of CTBN were cured with different curing agents, and their mechanical properties were characterized. It is found that no matter what grades of CTBN, also regardless of curing agents, the composites

prepared by the new method always exhibit much higher impact strength, yield strength and Young's modulus than the corresponding traditional composites

Another good elastomeric candidate for toughening epoxy is liquid amine terminated butadiene acrylonitrile copolymers (ATBN). Levita et al. (1985) studied the effects of temperature and cure on ATBN/epoxy blends and compared with those brought about by variations in rubber content. The fracture toughness changes by a factor of about 2.7 by varying the cure conditions and it has been shown that the addition of the rubber does not necessarily cause an increase in fracture resistance. Maximum toughness, measured by $K_{IC}$, is obtained in the 120-140 °C cure temperature range. Chikhi et al. (2002) used ATBN containing 16 % acrylonitrile content to improve the toughness of epoxy resin using polyaminoimidazoline as a curing agent. Upon addition of ATBN, the Izod impact strength increased drastically from 0.85 to 2.86 $kJ/m^2$ for notched specimen while $K_{IC}$ varies from 0.91 to 1.49 $MPa.m^{1/2}$ (1.5 fold increase by addition of 12.5 phr rubber). Latha et al. (1994) incorporated epoxidized hydroxy-terminated polybutadiene (EHTPB), to an epoxy resin cured at high temperature with 2,4,6- tris(N,N-dimethylaminomethyl)phenol resulted in significantly improved mechanical and bonding properties compared with the neat system. Maximum mechanical properties were obtained at a level of 10 parts EHTPB per 100 parts epoxy resin. In an attempt to toughen epoxy, Thomas et al. (2008) incorporated hydroxyl terminated polybutadiene (HTPB) liquid rubber and characterized their morphology and toughening mechanisms. Decrease in cross-link density was observed with the inclusion of elastomer. The elastomeric nature of the rubber caused reduction in tensile strength, but fracture toughness values increased and attained a maximum for 10 phr rubber inclusion. Figure 1.24 shows the SEM images of fracture surface of HTPB blends at various compositions

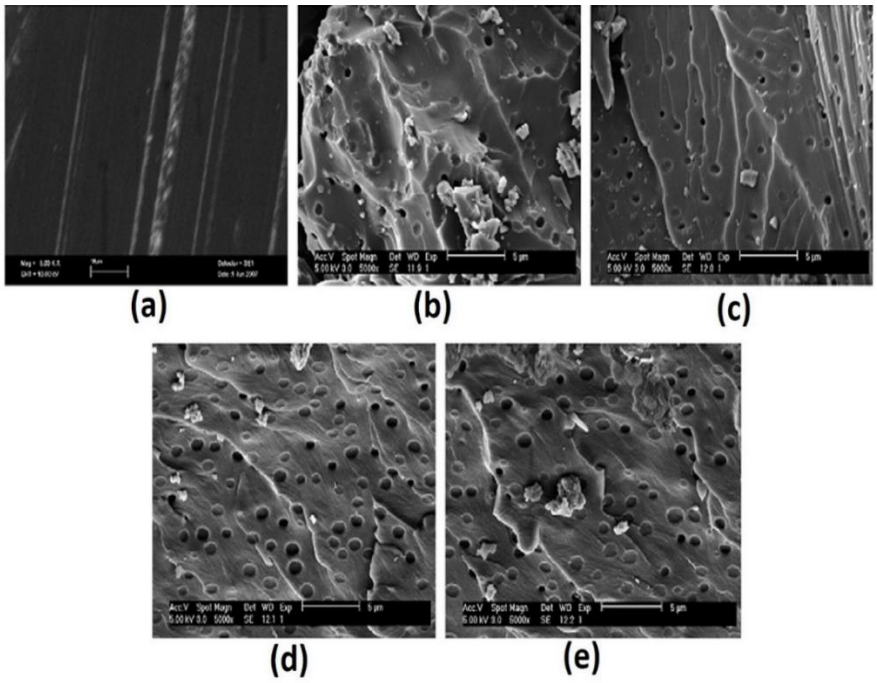


Figure 1.24: SEM micrographs of the fracture surface of (a) neat epoxy (b) 5 phr HTPB blend, (c) 10 phr HTPB blend, (d) 15 phr HTPB blend and (e) 20 phr HTPB blend (Thomas et al., 2008)

Chemorheology of curing as well as the phase separation behavior of carboxyl terminated poly(2-ethyl hexyl acylate) (CTPEHA) liquid-modified epoxy mixtures have been studied by Ratna (2001). The CTPEHA was incorporated into the epoxy matrix by a pre-react method. Addition of CTPEHA liquid rubber causes a delay in polymerization of the epoxy matrix. Optimum impact performance was achieved for the mixture containing 10 phr of CTPEHA and cured at 140 $^{o}$C, which contains both phase-separated rubber as well as dissolved rubber. The effect of synthesized epoxy terminated polybutadiene (ETPB) on the mechanical properties of DGEBA was investigated by Yahyaie et al. (2013). The maximum increase of toughness occurred at 7.5 wt% of ETPB content which was in accordance to the bulk properties of the samples.

Some of the important published data related to elastomeric toughening of epoxy are summarized in Table 1.1

Table 1.1: Toughness of epoxy systems modified by various types of elastomers

| **Author** | **Elastomeric toughener used** | **Composition at which maximum toughness achieved** | **% Improvement in toughness** |
|---|---|---|---|
| Chikhi et al. (2002) | ATBN | 12.5 phr | 60 |
| Chonkaew and Sombatsompop. (2012) | CTBN | 5 phr | 68 |
| Kunz et al . (1982) | CTBN<br>ATBN | 10 wt%<br>5 wt% | 180<br>153 |
| Akbari et al. (2013) | CTBN | 15 phr | 87.5 |
| Thomas et al. (2004) | CTBN | 15phr | 280 |
| Zhao et al. (2013) | CTBN nanorubber | 15 phr | 265 |
| Shukla and Srivastava. (2006) | CTPB | 15 wt% | 200 |
| Ratna. (2001) | CTPEHA | 10 phr | 60 |
| Latha et al. (1994) | EHTPB | 10 phr | 113 |
| Minfeng et al. (2008) | CRBN<br>HTBN | 5 wt% | 68<br>56 |
| Sankaran and Chanda. (1990) | HTBN | 3 wt% | 226 |
| Thomas et al. (2008) | HTPB | 10 wt% | 156 |

| | | | |
|---|---|---|---|
| Saadati et al. (2005) | HTPB | 20 wt% | 92 |
| Tripathi and Srivastava. (2008) | CTBN | 15 wt% | 280 |
| Chuayjuljit et al. (2006) | Epoxidied natural rubber | 5 phr | 48 |
| Mathew et al. (2010) | HLNR | 15 wt% | 68 |

### 1.3.3.2. Toughening of epoxy using engineering thermoplastics

The rubber-modified epoxies showed surprisingly higher fracture resistance, but, at the same time, significant reductions in modulus, yield strength and *Tg* were observed. In the early 1980s it was discovered that epoxy resins could be toughened by the addition of a rigid thermoplastic phase, thus the rigid-rigid polymer alloy concept was born (Bucknell and Partridge, 1983). The main advantage in using thermoplastics to toughen epoxy resins is that their incorporation will not result in significant decrease in desirable properties such as modulus and yield strengths as is generally the case when rubbers are used as toughening agents.

Bucknall and Gilbert (1989) prepared toughened epoxy resins by dissolving polyetherimide (PEI) in a TGDDM based resin with DDS as curing agent. Three-point bend tests show a linear increase in $K_{IC}$ with PEI content, from 0.5 MPa.m$^{1/2}$ in the parent resin to 1.42 MPa.m$^{1/2}$ at 25 phr of PEI. Kimoto and Mizutani (1997) modified bifunctional epoxy resins with polyimide in order to improve their toughness. The effects of polyimide content, curing conditions, curing agents, and types of polyimide on the fracture properties were examined. Although the fracture toughness, $K_{IC}$ increased in systems containing more than 20 wt% PEI, no improvement was noted for systems containing less than 14 wt% PEI. In 20 wt% PEI containing samples, the $K_{IC}$ values increased with an increase in the initial curing temperature. The $K_{IC}$ values of the DDM cured samples were larger than those of the

DDS cured samples for all the tested PEI contents. Min et al. (1993a) investigated the microstructure and fracture properties of DGEBA modified with hydroxyl-terminated polysulfone as a function of the molecular weight and the concentration of the modifier. The microstructure changed from a typical particulate structure to a phase-inverted co-continuous structure as the molecular weight and/or the concentration of the modifier increased. The fracture toughness increased with microstructural changes from the particulate structure to the phase-inverted structure. In another work, Min et al. (1993b) studied the microstructural effects on the total fracture toughness and the toughening mechanisms in polysulfone (PSF) modified resin systems under the same cure conditions. Although the microstructure changed significantly as the cure temperature increased, the fracture toughness of the modified resin remained essentially constant. Huang et al. (1997) prepared a miscible blend of PSF with uncured DGEBA. Miscibility between PSF and DGEBA is considered to be due mainly to entropy contribution. Both $K_{IC}$ and fracture energy $G_{IC}$ increased by about 20% with the addition of PSF to the system. Di Pasquale et al. (1997) studied the effect a reactive poly(ethersulfone) (PES) thermoplastic modifier on the fracture toughness properties an epoxy resin. They observed that the amino functionalization enables the thermoplastic to behave as a curing agent for the epoxy resin and it also promotes interfacial bonding between the thermoplastic and the thermoset which is postulated to be a major factor in improving the fracture toughness. Mimura et al. (2000) used PES to improve both the heat resistance and the toughness of cured epoxy resins. In the resin with a homogeneous phase morphology, the *Tg* of the resin containing 10 wt% PES increased about 208 $^{o}$C, and the value of the fracture toughness also increased by about 60% more than that of the unmodified resin which was attributed to the formation of the semi-interpenetrating polymer networks (semi-IPNs) composed of the epoxy network and linear PES. However, for the resin where phase separation occurred, a great increase in toughness was obtained only when the PES formed continuous phase morphology. The properties of DGEBA toughened with poly(ether sulfone ether ketone) (PESEK) and PES polymers were investigated by Francis et. al. (2006b). They observed homogeneity for the blends due to the

similarity in chemical structure of the modifiers and the cured epoxy resin. H-bonding interactions between the modifiers and epoxy resin also favored miscibility. Addition of PESEK or PES to epoxy resin increased the fracture toughness of epoxy resin. Wu et al. (2000) studied the effects of adding thermoplastic poly(phenyleneoxide) (PPO) in thermosetting epoxy systems. All the blends exhibit heterogeneity, and their morphology is found to be dependent on the PPO content. The tensile strength and modulus vary only within a narrow range in the blends. Blending-induced improvement in toughness is noticeably greater in the materials with high PPO content. Thermoplastic/epoxy blends of amine-cured epoxy polymer and a semi-crystalline thermoplastic: syndiotactic polystyrene (sPS) was prepared by Johnsen et al. (2005). Complete phase-separation of the initially soluble sPS from the epoxy occurred via 'reaction-induced phase-separation' (RIPS) or via 'crystallization-induced phase-separation' (CIPS), depending upon the thermal processing history employed (Figure 1.25). The addition of the sPS significantly increases the value of $G_{IC}$, though the toughness of the RIPS and CIPS blends differs markedly. Hydroxyl terminated poly (ether ether ketone) based on tert-butyl hydroquinone (PEEKTOH) was used by Francis et al. (2006a) to modify epoxy resin. The blends cured at various temperatures exhibited two phase morphology in which PEEKTOH domains were dispersed in the continuous epoxy matrix. The domain size was not much affected by changing the curing temperature. (He et al., 2013) used three different types of thermoplastics, PEI, polycarbonate (PC), and poly(butylene terephthalate) (PBT) to modify epoxy for cryogenic applications. The impact strength of the modified epoxies at cryogenic temperature increased with increasing thermoplastic content up to 1.5 wt% and then decreased for further loading (2.0 wt%). Both the PEI and PC were very effective in preventing micro-crack formation in the composites during thermal cycles at cryogenic condition due to their low CTE values and high impact strength. Jones et al. (2015) in their work, a thermoplastic resin poly(bisphenol A-co-epichlorohydrin) (PBAE) is blended with a high *Tg* epoxy matrix to serve as both a toughening additive and a healing agent in combination with an encapsulated solvent. The fracture toughness of the high *Tg* epoxy (EPON 828: DDS) is doubled by the

addition of 20 wt% PBAE alone and tripled by the addition of both microcapsules and the thermoplastic phase. Chaudhary et al. (2015) explored the potential of polystyrene microspheres as effective thermoplastic toughening agents for epoxy. Microspheres were prepared by suspension polymerization route and to aid their dispersion within the epoxy matrix, the surface of the microspheres were functionalized to generate pendant amino groups capable of forming covalent bonds with the epoxy resin. The amination of poly(styrene) (APS) led to improved dispersion of the rigid microspheres in the epoxy matrix, which was evident from higher impact strength and fracture energies ($G_{IC}$) as compared to its neat analogs. The Izod impact strength and $G_{IC}$ increased by 33% and 150%, respectively, on introduction of 3 wt% APS.

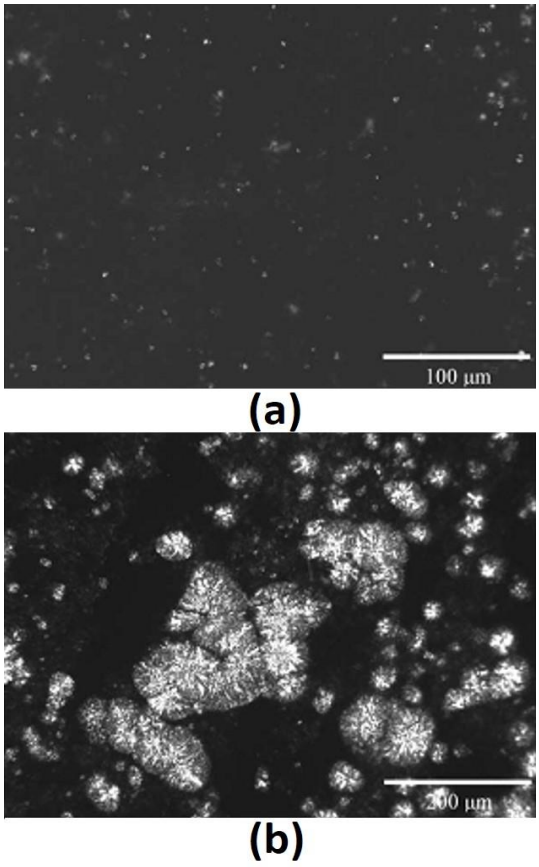


Figure 1.25: Transmission optical micrographs obtained using polarized light of the (a) RIPS and (b) CIPS blends containing 8 wt% sPS (Johnsen et al., 2005)

Table 1.2 presents a literature review in which engineering thermoplastics have been used as modifier to improve the toughness of epoxy.

Table 1.2: Toughness of epoxy systems modified by various types of thermoplastics

| **Author** | **Toughener used** | **Composition at which maximum toughness achieved** | **% improvement in toughness** |
|---|---|---|---|
| Bucknall and Gilbert. (1989) | PEI | 25 phr | 184 |
| Mimura et al. (2000) | PES | 10 wt% | 60 |
| Francis et al. (2006b) | PES<br>PESEK | 10 phr<br>15 phr | 41<br>35 |
| Di Pasquale et al. (1997) | Amine functionalied PES | 15 phr | 238 |
| Kimoto and Mizutani. (1997) | PEI | 20 phr | 67 |
| Johnsen et al. (2005) | Polystyrene | 8 wt% | 092 |
| Huang et al. (1997) | PSF | 7.5 wt% | 20 |
| Martinez et al. (2000) | PSF | 20 wt% | 169 |
| Yun et al. (2004) | PSF | 20 wt% | 220 |
| Min et al. (1993b) | PSF | 20 wt% | 300 |
| Chaudhary et al. (2015) | APS | 3 wt% | 33 |

### 1.3.3.3. Toughening of epoxy using particulate fillers

Apart from liquid rubbers and high performance thermoplastics, mineral fillers are also used to toughen thermosets. Different types of thermoplastics which have been used to modify epoxy resin include alumina, glass beads etc. N. Amdouni et al. (1992) studied the effect of toughness of epoxy by the introduction of glass beads with different volume fractions. The influence of surface treatment was also studied by comparing untreated, silane-treated glass beads, and beads coated with different thicknesses of an elastomeric adduct. An improvement in Charpy impact strength was observed by the addition of glass beads into epoxy. They found that the coating of glass beads with a thin layer of a crosslinked elastomer slightly affects the modulus of the composites and greatly enhances the fracture properties in comparison with untreated glass beads in composites. Kawaguchi and Pearson (2003) used three different types of glass reinforcements, large glass spheres, small glass spheres, and glass fibers, with different surface treatments and the effect of different surface treatments and moisture exposure on fracture toughness was carefully investigated (Figure 1.26). Under these conditions, fracture toughness was found to increase with increasing filler content and was not affected by changes in particle– matrix adhesion. McGrath et al. (2008) used alumina of different article size, size distribution, and shape to prepare alumina filled epoxy composites for its application in electronic packaging and dental restoratives. For all systems the fracture toughness of the composites increases with increasing filler loading. No trend with fracture toughness and particle size was observed in either resin systems. In addition, no impact of varying the filler shape was observed.

Table 1.3 presents a literature review in which inorganic particulate fillers have been used as modifiers to improve the toughness of epoxy.

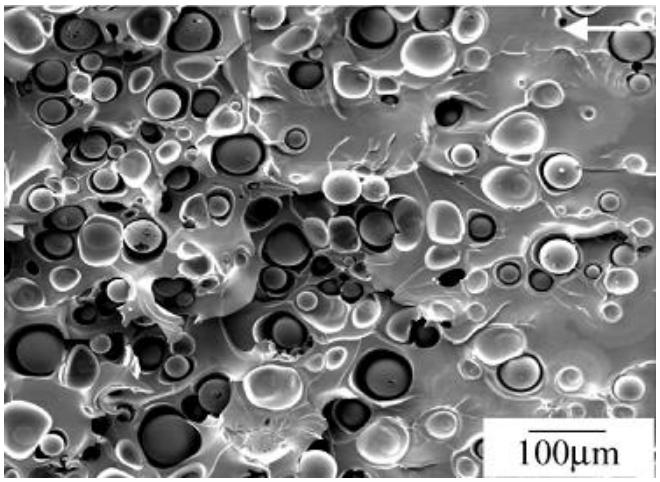


Figure 1.26: SEM image of the process zone on the fracture surfaces of glass sphere filled epoxy that shows significant particle-matrix debonding as well as increased matrix plasticity (Kawaguchi and Pearson, 2003)

Table 1.3: Toughness of epoxy systems modified by various types of particulate fillers

| **Author** | **Toughener used** | **Composition at which maximum toughness achieved** | **% improvement in toughness** |
|---|---|---|---|
| McGrath et al. (2008) | alumina | 50 wt% | 100 |
| Lee and Kim. (1997) | Glass beads | 30 wt% | 137 |
| Kawaguchi and Pearson. (2003) | Glass sphere<br>Glass fiber | 10 vol%<br>20 vol% | 178<br>200 |
| Amdouni et al. (1992) | Glass bead | 30 vol% | 25 |

### 1.3.3.4. Toughening of epoxy using core shell rubber particles

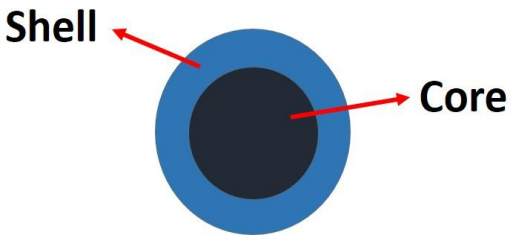


Figure 1.27: Schematic diagram showing a core shell rubber particle

An alternative route to increase the toughness of epoxy polymers is to use core-shell rubber (CSR) particles. These particles comprise of a soft rubbery core within a harder shell (Figure 1.27). The particles are typically formed by emulsion polymerization, and then dispersed in the epoxy resin. Hence, it is readily possible to produce particles with a controlled particle size, unlike with phase-separating rubber. Qian et al. (1995) employed poly(butadiene-co-styrene) [P(BS)] core-poly(methy1 methacrylate) (PMMA) shell particles to toughen epoxy polymer. The fracture toughness of the epoxies was successfully improved by the custom-made core-shell particles as evidenced by the increase of value from 0.78 to 2.69 $MPa.m^{1/2}$. The effects of particle size of the core-shell rubber on the fracture toughness of rubber-modified epoxies were investigated by Kim et al. (1996). Various sizes of core-shell rubber particles, from 0.16 to 1.2 μm in diameter, were synthesized by seeded emulsion polymerization. Fracture toughness increased as the particle size of core-shell rubber decreased from 1.2 to 0.4 μm. The fracture and toughening mechanisms of the clay/epoxy nanocomposite with and without the addition of CSR particles were investigated by Gam et al. (2003). The addition of both clay and CSR improved not only fracture toughness but also modulus. Giannakopoulos et al. (2011) modified epoxy resin by the addition of preformed CSR particles which were approximately 100 or 300 nm in diameter. The fracture energy increased from 77 $J/m^2$ for the unmodified epoxy to 840 $J/m^2$ for the epoxy with 15 wt% of 100-nm diameter CSR

particles. Chen et al. (2013) modified an epoxy resin cured using an anhydride hardener by the addition of pre-formed polysiloxane core-shell rubber (S-CSR) particles with a mean diameter of 0.18 μm. The addition of the S-CSR particles reduced the Young's modulus and tensile strength of the epoxy polymer, but at 20 C the fracture energy, $G_{IC}$, increased from 117 J/m$^2$ for the unmodified epoxy to 947 J/m$^2$ when 20 wt% of the S-CSR particles were incorporated. Quan and Ivankovic (2015) investigated the influence of nano-sized CSR particles on the mechanical properties, thermal properties and fracture toughness of epoxy polymer by using wide range of CSR particle content, volume fraction up to 38 vol%. An optimum CSR particles content, 30 vol% was found to exist, below which the fracture energy increased from 343 J/m$^2$ of neat matrix upto 2671 J/m$^2$, beyond which fracture energy $G_{IC}$ did not improve and even declined. The main toughening mechanism of CSR particles toughened epoxy adhesive is debonding of CSR particles from matrix, followed by large scale plastic void growth, which is accompanied by shear band yielding. Thitsartarn et al. (2015) achieved simultaneous enhancement of strength and toughness of epoxy using POSS-CSR nanoparticles. With the developed filler, with only 1 wt% of the filler in the epoxy matrix, the impact resistance and the $K_{IC}$ of the composite respectively increases by ~80%, and ~20%, as compared to the neat epoxy resin.

Table 1.4 presents a literature review in which core shell rubber particles have been used as modifier to improve the toughness of epoxy.

Table 1.4: Toughness of epoxy systems modified by various types of core shell rubber particles

| **Author** | **Core shell toughener used** | **Composition at which maximum toughness achieved** | **% Improvement in toughness** |
|---|---|---|---|
| Nguyen and Berg. (2008) | Core-Shell Dendrimer | 10 wt% | 107 |
| Chen et al. (2013) | Polysiloxane CSR | 20 wt% | 109 |
| Becu et al. (1997) | poly(butadiene-*co*-styrene) core/carboxy-functionalized poly(methyl methacrylate-*co*-styrene) shell | 24 wt% | 113 |
| Choi et al. (2004) | Styrene-butadiene copolymer CSR | 8 wt% | 50 |
| Gam et al. (2003) | CSR | 5.4 wt% | 172 |
| Kim et al. (1996) | Butyl acrylate core methyl methacrylate shell CSR particles | 10 phr | 277 |
| Lin and Shieh. (1998) | PBS core PMMA shell | 10 vol% | 245 |
| Sue et al. (1996) | Rigid Core Shell Particle (RCSP) | 7.5 wt% | 245 |
| Quan and | CSR | 22 wt% | 125 |

| | | | |
|---|---|---|---|
| Ivankovic. (2015) | | | |
| Thitsartarn et al. (2015) | POSS-CSR | 2 wt% | 30 |
| Giannakopoulos et al. (2011) | CSR particle | 9 wt% | 157 |

### 1.3.3.5. Toughening of epoxy using polysiloxanes

Recently, the use of liquid functional polysiloxanes as new modifiers for toughening of epoxy resins is triggering more and more interest. Functionally terminated siloxanes belong to the elastomeric materials. The morphology and fracture toughness of epoxy resins modified with amino-terminated polydimethylsiloxane (ATPDMS), differing in their molecular weight, and the degree of the preliminary reaction in the melt state were investigated by Lee and Kim (1997). Liu et al. (2010) synthesized a novel highly epoxidized polysiloxanes (HEPSO) to modify the DGEBA. The addition of 4 phr HEPSO resulted in the highest increase in tensile strength, impact strength and fracture toughness. The morphologies of the fracture surfaces of the cured epoxy resins show that the miscibility of polysiloxanes with epoxy resin increased with the increase of the epoxide group in HEPSO. Ma et al. (2010) used a novel dendritic polysiloxane (DPSO) bearing high epoxide groups to modify epoxy resin. An addition of 3 phr DPSO resulted in the 70.4% increase in the impact strength compared to that for the unmodified epoxy, and the glass transition temperature and thermal stability were also improved at relatively low addition levels. In another work, Ma et al. (2011) synthesized a novel polysiloxane ($G_xD_y$) containing a large number of epoxide groups and flexible segments by hydrolysis and condensation of 3-glycidoxypropyl trimethoxysilane (GPTMS) and dimethyldiethoxylsilane (DMDES) to toughen the 3,4 epoxycyclohexylmethyl-3,4 epoxycyclohexanecarboxylate. The addition of 10 phr $G_xD_y$ resulted in greatly improved toughness, but maintained the transmittance of

the epoxy resin and $G_xD_y$ can be used as a toughening agent for light emitting diode (LED)-packaging epoxy resins.

Table 1.5 presents a literature review in which polysiloxanes have been used as modifier to improve the toughness of epoxy.

Table 1.5: Toughness of epoxy systems modified by various types of polysiloxanes

| **Author** | **Toughener used** | **Composition at which maximum toughness achieved** | **% improvement in toughness** |
|---|---|---|---|
| Lee and Kim. (1997) | polysiloxane | 10 phr | 120 |
| Liu et al. (2010) | Highly epoxidised polysiloxane | 4 wt% | 126 |
| Ma et al. (2010) | Dendritic polysiloxane | 3 phr | 70 |
| Ma et al. (2011) | polysiloxane | 10 wt% | 29 |

### 1.3.3.6. Toughening of epoxy using hyperbranched polymers

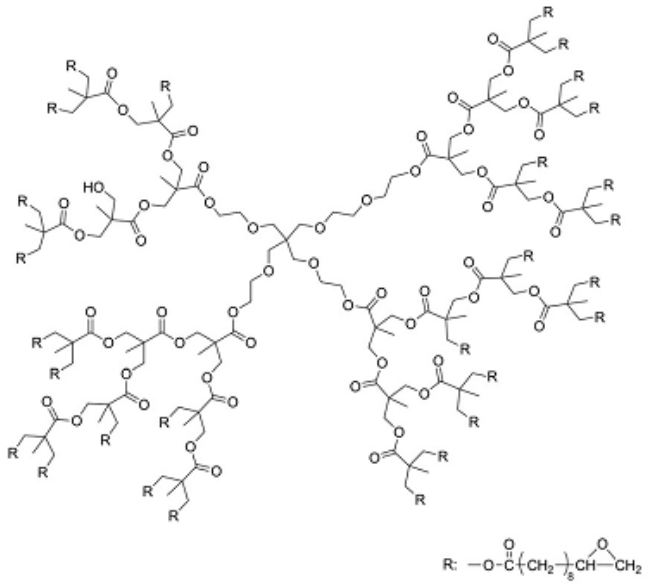

Figure 1.28: Idealized chemical structure of the hyperbranched polymer (Foix et al., 2012)

Dendritic hyperbranched polymers used by Mezzenga et al. (2001) was able to double the interlaminar fracture resistance of epoxy-based composites and to reduce the internal stress level by as much as 80% with only 10 phr of modifier. These property improvements were obtained without affecting the viscosity, processability, nor the glass transition temperature of the epoxy resin. Ratna et al. (2003) prepared epoxy/clay nanocomposites using DGEBA and its blend with an epoxy functionalized hyperbranched polymer (HBP). Both the strengthening and toughening of epoxy resin was achieved by incorporating HBP and clay. Strengthening effect of clay is slightly reduced by the presence of HBP. DeCarli et al. (2005) used another epoxy terminated HBP to toughen a carbon fiber reinforced epoxy anhydride composite. The increases in the mode I and II interlaminar fracture toughness of the composite material were found to be 224% and 265%, respectively, at a loading of 10 wt% of epoxy terminated HBP additive. Jin and Park (2006) prepared an amine-terminated hyperbranched polyimide (HBPI) by the condensation

polymerization of a commercially available triamine monomer with a dianhydride monomer. The *Tg* of the DGEBA/HBPI blends increased with the addition of HBPI. The $K_{IC}$ value and impact strength were 2.5 and 2 times the values of the neat epoxy resins with only 4 wt % HBPI. Foix et al. (2012) synthesized epoxy-functionalized HBP and used as toughening additive in epoxy based UV-curable formulations (Figure 1.28). The thermomechanical properties are only slightly affected by the presence of the HBP. Dhevi et al. (2013) attempted to improve the inherent brittleness in DGEBA using HBPs as toughening agents. Four different hyperbranched polyesters with increasing generations were synthesized by reacting calculated amount of dipentaerythritol (used as a core) and dimethylol propionic acid ($AB_2$ type monomer) through pseudo one-step melt polycondensation method. Further, toughening of the epoxy resin is carried out by reacting each generation of the HBP with epoxy using hexamethylene diisocyanate as an intermediate linkage resulting in the formation of HBP-Polyurethane/Epoxy-g-Interpenetrating Polymer Networks. It was found that the HBP modified epoxy samples exhibited higher toughness in comparison to that of neat epoxy and linear polyol based epoxy samples. Miao et al. (2015) developed a novel epoxide-terminated hyperbranched polyether sulfone (EHBPES) toughener for epoxy using $A_2 + B_3$ approach, which can form non-phase-separated network after cure. Effects of loading and molecular weight on mechanical and thermal properties of cured hybrids were studied. The general trend is that when EHBPES loading increases, the impact, elongation at break, and tensile strength all go through maxima at ca. 5 wt% loading. However, at higher loadings (10 wt%), mechanical performance decreases due to incomplete cure. Luo et al. (2013) synthesized a new epoxy-ended hyperbranched polyether (HBPEE) with aromatic skeletons through one-step proton transfer polymerization. Compared with the neat DGEBA, the hybrid curing systems showed excellent balanced mechanical properties at 5 wt% HBPEE loading. These great improvements were attributed to the increased cross-linking density, rigid skeletons, and the molecule-scale cavities brought by the reactive HBPEE. Tang et al. (2014) synthesized a hyperbranched polyurethane (HBPU), with low-molecular-weight polyethylene glycol space segments between the

branching points, by a pseudo one-pot procedure. Their impact fracture surfaces were investigated by scanning electron microscopy, and the results indicated that no phase separation occurred in the DGEBA/anhydride system after the introduction of HBPU, which was confirmed by dynamic mechanical analysis and thermogravimetric analysis. After addition of 10 wt% HBPU, the toughness of the modified thermosets was found to be significantly improved without sacrificing their processability and thermal and mechanical properties to a large extent. Li et al. (2015a) prepared an amino-terminated hyperbranched polymer ($HBPNH_2$) from diethylenetriamine (DETA) and methyl acrylate (MA) by melt polycondensation through $AB_3$ and $AB_2$ route and showed that HBP-$NH_2$ can enhance the toughness of epoxy cured system near 61 % than the neat DGEBA cured thermosets. Li et al. (2015b) in another work, synthesized a novel amino-terminated hyperbranched polymer (ATHBP) through the end-capping reaction between hyperbranched polymer with hydroxyl group (HBPH) and diethylenetriamine. The introduction of ATHBP improved the impact strength without sacrificing the *Tg* of epoxy resin. FESEM analysis indicated that the toughening mechanism may be attributed to plastic deformation mechanism.

Table 1.6 presents a literature review in which polysiloxanes have been used as modifier to improve the toughness of epoxy.

Table 1.6: Toughness of epoxy systems modified by various types of hyperbranched polymers

| **Author** | **Toughener used** | **Composition at which maximum toughness achieved** | **% improvement in toughness** |
|---|---|---|---|
| Jin and Park. (2006) | Amine terminated hyperbranched polyimide | 4 w% | 150 |

| | | | |
|---|---|---|---|
| DeCarli et al. (2005) | Epoxy terminated hyperbranched polyester | 10 wt% | 224 |
| Ratna et al. (2003) | Epoxy functionalized hyperbranched polymer | 15 wt% | 215 |
| Miao et al. (2015) | Epoxy terminated hyperbranched polyether sulfone | 5 wt% | 88 |
| Luo et al. (2013) | Epoxy ended hyperbranched polyether | 5 wt% | 100 |
| Tang et al. (2014) | Hyperbranched polyurethane | 10 wt% | 128 |
| Foix et al. (2012) | Epoxy functionalized hyperbranched polyester | 30 phr | 78 |
| Li et al. (2015a) | Amine terminated hyperbranched polymer | 30 wt% | 60 |
| Li et al. (2015b) | Amine terminated hyperbranched polymer | 25 wt% | 61 |

### 1.3.3.7. Toughening of epoxy using block copolymers

Block copolymers present a novel approach to the problem of toughening epoxy resins. During the last decade or so, there have been numerous reports of novel morphologies in block copolymers. Höfflin et al. (2000) used thermoplastic elastomers based on polyetheresters with polyoxytetramethylene soft segments and poly(hexamethyleneterephthalate) hard segments to toughen anhydride-cured epoxy resins. Epoxy resins blended with 10 wt% of the polyetherester exhibited an increase in toughness by 50–150%, while strength and modulus decreased by 20% or less. Dean et al. (2001) blended poly(ethylene oxide)– poly(ethylene-*alt*-propylene) (PEO–PEP) diblock copolymers containing 50 or 26 vol% PEO with various amounts of BPA348, a commercial epoxy resin. These block copolymer-modified BPA348/MDA resins exhibited increased fracture toughness without a large reduction in *T*g at low (5 wt%) block copolymer concentrations. This improvement is attributed to debonding of the vesicles followed by localized matrix deformation, crack deflection, and possibly crack-wake ligamentary bridging by the large vesicles. Dean et al. (2003) used a wide variety of block copolymers which can self-assemble into vesicles, spherical micelles, and wormlike micelles, in epoxy to improve fracture toughness. Spherical micelles and wormlike micelles are less effective than vesicles in improving $G_{IC}$ of this amine-cured bisphenol-A epoxy. Gerard et al. (2007) used different acrylic block copolymers for the toughening of a lightly crosslinked epoxy. Depending on the block composition and on the ratio of the blocks, micro interconnected filament-like or wormlike and spherical micelles are obtained. Liu et al. (2009) studied the fracture characteristics of PEP-PEO block copolymer nanoparticle (BCP)-modified epoxies with variations in matrix crosslink density. They found that toughenability of the epoxy resin has a strong dependence on its crosslink density. The lower the crosslink density is, the more capable the host resin can be toughened by the incorporation of the elastomeric phase. In another work, Liu et al. (2010b) employed an amphiphilic PEP-PEO block copolymer (BCP) to modify a bisphenol A-based epoxy resin formulation which is self-assembled into a wormlike

micelle structure (Figure 1.29). Incorporation of 5 wt% BCP wormlike micelles gives a 100% improvement in $K_{IC}$, which is more effective than that of the spherical micelle-modified epoxy. Li et al. (2014) employed two diblock copolymers, PEP–PEO and poly(1,2-butadiene)-bpoly(2-vinyl pyridine) (PB–P2VP) as modifiers for an amine-cured DGEBA epoxy resin, and their effect on the mechanical properties of bulk thermosets and 15 μ thick coatings was investigated. In the bulk epoxy thermosets, both block copolymers self-assembled into spherical micelles and effectively improved the fracture toughness. In coatings, spherical micelles were also formed and distributed throughout the coating with some segregation at the coating/substrate interface. Redline et al. (2014) modified epoxy thermosets with 0.6 wt% of PEP-PEO or polystyrene-b-poly(ethylene oxide) (PS-PEO) diblock copolymers. Both polymers self-assembled into spherical micelles with PEO coronas and either a rubbery PEP or glassy PS core. As block copolymer was added up to 2 wt% loading, both block copolymers provided similar improvements in $G_{IC}$. However, at 2 wt% and above, the epoxies containing PEP-PEO diblock copolymers outperform those containing PS-PEO by approximately a factor of two. Naguib et al. (2015) in their work, prepared reactive and non-reactive diblock copolymers based on PEO and a poly(glycidyl methacrylate) (PGMA, reactive) or polystyrene (non-reactive) block, respectively, via ATRP and those are incorporated into a cycloaliphatic epoxy matrix. The measurement of the critical stress factor, $K_{IC}$, showed that the fracture toughness of the composite materials is enhanced by inclusion of the non-reactive block copolymer. In contrary, the reactive block copolymer has negative effect on the fracture toughness especially in case of short PEO block. Boumbimba et al. (2015) investigated the effect of nanostructured tri-block acrylic copolymers on impact resistance in glass fibres epoxy laminate composites. The low velocity impact results indicate that the addition of modified tri-block copolymer lead to the improved impact resistance and an increase in absorbed energy, especially at high impact energy level. SEM observations, performed on ion polished samples, revealed the presence of micro-cracks for both composites. George et al. (2013) investigated the effect of addition of poly (styrene-block-butadiene-

block-styrene) (SBS) triblock copolymers on the morphology and mechanical properties of epoxy matrix cross-linked by DDM. They observed that the epoxidation reaction in SBS influences the compatibility of block copolymer in epoxy matrix and also in the toughness of epoxy matrix. Spherical micelle-like morphologies are obtained when the epoxidation degree is 47 mol%. The spherical micelle-like morphology changes to elongated vesicle-like domains in the blends with 39 mol% of epoxidation. The fracture toughness of the epoxy thermoset was significantly improved by the inclusion of a small amount of SBS triblock copolymer.

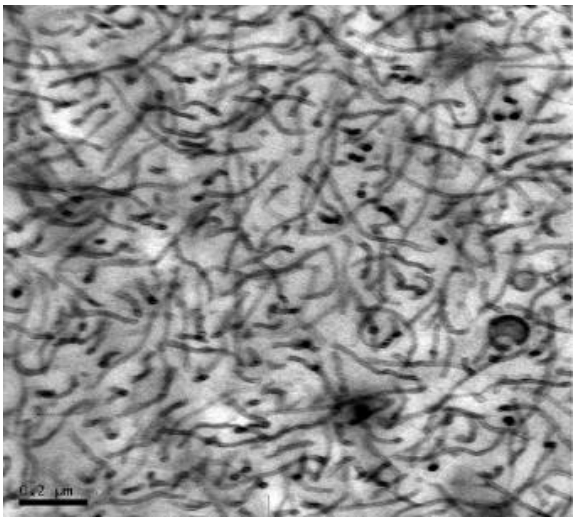

Figure 1.29: TEM micrographs of BCP wormlike micelle-modified epoxy (Liu et al., 2010)

Table 1.7 presents a literature review in which block copolymers have been used as modifier to improve the toughness of epoxy.

Table 1.7: Toughness of epoxy systems modified by various types of block copolymers

| **Author** | **Block co-polymer toughener used** | **Composition at which max toughness achieved** | **% Improvement in toughness** |
|---|---|---|---|
| Liu et al., (2010) | PEP-PEO BCP | 5 wt% | 144 |
| Larrañaga et al., (2007) | PEO-PPO-PEO | 10 wt% | 56 |
| Höfflin et al., (2000) | Polyetherester | 10 wt% | 150 |
| Dean et al., (2001) | PEO-PEP | 2.5 wt% | 177 |
| Dean et al., (2003) | PEO-PB | 5 wt% | 350 |
| Gerard et al., (2007) | MAM<br>MAM-D1<br>MAM-D2 | 10 wt% | 290<br>104<br>203 |
| Liu et al., (2009) | PEP-PEO | 5 wt% | 100 |
| Wu, Thio and Bates, (2005) | Aramid Silicone Block Copolymer | 4.2 wt% | 200 |
| Ritzenthaler et al., (2003) | SBM Triblock Copolymer | 10 wt% | 208 |
| Thio et al., (2006) | PHO-PEO | 5 wt% | 260 |
| Thompson et al., (2009) | PEO-PEP | 5 wt% | 200 |
| Wu et al., (2005) | PBO-PEO Diblock Copolymer | 5 wt% | 294 |
| Li et al., (2014) | PEP-PEO<br>PB-P2VP | 5 wt%<br>5 wt% | 94<br>112 |
| Redline et al., (2014) | PEP-PEO<br>PS-PEO | 4 wt%<br>2 wt% | 80<br>45 |

### 1.3.3.8. Toughening of epoxy using liquid crystalline polymers

Crystalline thermoplastics have also been utilized in modifying resin. Carfagna et al. (1992) observed that toughened epoxy resins can be achieved by blending a low percentage of liquid crystalline polymer (LCP) with the thermoset. The processing technique consisted of the spinning of blends of a thermoplastic (Ardel) with the LCP (PET/PHBGO) .The bundled filaments were subsequently dissolved in the uncured epoxy resin. After curing, the LCP phase separates from the matrix in the form of microfibers with a very high aspect ratio, which act as crack stoppers and improve fracture toughness of the material. Zhang et al. (1999) synthesized a series of novel reactive toughening agents (LCEUPPG) containing both a flexible spacer and rigid liquid crystalline unit to modify the bisphenol epoxy resin/dicyandiamide curing system. Compared with the unmodified system, LCEUPPG have enhanced the impact strength 3–7 times, and maintained high dynamic modulus and good thermal properties. Son et al. (2012) used a novel amino end-capped aromatic liquid crystalline copoly(ester amide) to improve the thermal and mechanical properties of DGEBA cured DDS. Upon addition of 10 phr of LCP, the impact strength of the modified epoxy was dramatically increased from 35.8 J/m to 51.8 J/m, which is an approximately 30% improvement compared to the un-modified system (Figure 1.30).

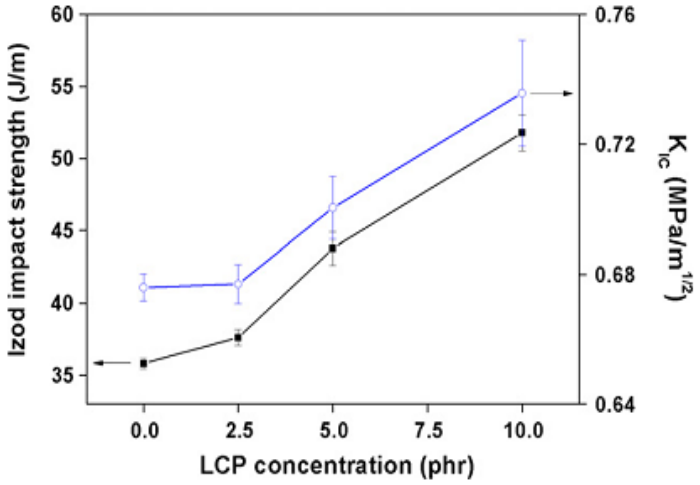


Figure 1.30: The Izod impact and fracture toughness of various LCP/DGEBA/DDS blends (Son et al., 2012)

Table 1.8 presents a literature review in which liquid crystalline polymers have been used as modifier to improve the toughness of epoxy.

Table 1.8: Toughness of epoxy systems modified by various types of liquid crystal polymers

| **Author** | **Toughener used** | **Composition at which maximum toughness achieved** | **% improvement in toughness** |
|---|---|---|---|
| Son et al. (2012) | LCP (liquid crystalline copoly(ester amide) | 10 phr | 39 |
| Zhang et al. (1999) | LCP | 20 wt% | 590 |

### 1.3.3.9. Toughening of epoxy using nanofillers

Since the advent of nanotechnology, nano-fillers, such as nanoparticles and carbon nanotubes, have been widely used in composites as reinforcements. Nano-reinforcements, as opposed to traditional reinforcements, have been shown to improve mechanical and thermal properties at much lower filler loadings. Due to their extremely high specific surface area, the nanoparticles exhibit high interfacial interactions between the particles and the polymer matrix that primarily leads towards the achievement of novel properties in materials (Yang et al., 2009). Thus, research on nanocomposite mechanical performance has continuously attracted great attention in both the scientific and industrial communities. Recently, some researchers showed that the incorporation of nano fillers in the epoxy matrix can improve the fracture toughness of the resultant composites. Adding reinforcements such as nanosilica, nano $TiO_2$, nano $CaCO_3$, nano clay, carbon nanotubes and graphene has attracted considerable attention as a means to enhance the toughening of epoxy resins. Ragosta et al. (2005) reported the preparation of a new nanocomposite system based on TGDDM/DDS resin and an isopropanol emulsion of silica nanoparticles. The addition of silica nanoparticles up to 10 wt% brings about a considerable increase in fracture toughness and an increase in critical crack length for the onset of brittle fracture. BB Johnsen and coworkers (Johnsen et al., 2007) introduced the silica nanoparticles to epoxy via a sole gel technique which gave a very well-dispersed phase of nanosilica particles which were about 20 nm in diameter. The measured modulus was compared to theoretical models, and good agreement was found. The fracture energy increased from 100 $J/m^2$ for the unmodified epoxy polymer to 460 $J/m^2$ for the epoxy polymer with 13 vol% of nanosilica. Blackman et al. (2007) also showed that the introduction of nano-silica particles into an epoxy polymer has increased both the fracture toughness, $K_{IC}$, and the cyclic-fatigue behaviour of the epoxy polymer. Shi et al.(2006) in their work observed that the nanocomposites epoxy resin/$CaCO_3$ nanocomposites prepared by in situ and inclusion polymerization showed a better nanoparticle dispersion compared to the nanocomposite prepared by

solution blending. These composites showed good improvement in toughness because of better dispersion. Jin and Park (2008) found that the fracture toughness and impact strength of the TGPAP/$CaCO_3$ nanocomposites significantly increased by the addition of nano-$CaCO_3$. He et al. (2011) also observed that even small contents (2–6 wt%) of nano-$CaCO_3$ in the epoxy cast can increase the thermal stability and mechanical properties of the nano-$CaCO_3$/epoxy cast. Hussain et al. (1996) evaluated the fracture toughness for an epoxy-$TiO_2$, composite system at room and liquid nitrogen temperature in which both the volume and the particle size of dispersoid have been changed. Fracture toughness was significantly increased by choosing the larger particle size of the dispersed second phase and low temperature testing environment. Carballeira and Haupert (2010) investigated the effect of mechanically dispersed titanium dioxide nanoparticles in an epoxy resin using a torus mill device on the mechanical properties of the polymer. The addition of $TiO_2$ nanoparticles in low volume concentrations to the epoxy resin could simultaneously improve the stiffness, toughness, maximum sustained strain, and resistance to crack propagation of the neat resin. Wang et al. (2006) developed a novel approach assisted with solvent to disperse clay into epoxy matrix. It was found that both stiffness and toughness of the materials were improved through incorporation of SMC clay. Mechanical properties and tribological behavior of epoxy resin epoxy nanocomposites containing different shape nanofillers, such as spherical silica ($SiO_2$), layered organo-modified montmorillonite (oMMT) and oMMT-$SiO_2$ composites, were investigated by Jia et al. (2006). Compared with pure epoxy, the fracture toughness of epoxy/oMMT improves a little but the tensile strength improves obviously, and the fracture toughness of epoxy/$SiO_2$ improves obviously but the tensile strength improves a little. However, oMMT-$SiO_2$ exhibits synergistic effects on toughening and reinforcing the epoxy simultaneously, because of its special spherical-platelet structure and the interaction between $SiO_2$ and oMMT. In order to improve the fracture toughness of epoxy adhesive, Kim and Park (2008) incorporated nano-particle additives such as carbon black and nanoclay into epoxy resin. It was found that reinforcement with nano-particles improved the fracture toughness at the room temperature, but decreased the

fracture toughness at the cryogenic temperature in spite of their toughening effect. In this study, carbon black and nanoclay were mixed with epoxy to investigate their toughening effect. Wang et al. (2015a) in-situ synthesized a modifying copolymer for clay modification during epoxy curing and it was incorporated to form an interpenetrating network (IPN) structure within epoxy network, leading to a double IPN structure. At an optimum clay loading of 1 wt%, tensile strength and modulus, elongation at break as well as $K_{1C}$ of the epoxy/clay nanocomposite was enhanced by 38%, 5%, 64%, 93%, respectively, indicative of a remarkable improvement of tensile and fracture toughness while maintaining reasonable strength. Ayatollahi et al. (2011) studied the effects of MWCNTs on the mechanical properties of epoxy/MWCNT nano-composites with emphasis on fracture toughness under bending and shear loading conditions. While the maximum mode I fracture toughness was obtained in nano-composites containing 0.5 wt% of MWCNT, the addition of MWCNTs improved the strength and mode II fracture toughness of epoxy continually. The presence of MWCNTs had a greater effect on the enhanced fracture toughness of nano-composites under shear loading compared with normal loading. Ma et al. (2015) used MWCNTs containing residual catalyst Ni particles to fabricate magnetically aligned epoxy composites under a relatively low applied magnetic field of 0.4 T. Significant toughness and fracture energy improvements were obtained in composites with magnetic field aligned CNTs and randomly oriented CNTs relative to neat epoxy. With CNTs aligned perpendicular to the crack plane, the composites displayed much higher $K_{IC}$ and $G_{IC}$ compared to those with randomly oriented CNTs or CNTs aligned parallel to the crack plane. Ladani et al. (2015) reported the use of an alternating current (AC) electric field to align carbon nanofibres in an epoxy. During the cure process of an epoxy resin, CNFs are observed to rotate and align with the applied electric field, forming a chain-like structure. The addition of 1.6 wt% of aligned CNFs increases the fracture energy, $G_{IC}$, by about 1600% from 134 to 2345 $J/m^2$. The three different sized chemical functionalized graphene (GO) sheets, namely GO-1 (D50 = 10.79 μm), GO-2 (D50 =1.72 μm) and GO-3 (D50 = 0.70 μm), were used by Wang et al. (2013) to fabricate a series of epoxy/GO nanocomposites.

Incorporation of a very small amount of the graphene sheets into the epoxy matrix resulted in a significant improvement on the fracture toughness of the polymer (See Figure 1.31). The enhancement of the epoxy toughness was strongly dependent on the size of the graphene sheets incorporated. Chandrasekaran et al. (2014) toughened epoxy composites with three kinds of nanofillers viz., graphite nano-platelets (GNP), thermally reduced graphene oxide (TRGO), and MWCNTs. It was observed that epoxy toughened with TRGO and GNP showed significant enhancement in toughness compared to MWCNT. Among the 2D fillers, TRGO showed two-fold increase in $K_{IC}$ compared to GNP toughened epoxy which is due to the partial functionalization and fewer numbers of layer stacked in TRGO. Lei et al. (2016) synthesized imidazole grafted GO and used as an effective co-curing reagent with DDM to the epoxy. The ultimate tensile strength, flexural strength, and impact strength increased by 40%, 10.8%, and 42% was achieved for the cured epoxy composite containing 0.80 wt% of imidazole grafted GO when compared with that without GO.

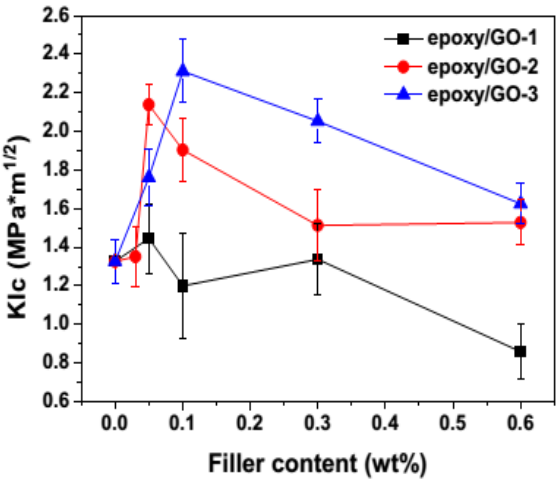


Figure 1.31: $K_{IC}$ versus GO content for the epoxy nanocomposites (Wang et al., 2013)

Table 1.9 presents a literature review in which nanofillers have been used as modifier to improve the toughness of epoxy.

Table 1.9: Toughness of epoxy systems modified by various types of nanofillers

| **Author** | **Toughener used** | **Composition at which maximum toughness achieved** | **% improvement in toughness** |
|---|---|---|---|
| Chandrasekaran et al. (2014) | GNP | 1 wt% | 57 |
| Kim and Park. (2008) | Carbon black | 3 wt% | 20 |
| Yang et al. (2009) | TETA-MWCNT | 0.6 wt% | 84 |
| Rafiee et al. (2009) | GNP | 0.1 wt% | 50 |
| Wetzel et al. (2006) | $Al_2O_3$ | 10 vol% | 120 |
| Ayatollahi et al. (2011) | MWCNT | 0.5 wt% | 27 |
| Ma et al. (2015) | Aligned MWCNT | 3 wt% | 51 |
| Wang et al. (2013) | GO | 0.1 wt% | 75 |
| Jin and Park. (2008) | Nano $CaCO_3$ | 6 wt% | 40 |
| He et al. (2011) | Nano $CaCO_3$ | 4 wt% | 106 |
| Ji et al. (2004) | Nano $Al_2O_3$ | 0.98 vol% | 19 |
| Wang et al. (2006) | nanoclay | 2 wt% | 77 |
| Wang et al. (2015a) | Organo modified nanoclay | 1 wt% | 98 |
| Blackman et al. (2007) | nanosilica | 20 wt% | 73 |
| Jia et al. (2006) | nanosilica | 3 wt% | 79 |

| | | | |
|---|---|---|---|
| Johnsen et al. (2007) | nanosilica | 13.4 vol% | 141 |
| Carballeira and Haupert. (2010) | $TiO_2$ | 10 vol% | 138 |
| Ragosta et al. (2005) | nanosilica | 10 wt% | 131 |
| Hussain et al. (1996) | $TiO_2$ | 10 vol% | 33 (at liquid N temp) |

## 1.3.4. Toughening mechanisms

Addition of a particulate phase to a glassy polymer often enhances fracture toughness without significantly compromising the other desirable engineering properties. Successful application of this technique to overcome the inherent brittleness of epoxy resins was first reported in the early 1970s (McGarry, 1970; Sultan and McGarry, 1973). Since then, many investigations have been performed to elucidate the exact role of these particles in toughening of brittle epoxies. In general, several toughening mechanisms operate simultaneously to produce the overall toughening effect of various rubber and thermoplastic modified epoxies. In many cases, they operate simultaneously to generate toughness properties. The important mechanisms responsible for enhancement of fracture toughness are given below.

### 1.3.4.1. The particle bridging mechanism

The proposed role of the rubber or plastic particles is to span two crack surfaces and apply surface tractions that effectively alleviate the stress applied at the crack tip (Kunz-Douglass et al, 1980; Kunz et al., 1982). In other words, the energy is consumed when the crack deforms and tears the particles. Physical evidence for the crack bridging mechanism has been inferred by the analysis of fracture surfaces using scanning electron microscopy (SEM) (Figure 1.32). Good interfacial adhesion is a prerequisite for this mechanism to operate. In rubber modified thermosets, early

toughening models were based on the rubber particle bridging mechanism and claimed that the work consumed in the tearing of the stretched rubber particles across the crack wake contributes significantly to toughening. This proposal could not be accepted as a major toughening mechanism since it did not take the role of matrix into account and could not explain other experimental observations. It has been shown that the fracture toughness of rubber-modified epoxies depends strongly on the structure of the matrix; looser epoxy networks result in higher toughness.

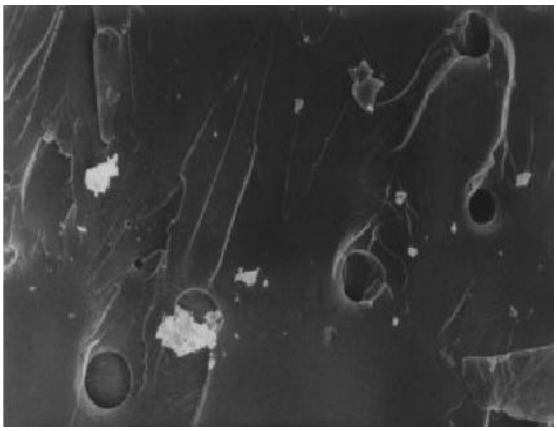

Figure 1.32: SEM image of the fracture surface of CTBN/epoxy blend showing crack bridging (Thomas et al., 2004)

### 1.3.4.2. Rubber particle cavitation and induced shear deformation in the matrix

Kinloch et al. (1983) suggested that the rubber-tear mechanism only makes a secondary contribution to toughening, but it does not represent the major toughening mechanism. Rubber particle cavitation is the primary toughening mechanism in rubber modified epoxies especially in relatively lower crosslink density epoxy resins. They proposed a mechanism that involves dilatational deformation of the matrix, and cavitation of the rubber particles in response to the triaxial stresses near the crack tip, combined with shear yielding between the holes formed by the cavitated rubber particles. The stress-whitening was attributed to light scattering by these holes, and the major energy absorption mechanism was suggested to be the plastic deformation

of the matrix (Figure 1.33). Plastic deformation blunts the crack tip, which reduces the local stress concentration and allows the material to support higher loads before failure occurs. Kim and Brown (1987) and Pearson (1990) provided evidence to show that shear-yielding also exists in thermoplastic particle modified epoxy system. The thermoplastic acts as stress concentrators owing to the significant modulus mismatch between the particle and the matrix. This stress concentration causes the matrix to undergo extensive shear deformation, generally in the form of massive shear banding between the particles. The formation of shear bands absorbs considerable energy, thereby increasing the fracture toughness.

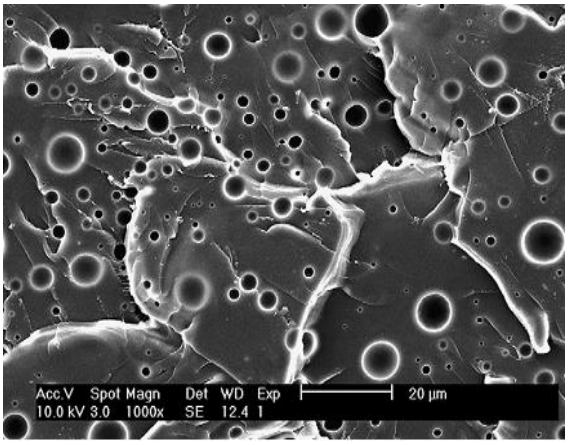


Figure 1.33: Stress whitened zone due to rubber cavitations in HTPB/epoxy blend (Thomas et al., 2008)

### 1.3.4.3. Crack-pinning mechanism

This theory states that as the crack begins to propagate through the resin, the crack front bows out between the filler particles but remains pinned at the particles which consumes additional energy (Lange, 1971a; Lange and Radford, 1971b). A schematic diagram of the crack-pinning mechanism is shown in Fig. 1.1 (Pearson, 1993). The crack pinning mechanism operates mainly with inorganic fillers that resist fracture during failure of the epoxy matrix resin. The crack-pinning mechanism

is generally less important in ductile matrix materials. Although thermosets can be toughened by a crack-pinning mechanism, this is generally less effective than the mechanisms present with soft or ductile particles. Indirect evidence for the occurrence of this mechanism is the observation of 'tails' near the particles on the fracture surface when viewed using SEM (Figure 1.34). Crack pinning is identified by the presence of bowing lines on the fracture surface.

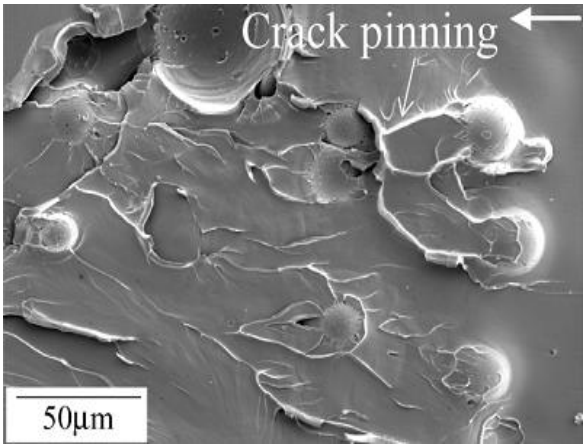


Figure 1.34: SEM micrograph of fracture surface of glass sphere filled epoxy showing crack pinning (Kawaguchi and Pearson, 2003)

### 1.3.4.4. Crack-path deflection mechanism

Another toughening mechanism often cited for producing the toughening effect especially in thermoplastic-modified epoxies is called crack path deflection. Thermoplastic particles change the crack path by causing the crack to deviate from its principal plane of propagation and/or the crack is split into several secondary cracks. The deflection of the crack path increases the total surface area of the crack surface and forces crack propagation into mixed mode. This mechanism was considered to be a secondary toughening mechanism and it accompanies other toughening mechanisms. This mechanism is important for highly crosslinked epoxies modified with relatively large particles. One of the most important fracture mechanisms in

nanocomposites is crack deflection. A SEM image of the crack-path deflection mechanism is shown in Figure. 1.35.

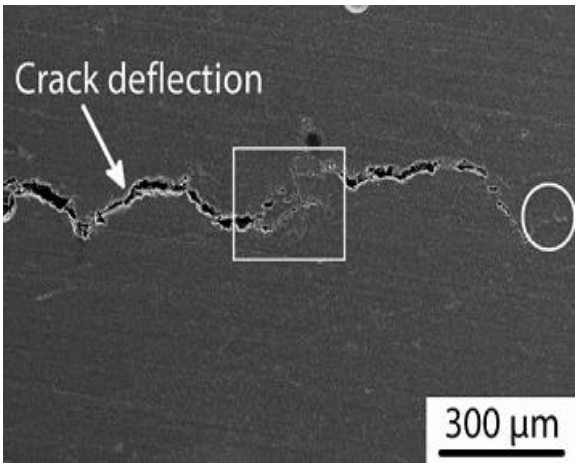


Figure 1.35: SEM micrograph of fracture surface of GnP/ epoxy nanocomposite showing crack deflection (Wu et. al., 2015)

### 1.3.4.5. Microcracking mechanism

This mechanism is effective for highly crosslinked epoxies when the particles are relatively rigid and capable of debonding. Microcracks due to rubber or thermoplastic particles cause stress concentration and initiate massive microcracks in the surrounding matrix. Voids result when the microcracks open, and these voids permit large strains (Figure 1.36). Debonding or microcracking effectively lowers the modulus in the frontal process zone around the crack tip, and thus effectively reduces the stress intensity there.

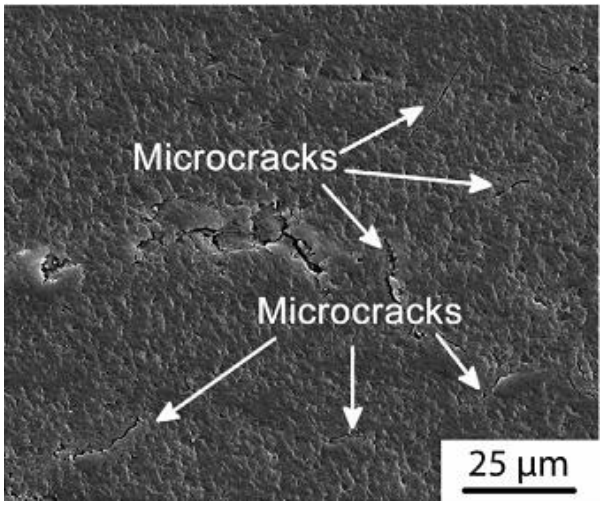


Figure 1.36: SEM micrograph of fracture surface of GnP/ epoxy nanocomposite showing microcracks (Wu et. al., 2015)

### 1.3.4.6. Crazing of matrix

Rubber particles act not only as stress concentrators, initiating crazes in the surrounding matrix, but also as craze terminators, preventing uninhibited growth of the crazes, which would result in the premature failure. Craze stabilization allows additional crazes to grow. The multiple crazing process consumes significant amount of energy and hence increase fracture toughness. This mechanism was proposed on the basis of interpretations of several observations, such as stress whitening ahead of the crack tip, and on the basis of the strong dependences on the particle size of the fracture toughness and pressure sensitivity of yielding. The relatively high cross-link density of epoxies should prevent crazing from occurring. Moreover, crazes have never been observed in epoxies with high cross-link densities

The rigid particulate nano-fillers like nanosilica and $TiO_2$ may toughen epoxy in a similar way as the soft rubber or thermoplastic particles do. That is, the filler debonding, and the subsequent void growth as well as the matrix shear band likely play the key roles in toughening. Hsieh et al. (Hsieh et al., 2010) reported that the

matrix shear band contributed more to the fracture toughness than the plastic void growth effect. It has been reported that the increase of fracture surface area because of crack path deflection is the major toughening mechanism in the epoxy MWCNT nanocomposites (Hsieh et al., 2011). Apart from crack deflection, pullout of nanotubes, debonding of MWCNTs and bridging mechanism also plays a significant role in improving the fracture toughness of composites. Shear banding and crack deflection or bifurcation is found to be the main contribution of toughness of polymer matrix in the case of layered nanofillers like nanoclay and graphene.

In recent years, many advances have taken place in the theoretical understanding of the toughening mechanisms for rubber, thermoplastic and nanofiller toughened epoxy resins. The relationships between microstructure and fracture behavior of toughened thermoset have been illustrated quantitatively. Several reviews have given detailed descriptions of the existing toughening mechanisms proposed to explain the improved toughness for rubber, thermoplastic and nanofiller toughened epoxy resins. Even though there are various toughening mechanisms proposed by different researchers, it seems that a single theory is not sufficient to explain every experimental result and phenomenon of toughening. One reason may be the discrepancy of the raw materials chosen by different researchers, because the initial properties of raw materials have significant influence on the final fracture properties of epoxy materials. Another reason lies in the fact that the fracture itself is a complex phenomenon, and a single theory cannot represent every detail.

## 1.4. Scope and Objectives of the Work

The realization of nanofiller reinforced epoxies with high toughness requires a homogeneous dispersion and strong interfacial interaction between the nanofiller and the polymer matrix. Generally nanoparticles have a tendency for agglomeration because of the weak van der Waals force of attraction. Surface modifications of nanofillers are an effective way to improve interfacial interaction between the

nanofillers and the epoxy matrix, which in turn leads to better filler dispersion, and enhanced mechanical performance in the nanocomposites (Davis et al., 2011; Sun et al., 2008). Recently, polymer functionalized nanofillers have attracted more interest in the field of polymer composites due to the presence of multiple anchor units for surface attachment and better interfacial interaction between the nanofillers and the polymer matrix (Díez-Pascual et al., 2010; Hu et al., 2012; Hu et al., 2015; Li et al., 2015; Wang et al., 2015b). However, a better improvement in toughness and mechanical strength can be expected if the nanofillers are previously functionalized with reactive polymers which consist of multiple functional groups. Besides homogeneous dispersion, the chemical modification of the nanofillers with reactive polymers can create a soft interface between nanofillers and polymer which can result in a better load transfer from matrix to filler. Apart from surface modification, nanofiller geometry of a composite also plays a crucial role in determining the mechanical performance of the composites. It is therefore significant to determine the influence of shape on the properties of the composites made with nanofillers. By judiciously selecting nanofillers of different geometry and size, and modifying the surface of these fillers with suitable polymers, tremendous improvement in fracture toughness and mechanical strength can be achieved.

Several investigations have been made in the area of toughening of epoxy resins. From the review on toughened epoxy resins, it was observed that relatively few systematic studies were conducted on surface engineered nanofiller toughened epoxy resins. In view of this, a detailed investigation has been carried out on the mechanical and thermomechanical properties of surface engineered epoxy nanocomposites.

The main objective of this research work is to study the influence of geometry and surface modification of nanofiller on the morphology, mechanical, thermal and viscoelastic properties of the epoxy composite system. We focus our work to develop epoxy systems with high toughness as well as mechanical strength. With this view, an

array of fillers of varying geometry and chemical functionalisation have been selected for the current study.

The specific objectives of this research work are summarized below:

- To develop a novel hybrid network system using polyhedral oligomeric silsesquioxane (POSS) and carboxyl terminated poly(acrylonitrile-co-butadiene) (CTBN) and the study of its cure kinetics.
- To develop POSS-CTBN/epoxy hybrid composite and to study its mechanical, thermal and viscoelastic performance.
- To study the effect of polymer functionalisation of multi-walled carbon nanotube (MWCNT) on the mechanical, thermal and viscoelastic performance of the MWCNT/epoxy composites.
- To study the effect of polymer functionalisation of graphite oxide (GO) on the mechanical, thermal and viscoelastic performance of the GO/epoxy composites.
- To study the shape dependence of titania nanofillers on the mechanical, thermal and viscoelastic performance of $TiO_2$/epoxy nanocomposites.

## 1.5. Organization of the Thesis

This thesis describes the research on the toughened epoxy nanocomposites based on surface engineered nanofillers. This research focuses on the effect of surface modification and shape dependence on the dispersion behavior and thermo-mechanical and fracture resistance of epoxy nanocomposites. The structure of the thesis is presented in the following seven chapters:

**Chapter 1** contains a general introduction on polymer nanocomposites, nanofillers, epoxy resins, curing process of epoxy systems and different types of curing agents used in the epoxy systems. It deals with an updated survey of literature

covering the toughening of epoxy with various modifiers with special reference to nanofiller. The objectives and the plan of the present investigation are stated at the end of this chapter.

**Chapter 2** describes the synthesis and cure kinetics of a novel organic–inorganic hybrid material from CTBN using glycidyl POSS as a crosslinking agent. The effect of catalyst on curing process and kinetic parameters were studied in detail using model free kinetic methods.

**Chapter 3** explains the preparation of a novel hybrid epoxy nanocomposite using CTBN as modifier, glycidyl POSS as nanofiller and DDS as curing agent. A comparative study of the properties of the hybrid systems with POSS/epoxy nanocomposites and CTBN/epoxy blends is discussed.

In **Chapter 4**, a systematic study has been conducted to investigate the thermo-mechanical and viscoelastic properties of epoxy nanocomposites prepared by the introduction of polymer grafted MWCNTs into epoxy resin. The samples were characterized using different types of spectroscopic and analytical methods. The effect of surface modification on the nanotube morphology and dispersion status was then evaluated. The mechanisms responsible for the improvement of toughness in polymer grafted MWCNT/epoxy composites is discussed.

In **Chapter 5**, polymer grafted GOs are prepared, and used as a modifier for epoxy resin. The enhancement in mechanical performance and fracture resistance of epoxy composites with different loadings of GO and polymer grafted GOs is described in this chapter. The effect of chemical modification on the dispersion and interfacial interaction in the resulting composites is also reported.

**Chapter 6** highlights the correlation between the shape of the titania nanostructures on the mechanical performance and fracture resistance of their epoxy

composites. $TiO_2$(B) nanowires were prepared using hydrothermal method and characterized. A comparative study of the mechanical, thermal and visco-elastic performance of epoxy nanocomposites prepared from $TiO_2$ nanoparticle and nanowires are reported. The fracture mechanism involved in reinforcement and the effect of particle shape on these mechanisms are discussed in detail.

**Chapter 7** summarizes the conclusions drawn from this research and offers recommendations for future scope of the work

# CHAPTER 2

# CURE KINETICS OF NOVEL POSS-CTBN NETWORK SYSTEM

*In this study, glycidyl polyhedral oligomeric silsesquioxane (POSS) was used as a crosslinking agent to prepare a new organic–inorganic hybrid material from carboxyl terminated poly(acrylonitrile-co-butadiene) (CTBN). The structure of the reacted material was characterized by Fourier Transform Infrared Spectroscopy (FTIR). Differential Scanning Calorimetry (DSC) at different heating rates in the presence and absence of catalyst, triphenyl phosphine (TPP), was conducted to investigate the cure kinetics. Different kinetic models were used to analyze the kinetic parameters. We investigated the dependence of activation energy of the curing of CTBN using Glycidyl POSS on factors such as extent of conversion, heating rate and catalyst. The activation energy of gelation was estimated by rheology and DSC analyses.*

**Part of this chapter has been published in Journal of Thermal Analysis and Calorimetry, (2016), Vol.123: 1479-1489**

# 2.1. Introduction

Nitrile rubber, a copolymer of acrylonitrile and butadiene is a synthetic rubber with good chemical resistance, hot air aging resistance, mechanical performance, abrasion resistance etc. (Liu et al., 2011a). The usual way of crosslinking such polymers is by a reaction of the unsaturation by sulfur or peroxide. This often poses problems of loss of rubbery character and toughness. Another possibility for crosslinking is by a reaction of the end groups. For instance, carboxyl end groups offer possibility for crosslinking by reaction with polyepoxide (Varghese et al., 1989). In fact, carboxyl terminated poly (acrylonitrile-co-butadiene) (CTBN) is conventionally used as a toughener in epoxy by making use of the carboxyl-epoxy reaction (Wang et al., 2012). The incorporation of polyhedral oligomeric silsesquioxane (POSS) into the polymer offers the opportunity to enhance the mechanical, thermal, oxidative, dielectric properties and reductions in flammability of polymer system (Kuo and Chang, 2011; Lee et al., 2006). However, only a limited number of studies have been reported for the use of POSS as crosslinker in the nitrile rubber. Very recently, Liu et al (2012) studied the cure kinetics, dielectric and viscoelastic properties of hydrogenated carboxylated nitrile rubber-POSS composites. Octa-functional POSS can react with carboxyl group of CTBN to get a highly crosslinked network system. The performance of rubber depends on the curing condition opted for the reaction. An optimal curing process depends on understanding the accurate kinetic modeling of the curing process. This modeling includes determination of the mechanism, measurement of the reaction orders, and activation energies of the reaction. The cure kinetics of CTBN rubber and POSS are not yet clearly understood, and an accurate model of an optimal curing process has yet to be clearly established. To date, no detailed study has been reported on modeling the curing of the CTBN rubber using POSS. In this work, a new organic–inorganic hybrid material by a reaction of CTBN with glycidyl POSS is reported. The curing kinetics is studied by model free kinetic methods.

## 2.2. Theoretical background

The kinetics of the reaction is usually described by the following rate Eq. (Brown et al., 1980; Murias et al., 2015; Tripathi et al., 2015)

$$\frac{\mathrm{d}\alpha}{\mathrm{d}t} = Af(\alpha)\exp\left(-\frac{E_a}{RT}\right) \tag{2.1}$$

where $\alpha$ is the conversion, $t$ is time, $A$ is the pre-exponential factor, $E$ is the activation energy, $T$ is the absolute temperature, R is the gas constant (8.3145 $JK^{-1}mol^{-1}$), and $f(\alpha)$ is the differential conversion function.

When a sample is heated at a constant rate, $\beta = \mathrm{d}T/\mathrm{d}t$, Eq. (2.1) is rewritten as

$$\frac{\mathrm{d}\alpha}{\mathrm{d}T} = \left(\frac{A}{\beta}\right) f(\alpha)\exp\left(-\frac{E_a}{RT}\right) \tag{2.2}$$

The integral kinetic methods are based on the following integral form of the Eq. (2.1) (Vyazovkin and Wight, 1997)

$$g(\alpha) = \left(\frac{A}{\beta}\right) I(E, T_\alpha) \tag{2.3}$$

where

$g(\alpha) = \int_0^\alpha \frac{\mathrm{d}\alpha}{f(\alpha)}$ and $I(E_\alpha, T_\alpha) = \int_0^{T_\alpha} \left[\exp\left(-\frac{E}{RT}\right)\right]\mathrm{d}T$ is the temperature integral.

Several kinetic models have previously been proposed to adequately describe the cure behavior of thermosets. Kinetic parameters can be obtained by both model

fitting and isoconversional methods. For non-isothermal experiments, model fitting method involves fitting different models to $\alpha$–$T$ curves and simultaneously determining $E_a$ and $A$ (Janković, 2008). The Model free kinetic methods do not assume any kinetic models in data analysis. Instead, they assume that the activation energy during cure only depends on conversion. The basic assumption of these methods is that the reaction rate at constant conversion is only a function of the temperature (Ozawa, 1992).

The Friedman isoconversional differential method (Friedman, 1969) is derived by taking the logarithms of Eq. (2.1)

$$\ln\left(\beta\frac{\mathrm{d}\alpha}{\mathrm{d}t}\right)_{\alpha} = \ln\left[A_{\alpha} f(\alpha)\right] - \frac{E_{\alpha}}{RT_{\alpha}} \tag{2.4}$$

where $E_\alpha$ and $T_\alpha$ are the activation energy and temperature at different conversions respectively. The linear plots between $\ln(\mathrm{d}\alpha/\mathrm{d}t)_\alpha$ and $1/T_\alpha$ make it possible to determine the values $E_\alpha$ and $\ln\left[A_\alpha f(\alpha)\right]$ at different conversions.

According to the Kissinger method (Kissinger, 1957), the activation energy can be obtained from the maximum reaction rate where $d\alpha^2/\mathrm{d}t^2$ is zero under a constant heating rate condition. Kissinger method uses Coats Redfern approximation of the temperature integral which leads to

$$\ln\left(\frac{\beta}{T_p^2}\right) = \ln\left(\frac{AR}{E}\right) - \frac{E}{RT_p} \tag{2.5}$$

where $T_p$ is the peak exotherm temperature. Thus, for $\alpha$ = const., the plot $\ln(\beta/T_p^2)$ versus $1/T_p$ should be a straight line whose slope can be used to evaluate the activation energy.

The isoconversional integral method suggested independently by Flynn and Wall (Flynn and Wall, 1966) and Ozawa (Ozawa, 1992) uses Doyle's approximation for the temperature integral which leads to the Eq.

$$\log \beta = \log\left(\frac{AE_\alpha}{R}\right) - 2.315 - 0.4567\frac{E_\alpha}{RT_\alpha} \tag{2.6}$$

Thus, for $\alpha$ = const., the plot log $\beta$ versus ($1/T_\alpha$), obtained from thermograms recorded at several heating rates, should be a straight line whose slope can be used to evaluate the activation energy.

Vyazovkin (Vyazovkin, 2001) developed an enhanced isoconversional method that allows evaluation of $E\alpha$ as a function of the extent of reaction (α)

$$\varphi(E_\alpha) = \sum_{i=1}^{n}\sum_{j\neq i}^{n}\frac{I\left[E_\alpha, T_i\left(t_\alpha\right)\right]\beta_j}{I\left[E_\alpha, T_j\left(t_\alpha\right)\right]\beta_i} \tag{2.7}$$

where n is the number of heating rates, $I\left[E_\alpha, T_i\left(t_\alpha\right)\right]$ the exponential integral *p(x)* that results from heating rate $\beta_i$ while $I\left[E_\alpha, T_j\left(t_\alpha\right)\right]$ is the exponential integral from heating rate $\beta_j$ and it can be given by

$$I\left[E_\alpha, T_i\left(t_\alpha\right)\right] = \int_{t_\alpha-\Delta t_\alpha}^{t_\alpha} \exp-\left[\frac{E_\alpha}{RT_i\left(t_\alpha\right)}\right]dt \tag{2.8}$$

The above integral can be solved by using trapezoidal rule. The activation energy at a given extend of conversion is the value that minimizes $\varphi$ in the above equation.

In this work, the above mentioned methods were used for calculation of the kinetic parameters of the reaction between POSS and CTBN. The main objective of this study is investigating the dependence of activation energy of the curing of CTBN using Glycidyl POSS on factors such as extent of conversion, heating rate and catalyst. Also, in this study we have evaluated activation energy of gelation by rheology and DSC analyses.

# 2.3. Experimental

## 2.3.1. Materials

CTBN (average Mn~3800 $gmol^{-1}$, acrylonitrile 8-12 wt%, 1.9 carboxyl groups per molecule, and glass transition −66 °C) was obtained from Aldrich India. Triphenyl phosphine (TPP) was purchased from Aldrich India and glycidyl POSS (molecular mass 1378 $gmol^{-1}$) was supplied by Hybrid Plastics USA. The molecular structure of the materials are shown in Figure 2.1.

(a)

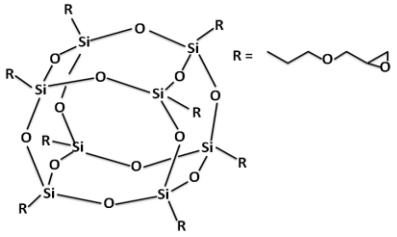

(b)

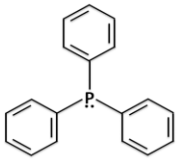

(c)

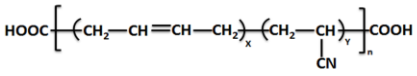

Figure 2.1: Chemical structure of (a) Glycidyl POSS (b) TPP and (c) CTBN

## 2.3.2. Preparation of samples

Samples for DSC analysis were prepared by the following method. 1 gram of CTBN was dissolved in 20 mL acetone and stirred for 15 minutes using magnetic stirrer. 90 mg of POSS and catalytic quantities of TPP with different mass percentage (0.1, 0.3 and 0.5 wt% with respect to CTBN) were added and stirring was continued for 30 minutes. Acetone was evaporated off by heating at 50 $^{o}$C for 1 h and kept in vacuum oven for 4 h at room temperature.

## 2.3.3. Characterization

### 2.3.3.1. Fourier Transform Infrared Spectroscopy

The reaction between POSS and CTBN was monitored using Fourier Transform Infrared (FTIR) spectrometer (Spectrum 100, Perkin Elmer, USA) in the wavenumber ranges from 4000 to 650 $cm^{-1}$ with a spectral resolution of 4 $cm^{-1}$. The spectra were recorded using an attenuated total reflectance accessory.

### 2.3.3.2. Differential Scanning Calorimetry

Cure kinetics of the system was investigated using Differential Scanning Calorimetry (DSC, Q-20, TA Instruments, USA). In order to carry out the cure studies, dynamic DSC scans were performed in the temperature ranges from 40-350 $^{o}$C at different heating rates (2.5, 5, 10, 15 and 20 $Kmin^{-1}$) in nitrogen atmosphere. The peak area integration and subsequent fractional conversion ($\alpha$)–temperature calculations were done by TA Instruments Universal Analysis 2000 software.

### 2.3.3.3. Rheological measurements

Rheological analysis was done using Modular Rheometer (MCR 102 Modular Compact Rheometer, Anton Paar, USA), using a 50 mm parallel plate. Isothermal measurements were done at 145, 150, 160 and 170 $^{o}$C in order to study the kinetics of gelation.

# 2.4. Results and Discussion

## 2.4.1. FTIR analysis

The success of the reaction between CTBN and POSS was monitored by FTIR. To prepare POSS-CTBN, 1 gram of CTBN was treated with 90 mg of POSS at 150 $^{o}$C for 4 h. The FTIR spectra of gycidyl POSS, CTBN and POSS-CTBN polymer are shown in Figure 2.2. In Figure 2.2 (a), the peaks at 910 $cm^{-1}$ and 850 $cm^{-1}$ are due to the stretching of oxirane ring in Glycidyl POSS. The peak at 1098 $cm^{-1}$ is the characteristic of Si-O-Si stretching in Glycidyl POSS (Liu et al., 2006; Ramírez et al., 2008). In Figure 2.2 (b), the peak at 964 $cm^{-1}$ corresponds to =C−H out of plane bending vibration of 1, 4 trans olefin in CTBN, peak at 1640 $cm^{-1}$ is due to C=C stretching and peak at 1712 $cm^{-1}$ corresponds to C=O stretching of carbonyl group in CTBN. The peak at 2238 $cm^{-1}$ can be assigned to C≡N stretching. After the POSS-CTBN reaction, as shown in Figure 2.2 (c), it is clear that the peak at 850 $cm^{-1}$ from the compound glycidyl POSS disappeared and peak at 1712 $cm^{-1}$ of CTBN shifted to 1738 $cm^{-1}$ which corresponds to the carbonyl stretching frequency of ester from the composite. This implies that epoxide group of glycidyl POSS reacted with carboxyl group of CTBN rubber forming an ester.

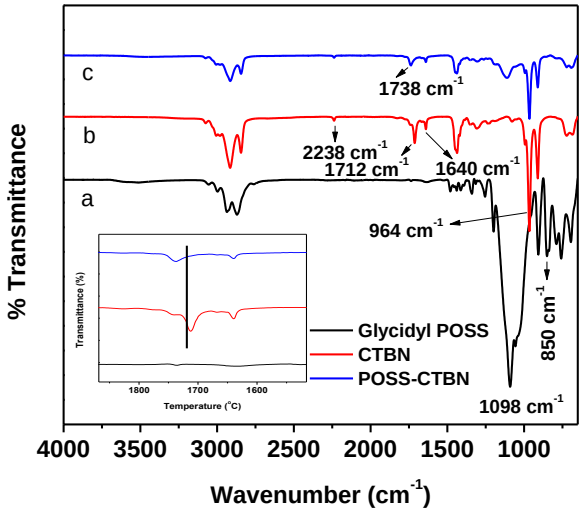


Figure 2.2: FTIR spectra of (a) Glycidyl POSS, (b) CTBN and (c) POSS-CTBN network

## 2.4.2. Cure kinetic analysis from DSC

Representative non-isothermal DSC curves for the reaction between POSS and CTBN by varying the concentration of catalyst (TPP) and heating rates are given in Figure 2.3 (a) and 2.3 (b). The heat flow curves from non-isothermal DSC measurements show a single exothermic peak for all samples. The exothermic peak temperature *($T_p$)* is shifted to higher temperature region with increasing heating rate. This is because, as the heating rate is increased, the reactant mixture has little time to react and hence $T_p$ is shifted to higher temperature region. On the other hand, when the catalyst was added, the curing shifted to a lower temperature as observed from a systematic drift in $T_p$. TPP is used as a pre-reaction catalyst to promote the reaction between the epoxy group of POSS and carboxyl group of CTBN. Table 2.1 shows the $T_p$ of all the samples studied by varying the concentration of the catalyst and heating rate. It is important to mention that an increase in $T_p$ with increasing heating rate with or without catalyst was observed. On the other hand a decrease in $T_p$ with the addition of catalyst irrespective of the heating rate was observed.

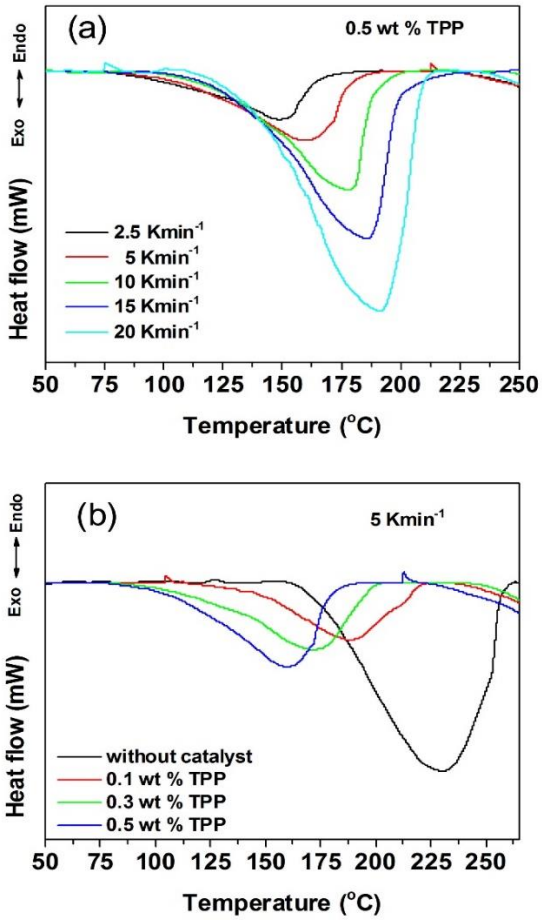


Figure 2.3: Representative DSC curves for the reaction between POSS and CTBN by (a) varying the heating rate with a catalytic concentration of 0.5 wt% and (b) varying catalytic concentration at a heating rate of 5 $Kmin^{-1}$

A schematic illustration of the reaction between epoxide group of glycidyl POSS with carboxyl group of CTBN in presence of catalyst is illustrated in Figure 2.4. The first step of the reaction involves a nucleophilic attack of TPP on the epoxide which results in a ring opening reaction followed by the generation of a betaine complex (Konnola et al., 2015b). The betaine complex formed as a result of the first step, attacks the CTBN entity and deprotonates the carboxylic acid group of CTBN resulting in the formation of the corresponding carboxylate anion. The carboxylate

anion will then attack the alpha carbon atom of the phosphonium ion to form an ester with subsequent regeneration of TPP catalyst.

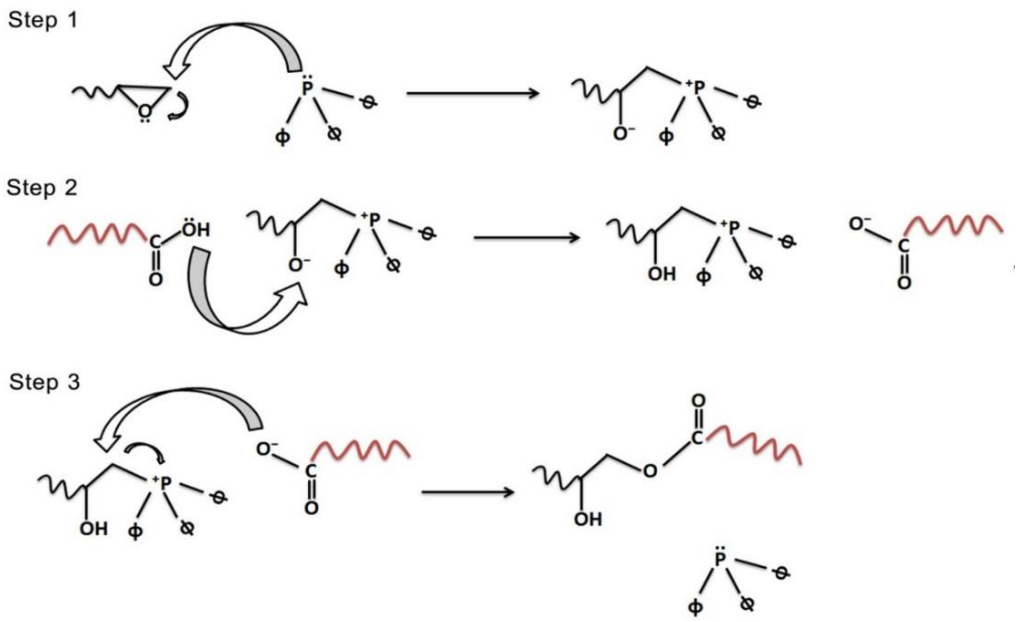


Figure 2.4: Schematic illustration of possible reaction between epoxide group of POSS with carboxyl group of CTBN in presence of TPP

Table 2.1: Variation of peak temperature of exotherm with catalyst concentration

| **Heating rate (Kmin$^{-1}$)** | **exothermic peak temperature ($T_p$) (K)** | | | |
|---|---|---|---|---|
| | **Without catalyst** | **0.1 wt% TPP** | **0.3 wt% TPP** | **0.5 wt% TPP** |
| 2.5 | 218 ± 2 | 177 ±1 | 158 ±2 | 149 ±1 |
| 5 | 230 ±3 | 189 ±1 | 172 ± 3 | 160 ± 2 |
| 10 | 240 ± 3 | 205 ±2 | 186 ± 0.5 | 178 ±3 |
| 15 | 252 ±1 | 214 ±0.5 | 195 ±2 | 186 ±1 |

| | | | | |
|---|---|---|---|---|
| 20 | 258 ±1 | 218 ±1 | 202 ±3 | 1910.5 |

### 2.4.2.1. Effect of catalyst and heating rate on extent of conversion

The exothermic curves obtained from the DSC dynamic measurements were integrated to obtain extent of conversion ($\alpha$) with respect to temperature. The variation in $\alpha$ with temperature for the curing of CTBN using POSS with varying concentration of catalyst at a typical heating rate (5 $Kmin^{-1}$) is illustrated in Figure 2.5 (a). The $\alpha$ shift to the lower temperature on adding 0.1 wt% TPP to the CTBN matrix and this effect is more pronounced at higher concentrations of catalyst. As mentioned in the previous section, the catalyst promotes the reaction between the epoxy group of POSS and carboxyl group of CTBN and hence $\alpha$ shift to the lower temperature at higher concentrations of TPP. On the other hand, upon increasing the heating rate, $\alpha$ shifted to higher temperature for all the CTBN systems due to the thermal lag at higher heating rates, due to which the effective temperature required for the reaction between carboxyl and epoxy group attains a higher temperature on increasing the heating rate (Figure 2.5 (b)).

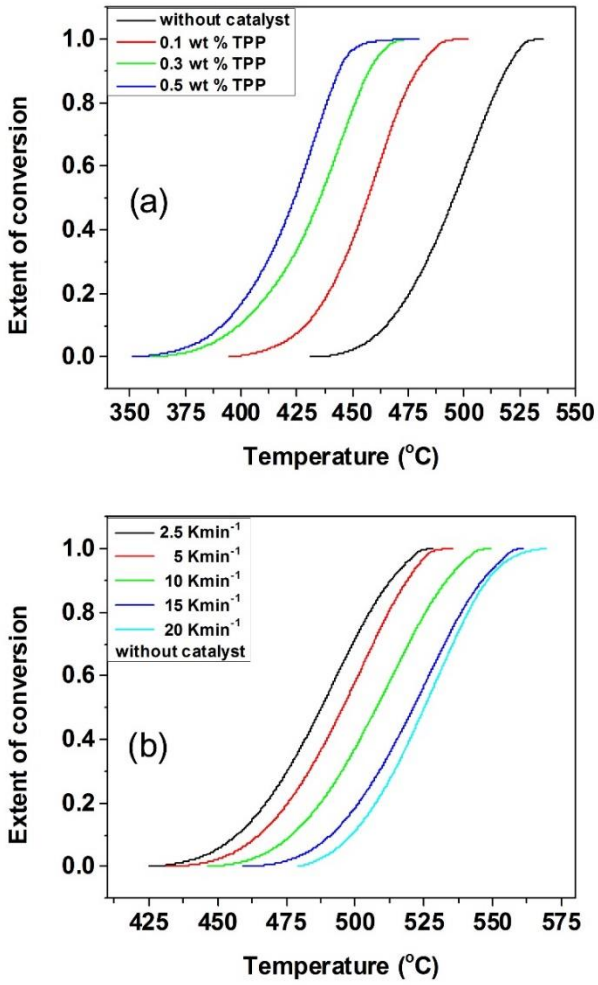


Figure 2.5: Variation of extent of reaction with temperature for (a) different concentration of catalyst at 5 $Kmin^{-1}$ heating rate and (b) different heating rate in the absence of catalyst

### 2.4.2.2. Effect of catalyst on activation energy

In Kissinger method, the reciprocal peak temperature $(1/T_p)$ values obtained at different heating rates were plotted against $\ln(\beta/T_p^2)$ , where $(\beta)$ is the heating rate. There is an excellent linear fit in all systems studied, indicating that the model fit the experimental data quite well (determination coefficients ($R^2$) is above 0.98). The slope of the straight line fit of $\ln(\beta/T_p^2)$ vs $1/T_p$ gives the apparent activation energy

(*Ea*) for the system (Figure 2.6). Kissinger method is based on the assumption of a single reaction that happens during the curing of CTBN with POSS. Thus the activation energy obtained in Kissinger model is an overall value representing all the complex reactions that occur during curing. Table 2.2 shows the kinetic parameters obtained from Kissinger method for POSS-CTBN system with varying concentration of catalyst. For uncatalyzed system, Kissinger method gives the value of $E_a$ as 104 kJmol$^{-1}$ and the value of ln $A$ as 23.49 min$^{-1}$. By the addition of 0.1 wt% of catalyst, $E_a$ decreases from 104 to 82 kJmol$^{-1}$. This is a clear evidence of a catalytic effect of the TPP in the curing reaction of CTBN by POSS. $E_a$ decreases further as the concentration of catalyst increases. Figure 2.7 shows the variation of $E_a$ as a function of concentration of catalyst.

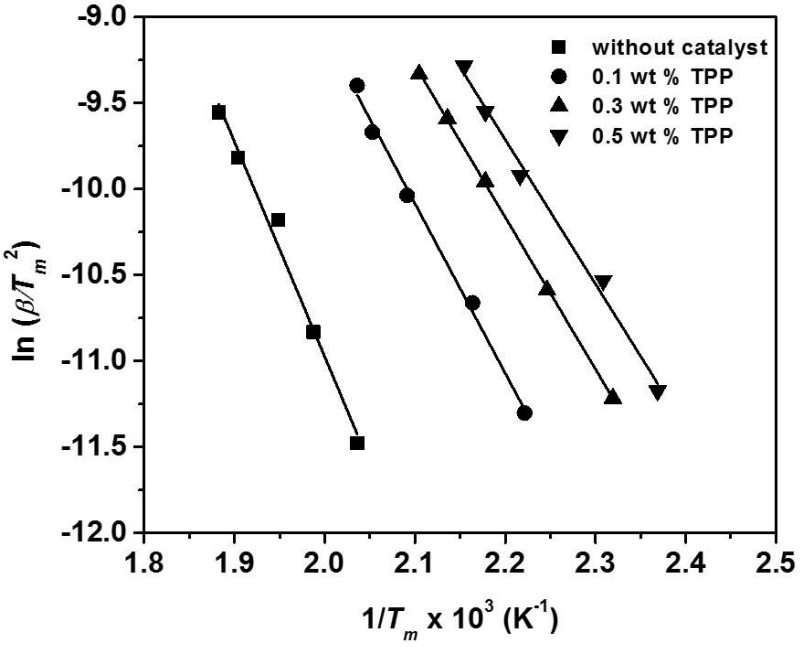


Figure 2.6: Kissinger plot for POSS-CTBN system with varying amount of catalyst

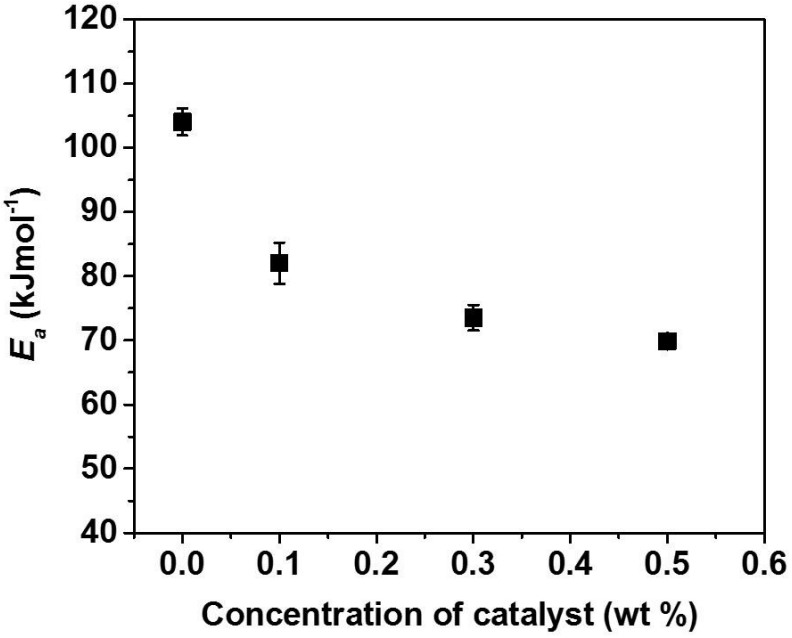


Figure 2.7: Variation of $E_a$ with concentration of catalyst

Table 2.2 Kinetic parameters obtained using Kissinger analysis

| **Catalyst concentration** | **$E_a$ (kJmol$^{-1}$)** | **ln $A$ (min$^{-1}$)** | **$R^2$** |
|---|---|---|---|
| Without catalyst | 104 ±2.1 | 23.49 ±0.7 | 0.9831 ±0.005 |
| 0.1 wt% TPP | 82 ±3.2 | 19.83 ±0.8 | 0.9873 ±0.006 |
| 0.3 wt% TPP | 73 ±2.0 | 18.38 ±0.5 | 0.9907 ±0.006 |
| 0.5 wt% TPP | 69 ±0.7 | 17.81 ±0.2 | 0.9898 ±0.003 |

### 2.4.2.3. Variation of activation energy with extent of conversion

The dependence of the $E_a$ on the extent of conversion is a source of additional kinetic information of process. If the $E_a$ is not assumed to be constant throughout the curing reaction, but rather allowed to vary with the degree of cure, then the model free isoconversional methods are useful to track how the activation energy changes throughout the entire reaction. The dominant curing reaction is expected to be the

reaction between epoxy of POSS and carboxyl group of CTBN. Towards the end of the cure process, i.e., at higher temperatures, other reactions such as etherification and homopolymerization of epoxide groups are expected to be important.

The cure reaction between POSS and CTBN without any catalyst and by the addition of 0.5 wt% TPP was analyzed by isoconversional methods of Friedman (FR), Flynn–Wall–Ozawa (FWO) and Vyazovkin (V). Figure 2.8 plots the values of the $E_a$ calculated by the different isoconversional methods for different values of the conversion ranging from 5 to 95 %, showing $E_a$ of both systems gradually increase with the extent of cure. The increase of $E_a$ at higher conversion is due to increased viscosity of the medium leading to more constrains of mobility of chains and consequently the difficulty of reactive species to undergo reaction. Similar observations have been reported (Deng and Martin, 1994). The mean value of activation energies from isoconversional FWO method for POSS-CTBN system without catalyst and using 0.5 wt% TPP were 103.4 kJ $mol^{-1}$ and 70.2 $kJmol^{-1}$ respectively. These values are in good agreement with the obtained value of $E_a$ using by Kissinger method. The values of $E_a$ for FWO method obtained for POSS-CTBN system without catalyst is comparatively lower than the values of $E_a$ obtained for FR and V methods. The deviation of $E_a$ of FWO is due to the assumption of constant activation energy while deriving the Eq. (2.6). This assumption introduces a significant systematic error for a process whose activation energy strongly varies with the degree of conversion (Vyazovkin and Wight, 1997; Vyazovkin and Wight, 1999). Such an error does not appear in the differential isoconversional FR method. The nonlinear V method uses integration as a part of the procedure for estimating the activation energy. Compared to linear integral procedures, nonlinear V method was found to be a very accurate method (Vyazovkin and Wight, 1999).

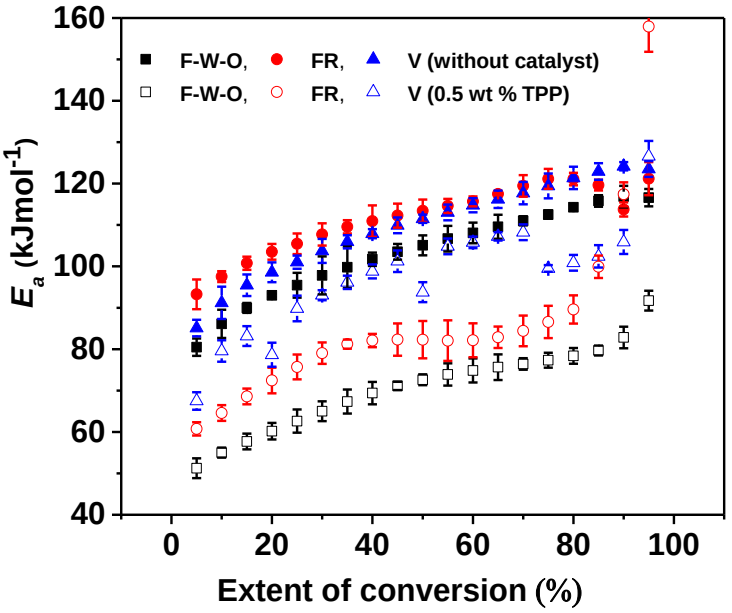


Figure 2.8: Variation of activation energy with extent of conversion for POSS CTBN system without catalyst and the presence of 0.5 wt% TPP. FWO: Flynn-Wall-Ozawa method, FR: Friedman isoconversional method, V: Vyazovkin method.

### 2.4.2.4. Kinetic model prediction

Malek (Zhang et al., 2015) method is the most reliable method for the determination of probable mechanism function in the kinetic model. In Malek method, once activation energy is determined, two characteristic functions, *y(α)* and *z(α)* were defined in order to find the kinetic model and the kinetic parameters. The shape and maximum value of these functions provides valuable information for determining the most suitable kinetic model (Bai et al., 2015). In non-isothermal conditions, the two functions can be described as follows:

$$y(\alpha) = \left(\frac{\mathrm{d}\alpha}{\mathrm{d}t}\right)\exp(x) \tag{2.9}$$

$$z(\alpha) = \pi(x)\left(\frac{\mathrm{d}\alpha}{\mathrm{d}t}\right)\frac{T}{\beta} \tag{2.10}$$

where $x$ represents ($E_a/RT$), $\beta$ is the heating rate, $T$ is the absolute temperature and $\pi(x)$ function can be approximated using the 4th order rational expression of Senum and Yang (Kasemsiri et al., 2015) as shown in Eq. (2.11).

$$\pi(x) = \frac{x^3 + 18x^2 + 88x + 96}{x^4 + 20x^3 + 120x^2 + 240x + 120} \tag{2.11}$$

The $y(\alpha)$ and $z(\alpha)$ functions are normalized within the (0,1) range. These curves show the conversion $\alpha_M$ for the maximum value of $y(\alpha)$ and $\alpha_p^\infty$ for the maximum value of $z(\alpha)$. Both $\alpha_M$ and $\alpha_p^\infty$ suggest the choice of the most suitable kinetic model.

Figure 2.9 shows the the curves of $y(\alpha)$ and $z(\alpha)$ of POSS-CTBN system without and by the addition of 0.5 wt% TPP catalyst. From the figure, it can be seen that for both systems, the values of $\alpha_M$ and $\alpha_p^\infty$ satisfy the conditions: $0 < \alpha_M < \alpha_p^\infty$ and $\alpha_p^\infty \neq 0.632$, which strongly indicate that the two-parameter autocatalytic Sestak–Berggren model (SB($m$,$n$)) (Xiong et al., 2014) is suitable for kinetic modeling of the reactions in this work.

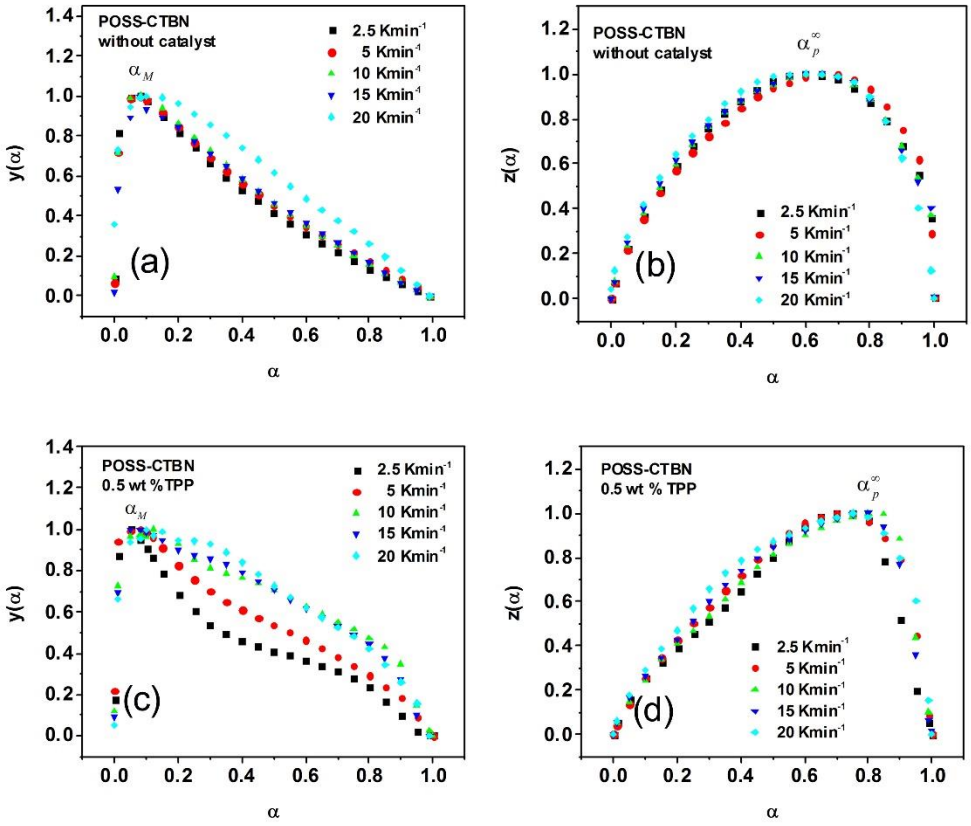


Figure 2.9: (a) and (b) represents *y(α)* and *z(α)* curves of POSS-CTBN system without catalyst and (c) and (d) represents *y(α)* and *z(α)* curves of POSS-CTBN system with 0.5 wt% catalyst

The SB (*m*, *n*) model can be expressed by Eq. (2.12)

$$f(\alpha) = \alpha^m (1-\alpha)^n \tag{2.12}$$

where *m* and *n* are the kinetic parameters. Substituting Eq. (2.12) in Eq. (2.1)

$$\frac{\mathrm{d}\alpha}{\mathrm{d}t} = A\exp\left(-\frac{E_a}{RT}\right)\alpha^m (1-\alpha)^n \tag{2.13}$$

Eq. (2.13) can be transformed into the following form (Zabihi et al., 2013)

$$\ln\left[\left(\frac{\mathrm{d}\alpha}{\mathrm{d}t}\right)\exp\left(\frac{E_a}{RT}\right)\right]=\ln A+n\ln\left[(1-\alpha)\alpha^{\left(\frac{\alpha_M}{1-\alpha_M}\right)}\right] \tag{2.14}$$

Where

$$\alpha_M=\frac{m}{m+n} \tag{2.15}$$

The kinetic parameters *n* and ln*A* are obtained from the slope and the intercept of $\ln\left[\left(\frac{\mathrm{d}\alpha}{\mathrm{d}t}\right)\exp\left(\frac{E_a}{RT}\right)\right]$ versus $\ln\left[(1-\alpha)\alpha^{\left(\frac{\alpha_M}{1-\alpha_M}\right)}\right]$ (from Eq. (2.14)) as well as the kinetic parameter, m can be calculated from Eq. (2.15). All of the kinetic parameters *n*, *m*, and ln *A*, are listed in Table 2.3. Figure 2.10 shows the dependence of $\ln[(\mathrm{d}\alpha/\mathrm{d}t)\exp(Ea/RT)]$ on $\ln[(1-\alpha)\alpha^{(\alpha_M/1-\alpha_M)}]$ at the heating rate of 20 $Kmin^{-1}$ in both systems in the conversion range from 0.2 to 0.95 .

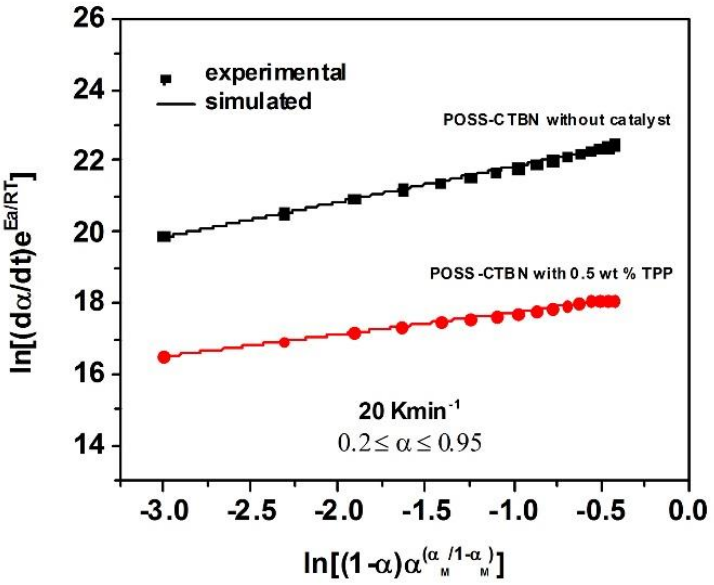


Figure 2.10: $\ln[(\mathrm{d}\alpha/\mathrm{d}t)\exp(E_a/RT)]$ versus $\ln[(1-\alpha)\alpha^{(\alpha_M/1-\alpha_M)}]$ at heating rate of 20 $Kmin^{-1}$ in the conversion range from 0.2 to 0.95

Table 2.3 Calculated kinetic parameters

| **Polymer system** | **Heating rate ($Kmin^{-1}$)** | ***m*** | **Average *m*** | ***N*** | **Average *n*** | **ln *A*** | **Average ln *A*** |
|---|---|---|---|---|---|---|---|
| POSS-CTBN without catalyst | 2.5 | 0.099 | 0.096 | 1.140 | 1.043 | 23.270 | 22.978 |
| | 5 | 0.085 | | 0.985 | | 23.222 | |
| | 10 | 0.093 | | 1.073 | | 22.900 | |
| | 15 | 0.088 | | 1.017 | | 22.650 | |
| | 20 | 0.111 | | 1.002 | | 22.847 | |
| POSS-CTBN 0.5 wt% TPP | 2.5 | 0.044 | 0.059 | 0.836 | 0.656 | 18.210 | 18.292 |
| | 5 | 0.064 | | 0.740 | | 18.316 | |
| | 10 | 0.067 | | 0.493 | | 18.259 | |
| | 15 | 0.050 | | 0.580 | | 18.298 | |
| | 20 | 0.070 | | 0.633 | | 18.375 | |

The explicit rate equations of the curing reaction can be obtained by substituting the calculated kinetic parameters $E_a$, $n$, $m$, and ln$A$ into Eq. (2.13).

The kinetic model evaluation for POSS-CTBN system without any catalyst and using 0.5 wt% TPP catalyst are given in Eq. (2.16) and (2.17) respectively

$$\frac{\mathrm{d}\alpha}{\mathrm{d}t} = 9.796X10^{9}\exp\left(-\frac{100319}{RT}\right)\alpha^{0.096}(1-\alpha)^{1.043} \qquad (2.16)$$

$$\frac{\mathrm{d}\alpha}{\mathrm{d}t} = 8.804\mathrm{x}10^{7}\exp\left(-\frac{70687}{RT}\right)\alpha^{0.059}(1-\alpha)^{0.656} \qquad (2.17)$$

To demonstrate the validity of the proposed model, a comparison has been made using the experimental curves and predicted curves based on the determined cure parameters for POSS-CTBN system without catalyst and by the addition of 0.5

wt% catalyst at different heating rates (Figure 2.11). From the figure, it can be clearly seen that the calculated DSC curve fits relatively well using the obtained model parameters of the cross-linking reaction.

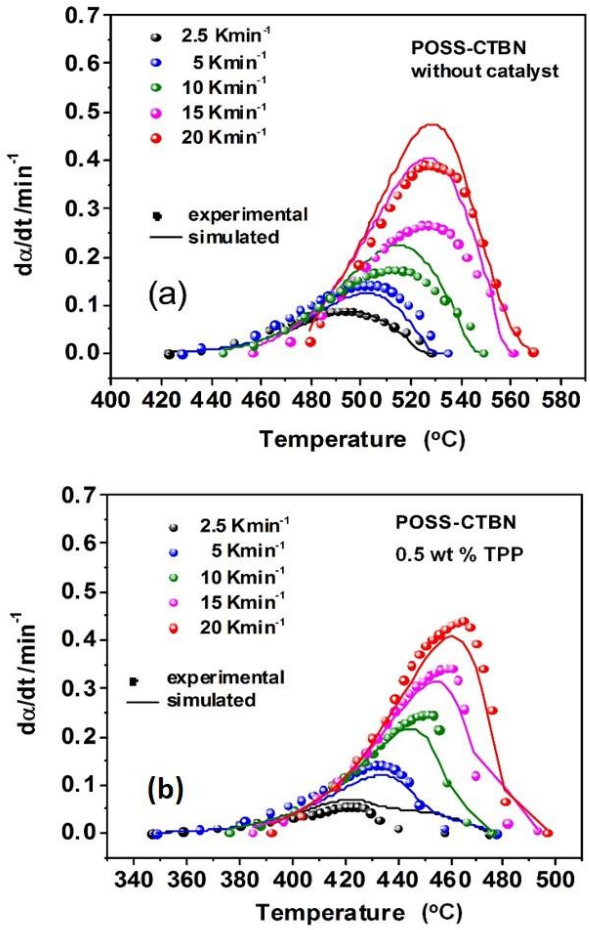


Figure 2.11: Comparison of simulated curves of SB(*m*,*n*) model to experimental curves for (a) POSS-CTBN system without catalyst and (b) POSS-CTBN system with 0.5 wt% catalyst

## 2.4.3. Time of gelation from rheokinetics

The gel point is one of the most important kinetic characteristics of curing. As the cure reaction proceeds, the molecular mass increases and several chains link together into networks of infinite molecular mass. This sudden and irreversible transformation from a viscous liquid to an elastic gel is defined as gelation point; and

the time at which occurs, at a given isothermal cure temperature, is the gelation time (Fernandez et al., 2001; NEZ et al., 1997). The critical gel is an isoconversion property of any given thermosetting system and will occur at the same conversion regardless of cure temperature if the polymerization proceeds with a single mechanism. Gelation time was determined by the intersection of storage modulus (*G'*) and loss modulus (*G"*) where the material began to develop mechanical properties characteristics of the elastic solids (Auad et al., 2006; Zlatanic and Dunjic, 1999). Times of gelation ($t_{gel}$) for curing of CTBN with POSS at different isothermal temperatures were measured (Figure 2.12). The time of gelation decreases on increasing the isothermal temperature. $1/t_{gel}$ is indicative of the rate of gelation. Activation energy of gelation can be determined by plotting the $\ln(1/t_{gel})$ against $1/T$ (Figure 2.13) (Kumar et al., 2006). The slope of the plot gives $-E_a/R$. For POSS-CTBN system without catalyst, the activation energy of gelation calculated from rheological measurement is 111.5 kJmol$^{-1}$.

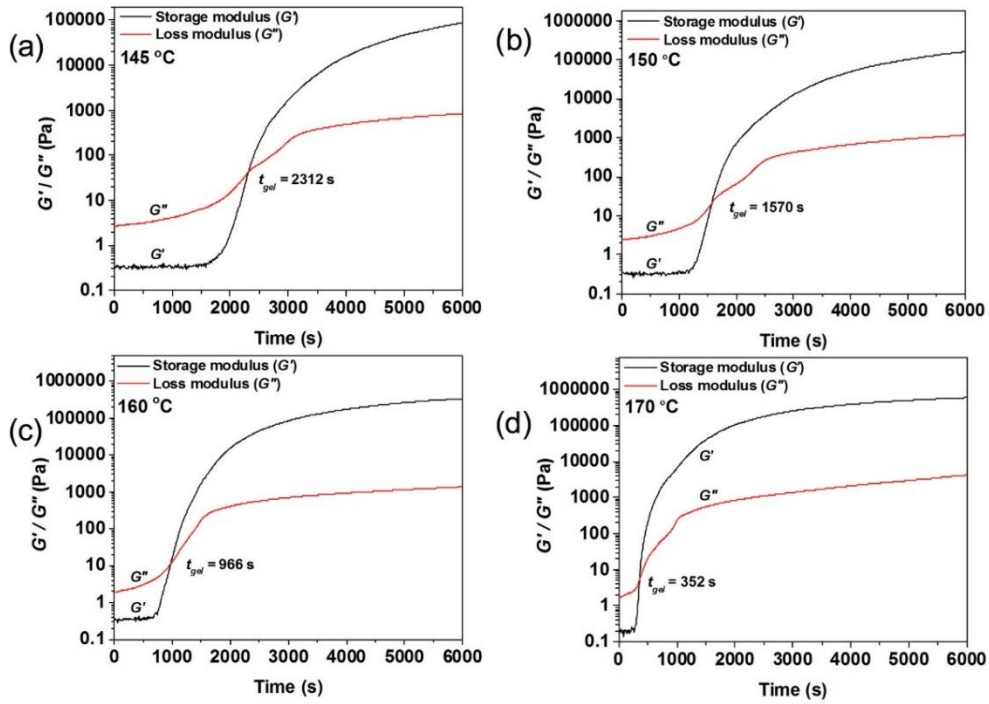


Figure 2.12: Variation of storage and loss moduli with time for POSS-CTBN system without catalyst at (a) 145 °C (b) 150 °C (c) 160 °C and (d) 170 °C

By knowing the extent of reaction from Flory's theory, it is possible to compare the $E_a$ of gelation obtained from rheological studies and thermal studies. According to the classical statistical theory of gelation developed by Flory (Flory, 1953), the gel point is characterized by the appearance in the reactive system of a macromolecule with infinitely large molecular mass. Based on this theory, this phenomenon occurs for a determined extent of reaction, which can be expressed as

$$\chi_{gel} = \left[ \frac{1}{(f_e - 1)(f_c - 1)r} \right]^{1/2} \tag{2.18}$$

where $\chi_{gel}$ is the extent of reaction at gelation point, $f_e$ and $f_c$ are the epoxy and carboxyl functionalities, respectively, and $r$ is the carboxyl/epoxy stoichiometric ratio.

From Flory's theory, $\chi_{gel}$ for the system is found to be 0.39. The activation energy of curing of CTBN with POSS near conversion of 0.4 (Figure 2.8) according to Vyazovkin model is 108 kJmol$^{-1}$, which is reasonably in good agreement with activation energy of gelation predicted from rheological analysis. Here $E_a$ from Vyazovkin model is used for comparison as Vyazovkin model shows extremely low errors in the activation energy (Janković, 2008; Vyazovkin and Wight, 1999).

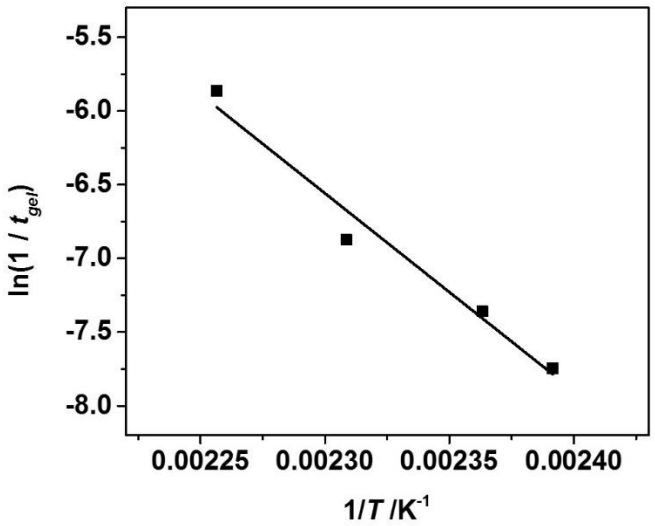


Figure 2.13: Plot of ln(1/$t_{gel}$) vs 1/$T$ for curing of POSS-CTBN system without catalyst with different isothermal temperature

## 2.5. Conclusions

A new organic–inorganic hybrid material was prepared by cross linking CTBN with glycidyl POSS. FTIR confirms the successful reaction between carboxyl group of CTBN and epoxide group of POSS. The differential scanning calorimetry (DSC) at different heating rates was conducted to investigate the curing kinetics. Isoconversional kinetic models using differential scanning calorimetry showed an increase in activation energy with an increase in extent of conversion which is due to a restriction in mobility of reactants as the system tends to be more viscous. The activation energy obtained from FWO method is found to be less than that from FR and V method because of the difference in approximation used while deriving the model equation. There is a kinetic evidence for a catalytic effect of TPP on the curing reaction of the CTBN by POSS. Activation energy is found to decrease as the concentration of the catalyst increased from 0.1 to 0.5 wt%. A two-parameter (*m, n*) autocatalytic model (Sestak-Berggren equation) was found to be the most adequate to describe the cure kinetics of the studied POSS-CTBN systems. Evidently, the kinetic

models of the curing reactions of the both systems are in good agreement with non-isothermal DSC data. The activation energy of gelation obtained from rheological studies is comparable with activation energy obtained from DSC study in league with Flory's theory of gelation.

# CHAPTER 3

# DEVELOPMENT OF POSS-CTBN/EPOXY HYBRID NANOCOMPOSITES

*This study focuses on the preparation of a novel hybrid epoxy nanocomposite with glycidyl POSS as nanofiller, CTBN as modifying agent and DGEBA as matrix polymer. The reaction between DGEBA, CTBN and glycidyl POSS was carefully monitored and interpreted by using FTIR and DSC. The mechanical properties such as tensile strength and fracture toughness were also carefully examined. The fracture toughness increases for CTBN/epoxy, POSS/epoxy and POSS-CTBN/epoxy hybrid systems with respect to neat epoxy, but for hybrid composites toughening capability of soft rubber particles is lost by the presence of POSS. High resolution scanning electron micrographs (HRSEM) of fractured surfaces were examined to understand the toughening mechanism. The viscoelastic properties of CTBN/epoxy, POSS/epoxy and POSS-CTBN/epoxy hybrid systems were analyzed using dynamic mechanical analysis. Finally TGA studies were employed to evaluate the thermal stability of prepared blends and composites.*

**The results of this chapter have been published in Polymer Composites, (2015).**

**DOI: 10.1002/pc.23390**

# 3.1. Introduction

In the last few decades, much attention has been given to improve the thermal and mechanical properties of epoxy resins, especially by making them tough. Enhancing the toughness of epoxy resins by addition of a second polymer such as an elastomeric or a thermoplastic modifier has been widely reported (Chikhi et al., 2002; Guild and Kinloch, 1995; Ozturk et al., 2001; Ratna, 2001). The rubber-modified epoxies exhibit significant improvement in fracture toughness but considerable reduction in mechanical properties and glass transition temperature *($T_g$)* (Karger-Kocsis and Friedrich, 1993). Recently, many researchers have shown that the incorporation of nano fillers in the epoxy matrix can improve the mechanical properties of the resultant composites. Due to the extremely small particle size, the interactions between nano-fillers and matrix are not fully understood, though many interesting and useful results have been published to date to identify the toughening potential of nanotube (Deng et al., 2008), nanoclay (Miyagawa and Drzal, 2004), nano-silica (Kinloch et al., 2003) and nano-aluminum (Zunjarrao and Singh, 2006) in brittle epoxy resins.

POSS can be considered as a nano form of silica. The inner inorganic silicon and oxygen core, surrounded by organic substituents renders high reactivity and compatibility to POSS molecules which make them a preferred additive for altering the properties of a variety of polymer matrices. Since POSS is having a hollow inorganic core, it can act as stress concentrators and this property can be utilized for improving the fracture toughness of the nanocomposite. A few works have reported the use of POSS as a toughening agent (Kim et al., 2003; Mishra and Singh, 2013). Mishra and Singh (2013) studied the fracture toughness behavior of POSS in both room temperature and cryogenic condition. Modification of POSS with a toughening polymer can impart a positive effect on the fracture toughness behavior of epoxy nanocomposite. Better improvement in toughness is expected by the presence of this

third phase in the epoxy matrix system. The idea of using these hybrid composite systems with nanofillers and rubber has already been explored in the literature and it has been demonstrated that improved composite performance can be achieved by combining the advantages of each of the additives. Lee et al. (2010) used CTBN with nano clay to improve the toughness and mechanical strength of bisphenol A type epoxy. The effects of incorporating MWCNTs at low weight percent on the tensile behavior and thermal conductivity properties of a DGEBA type epoxy toughened with rubber particles have been investigated by Balakrishnan et al. (2011). Asif et al. (2010) studied the effect of PES and processing techniques on phase morphology, surface morphology, fracture toughness, barrier properties and thermomechanical properties of epoxy clay ternary nanocomposites. Loh et al. (2010) studied the effect of particle size of nanosilica on the fracture behavior of rubber modified epoxy system. Jyotishkumar et al. (2013) used ABS as a modifier for DGEBA type epoxy resin, and the modified epoxy resin was used as a matrix for making MWCNTs reinforced composites for better mechanical and thermal properties.

In this work, we prepared hybrid epoxy nanocomposites using CTBN as modifier, glycidyl POSS as nanofiller and DDS as curing agent (a high-performance hardener). Though a few works have been reported with the incorporation of CTBN, POSS and DDS independently or in combination with other materials in the epoxy matrix, none of them has utilized the combination of modifier, curing agent and nanofiller and hence our effort is to bridge the gap in the relevant literature. We examined the viscoelastic behavior, thermal stability, mechanical performance and fracture toughness of the hybrid nanocomposites. We have also carried out a comparison of the properties of these hybrid systems with POSS/epoxy nanocomposites and CTBN/epoxy blends.

# 3.2. Materials and Method

## 3.2.1. Materials

Diglicidyl ether of bisphenol A (DGEBA) (Lapox ARL-135) and hardener 4, 4' diamino diphenyl sulfone (Lapox K10) were purchased from Atul India Pvt Ltd. The toughening polymer CTBN (average $M_n$ ~3,800, acrylonitrile, 8-12 wt%, 1.9 carboxyl groups per molecule, $T_g$ −66 °C) and triphenylphosphine ($P(C_6H_5)_3$ were obtained from Aldrich, India and Glicidyl POSS mixture (molecular weight 1378 g/mol) was supplied by Hybrid Plastics USA. The molecular structures of the materials used are shown in Figure 3.1.

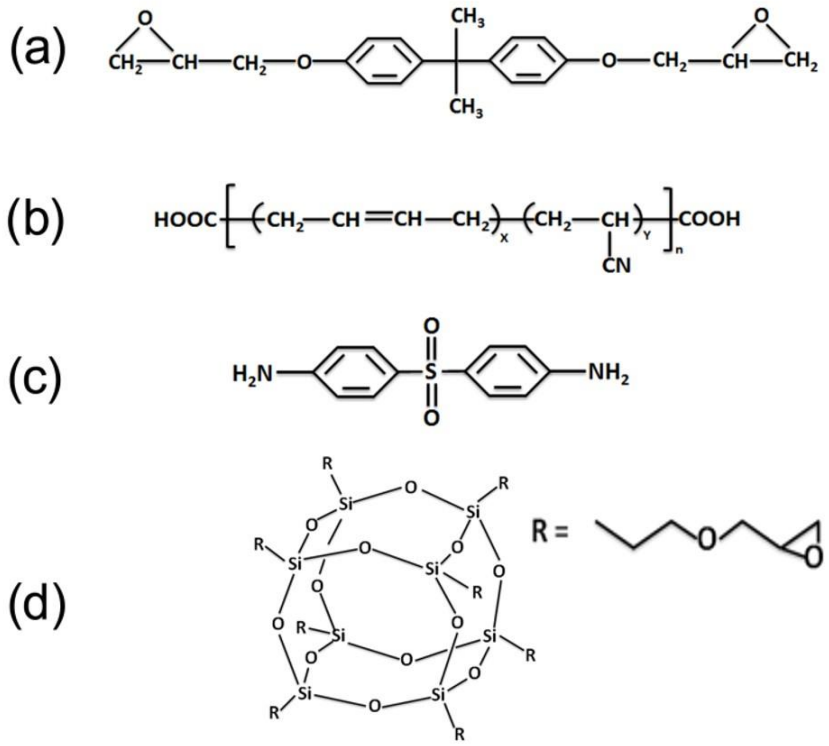


Figure 3.1: Chemical structure of (a) digycidyl ether of bisphenol A, (b) carboxyl terminated poly(acrylonitrile-co-butadiene) (c) diamino diphenyl sulfone and (d) glycidyl POSS

## 3.2.2. Characterization

### 3.2.2.1. Scanning electron microscopy (SEM)

The morphology of fractured surface of the samples was analyzed using scanning electron microscope (SEM, FEI Quanta FEG200). Prior to analysis, the sample is sputter coated with gold to make it conducting surface.

### 3.2.2.2. Mechanical measurements

Tensile tests were performed with dumbbell shaped specimens using an Instron model 5900 tensile tester at a crosshead speed of 1 mm/min as per ASTM standard D638. The results are the average of at least five measurements. Fracture toughness of the sample was measured using UTM (Instron 5900, Instron, USA) at a crosshead speed of 10mm/min (as per ASTM standard D5045). Single edge notch specimens of 46 x 6 x 3 $mm^3$ (span length = 24 mm) were used to measure the fracture toughness of the epoxy nanocomposites. A notch of 2.7 mm was made at one edge of the specimen. A natural crack was made by pressing a fresh razor blade into the notch. The fracture toughness was expressed as stress intensity factor ($K_{IC}$) calculated using equation

$$K_{IC} = \frac{L}{BW^{0.5}} f(x) \tag{3.1}$$

where $0 < x < 1$ and

$$f(x) = \frac{6x^{0.5}\left[1.99 - x(1-x)\left(2.15 - 3.93x - 2.7x^2\right)\right]}{(1+2x)(1-x)^{1.5}} \tag{3.2}$$

and L is the load at crack initiation, B is the specimen thickness, W is the specimen width, a is the crack length and x = a /W.

#### 3.2.2.3. Dynamic mechanical analyzer (DMA)

Dynamic Mechanic Analysis (DMA) was performed on a DMA Q800, operating in the single cantilever mode at an oscillation frequency of 1 Hz. Data was collected from room temperature to 250 $^{o}$C at a scanning rate of 2 $^{o}$C/min. The sample specimens were cut into rectangular bars measuring 20 x 5 x 2 $mm^3$.

#### 3.2.2.4. Thermogravimetric analyzer (TGA)

Thermal stability of nanocomposites was analyzed using a thermogravimetric analyzer (Q-50, TA Instruments, USA). The samples were heated from ambient to 800 $^{o}$C at a ramp rate of 10 $^{o}$C/ min.

### 3.2.3. Preparation of blends and composites

For the preparation of POSS-CTBN/epoxy hybrid nanocomposite, 2.5 phr glycidyl POSS, 5 phr CTBN and DGEBA were pre reacted for 4 hours at 120 $^{o}$C using a pinch of triphenylphosphine (TPP) as catalyst. Stoichiometric amount of curing agent (DDS) was added, mixed and degassed for 5 minutes. The resulting mixture was poured into a preheated teflon mould and cured for 4 hours at 180 $^{o}$C. Post curing was done at 200 $^{o}$C for an hour. CTBN/epoxy blends with various compositions were prepared by mixing CTBN (2, 5, 10 and 15 phr) in the epoxy resin for 4 hours at 120 $^{o}$C in presence of TPP catalyst. Stoichiometric amount of curing agent (DDS) was added and cured using the same cure schedule as mentioned above. For the preparation of POSS/epoxy nanocomposites, the required amounts of POSS (1, 2.5, 5 and 10 phr) was dissolved in a mixture of THF and DGEBA and sonicated for 30 minutes. THF was evaporated off by heating at 80 $^{o}$C for 1 hour. The trace

amounts of solvent were removed by keeping the mixture in vacuum oven. It was then added to molten hardener and stirred for 10 minutes. Same cure schedule as described above was followed for the preparation of the POSS nanocomposite.

## 3.3. Results and Discussion

### 3.3.1. Characterization using FTIR analysis

The FTIR spectra of DGEBA-POSS-CTBN hybrid network (before and after reaction) are shown in Figure 3.2. The peak at 1098 $cm^{-1}$ is characteristic of the Si-O-Si stretching in glycidyl POSS. The peak at 964 $cm^{-1}$ corresponds to =C−H out of plane bending vibration of 1, 4 trans olefin in CTBN, peak at 1640 $cm^{-1}$ is due to C=C stretching and peak at 1712 $cm^{-1}$ corresponds to C=O stretching of carbonyl group in CTBN. The peak at 2238 $cm^{-1}$ can be assigned to C≡N stretching. After the reaction, it can be seen that the intensity of peak at 840 $cm^{-1}$ corresponding to C-H stretching of oxirane rings in POSS and DGEBA has reduced significantly (shown in circle) and peak of CTBN at 1712 $cm^{-1}$ has shifted to 1740 $cm^{-1}$ (shown as dotted line). The appearance of a peak at 1740 $cm^{-1}$ corresponds to the carbonyl stretching frequency of ester of the composite. This implies that the epoxide groups of glycidyl POSS and DGEBA have reacted with carboxyl group of CTBN rubber in forming an ester.

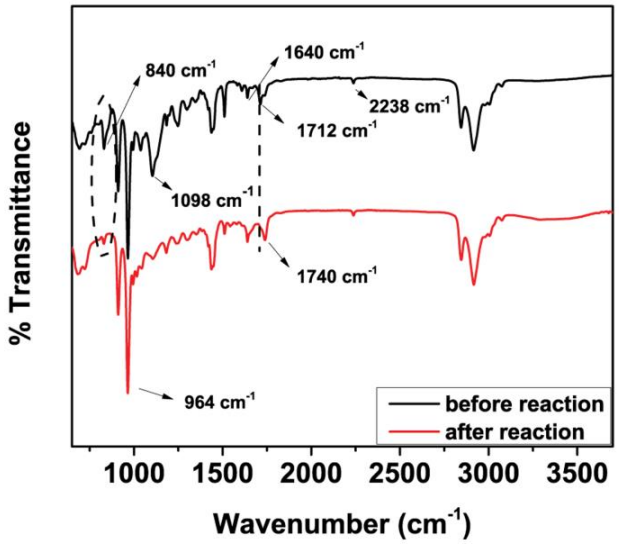


Figure 3.2: FTIR spectra of the reaction between POSS, CTBN and DGEBA

The mechanism of catalytic action of TPP in the reaction was discussed in detail in chapter 2. The proposed mechanism clearly reveals the nature of the reaction occurring during the synthesis of the nanocomposite leading to the formation of a convoluted network structure as illustrated in Figure 3.3 which paves way for the explanation of all the interesting properties exhibited by the novel in-situ epoxy nanocomposite system.

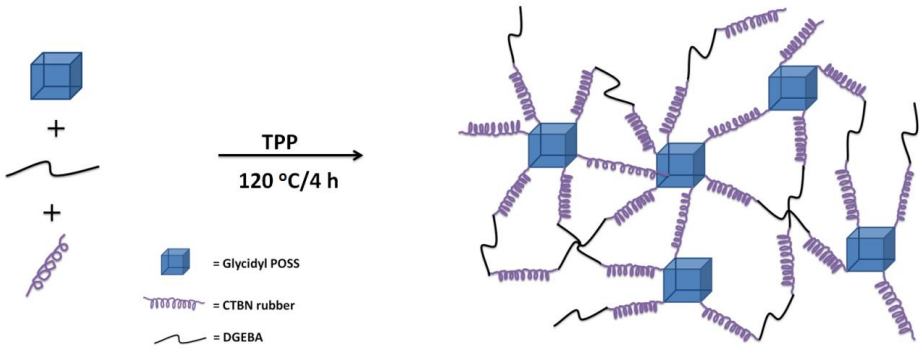


Figure 3.3: Schematic illustration showing the network formation during the pre-reaction between POSS, CTBN and DGEBA

### 3.3.2. Characterization using DSC analysis

DSC analysis confirmed the reaction between DGEBA, CTBN and Glycidyl POSS. DSC curves of reaction between equivalent quantities of DGEBA and CTBN, POSS and CTBN and half equivalence of DGEBA and POSS together with CTBN are given in Figure 3.4. The presence of a single sharp exothermic peak in all the three cases clearly substantiates that the reaction of the epoxy groups of both DGEBA and POSS occurs within similar temperature range.

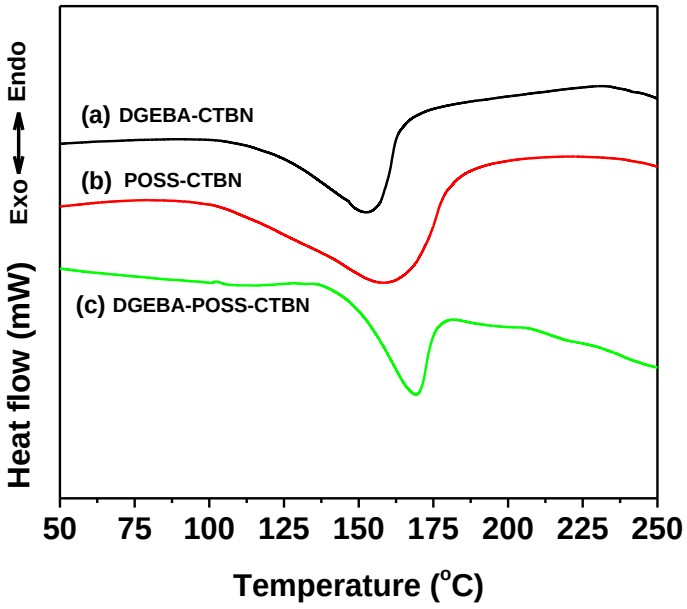


Figure 3.4: DSC curves showing the cure reaction of (a) DGEBA and CTBN (b) POSS and CTBN and (c) DGEBA, POSS and CTBN

### 3.3.3. Tensile strength of epoxy blends and composites

The changes in tensile strength for the prepared blends and composites are shown in Figure 3.5 and 3.6. The tensile strength decreases with increasing CTBN content. This decrease in tensile strength is due to the increase in the relative amount of dissolved rubber in the epoxy phase as the rubber content increases (Tripathi and

Srivastava, 2007). The decrease in tensile strength for CTBN/epoxy blends can also be attributed to the stiffness of the modified epoxy network. The addition of rubber decreases stiffness of the epoxy network due to the lowering of crosslink density. The addition of POSS particles in neat epoxy slightly reduced their tensile strength, and a higher loading led to a larger drop in strength (Figure 3.5). Highly crosslinked network formed by the octa-functional POSS will tend to create internal stress in the matrix which results in the premature failure of the matrix on loading. For POSS-CTBN/epoxy hybrid nanocomposite, further loss of tensile strength could be due to the internal stresses induced by the different cure speeds between the bulk epoxy, CTBN/epoxy, CTBN/POSS and POSS/epoxy reactions (Zilg et al., 2000).

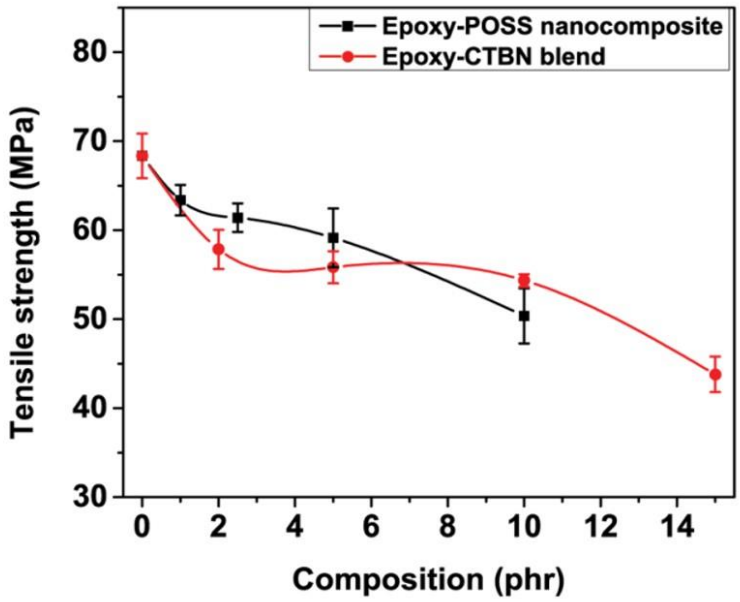


Figure 3.5: Tensile strength of neat epoxy, POSS/epoxy nanocomposite and CTBN/epoxy blends at various compositions

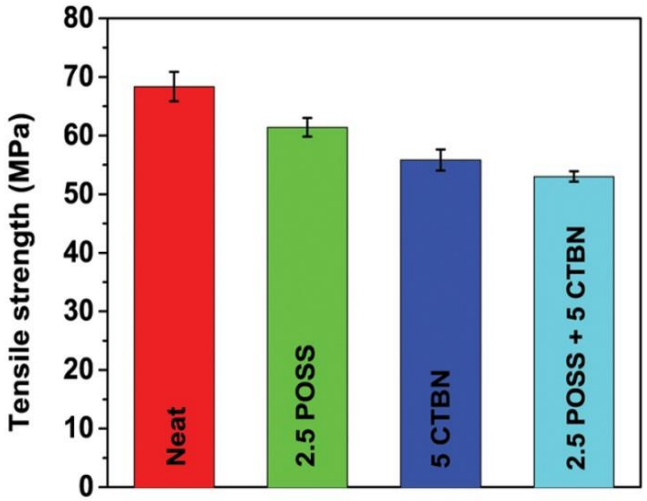


Figure 3.6: Comparison on tensile strength of neat epoxy, phr POSS/epoxy nanocomposite, 5 phr CTBN/epoxy blend and POSS-CTBN/epoxy hybrid nanocomposite

### 3.3.4. Fracture toughness of the epoxy blends and composites

The fracture toughness values of blends and nanocomposites are expressed in terms of the stress intensity factor ($K_{IC}$), are shown in Figure 3.7 and 3.8. Fracture toughness of the blends are found to be higher compared to neat epoxy resin due to the incorporation of CTBN, which is reported widely (Konnola et al., 2015b; Tripathi and Srivastava, 2007; Zilg et al., 2000). A maximum increase of around 62% in $K_{IC}$ for rubber content of 5 phr was observed with respect to the neat crosslinked epoxy system (Figure 3.7). No further increase was found on increasing the loading of rubber. This might be attributed to the bigger size of rubber particles at higher concentrations (Thomas et al., 2008). It is important to mention that the fracture toughness is also improved remarkably by the inclusion of POSS into epoxy matrix. Addition of 2.5 phr POSS gives the maximum toughness for the system (59% increase). A decrease in $K_{IC}$ was observed on further loading which might be due to the agglomeration of POSS nanoparticles. However, the modification of POSS with CTBN gave only 38 % improvement compared to neat epoxy (Figure 3.8). This is

due to the occurrence of high crosslink density created by octa-functional POSS particles near rubber particles which might have reduced the toughening capability of soft rubber particles.

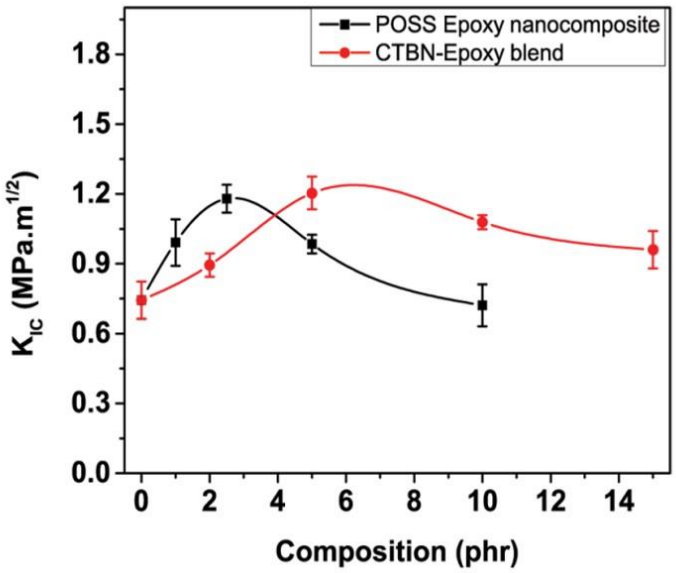


Figure 3.7: Fracture toughness of neat epoxy, POSS/epoxy nanocomposite and CTBN/epoxy blend at various compositions

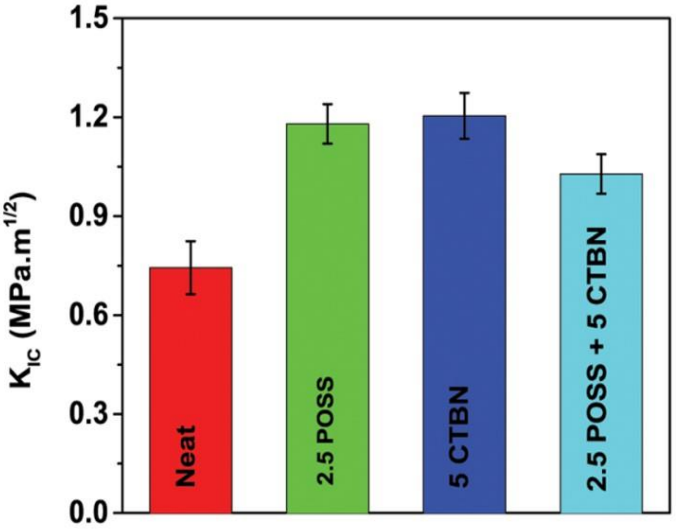


Figure 3.8: Comparison on fracture toughness of neat epoxy, 2.5 phr POSS/epoxy nanocomposite, 5 phr CTBN/epoxy blend and POSS-CTBN/epoxy hybrid nanocomposite

### 3.3.5. Fracture surface morphology by SEM analysis

The HRSEM micrographs of the samples taken after the $K_{IC}$ fracture test are shown in Figure 3.9. The neat epoxy shows a smooth glassy fracture surface with cracks in different planes, which is an indicative of the brittleness of the sample, with no plastic deformation. The fracture surface of rubber/epoxy blends are rougher indicating massive shear deformation (Figure 3.9 (b) and (c)). CTBN/epoxy blends reveals matrix droplet morphology, with rubber particles dispersed in the epoxy matrix. From the micrographs, the particle size increases with increase in rubber content due to coalescence process. The domain size of 5 phr CTBN/epoxy blend is 8 μm and it increases to 15 μm for 10 phr CTBN/ epoxy system. As observed in the previous session, the fracture toughness first increases and a maximum of 1.20 ± 0.07 $MPa.m^{1/2}$ was observed for 5 phr CTBN/epoxy blends. This means that, the optimum particle size is 8 μm for 5 phr CTBN/epoxy blends. The larger particles are very easy to cavitate or get debonded from the epoxy matrix and hence results in reduced toughness for 15 phr CTBN/epoxy blends. (Tian et al., 2011).

From the SEM micrographs, the particles remains intact, reveals good adhesion between the epoxy phase and CTBN phase, hence effective stress transfer between the epoxy matrix and rubber particles is possible. The dispersed rubber particles have white ring marks around it. The white ring mark is because the rubber particles act as stress concentrators upon the application of external load. This will lead to the formation of rubber cavitations (Yee and Pearson, 1986) and plastic deformation of the matrix surrounding the rubber particles. The formation of cavities in the rubber particles is regarded as one of the most important energy dissipating mechanism for rubber toughened epoxies (Zhang et al., 2014). Cavitations of CTBN particles can absorb energy and hence increases the fracture toughness by lowering the local yield stress and provokes extensive shear yielding. The cracks propagate through rubber particles, promoting stress transfer between the epoxy matrix and CTBN particles. The micrographs also reveal some other interesting observations (1)

the cracks are deviated from the original plane due to the rubber particles resulting in an increased surface area of the crack, which also increase the toughness, (2) cracks are pinned by the rubber particles and hence prevent the crack growing to a catastrophic size, (3) rubber particles are able to bridge the cracks and hence prevent the crack growth, (4) restriction of crack propagation by rubber domains. The increase in toughness is due to the combined effect of all these phenomena acting simultaneously on the polymer blend matrix during the applied load.

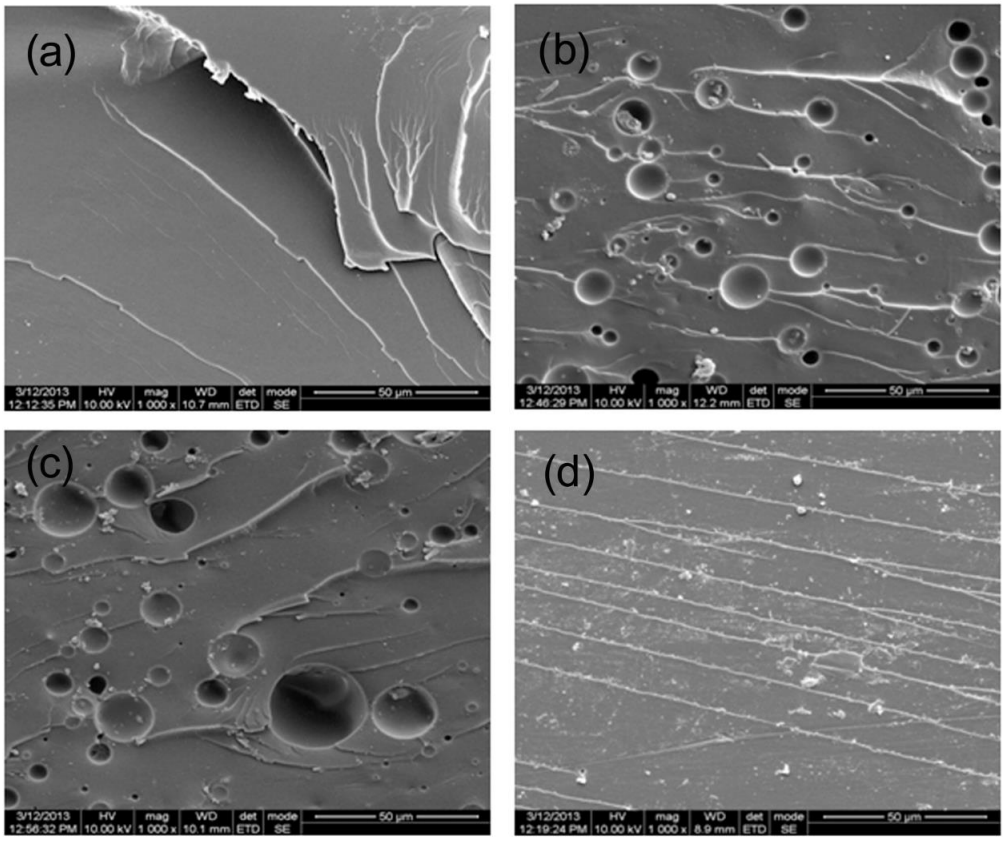


Figure 3.9: FESEM images of fracture surface of (a) neat epoxy (b) 5 phr CTBN/epoxy (c) 10 phr CTBN/epoxy blend and (d) 2.5 phr POSS/epoxy nanocomposite

Figure 3.9 (d) shows the SEM micrograph of 2.5 phr POSS/epoxy system. With the addition of POSS particles, the crack propagation is accompanied by numerous crack steps, which are indicative of the localized crack deflection. The high

degree of roughness on the fractured surface also indicates the deviation of crack from its original plane, resulting in an increased surface area of the crack, which may also lead to an increase in the toughness. FESEM image of fracture surface of POSS-CTBN/epoxy hybrid nanocomposite is shown in Figure 3.10. The micrograph shows some interesting features (1) the rubber particles become different from the smooth quasisphere usually observed in the rubber/epoxy systems, due to the high crosslink density created by octa-functional POSS particles near rubber particles, (2) the rubber particle size decreases from 8 μm to 3 μm which means POSS prevent the coalescence of the CTBN phase. The occurrence of high crosslink density created by octa-functional POSS particles near rubber particles which might have reduced the toughening capability of soft rubber particles, causes decrease in toughness of the hybrid composites. It is important to mention that, the rubber particle size formed in the hybrid composite is less than the optimum size; this may also contribute to the reduction in toughness.

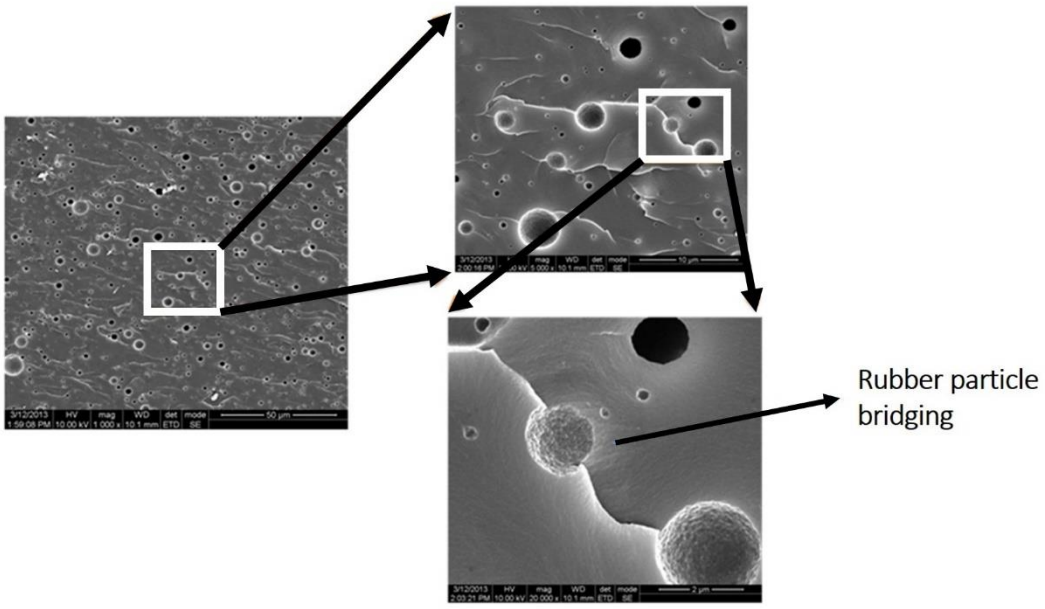


Figure 3.10: FESEM images of fracture surface of POSS-CTBN/epoxy hybrid nanocomposite at different magnifications

### 3.3.6. Dynamic mechanical analysis

Dynamic mechanical analysis helps to study the relaxation behavior and to detect the thermal transitions as well as the changes in storage modulus, loss modulus and tan delta by varying the temperature. This method provides information on the phase separation and the mechanical behavior of a polymer. Dynamic mechanical storage modulus versus temperature of the neat epoxy and representative modified networks containing different loadings of POSS are depicted in the Figure 3.11 (a). Neat crosslinked epoxy shows only one inflection point at the glass transition temperature (*Tg*) of the epoxy. But the crosslinked POSS/epoxy composites shows two inflection points, one at 60 $^{o}$C, which is due to some sites with lower cross-link density in the epoxy network and the other at the glass transition temperature of the cross-linked epoxy system (at around 200 $^{o}$C). The storage modulus (G') decreases with an increase in temperature. The storage modulus values at glassy region and rubbery region are tabulated in Table 3.1. The storage modulus of the POSS/epoxy composites is less than that of the unmodified epoxy network in the glassy region. The *G'* value of neat epoxy and 10 phr POSS at 30$^{o}$C, are 1995 and 1827 MPa respectively. The *G'* value in the glassy region decreases with increasing amount of POSS. On the other hand, the storage modulus of the composites in the rubbery region is higher than neat epoxy. The *G'* value of neat epoxy and 10 POSS at 230 $^{o}$C, are 24.75 and 36.93 MPa respectively. The G' value in the rubbery region increases with increasing amount of POSS. In POSS/epoxy composites there exists lower cross-link density sites in the epoxy network, especially at higher POSS content hence the decrease in the storage modulus in the glassy region. However, at the same time the $T_g$ increases from 208.6 to 214.3 $^{o}C$ and the modulus increase from 24.75 and 36.93 MPa in the rubber state for 10 phr POSS/epoxy composite, clearly indicates there are sites with higher crosslink density in POSS/epoxy composites than neat epoxy. That means that the DMA profile confirms the existence lower and higher crosslink density sites in the POSS/epoxy nanocomposites. Figure 3.11 (b) shows the storage modulus profile of rubber modified epoxy matrix. Storage modulus

decreases as amount of CTBN rubber increases in the epoxy matrix. The inclusion of a soft rubber particle into the epoxy system reduces the stiffness of epoxy matrix thereby reducing the storage modulus.

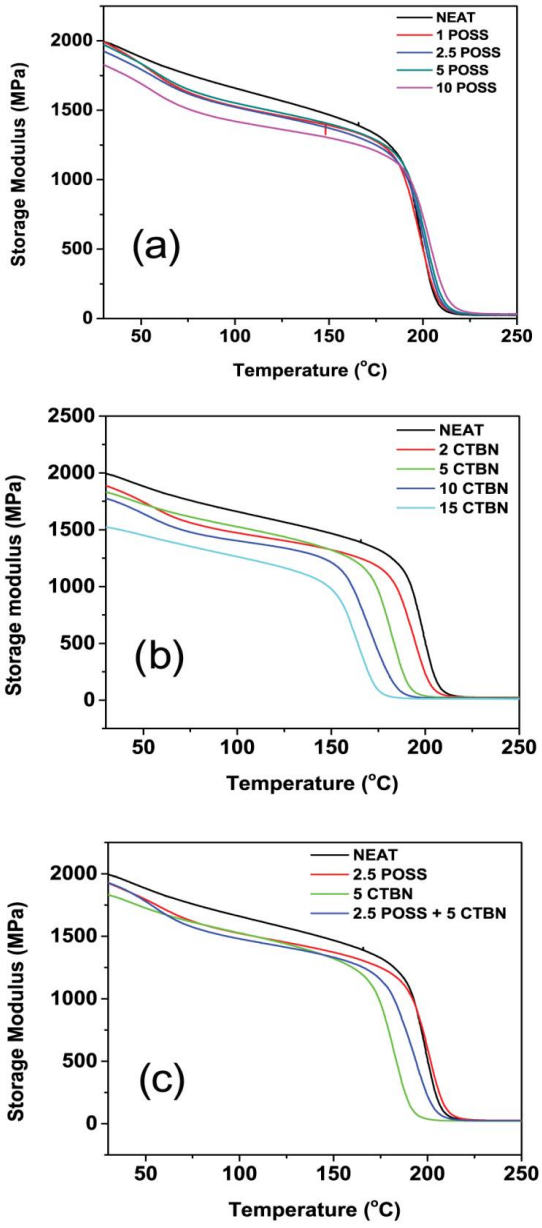


Figure 3.11: Storage modulus versus temperature plot for (a) POSS/epoxy nanocomposites (b) CTBN/epoxy blends (c) neat epoxy, 2.5 phr POSS/epoxy nanocomposite, 5 phr CTBN/epoxy blend and POSS-CTBN/epoxy hybrid nanocomposite

Table 3.1**.** Values of storage modulus (G') at rubbery and glassy region and $T_g$ for the prepared blends and composites

| **POSS content (phr)** | **CTBN content** | **Storage modulus (G') at 30 ºC(MPa)** | **Storage modulus (G') at 230 ºC (MPa)** | ***Tg* (ºC)** | **Constrained region ($C_r$)** |
|---|---|---|---|---|---|
| 0 | 0 | 1995 | 24.75 | 208.6 | - |
| 1 | 0 | 1992 | 28.02 | 210.2 | 0.0183 |
| 2.5 | 0 | 1926 | 27.99 | 212.0 | 0.0187 |
| 5 | 0 | 1973 | 29.93 | 212.6 | 0.0303 |
| 10 | 0 | 1827 | 36.93 | 214.3 | 0.0642 |
| 0 | 2 | 1888 | 24.28 | 204.6 | - |
| 0 | 5 | 1831 | 22.37 | 193.2 | - |
| 0 | 10 | 1777 | 16.49 | 188.1 | - |
| 0 | 15 | 1522 | 10.93 | 176.2 | - |
| 2.5 | 5 | 1929 | 24.55 | 206.2 | - |

The tan $\delta$ curves for neat epoxy system and for the POSS modified epoxy composites are given in the Figure 3.12 (a). The tan $\delta$ peak represents the $T_g$ of the epoxy phase, which increases with the addition of POSS and is maximum for 10 phr POSS modified epoxy system. The decrease in the height of the tan $\delta$ peak of POSS/epoxy nanocomposites is associated with changes in the cross-link density (Li et al., 2001). The addition of the POSS to the epoxy resin increases the cross-link density and hence increases the $T_g$ and lowers the segmental mobility at the $T_g$; hence the peak height decreases. Moreover, the presence of inorganic cages inside the epoxy matrix may hinder the chain mobility of the polymer molecules which generates a constrained polymer around the POSS, which results in an increase in the glass transition temperature. The presence of CTBN decreases the $T_g$ of the epoxy phase, this is also reflected in the epoxy transition peak from the tan $\delta$ profile (Figure

3.12 (b)). This may be attributed to the lowering of cross-linking density of the modified samples. During the curing of epoxy resin, phase separated rubber domains will come in between the reaction sites, thus hindering the cross-linking reaction. This, in turn, reduces the cross-linking density of the cured systems. The lowering of cross-linking density is also due to the dilution effect imparted by the CTBN molecules (Thomas et al., 2007). A comparison of storage modulus versus temperature and tan delta versus temperature of neat, 5 phr CTBN/epoxy blend, 2.5 phr POSS/epoxy and POSS-CTBN/epoxy hybrid nanocomposite are given in Figure 3.11 (c) and 3.12 (c). Modification of POSS with rubber does not have any profound effect on the viscoelastic properties of POSS/epoxy nanocomposite.

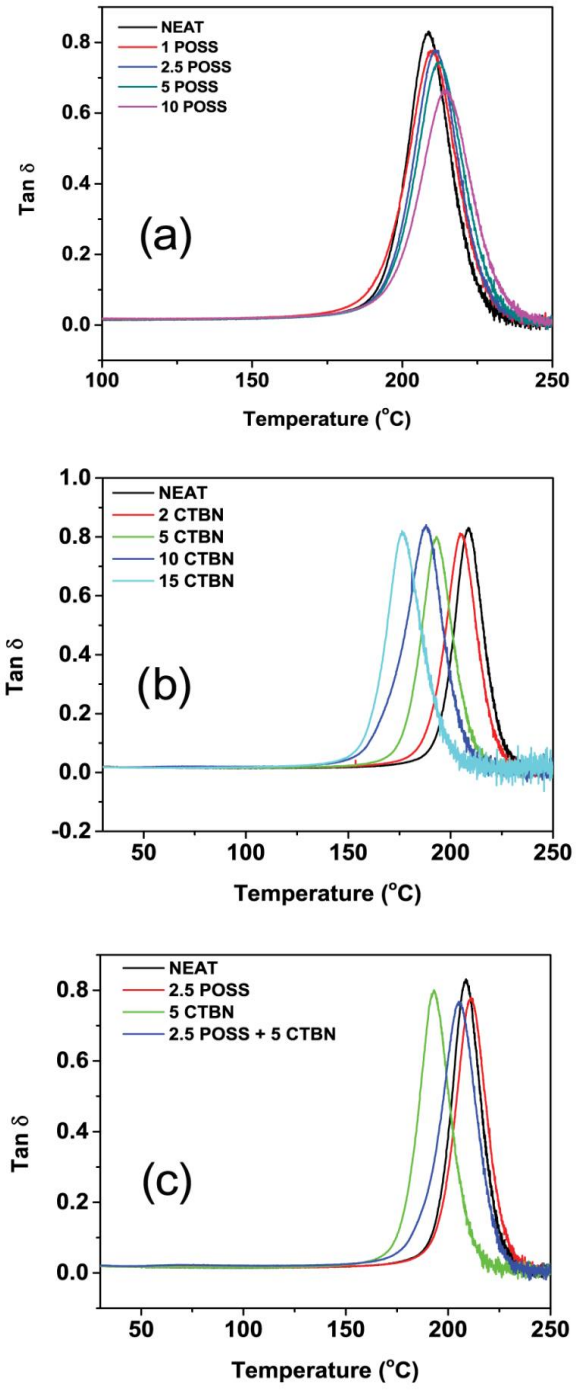


Figure 3.12: Tan delta versus temperature plot for (a) POSS/epoxy nanocomposites (b) CTBN/epoxy blends, (c) neat epoxy, 2.5 phr POSS/epoxy nanocomposite, 5 phr CTBN/epoxy blend and POSS-CTBN/epoxy hybrid nanocomposite

The height depression in the *tan δ* peak indicates that there is a reduction in the amount of mobile polymer chains during the glass transition; therefore the height depression in tan delta peak was used to determine the amount of constrained region in epoxy phase in POSS/epoxy nanocomposites with different POSS content. In polymer nanocomposites, the nanoparticles may interact with the polymer chains thereby limiting the mobility of surrounding polymer chains and hence the formation of constrained regions around the nanofiller with higher $T_g$ (Liang, 2010; Rao and Pochan, 2007). The height depression in the *tan δ* peak and the increase in $T_g$ is considerable for the POSS/epoxy system. The constrained region in each sample can be estimated from the height of the tan *δ* peak.

For linear viscoelastic behavior, the relationship among the energy loss fraction of the polymer nanocomposite *W* and *tan δ* is given by the following equation (Kojima et al., 1993; Varghese et al., 1999).

$$W = \frac{\pi \tan \delta}{\pi \tan \delta + 1} \tag{3.3}$$

The energy loss fraction *W* at the *tan δ* peak is expressed by the dynamic viscoelastic data in the form.

$$W = \frac{(1 - C_r) W_o}{1 - C_o} \tag{3.4}$$

where $C_r$ is the volume fraction of the constrained region, $W_o$ and $C_o$ denote the energy fraction loss and volume fraction of the constrained region of neat epoxy. This equation can be rearranged as follows

$$Cr = 1 - (1 - C_o)\frac{W}{W_o} \tag{3.5}$$

$C_o$ is taken to be *0* (totally amorphous phase in epoxy). The height of the *tan δ* peak is used to calculate *W* according to Eq. (3.3). The calculated constrained region is given in the *Table 3.1*.

Among the POSS/epoxy nanocomposites, 10 phr POSS/epoxy has the highest fraction of constrained region. This means that the maximum interaction between the POSS and epoxy polymer chains is with 10 phr modified POSS. Figure 3.13 shows schematic of POSS nanoparticles covered by a layer of immobilized polymer chains.

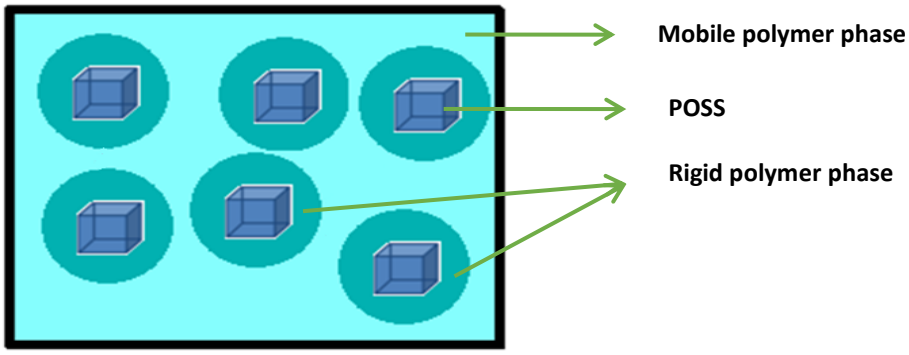


Figure 3.13: Sketch of POSS nanoparticles covered by a layer of immobilized polymer chains

## 3.3.7. Thermal analysis by TGA

Thermal degradation behavior of the blend and composite systems are shown in Figure 3.14. The decomposition of all the systems studied, starts at around 320 $^oC$. For better understanding of the thermal stability of the blend and composite, the weight percentage at different temperatures were taken and are given in Table 3.2. The average weight loss of around 1-2 % up to 300 $^oC$ is due to the release of moisture if any. On the other hand, the weight loss above 320 $^oC$ is related to the decomposition of the polymer. From the thermogram, it is clear that the initial decomposition temperature *(Ti)* for all the composites remain the same indicating that the thermal stability of cured epoxy system was not much affected by the addition of CTBN and POSS. Improvement in char residue from 420-600 $^oC$ is observed by the

addition of POSS which is due to the presence of inorganic core of POSS. To conclude, the modification of POSS with CTBN did not alter the thermal stability of the nanocomposite.

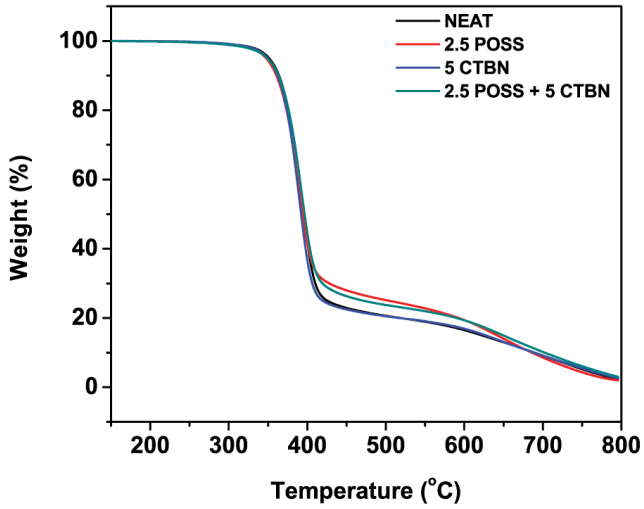


Figure 3.14: TGA curves of neat, 2.5 phr POSS, 5 phr CTBN and POSS-CTBN/epoxy hybrid nanocomposite

Table 3.2. TGA data of epoxy composites at different temperatures

| **Temperature (°C)** | **% residue** | | | |
|---|---|---|---|---|
| | **Neat** | **2.5 POSS** | **5 CTBN** | **Hybrid** |
| 100 | 99.3 | 99.3 | 99.4 | 99.3 |
| 200 | 99.1 | 99.1 | 99.3 | 99.2 |
| 300 | 98.4 | 98.3 | 98.4 | 98.2 |
| 400 | 41.43 | 41.2 | 42.7 | 44.29 |
| 500 | 20.48 | 25.0 | 19.9 | 23.6 |
| 600 | 16.4 | 19.3 | 16.5 | 19.2 |
| 700 | 9.1 | 8.5 | 9.9 | 10.1 |
| 800 | 2.5 | 2.0 | 3.9 | 3.0 |

## 3.4. Conclusions

A novel in-situ hybrid network of DGEBA with glycidyl POSS and CTBN rubber was prepared. The reaction process was carefully monitored and characterized using FTIR and DSC techniques. A comparative study of the properties of the synthesized novel in-situ hybrid nanocomposite was done with POSS/epoxy nanocomposites and CTBN/epoxy blends. The reduction in crosslink density of epoxy network caused by the presence of rubber and POSS resulted in a decrease in tensile strength and storage modulus. DMA profile confirmed the existence of lower and higher crosslink density sites in the POSS/epoxy composites and hybrid nanocomposites. A quantitative analysis of constrained region in POSS/epoxy and hybrid epoxy network was done and found that 10 phr POSS/epoxy has the highest fraction of constrained region and hence better interaction with the matrix. Modification of POSS with rubber does not have any profound effect on the visco-elastic properties of POSS/epoxy nanocomposite. Fracture toughness measurement showed 59 % improvement in $K_{IC}$ for 2.5 phr POSS/epoxy composites as compared to neat epoxy, whereas only 38 % improvement was observed for hybrid nanocomposite. The nature of the fracture surface was studied using FESEM and elucidated the micro-deformation mechanisms occurring at the crack tip that dissipate energy to produce the resulting toughening effect. The decrease in toughness for the hybrid nanocomposites observed is due to the occurrence of high crosslink density created by octa-functional POSS particles near rubber particles which might have reduced the rubber particle size and this in turn, causes the toughening capability of soft rubber particles. The thermal stability of cured epoxy network was not affected by the addition of CTBN, POSS or the chemically modified filler.

# CHAPTER 4

# TOUGHENED EPOXY NANOCOMPOSITES BASED ON POLYMER GRAFTED MULTI-WALLED CARBON NANOTUBES

*The challenges for developing multi-walled carbon nanotube (MWCNT)/epoxy composite with enhanced properties are the dispersion of carbon nanotubes (CNTs) and strengthening the interfacial interaction of CNTs with epoxy matrix. We addressed these issues by doing a novel chemical modification of nanotubes with CTBN and PES. Surface modification was characterized by XPS, Raman and TGA analysis. The effect of surface modification on the nanotube morphology and dispersion status was then evaluated by the TOM, SEM and TEM observations. The tensile tests were performed on the nanocomposites with different amounts of nanotubes. The Halpin–Tsai model was used to study the mechanical behavior. Change in the values of glass transition temperature and storage moduli were determined using dynamic mechanical analysis.*

**Part of this chapter has been published in Polymer for Advanced Technologies, (2016), Vol.27: 82-89 and RSC Advances, (2016), Vol.6: 23887-23899**

# 4.1. Introduction

Owing to its outstanding thermo-mechanical and multifunctional properties, carbon nanotubes (CNTs) are used as reinforcing fillers to fabricate polymer composites. It has been shown that the inclusion of only a small amount of CNTs can significantly improve the functional and mechanical properties of polymer composites (George et al., 2015; Gong et al., 2015; Kuang and Huang, 2015; Kumar et al., 2015). These properties result from the high aspect ratio, low density, exceptional strength and high surface area to volume ratio of the CNTs (Thostenson et al., 2001). But the thermo-mechanical properties of the CNT/polymer nanocomposites were observed to be lower than the theoretical calculations (Coleman et al., 2006; Montazeri et al., 2010). It is attributed to the intrinsic van der Waals force of attraction and high aspect ratio nature of the CNTs due to which they exist in the form of bundles and ropes. Moreover, the weak interfacial bonding between CNTs and polymer matrices may limit the load transfer. A homogeneous dispersion of the CNTs in the polymer matrix is an essential parameter to obtain uniform properties and efficient load transfer during mechanical loading. Surface modification of carbon nanotubes seems to be the most effective way to overcome these problems (Gojny and Schulte, 2004; Sun et al., 2008; Yang et al., 2009). There are two main methods for the surface functionalisation of CNTs. One is the noncovalent attachment of molecules and the second is covalent attachment of functional groups to the walls of the carbon nanotubes (Spitalsky et al., 2010; Tasis et al., 2006). The noncovalent functionalisation involves the adsorption or wrapping of functional molecules on the surface of CNTs. But the lack of chemical bonding results in poor interfacial interaction between CNTs and the polymer matrix, which in turn results in reduction of the effective reinforcement of CNTs. The covalent attachment of functional groups to the surface of nanotubes offers the opportunity for chemical interactions with the epoxy systems and improve the efficiency of load transfer. These functional groups attached could be small molecules or polymer chain (Bahr and Tour, 2001; Datsyuk

et al., 2008; Gónzalez-Dominguez et al., 2011; Yoonessi et al., 2014). Polymer functionalized CNTs have attracted more attention due to the presence of multiple anchor units for surface attachment as well as effective compatibility between the functionalised CNTs and the hosting polymer matrix. There are some previous works demonstrating the grafting of a variety of polymers on the surface of nanotubes. Hayashida et al. (2015) covalently anchored poly(methyl methacrylate) (PMMA)-grafted multi-walled CNTs, and then dispersed into additional PMMA matrix, yielding highly insulated PMMA–CNT composites. In the work of Ilcíková et al. (2014) multi-walled carbon nanotubes (MWCNT) has been covalently modified by short polystyrene chains to improve their dispersion in polystyrene-b-polyisoprene-b-polystyrene (SIS) thermoplastic elastomer and prevent deterioration of its elastic properties after incorporation of the MWCNTs. Daugaard et al. (2014) prepared Poly(lauryl acrylate) and poly(stearyl acrylate) grafted multi-walled carbon nanotubes and tested in PP composites to elucidate their efficiency for compatibilization. Diez-Pascual et al. (2010) described the grafting of a hydroxylated poly(ether ether ketone) (HPEEK) derivative onto the surface of acid-treated single-walled carbon nanotubes (SWCNTs). The HPEEK-grafted SWCNTs has been used as fillers to prepare PEEK nanocomposites with enhanced performance.

Recently, the incorporation of CNTs into epoxy matrix is gaining significant interest in the structural composite application, where strength, stiffness, durability, lightweight, design, and process flexibility are required such as in aerospace and automobile industry (Jakubinek et al., 2015). The inherent brittle nature of the epoxy matrix can be improved by the presence of nanotube in the matrix (Jyotishkumar et al., 2013; Martinez-Rubi et al., 2011). However, a better improvement in toughness and mechanical strength can be expected if the CNTs are previously functionalized with reactive liquid rubbers which consist of multiple functional groups. Besides homogeneous dispersion, the chemical modification of the CNTs with reactive liquid rubbers can create a soft interface between CNTs and polymer which can result in a better load transfer from matrix to filler. CTBN is a liquid rubber whereas hydroxyl

terminated poly(ether sulfone) PES is an engineering thermoplastic. Both these polymers are conventionally used as toughening in epoxy system. The functionalisation of these polymers to MWCNTs ensures a uniform coating of polymer on the CNT surface and offers the opportunity to enhance both the mechanical and toughening properties of the epoxy system.

This work discusses the benefits of polymer functionalisation of MWCNTs using CTBN and PES and its use as filler to epoxy so as to develop improved matrix material with the aim of attaining higher fracture energy without compromising the mechanical and thermal properties of the epoxy resin. The specific objective of this study is to examine the influence of grafting CTBN and hydroxyl terminated PES on MWCNTs and hence to examine its influence on the morphology, mechanical, thermal and viscoelastic properties of the polymer grafted MWCNT/epoxy system.

# 4.2. Materials and Methods

## 4.2.1. Materials

DGEBA (Lapox ARL-135) and hardener DDS (Lapox K10) were purchased from Atul India Pvt Ltd, Gujarat. MWCNT (Nanocyl 3100) was procured from Nanocyl, Belgium. It was synthesized by chemical vapor deposition and had an average diameter 9.5 nm, average length 1.5 micron and purity of > 95 %. CTBN (MW-3600 g/mol),2-(2-chloroethoxy)ethanol, sodium azide, Thionyl chloride ($SOCl_2$), Dicyclohexylcarbodiimide (DCC),4-(Dimethylamino)pyridine (DMAP), N-Methyl-2-pyrollidone (NMP), and N,N-Dimethylformamide (DMF, 99.5 %)were purchased from Sigma-Aldrich, Bangalore, India. The engineering thermoplastic PES was obtained from Vikram Sarabhai Space Centre, Thiruvananthapuram. All the chemicals were used as received without further purification.

## 4.2.2. Chemical modifications on carbon nanotubes

### 4.2.2.1. Synthesis of 2-(2-azidoethoxy)ethanol

2-(2-azidoethoxy)ethanol was synthesized from 2-(2-chloroethoxy)ethanol using a procedure similar to the one developed by Matyjaszewski et al. (2005). In a typical experiment,2-(2-chloroethoxy)ethanol (124.5 g, 1 mol) and sodium azide (130 g, 2 eq.) were added to 1000 mL water in a 2 L two-necked round-bottom flask equipped with mechanical stirrer. Subsequently, the mixture was stirred at 75 °C for 96 h. After cooling to room temperature, the mixture was extracted with diethyl ether (5 × 100 mL). The organic mixture was dried over magnesium sulfate overnight and concentrated on a rotary evaporator. The obtained residues were distilled under reduced pressure to give colorless oil in 78 % yield. $^{1}$H NMR (500 MHz; $CDCl_3$): δ 2.69 (b, 1 H), 3.40 (t, 2 H, *J* = 4.9 Hz), 3.57-3.60 (m, 2 H), 3.65-3.69 (m, 2 H), 3.70~3.75 (m, 2 H). $^{13}$C NMR (125 MHz; $CDCl_3$): δ 50.7, 61.7, 70.0, 72.5. MALDI-TOF/TOF MS $(M)^+$ 131.22.

### 4.2.2.2. Preparation of MWCNT-g-CTBN

For the preparation of CTBN grafted MWCNTs (MWCNT-g-CTBN), hydroxyl functionalisation of MWCNTs was carried out. Hydroxyl functionalized nanotubes (MWCNT-OH) was prepared via the addition of nitrene formed by thermolysis of 2-(2-azidoethoxy)ethanol to strained double bonds of MWCNTs (Zhang et al., 2008). A 100 mg portion of MWCNTs were dispersed in 15 mL of NMP in an R.B flask by ultrasonication for 2 h to give a homogeneous suspension. The functionalization was performed by the addition 5 g of 2-(2-azidoethoxy) ethanol at room temperature and the mixture was heated at 160 °C for 18 h in a nitrogen atmosphere. After cooling to room temperature, the mixture was filtered through a 0.22-μm Teflon membrane and washed multiple times with acetone (100 mL) and distilled water (100 mL) to completely remove the unreacted 2-(2-

azidoethoxy)ethanol. After being dried under vacuum at 60 $^{o}$C for overnight, the functionalized MWCNTs containing hydroxyl groups were obtained (108 mg).

For the preparation of MWCNT-g-CTBN, 500 mg of MWCNT-OH was dispersed in 125 mL of anhydrous dimethylformamide (DMF) by sonication for 30 minutes. The MWCNT-OH solution was added to a two-necked flask containing a 5 gram solution of CTBN in 125 mL of DMF. Subsequently, a solution of DCC (20.6 g, 100 mmol) and DMAP (1.2 g, 10 mmol) in DMF (250 mL) was added under nitrogen and the reaction was allowed to proceed at 40 $^{o}$C for 68 h. The resulting product was filtered, washed with methanol, and dried under vacuum at 60°C for 24 h to get MWCNT-g-CTBN (645 mg). Schematic of the preparation of MWCNT-g-CTBN from pristine MWCNTs is given in Figure 4.1.

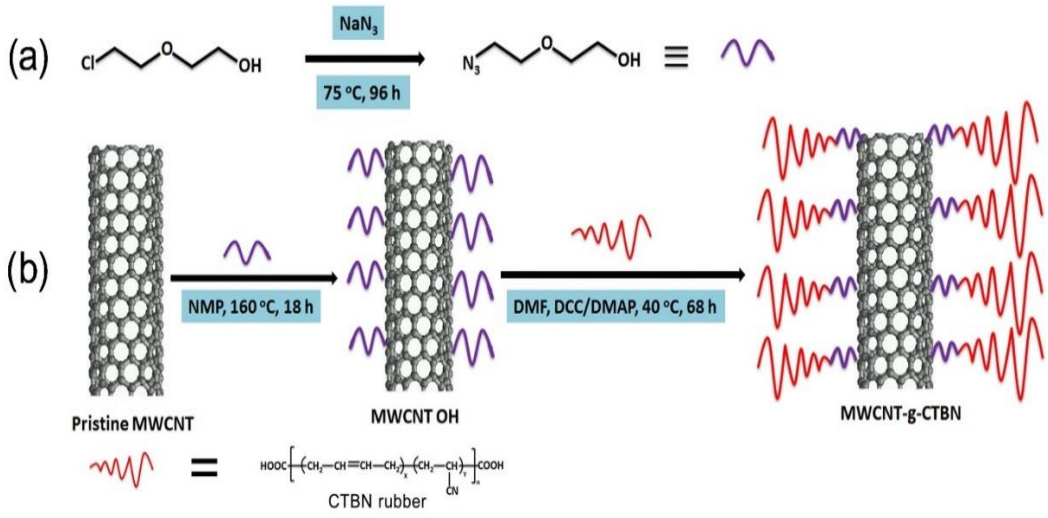


Figure 4.1: Schematic showing the preparation of (a) 2-(2-azidoethoxy)ethanol and (b) MWCNT-g-CTBN from pristine MWCNTs

### 4.2.2.3. Preparation of the MWCNT-g-PES

The nanotube was first oxidized with nitric acid to attach carboxylic acid groups on their surface. The carboxylation procedure was done using existing

procedure reported elsewhere (Datsyuk et al., 2008). Typically, 300-mg portion of pristine nanotubes was added to 25 mL of 70% concentrated nitric acid. The mixture was refluxed at 90$^{o}$C for 6 hours. Then, the mixture was diluted five times its original volume with distilled water, and then filtered through a PTFE filter (0.45-μm pore size). It was washed with excess of water until no residual acid was present.

PES grafted MWCNTs (MWCNT-g-PES) was prepared by the following procedure. Carboxylated MWCNTs (100mg) were dispersed in anhydrous DMF (25 mL) using an ultrasound bath for 30 minutes. Subsequently, they were treated with excess $SOCl_2$ (30 mL) for 18 h under reflux and the residual $SOCl_2$ was removed by distillation under reduced pressure to yield the acyl-chloride-functionalized MWCNTs. Hydroxyl terminated PES (1 g) was dissolved in DMF (65 mL) and 2 mL pyridine was added. The chloroacylated nanotubes were then added to the polymer solution and the reaction was allowed to continue for 4 days at 60$^{o}$C under nitrogen flow and mechanical stirring to yield MWCNT-g-PES. After cooling to room temperature, the resulting compound was filtered through a PTFE membrane (0.45 μm pore size) and washed thoroughly with DMF to remove excess PES and then with distilled water. Then it was rinsed with distilled ethanol and dried under vacuum at 100$^{o}$C for 2 days. Schematic of the preparation of MWCNT-g-PES from pristine MWCNTs is given in Figure 4.2.

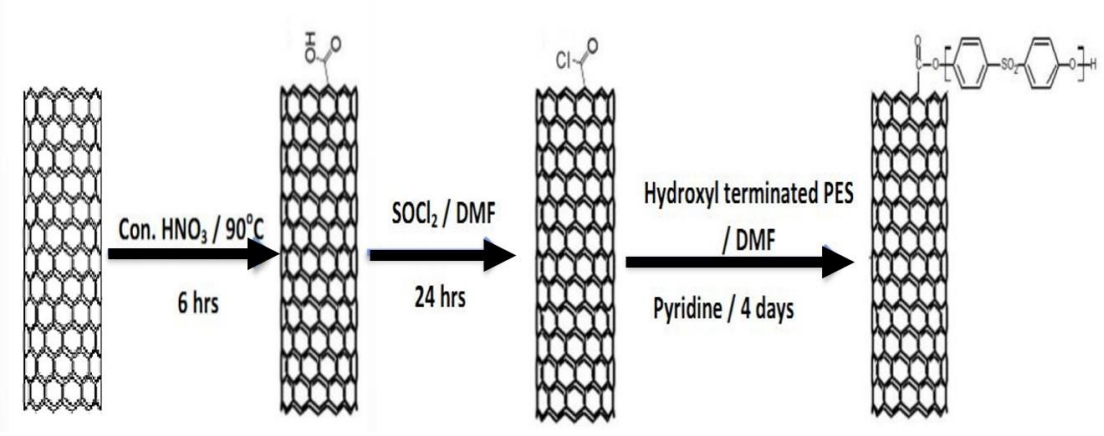


Figure 4.2: Schematic showing the preparation of MWCNT-g-PES from pristine MWCNTs

### 4.2.3. Preparation of unmodified and modified MWCNT/epoxy nanocomposites

MWCNT/epoxy nanocomposites containing different compositions of nanotube were prepared as follows. Epoxy resin was sonicated with required amount nanotubes in acetone for 30 minutes. Acetone was evaporated off by heating at 90 $^{o}$C for 2 hours. This MWCNT/epoxy nanosuspension was mixed with molten hardener in the 100:35 ratio and degassed for 5 minutes in a vacuum oven. The mixture was then transferred into pre heated mold and cured at 180 $^{o}$C for 4 h. Post curing was done at 200 $^{o}$C for 1 h. Flow chart of the preparation of MWCNT/epoxy composite is shown in Figure 4.3.

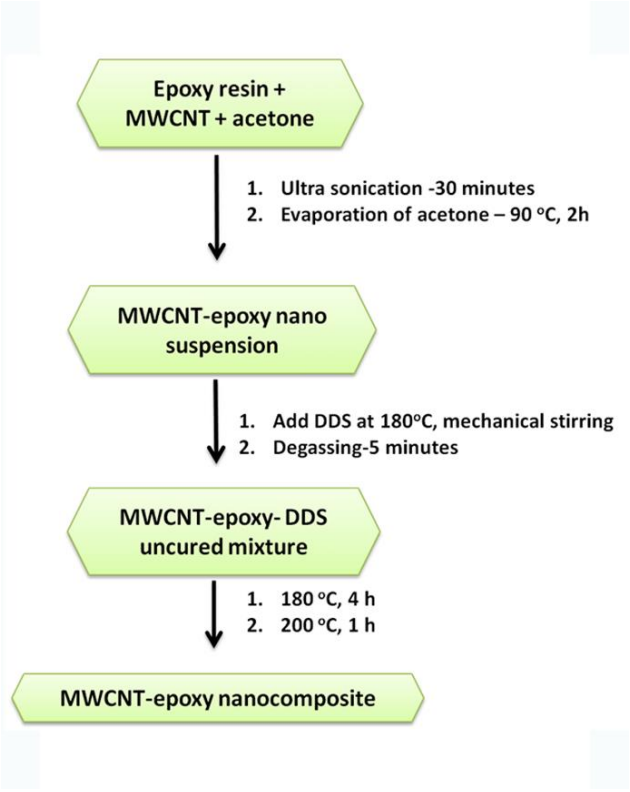


Figure 4.3: Flow chart of the preparation MWCNT/epoxy composites

## 4.2.4. Characterization

Fourier transform infrared spectroscopy (FTIR) analysis was carried out using a Perkin Elmer System series 100 spectrophotometer in a frequency range of 4000–500 $cm^{-1}$ with a spectral resolution of 4 $cm^{-1}$. Rheological analysis was done using modular rheometer (MCR102, Anton Paar, USA), using a 50 mm parallel plate assembly at room temperature. The morphology of a fractured surface of the sample was analyzed using Scanning electron microscope (SEM, FEI Quanta FEG200). The investigation of viscoelastic properties was performed using dynamic mechanical analyzer (DMA 800, Perkin Elmer, USA). Rectangular specimens of 20 x 5 x 2 $mm^3$ were used for the analysis. The analysis was done in single cantilever mode at a frequency of 1 Hz, from ambient to 250 $^oC$ and at a heating rate of 2 $^oC$/min. Thermal stability of nanocomposites was analyzed using a thermogravimetric analyzer (Q-50, TA Instruments, USA). The samples were heated from ambient to 800 $^oC$ at a ramp rate of 10 $^oC$/ min. The tensile strength of the sample was measured using universal testing machine (Instron 5984, Instron, USA) at a crosshead speed of 1mm/min (as per ASTM standard D638). Fracture toughness of the specimens was determined according to ASTM D 5045-99. Single edge notch specimens of 46 × 6 × 3$mm^3$ (span length =24 mm) were used to measure the fracture toughness of the epoxy nanocomposites.

### 4.2.4.1. Nuclear magnetic resonance spectroscopy (NMR)

NMR spectra of 2-(2-azidoethoxy)ethanol dissolved in $CDCl_3$ were recorded on a Bruker AVANCE II-500 spectrometer. The spectra were internally referenced to a tetramethylsilane (TMS) standard.

#### 4.2.4.2. X-ray photoelectron spectroscopy (XPS)

XPS was carried out with a Kratos Axis Ultra DLD spectrometer, using Al Kα excitation radiation.

#### 4.2.4.3. Raman spectroscopy

Raman spectra were recorded from 100 to 3000 $cm^{-1}$ on a Raman spectrometer (INVIA, England) with a 514 nm argon ion laser.

#### 4.2.4.4. High resolution transmission electron microscopy (HRTEM)

The high-resolution transmission electron microscopy (HRTEM) was conducted using JEOL JEM-2100 with an acceleration voltage of 200 kV being equipped with an EDX spectrometer. Sliced thin sections of MWCNT/epoxy composites with a thickness of about 60-80 nm, prepared by ultra-microtomy, were used to take the TEM images of the composites.

#### 4.2.4.5. Transmission optical microscopy (TOM)

Optical microscopy analysis was carried out with Leica DM1000 LED (Leica Microsystems, Germany) in transmitted light configuration. The analysis was done on a small droplet of the epoxy suspension placed on a microscope glass.

# 4.3. Results and Discussion

## 4.3.1. Characterization of 2-(2-azidoethoxy)ethanol

Figure 4.4 shows the FTIR spectra of (a) 2-(2-chloroethoxy)ethanol and (b) 2-(2-azidoethoxy)ethanol. 2-(2-chloroethoxy)ethanol shows a characteristic absorption peak of C-Cl at around 745 $cm^{-1}$. Apart from this, a broad band centered around 3400 $cm^{-1}$, referred to the stretching of OH groups, as well as peaks at 2870 and 2930 $cm^{-1}$, attributed to the C–H stretching vibrations were also observed. The peak at 1121 $cm^{-1}$ of chloroethoxyethanol is due to the C-O stretching. In the FTIR spectrum of 2-(2-azidoethoxy)ethanol, the disappearance of the C-Cl stretch after the reaction with sodium azide and the appearance of the characteristic absorption of azido groups at ca. 2094 $cm^{-1}$ indicates that most of the chloride groups have been substituted with azide groups. Furthermore, a band appears at 1284 $cm^{-1}$ referring to the C–N stretching vibration.

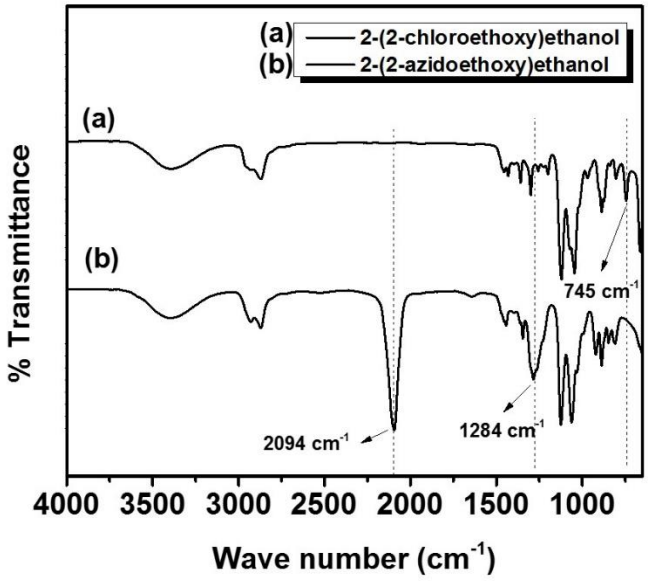


Figure 4.4: FTIR spectra of (a) 2-(2-chloroethoxy)ethanol and (b) 2-(2-azidoethoxy)ethanol

## 4.3.2. Characterization of grafting of CTBN and PES on MWCNTs

### 4.3.2.1. XPS analysis

XPS was employed to evaluate the chemical bonds formed on the surface of nanotube before and after its functionalization with CTBN and PES. Figure 4.5 and 4.6 shows the survey data of the pristine and chemically modified nanotube samples. Pristine MWCNTs exhibit a strong peak at 285 eV due to C 1s and a peak of very low intensity at 532 eV due to O1s from the defects of nanotube. After functionalization with CTBN, a significant increase in the O1s peak is observed. A new peak at 400 eV is observed (N1s) for MWCNT-OH and MWCNT-g-CTBN. In additional to this, two new peaks are observed at 164 eV and 232 eV are observed for MWCNT-g-PES which corresponds to the S2p and S1s respectively. This increased intensity of elements is originated from the presence of organic moieties which confirmed the success of the modification. The higher resolution data of C1s area of the CNTs, MWCNT-OH and MWCNT-g-CTBN are shown in Figure 4.7 (a), 4.7 (b), and 4.7 (c) respectively. For pristine MWCNT, the main peak at 284.5 eV is attributed to the $sp^2$ hybridized graphite-like carbon atoms (C=C), a peak at 285.1 eV corresponds to $sp^3$ hybridized carbon atoms arising from defects on the nanotube structure (C-C), a peak at 286.2 eV related to carbon–oxygen single bonds in alcohols, phenols and ethers (C–O), a peak at 288.9 eV attributed to carbon–oxygen double bonds in carboxylic acids, carboxylic anhydrides and esters (O-C=O) and finally a peak at 291.6 eV, the typical position of the π–π* shake-up satellite peak from the $sp^2$-hybridised carbon atoms (Datsyuk et al., 2008; Kolacyak et al., 2011; Lee et al., 2011). In the C1s spectra of the MWCNT-OH, the peak intensity of hydroxyl groups is much higher than that in pristine MWCNT, indicating the reaction has occurred between nanotube and the organic moiety. The disappearance of π–π* shake-up transition can be ascribed to the increased disruption of the π-electron system, indicating a significant change in the electronic structure of the CNT sidewalls. In the case of C1s high resolution spectrum of MWCNT-g-CTBN, the significant intensity increment of the

band at 288.9 eV (corresponds to O-C=O groups) suggests the covalent grafting of MWCNT with CTBN. Deconvolution of the N 1s spectrum shown in Figure 4.7d displays two contributions with binding energies of 399.6 eV and 401 eV, respectively. The former is ascribed to the C≡N from the polymer, while the latter is due to C-N, suggesting the successful covalent functionalization of MWCNT by CTBN (Górka et al., 2013). Figure 4.8 (b) shows the high resolution C1s spectra of MWCNT-g-PES which showed an increase in the intensity of peak at 285.1 eV due to the presence of C-S bond.

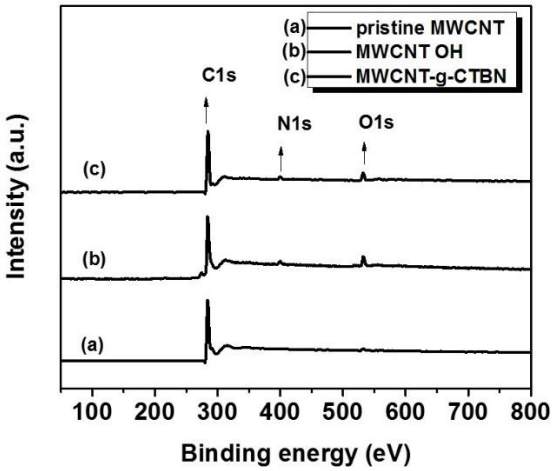


Figure 4.5: XPS survey spectra of (a) pristine MWCNTs, (b) MWCNT-OH and (c) MWCNT-g-CTBN

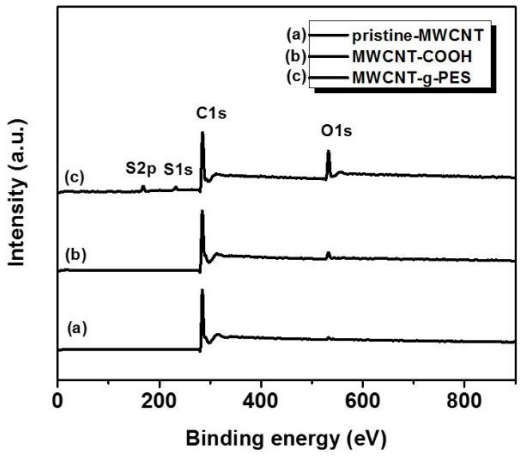


Figure 4.6: XPS survey spectra of (a) pristine MWCNTs, (b) MWCNT-COOH and (c) MWCNT-g-PES

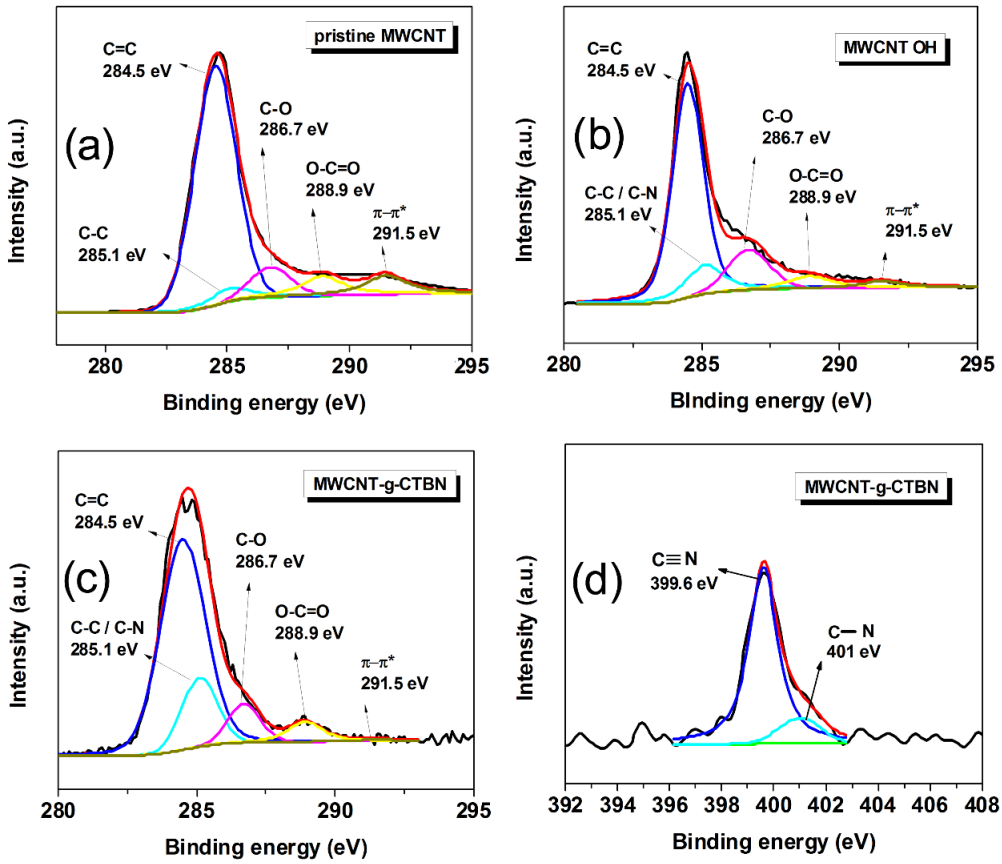


Figure 4.7: High resolution C1s spectra of (a) pristine MWCNTs, (b) MWCNT-OH and (c) MWCNT-g-CTBN; (d) High resolution N1s spectra of MWCNT-g-CTBN.

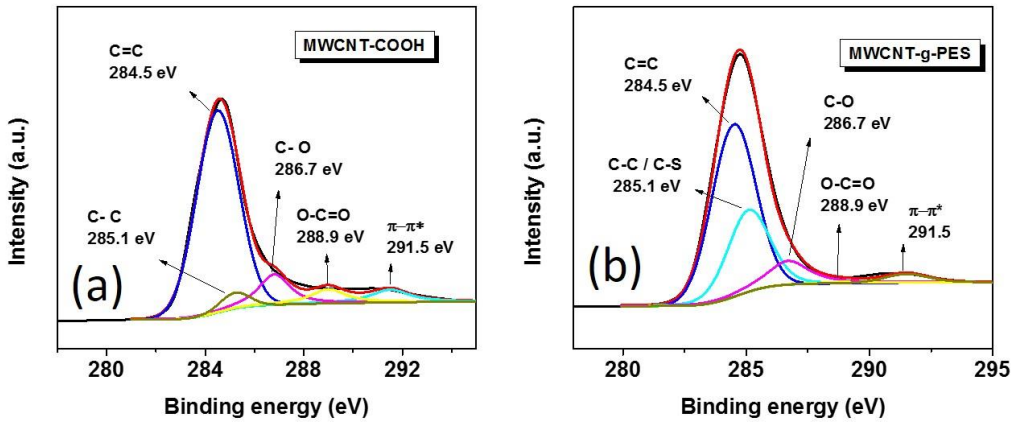


Figure 4.8: High resolution C1s spectra of (a) MWCNT-COOH and (b) MWCNT-g-PES

#### 4.3.2.2. Raman spectroscopy

Because of its high sensitivity to the structural change, Raman spectroscopy is commonly used to characterize the structural and electronic properties of carbon-based materials. Raman spectroscopy of three different MWCNTs is shown in the Figure 4.9. Raman spectrum of the carbon nanotube is usually characterized by three main features. The band at around 1572 $cm^{-1}$ is from the in-plane vibrations of $sp^2$-hybridized graphitic carbon, and hence is called the tangential or G-band. Defects and functional groups on the walls or ends of the CNTs, or amorphous carbon give rise to the so-called disorder (D) band corresponding to $sp^3$-carbon, which is located around 1340 $cm^{-1}$. The D' band which is a weak shoulder of the G-band at higher frequencies is also a double resonance feature induced by disorder and defects (Datsyuk et al., 2008). The intensity area ratio of the D to G bands, $I_D/I_G$, can serve as a standard to measure the defects of CNTs. The bigger the ratio, the greater is the defect which in turn indicates the presence of more groups on the surface of MWCNTs. The values of $I_D/I_G$ for MWNT-OH (1.87), MWCNT-g-CTBN (1.89), MWCNT-COOH (1.82) and MWCNT-g-PES (1.86) are greater than that of pristine MWNTs (1.60), which indicate the increase of defects in MWCNTs due to the chemical functionalization. The sequential functionalization of polymer functionalized nanotubes did not result in the obvious increase in the D-band intensity, which likely because the polymer was not directly linked on the carbons of CNTs.

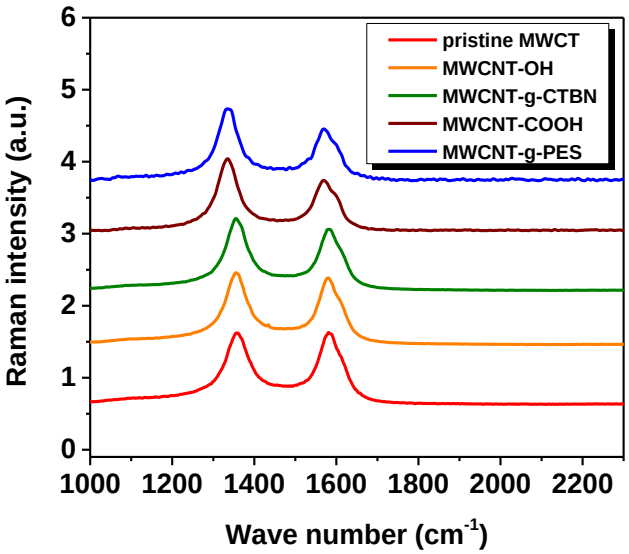


Figure 4.9: Raman spectra of pristine and functionalized multi-walled carbon nanotubes

### 4.3.2.3. Thermogravimetric analysis

Figure 4.10 shows representative TGA thermograms under nitrogen atmosphere of the pristine MWCNT, MWCNT-OH and MWCNT-g-CTBN. Due to the differences in the thermal stability of the carbon nanotube structure and the polymer moieties, by TGA analysis it is possible to gain a reliable estimation of the relative amount of introduced functionalities. The pristine MWCNTs are thermally stable up to about 550 $^{o}$C. For the MWCNT-OH, however, a slight decrease in weight was observed at approximately 200 $^{o}$C, corresponding to decomposition of organic groups. In the case of MWCNT-g-CTBN, the weight-loss region from 250 °C to 450 °C, has a weight loss of 50 wt % that is caused by the pyrolysis of the CTBN polymer. With the weight loss of the pure CTBN below 500 $^{o}$C as a reference, the concentration of CTBN in MWCNT-g-CTBN was estimated as 38 %. Figure 4.11 shows representative TGA thermograms of the pristine MWCNT, MWCNT-COOH and MWCNT-g-PES. The carboxylated nanotubes degrade faster than the pristine nanotubes due to the presence of more ‘kink’ structures from the carboxylation of the backbone. The PES grafted MWCNTs shows TGA pattern similar to that of the PES.

Major decomposition due to the graft occurs at the temperature of 550 $^{o}$C. 60 % weight loss was observed for the polymer alone in the TGA analysis. Based on these mass loss data, the concentration of PES in MWCNT-g-PES was estimated as 58 % (mass loss is 35 %).

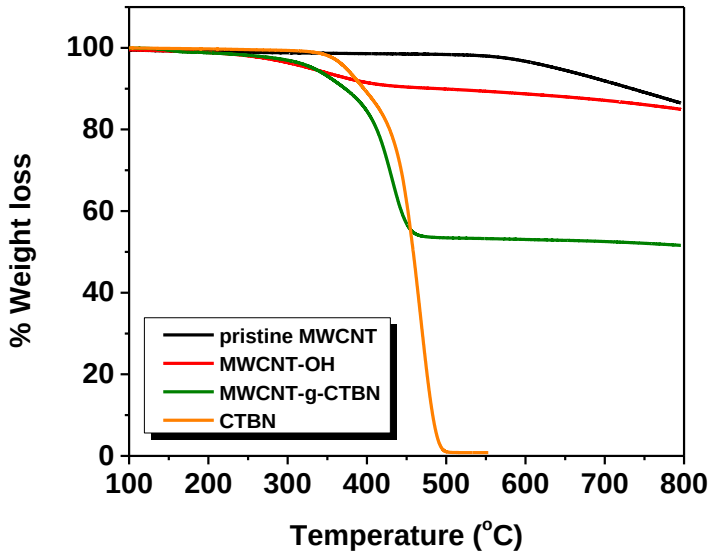


Figure 4.10: TGA of CTBN, pristine MWCNTs, MWCNT-OH and MWCNT-g-CTBN

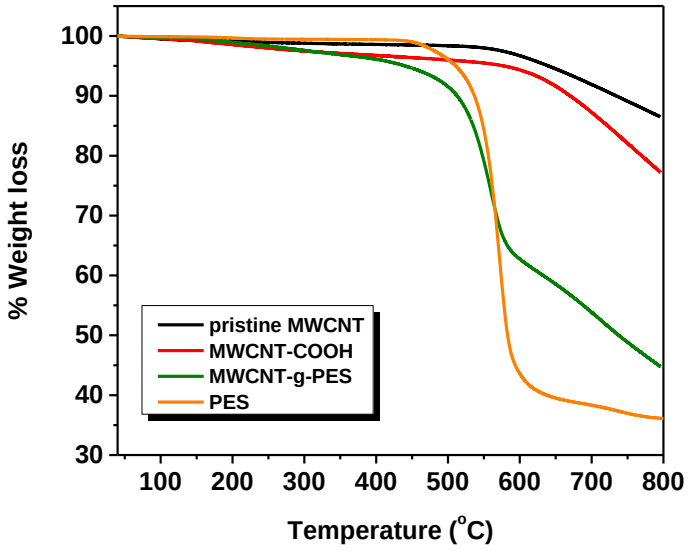


Figure 4.11: TGA of PES, pristine MWCNTs, MWCNT-COOH and MWCNT-g-PES

#### 4.3.2.4. TEM analysis

The microstructures of pristine MWCNTs, MWCNT-g-CTBN and MWCNT-g-PES were further characterized by HRTEM. Figure 4.12 (a) is the image of the pristine MWCNTs, in which the tube surface is relatively smooth and clean. The TEM microphotograph of polymer functionalized nanotubes shows that the surface of MWCNT is fully enwrapped with the amorphous polymer which is quite continuous all along the CNTs (Figure 4.12 (b) and (c)), implying that the covalent attachment of polymers had been achieved. The thickness of the wrapped polymer layer for MWCNT-g-CTBN is about 10 to 20 nm whereas for MWCNT-g-PES, the thickness is around 6-12 nm.

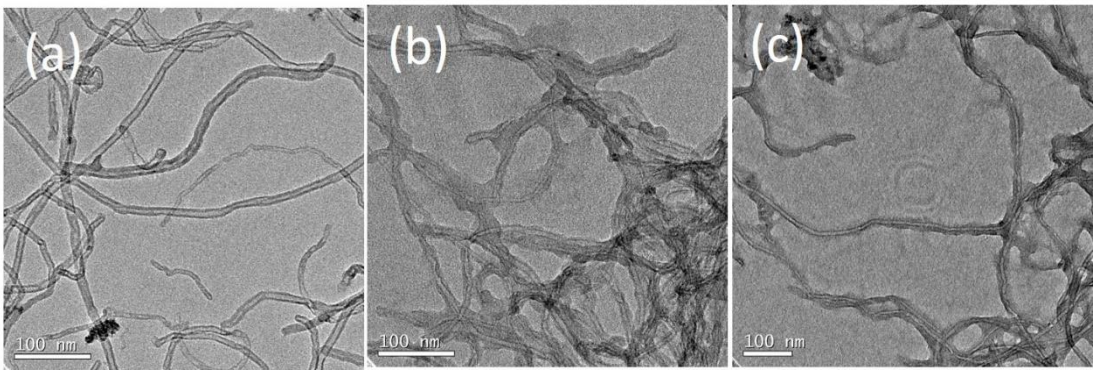


Figure 4.12: TEM images of (a) pristine MWCNTs and (b) MWCNT-g-CTBN and (c) MWCNT-g-PES

### 4.3.3. Dispersion behavior of epoxy nanosuspension and composites

#### 4.3.3.1. Transmission Optical Microscopy (TOM)

TOM observation of dispersion level of CNTs in epoxy is useful to examine changes in dispersion state and interfacial bonding affected by the surface modification. TOM observations of the epoxy suspensions revealed the presence of MWCNTs aggregates. There were some zones with very high local MWCNT

concentrations, as shown in Figure 4.13. In fact, the pristine MWCNT samples were very viscous, and the homogenization process was difficult. The agglomerates that result from the existence of strong van der Waals interactions between individual tubes together with large aspect ratio of CNTs is due to which nanotubes exists as a highly entangled network. By contrast, after the surface functionalization with polymer molecules, the dispersion of polymer functionalized nanotubes becomes relatively better although some small agglomerates are still observed. The reason for the differences in the MWCNT dispersion between both pristine and polymer functionalized nanotubes was the uncoiling of nanotubes during functionalisation and enhanced interfacial interaction between the nanotube and resin. The functionalisation seems to be favorable for the dispersion for the MWCNT in epoxy matrix.

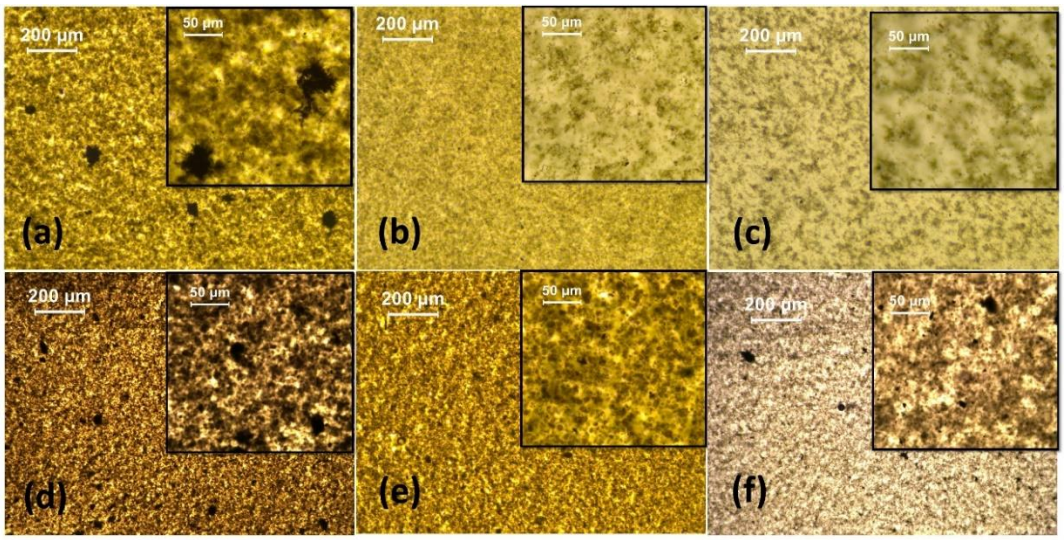


Figure 4.13: TOM images of epoxy nanosuspensions containing (a) 0.2 wt% pristine MWCNTs, (b) 0.2 wt% MWCNT-g-CTBN, (c) 0.2 wt% MWCNT-g-PES(d) 0.4 wt% pristine MWCNTs (e) 0.4 wt% MWCNT-g-CTBN and (f) 0.4 wt% MWCNT-g-PES. Insets show high magnification images

### 4.3.3.2. Rheology

The rheological properties of the MWCNT/epoxy dispersions play a crucial role in the processing and mechanical features of epoxy nanocomposites. Plots of viscosity vs shear rate of the pure epoxy, the pristine-MWCNT/epoxy composites, and the surface modified MWCNT/ epoxy composites are shown in Figure 4.14 to demonstrate the significance of viscosity build up and shear thinning in the epoxy nanosuspension system. The addition of pristine MWCNTs to epoxy resulted in an abrupt increase in viscosity at low shear rates. The pristine-MWCNTs were composed of bundles of nanotubes which are highly entangled. These nanotubes exist as many aggregates of different sizes in the epoxy resin. The aggregates would be obstacles to uniform dispersion of the MWNTs and were hardly broken into individual tubes in the epoxy resin. The dispersion and homogenization was very difficult. The viscosity of polymer functionalized MWCNT epoxy suspension is observed to be much lower than that of MWCNT/epoxy suspension at low shear rates. This arises from a better dispersion of functionalized MWNTs within the epoxy resin suspensions. At high shear rates, both nano-fillers show good dispersion due to disentanglement of nanotubes at very high shear forces.

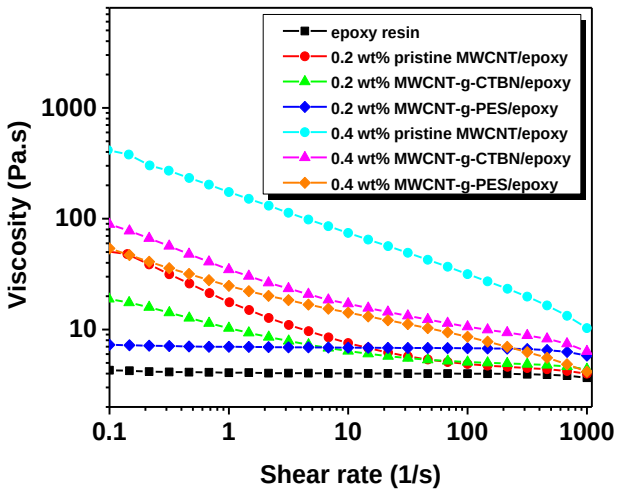


Figure 4.14: Variation of viscosity with shear rate for epoxy nano suspension of pristine MWCNTs, MWCNT-g-CTBN and MWCNT-g-PES

The epoxy composites filled with the poorly dispersed CNTs exhibit stronger non-Newtonian behavior than ones with the well dispersed CNTs. The shear thinning effects of the suspensions were quantified by calculating the pseudo-plasticity index n. The shear dependency of the viscosity of solutions is usually given by the power law (Devasia et al., 2005).

$$\tau = \eta\gamma^{n} \tag{4.1}$$

Experimental data were fitted by the power law equation for different epoxy nano suspension systems. A typical plot between shear rate (log $\gamma$) and shear stress (log $\tau$) is presented in Figure 4.15 for epoxy resin, pristine MWCNT/epoxy nanosuspension and polymer functionalized MWCNT/epoxy nanosuspensions. The slope of the plots of shear rate (log $\gamma$) vs shear stress (log $\tau$) provided the pseudo plasticity index ($n$). Usually, n is in the range of 0 to 1. At n=1, the equation reduces to the constitutive equation of a Newtonian fluid. When n<1, shear thinning behavior is observed. The lower the n value, the more pronounced is the shear thinning behavior. As seen from data in Table 4.1, the pseudo-plasticity index $n$ of the solution decreases by the addition of CNTs. On adding pristine CNTs, the $n$ value shows an abrupt decrease. After chemical modification of CNTs, shear thinning behaviour is observed but it is less pronounced; in other words, after chemical modification of CNTs, the extent of Newtonian plateau is greater than with the pristine CNT epoxy suspension.

Table 4.1: Rheological data of MWCNT/epoxy nanosuspensions

| Sample code | Viscosity at shear rate of 1 $s^{-1}$ (Pa.s) | Flow index (n) |
|---|---|---|
| Epoxy resin | 4.07 | 0.99 |
| 0.2 wt% pristine MWCNT | 17.6 | 0.73 |
| 0.2 wt% MWCNT-g-CTBN | 10.3 | 0.84 |
| 0.2 wt% MWCNT-g-PES | 6.98 | 0.98 |
| 0.4 wt% pristine MWCNT | 174 | 0.62 |
| 0.4 wt% MWCNT-g-CTBN | 34.7 | 0.73 |
| 0.4 wt% MWCNT-g-PES | 26.7 | 0.78 |

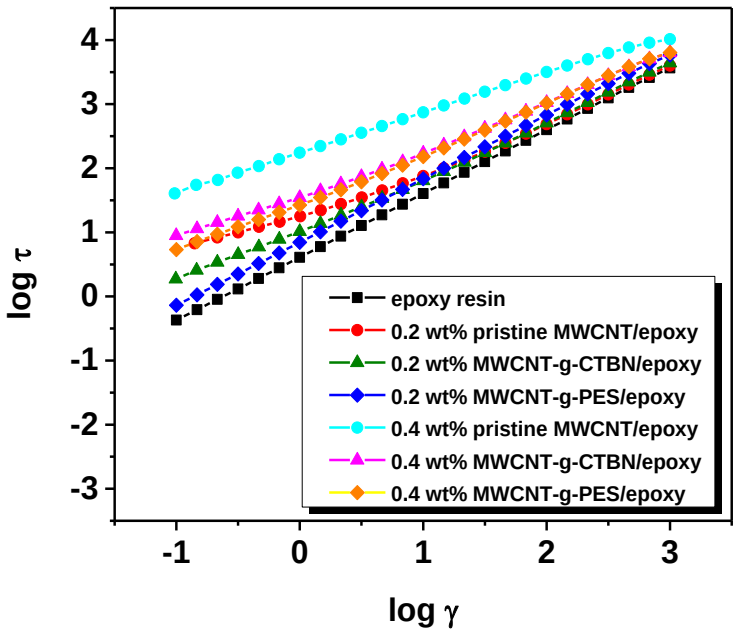


Figure 4.15: Variation of shear stress with shear rate for epoxy nano suspensions of pristine MWCNTs, MWCNT-g-CTBN and MWCNT-g-PES

#### 4.3.3.3. TEM micrographs of epoxy composites

To analyze the state of the dispersion of the filler in the polymer matrix of composite, TEM micrographs were taken for the epoxy composites prepared by the addition of 0.2 wt% of pristine and surface modified nanotubes (Figure 4.16). In the pristine MWCNT/epoxy composite, agglomerates of MWCNTs were observed. On the other hand, a significant improvement in the dispersion was observed by the grafting of CTBN and PES with MWCNTs.

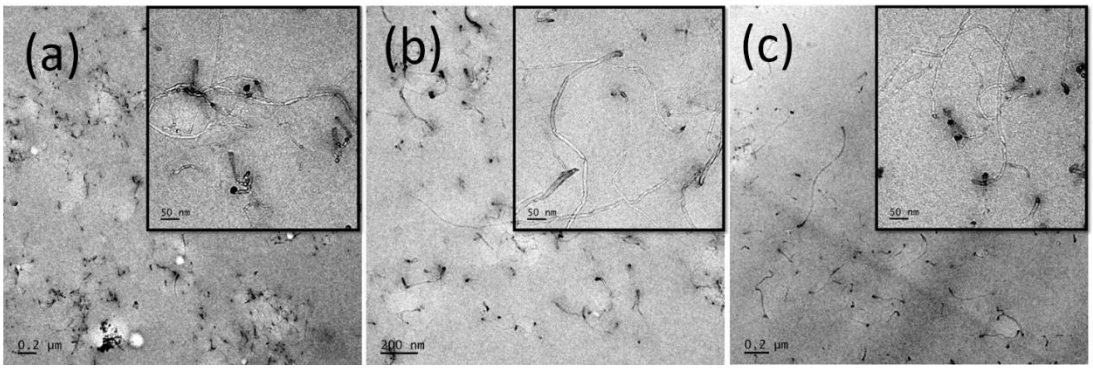


Figure 4.16: TEM images of epoxy nanocomposites containing (a) 0.2 wt% pristine MWCNTs (b) 0.2 wt% MWCNT-g-CTBN and (c) 0.2wt% MWCNT-g-PES

### 4.3.4. Tensile strength of epoxy composites

There is a significant interest to greatly improve the mechanical properties of epoxy-composites for aerospace and automobile applications. The tensile properties of the composites as a function of nanotube concentrations are plotted in Figure 4.17 and also summarized in Table 4.2. Representative tensile stress versus strain curves are shown in Figure 4.17 (a). The tensile strength of nanocomposites increased initially with increasing the nanotube content and attained the maximum value at the 0.2 wt% nanotube content corresponding to an increase of 11% compared with the pure epoxy. The decreased tensile strengths beyond 0.2 wt% might be probably due to the aggregation of the nanotube which can result in the stresses concentrating at the aggregation points. By comparison, the composites containing the polymer

functionalized MWCNTs exhibit higher strength and modulus values than the pristine MWCNTs over the whole filler contents studied. Functionalisation of nanotubes resulted in better dispersibility, leading to reduction in agglomeration of nanotubes. For epoxy composite with 0.3wt% MWCNT-g-CTBN, the tensile modulus and strength increased by 17% (2.21 ± 0.02GPa) and 25% (85.4 ± 3.1 MPa), respectively. Similarly, the tensile strength and modulus of MWCNT-g-PES/epoxy composite is also higher than the neat epoxy. Compared to neat epoxy, tensile modulus of MWCNT-g-PES/epoxy composite is increased by 16% at filler loading of 0.3 wt%, whereas tensile strength is increased by 26% at a filler loading of 0.2 wt%. This can be attributed due to the soft layer of polymer grafted on MWCNTs ensuring a better interfacial interaction enabling efficient load transfer to the nanotube. In order to compare the experimental modulus of composites with theoretical value, a modified Halpin-Tsai model was used. The predicted modulus of the MWCNT/epoxy composite using modified Halpin-Tsai equation given by (Sun et al., 2008),

$$E = \frac{1+\varphi\eta\upsilon_f}{1-\eta\upsilon_f} E_m \tag{4.2}$$

$$\eta = \frac{E_f / E_m - 6}{E_f / E_m + 6\varphi} \tag{4.3}$$

where E, $E_m$ and $E_f$ are moduli of composite, matrix and carbon nanotube, respectively; $\upsilon_f$ is the volume fraction of the filler, $\varphi$ is the shape factor which is equal to twice the aspect ratio of the filler.

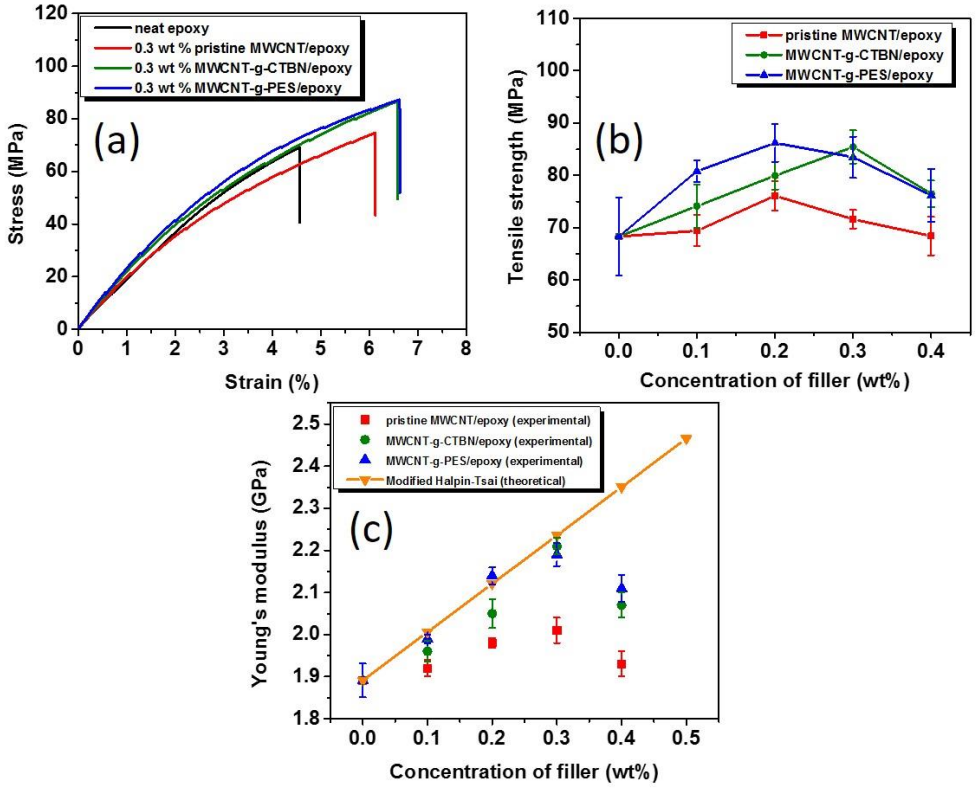


Figure 4.17: (a) Representative stress-strain curves (b) tensile strength and (c) tensile modulus of epoxy nanocomposites containing pristine MWCNTs, MWCNT-g-CTBN and MWCNT-g-PES.

Figure 4.17 (c) shows a comparison of the variation in theoretical and experimental tensile modulus values of composites with weight fraction of MWCNTs. It is found that the results obtained from the modified Halpin–Tsai equation on Young's moduli fit successfully the experimental ones at low concentration and the predicted values are slightly higher than the experimental ones for some compositions of MWCNT/epoxy composites. The discrepancy is caused by the aggregation of MWCNTs. However, the experimental tensile modulus of the MWCNT-g-CTBN/epoxy and MWCNT-g-PES/epoxy composites are found to be comparable to the modulus predicted using the Halpin-Tsai modeling. It means that a high reinforcing effectiveness is achieved by introduction of polymer functionalized nanotube as reinforcement. In this case, more homogeneous dispersion and a better

interface between the nanotubes and the epoxy matrix resulted in better mechanical properties. In the MWCNT-g-CTBN/epoxy composites, terminal carboxyl groups of CTBN react with epoxy matrix during curing reactions, which provide interfacial adhesion for load transfer between epoxy and nanotubes, and therefore, mechanical properties of the composites are enhanced. In the case of MWCNT-g-PES/epoxy composite, the soft layer of thermoplastic polymer grafted on nanotube enhances the interfacial adhesion through hydrogen bonding interaction between hydroxyl group of epoxy matrix and sulfonyl group of PES. Another reason for the observed behavior is the presence of voids which are developed during the mixing of hardener with the MWCNT/epoxy-suspension via stirring. The high viscosity disabled degassing of the nanocomposite samples with voids remaining in the matrix.

Table 4.2: Fracture toughness and tensile properties of epoxy nanocomposites

| **SI No** | **Sample code** | **$K_{IC}$ (MPa.m$^{1/2}$)** | **Tensile strength (MPa)** | **Tensile Modulus (GPa)** | **Elongation at break (%)** |
|---|---|---|---|---|---|
| 1 | Neat epoxy | 0.74 ± 0.08 | 68.4 ± 1.7 | 1.89 ± 0.04 | 5.66 ± 0.63 |
| 2 | 0.1 wt% pristine MWCNT | 1.14 ± 0.07 | 69.4 ± 3.0 | 1.92 ± 0.02 | 6.01 ± 0.88 |
| 3 | 0.2 wt% pristine MWCNT | 1.35 ± 0.11 | 76.1 ± 2.8 | 1.98 ± 0.01 | 6.53 ± 1.07 |
| 4 | 0.3 wt% pristine MWCNT | 1.15 ± 0.01 | 71.6 ± 1.8 | 2.01 ± 0.03 | 6.09 ± 0.99 |
| 5 | 0.4 wt% pristine MWCNT | 1.12 ± 0.05 | 68.4 ± 3.7 | 1.93 ± 0.03 | 5.75 ± 0.41 |
| 6 | 0.1 wt% MWCNT-g-CTBN | 1.39 ± 0.08 | 74.1 ± 4.1 | 1.96 ± 0.02 | 6.12 ± 0.11 |
| 7 | 0.2 wt% MWCNT-g-CTBN | 1.47 ± 0.01 | 79.9 ± 2.6 | 2.05 ± 0.03 | 7.05 ± 0.40 |
| 8 | 0.3 wt% MWCNT-g-CTBN | 1.62 ± 0.06 | 85.4 ± 3.1 | 2.21 ± 0.02 | 6.76 ± 0.31 |
| 9 | 0.4 wt% MWCNT-g-CTBN | 1.24 ± 0.07 | 76.5 ± 2.5 | 2.07 ± 0.03 | 6.96 ± 0.88 |
| 10 | 0.1 wt% MWCNT-g-PES | 1.28 ± 0.17 | 80.8 ± 2.1 | 1.99 ± 0.01 | 6.21 ± 0.87 |
| 11 | 0.2 wt% MWCNT-g-PES | 1.50 ± 0.11 | 86.2 ± 3.6 | 2.14 ± 0.02 | 6.98 ± 0.56 |
| 12 | 0.3 wt% MWCNT-g-PES | 1.67 ± 0.11 | 83.5 ± 4.0 | 2.19 ± 0.03 | 6.57 ± 0.21 |
| 13 | 0.4 wt% MWCNT-g-PES | 1.19 ± 0.17 | 76.2 ± 5.1 | 2.11 ± 0.03 | 6.02 ± 1.02 |

## 4.3.5. Fracture toughness of epoxy composites

Fracture toughness ($K_{IC}$) values of neat epoxy, pristine MWCNT, MWCNT-g-CTBN and MWCNT-g-PES epoxy nanocomposites are given in Table 4.2. The addition of nanotubes into the epoxy matrix resulted in an improvement in fracture toughness (Figure 4.18). Neat epoxy showed the fracture toughness of 0.74 ± 0.8 MPa.m$^{1/2}$, which increased up to 1.35 ± 0.11 MPa.m$^{1/2}$ (82% improvement) by adding 0.2 wt% pristine MWCNTs. Composites with MWCNT-g-CTBN improved the fracture toughness of epoxy significantly, achieving an 117% improvement at 0.3 wt% filler loading. The composite prepared by PES grafted nanotube showed the maximum improvement in fracture toughness (125% improvement compared to neat epoxy for 0.3 wt% MWNCT-g-PES). This is followed by a decrease in the value of $K_{IC}$ at higher MWCNT concentrations due to the presence of agglomerates and defects.

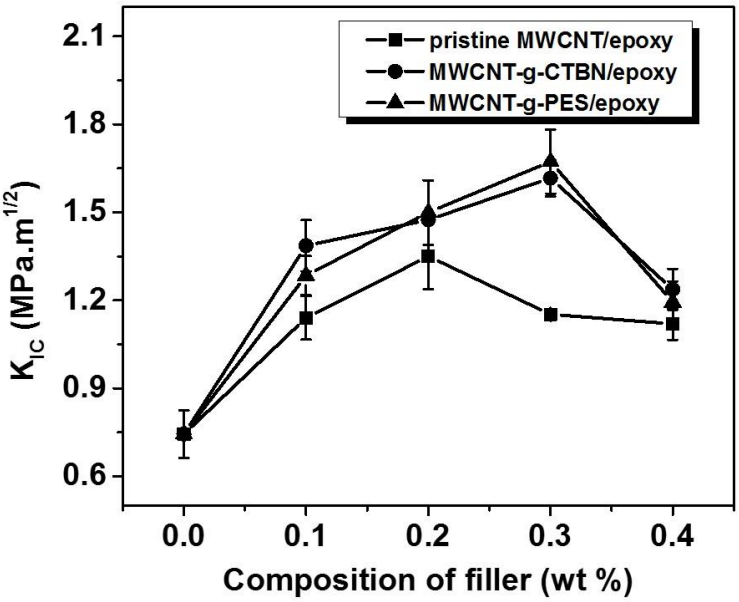


Figure 4.18: Fracture toughness of epoxy nanocomposites containing pristine MWCNTs, MWCNT-g-CTBN and MWCNT-g-PES.

The toughening mechanisms can be understood by observing the representative HRSEM images of the fracture surface of the neat epoxy and MWCNTs/epoxy composite with 0.3 wt% MWCNTs resulting from the fracture testing of the samples. Neat epoxy resin as shown in Figure 4.19 (a) exhibits a relatively smooth fracture surface, which indicates a typical fractography feature of brittle fracture behavior, thus revealing low fracture toughness of the neat epoxy. Compared to the case of neat epoxy, the fracture surfaces of the nanocomposites show considerably different fractographic features. The rough surface of the composites containing MWCNTs as seen in the Figure 4.19 (b) is most likely the result of crack deflection produced by the interaction of nanofillers and the epoxy matrix. Well dispersed nanotubes with proper adhesion to the epoxy could resist crack propagation and lead to crack deflection. Apart from crack deflection, pullout of nanotubes, debonding of MWCNTs and bridging mechanism also plays a significant role in improving the fracture toughness of composites. At higher magnification, some pulled out CNTs can be observed on the fracture surface (see Figure 4.19 (d) and (f)) in the polymer functionalized MWCNT/epoxy composites.

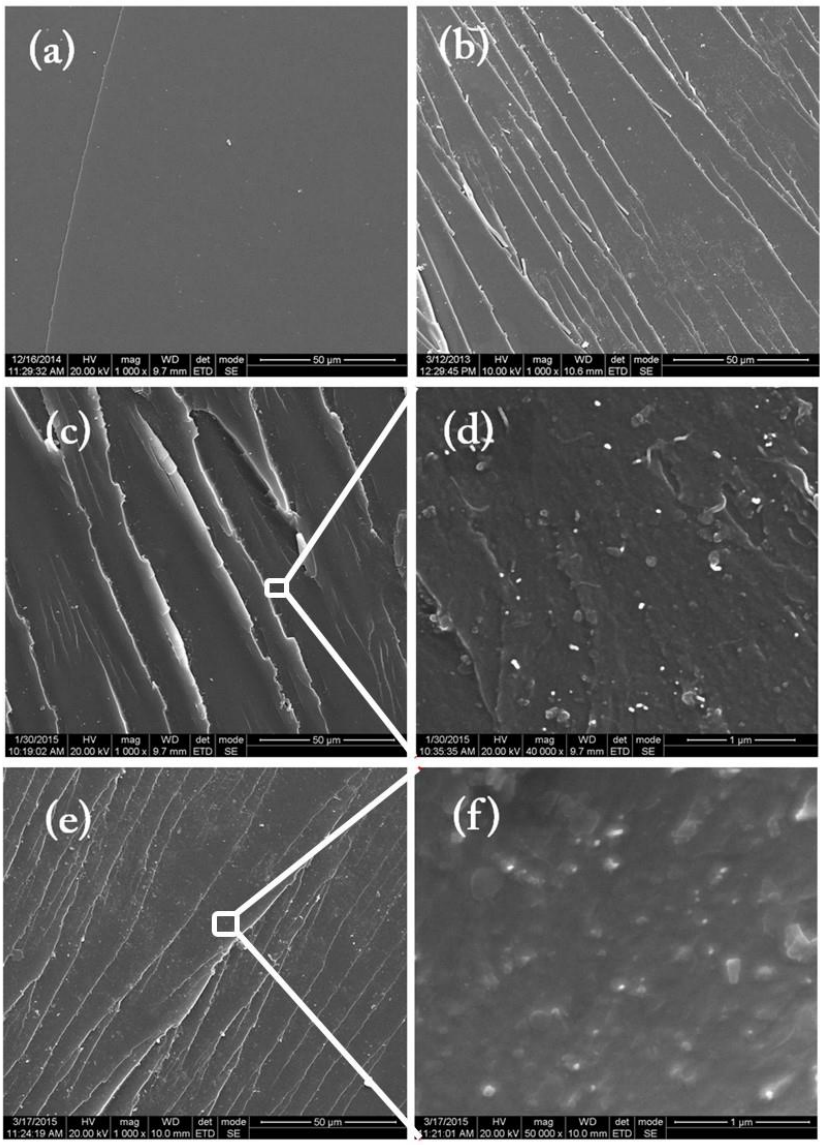


Figure 4.19: FESEM images of fractured surface of sample: (a) neat epoxy (b) 0.3 wt% pristine MWCNT/epoxy (c) 0.3 wt% MWCNT-g-CTBN/epoxy (d) 0.3 wt% MWCNT-g-CTBN/epoxy at high magnification (e) 0.3 wt% MWCNT-g-PES/epoxy and (f) 0.3 wt% MWCNT-g-PES/epoxy at high magnification

## 4.3.6. Dynamic mechanical analysis of epoxy composites

The effect of surface MWCNT functionalization on the viscoelastic performance of nanocomposites was investigated by DMA analysis by comparing the

storage modulus, and tan δ values with those of neat epoxy. The Figure 4.20 and 4.21 shows the storage modulus (G') and tan δ obtained by DMA in a range between 30 and 250 $^{o}$C for neat epoxy and composites prepared by the addition of 0.3 wt% polymer functionalized MWCNTs. Addition of pristine nanotubes into epoxy resulted in an improvement in the storage modulus. In the glassy state, an improvement of 9% from 1995 MPa to 2178 MPa in the storage modulus is observed at 30 $^{o}$C by the addition of 0.3 wt% pristine MWCNTs to epoxy matrix. The epoxy nanocomposite with MWCNT-g-CTBN nanofiller shows an enhanced storage modulus compared with pure epoxy resin and pristine MWCNT/epoxy nanocomposite with the same filler content. At 30 $^{o}$C, the storage modulus of the epoxy nanocomposite with 0.3 wt% MWCNT-g-CTBN is 2417 MPa, which is around 21% larger than that of neat epoxy resin (1995 MPa). The storage modulus in the rubbery region is also significantly increased for MWCNT-g-CTBN/epoxy, which is believed to be due to improved dispersion and the strong interfacial adhesion with epoxy which ensures an efficient load transfer at the interface. Although an improvement in storage modulus was observed for composite of PES grafted nanotube compared to neat epoxy, there is no significant change in the modulus by comparison with composite prepared by pristine nanotube. A reduction in *Tg* was observed by the addition of pristine nanotubes. The lowered *Tg* of MWCNT/epoxy composite is possibly due to either lower crosslink density of epoxy or poor adhesion between MWCNTs and epoxy, or both. After adding the MWCNT-g-CTBN, CTBN grafting provides carboxylic acid groups that can react with the oxirane rings of epoxy resin to form a strong bonding between matrix and MWCNTs, leading to a higher cross-linking density of the composites. This results in a confinement of the filler-matrix interface and reduce the chain mobility (Konnola et al., 2015a; Konnola et al., 2015b). As a result, the increase of *Tg* occurs. Similarly, an improvement in *Tg* was observed for MWCNT-g-PES/epoxy composite when compared with composites prepared from pristine MWCNTs.

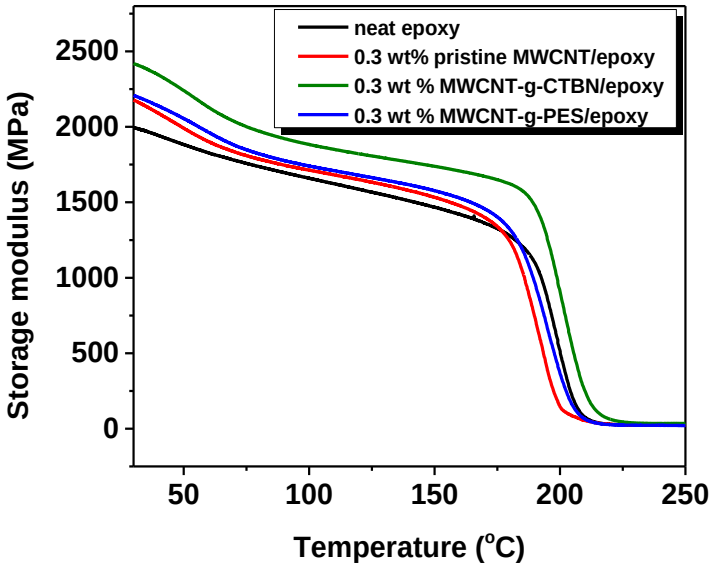


Figure 4.20: Storage modulus curves for pristine MWCNT, MWCNT-g-CTBN and MWCNT-g-PES epoxy composites

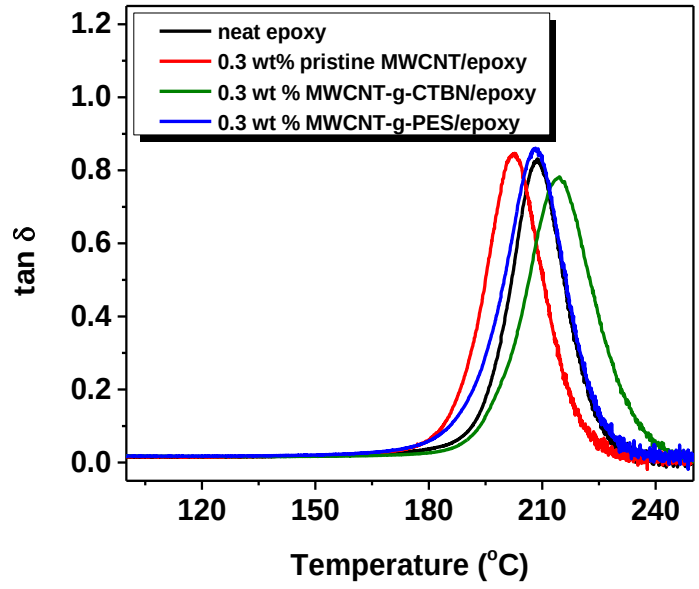


Figure 4.21: Tan delta versus temperature curves for pristine MWCNT, MWCNT-g-CTBN and MWCNT-g-PES epoxy composites

### 4.3.7. TGA of epoxy composites

Thermal stability of the epoxy composites was traced using TGA. The thermal stability of epoxy composites with 0.3 wt% loading of pristine MWCNTs and polymer functionalized MWCNTs were compared with neat epoxy system in Figure 4.22. The thermal stability of epoxy matrix was not affected by the addition of nanotubes. As shown in the figure, the main weight loss for the composites takes place at around 320 $^{o}$C, which is attributed to the degradation of the epoxy network. This means that all the composites prepared are very stable and show little degradation below 320 $^{o}$C and therefore can be used for many high-temperature applications.

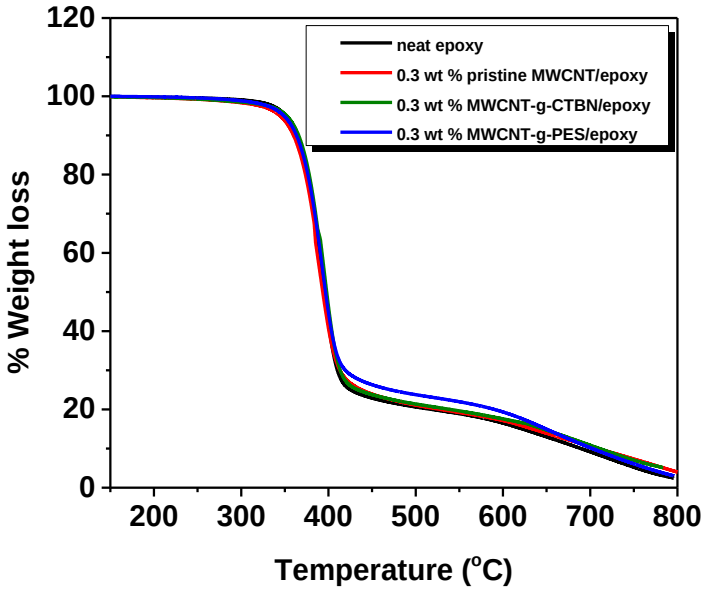


Figure 4.22: TGA curves of epoxy nanocomposites

## 4.4. Conclusions

In this work, CTBN and PES grafted MWCNTs have been proposed as an innovative filler for the preparation of epoxy nanocomposites with enhanced

thermomechanical properties The functionalized nanotubes were characterized by FTIR, Raman spectroscopy, TEM and TGA. The studies reveal the grafting of polymers on MWCNTs. Incorporation of polymer grafted MWCNTs in epoxy matrix composites imparted tremendous improvement in fracture toughness and tensile strength when compared to pristine MWCNT/epoxy composites It has been possible to obtain an improvement of ~117% in fracture toughness and 25% improvement in tensile strength in the CTBN functionalized MWCNT based epoxy composites with only 0.3 wt% loading. PES grafted MWCNT/epoxy nanocomposite also induces a significant increase in both tensile strength (26%) and fracture toughness (125%) of the epoxy matrix at a filler loading of 0.3 wt%. The improvement in fracture toughness is attributed to the better dispersion of the MWCNTs in epoxy matrix aided by the polymer graft that has better miscibility with epoxy which in turn influences the crack path deflection. Dynamic mechanical studies show an increase in the storage modulus for the nanocomposite prepared using polymer grafted MWCNTs compared to neat epoxy system. The obtained results can be considered as beneficial in the manufacture of components with higher strength-to-weight ratios for such uses as windmill blades or aircraft components.

# CHAPTER 5

# TOUGHENED EPOXY NANOCOMPOSIES BASED ON POLYMER GRAFTED GRAPHITE OXIDE

*This work is focused on the chemical modification of graphite oxide (GOs) with two types of liquid rubbers, in an attempt to achieve high dispersion and enhanced interaction in an epoxy matrix and hence to prepare composites with improved thermo-mechanical properties. Polymer grafted GOs were characterized using FTIR, XPS, Raman spectroscopy, TGA and TEM. Epoxy nanocomposites using the modified fillers were prepared. The fracture toughness of the systems were examined and compared with GO/epoxy nanocomposite. Field emission scanning electron micrographs (FESEM) of fractured surfaces were examined to understand the toughening mechanism. Considerable improvement in toughness as well as mechanical strength were observed by the modification of GOs with polymers. The enhancement in properties were attributed to the better interfacial interaction between filler and matrix.*

**Part of this chapter has been published in RSC Advances, (2015), Vol.5: 61775-61786**

# 5.1. Introduction

Due to unique mechanical properties such as high strength and stiffness and aspect ratio, graphite oxide (GO) have many potential applications especially in the field of advanced composites. The major problem associated with GO based polymer nanocomposites is the poor dispersion of the GO in the polymer matrix. Generally nanoparticles have a tendency for agglomeration because of the weak van der Waals force of attraction. In fact, GO has a strong tendency of aggregation inside epoxy matrix which limits the equal distribution of load into matrix. Chemical modifications of GO sheets are an effective way to improve interfacial interaction between the GO sheets and the epoxy matrix, which in turn leads to better filler dispersion, and enhanced mechanical performance in the nanocomposites (Cano et al., 2013; Dreyer et al., 2010; Sengupta et al., 2011; Song et al., 2013). Naebe et al. (2014) functionalized thermally reduced graphene nanoplatelets via Bingel reaction to evaluate the effect of functionalization on the dispersion status and interface in the graphene/epoxy composites. A good improvement in fracture toughness was observed in the work. In an another study, Park et al. (2015) investigated the toughening behavior of epoxy nanocomposites using amine terminated poly(acrylonitrile-co-butadiene) functionalized GO as reinforcing filler and they found a significant improvement in toughness at very small filler loadings. Similarly, Guan et al. (2014) introduced amine groups of polyetheramine (PEA) with different molecular lengths onto the GO surface, and studied sheet/matrix interfacial interaction between filler and epoxy matrix to understand the influence of different interphase structures on the mechanical properties of resulting nanocomposites. Wang et al. (2014) synthesized polyphosphamide (PPA) and covalently grafted it onto the surface of graphene nanosheets (GNSs). These modified sheets were incorporated into epoxy resins (EPs) to obtain a novel flame retardant nanocomposite. Tang and coworkers (Tang, 2014) were able to achieve an electrical conductivity of nearly 11 orders of magnitude higher than that of neat epoxy by the addition of 2.7 vol% of

polyetheramine functionalized GOs. The above studies reveal the potential behind the chemical modification of GO sheets for the improvements in properties at low filler loading, provides opportunity to produce cost effective high performance epoxy graphene composites.

Grafting of GO sheets with polymer can create a soft interface between filler and matrix which can result in a better load transfer from matrix to filler. To date, no systematic study of grafting liquid rubbers onto GO to improve the compatibility and performance in the epoxy composites is available in the literature. In this work, CTBN and polyethylenimine (PEI) were grafted onto GO and used as a modifier for epoxy resin. We investigated thermal, viscoelastic and mechanical performance of polymer grafted GO modified epoxy nanocomposites and thereby evaluated the effect of chemical modification on the dispersion and interfacial interaction in the resulting composites.

# 5.2. Materials and Methods

## 5.2.1. Materials

Graphite was supplied by Anthracite industries, USA, concentrated sulphuric acid ($H_2SO_4$, 98%), concentrated hydrochloric acid (HCl, 35 %), potassium permanganate ($KMnO_4$), hydrogen peroxide ($H_2O_2$, 30%) and acetone were purchased from Merck India Pvt Ltd, Bangalore India. The polymer matrix used in the present study was epoxy resin Lapox ARL-135 based on DGEBA (epoxy equivalent 187 g/eq) and diaminodiphenyl sulfone (DDS) hardener under the commercial name Lapox K10 and was purchased from Atul India private limited, Gujarat. Dimethyl formamide (DMF) purchased from Spectrochem, India. Triphenylphosphine (TPP, 99% $M_W$-262.92 g/mol), PEI and CTBN purchased from

Sigma Aldrich, Bangalore, India. All the chemicals were used as received without further purification.

## 5.2.2. Polymer grafting on graphite oxide

### 5.2.2.1. Preparation of GO

The graphite was first exfoliated to form GO using the improved method reported by Tour group (Marcano et al., 2010). In a typical process a 9:1 mixture of concentrated $H_2SO_4$/$H_3PO_4$ (360:40 mL) was added to a mixture of expandable graphite (3.0 g, 1 wt equiv) and $KMnO_4$ (18.0 g, 6 wt equiv). The reactants were heated to 50 $^oC$ and stirred for 12 h. The mixture was cooled to room temperature and it was kept in an ice bath. To this solution, 400 mL deionised water was added dropwise with stirring for 30 minutes. 30% $H_2O_2$ was slowly added into the mixture until the solution turned bright yellow. The resulting yellowish brown mixture was centrifuged and the solid material was then washed in succession with 200 mL of water, 200 mL of 30% HCl and 200 mL of ethanol. After this multiple wash, it was coagulated with 200 mL of ether. The solid GOs obtained after the evaporation of ether, was vacuum-dried overnight at room temperature.

### 5.2.2.2. Preparation of GCTBN

For the preparation of CTBN grafted GO (GCTBN), 500 mg of GOs was sonicated in DMF for 30 minutes. In a separate beaker, 2 g CTBN in 20 ml DMF solution was sonicated for 30 minutes and this solution was added to GO solution with mechanical stirring. 0.50 wt % TPP was added and the solution was heated at 125 $^oC$ for 36 h. The suspension was filtered and washed with DMF followed by acetone. The black powder obtained was dried well and powdered. A schematic illustration of the reaction is given in Figure 5.1.

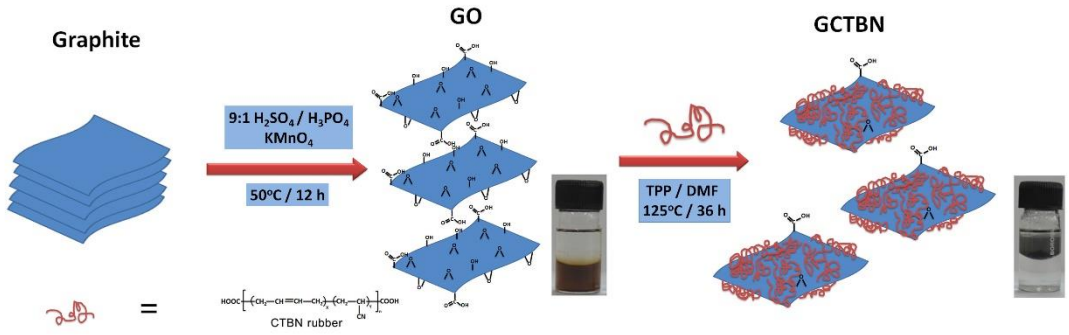


Figure 5.1: Schematic showing the preparation of GO and GCTBN

### 5.2.2.3. Preparation of GOPEI

For the preparation of PEI grafted GO (GOPEI), 500 mg of graphite oxide was sonicated in DMF for 30 minutes. In a separate beaker, 3g PEI in 20 ml DMF solution sonicated for 30 minutes and this solution was added to graphite oxide solution and the solution was heated at $50^0$ C for 72h. The suspension was filtered, washed with DMF followed by acetone. The black powder obtained is dried well in an air oven. A schematic illustration of the reaction is given in Figure 5.2.

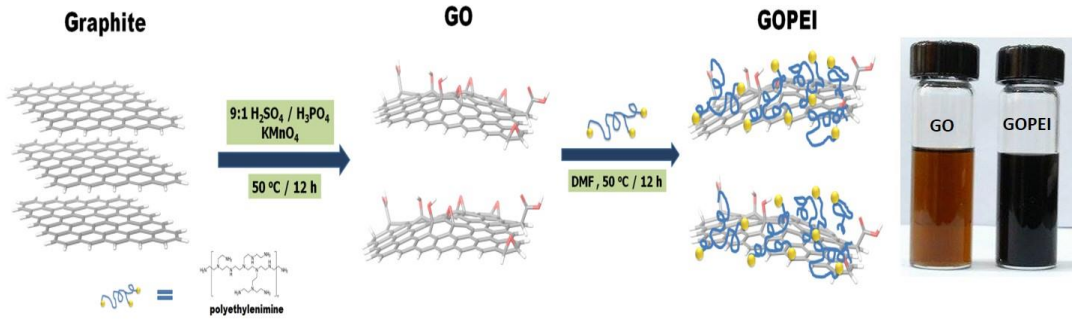


Figure 5.2: Schematic showing the preparation of GO and GOPEI

## 5.2.3. Preparation of GO/epoxy nanocomposites

Epoxy composites with different GO loadings were prepared by the following procedure. Required amounts of GOs (0.2, 0.4, 0.6 and 0.8 wt% with respect to

DGEBA) was initially dissolved in a mixture of acetone by sonication for 15 minutes and mixed the solution with DGEBA. The solution was again sonicated for 15 minutes to obtain a black suspension. Acetone was evaporated off by heating at 50 $^{o}$C for 1 h. The trace amount of solvent was removed by keeping in a vacuum oven. It was then added to molten hardener (35 g/100 g DGEBA), stirred for 10 minutes and degassed for 10 minutes until there was no trace of trapped bubbles. The mixture was poured into a preheated mould and cured for 4 h at 180 $^{o}$C. Post curing was done at 200 $^{o}$C for an hour. The same procedure was followed for the preparation of modified GO/epoxy composite. The preparation process of epoxy composites filled with GOs is shown in Figure 5.3.

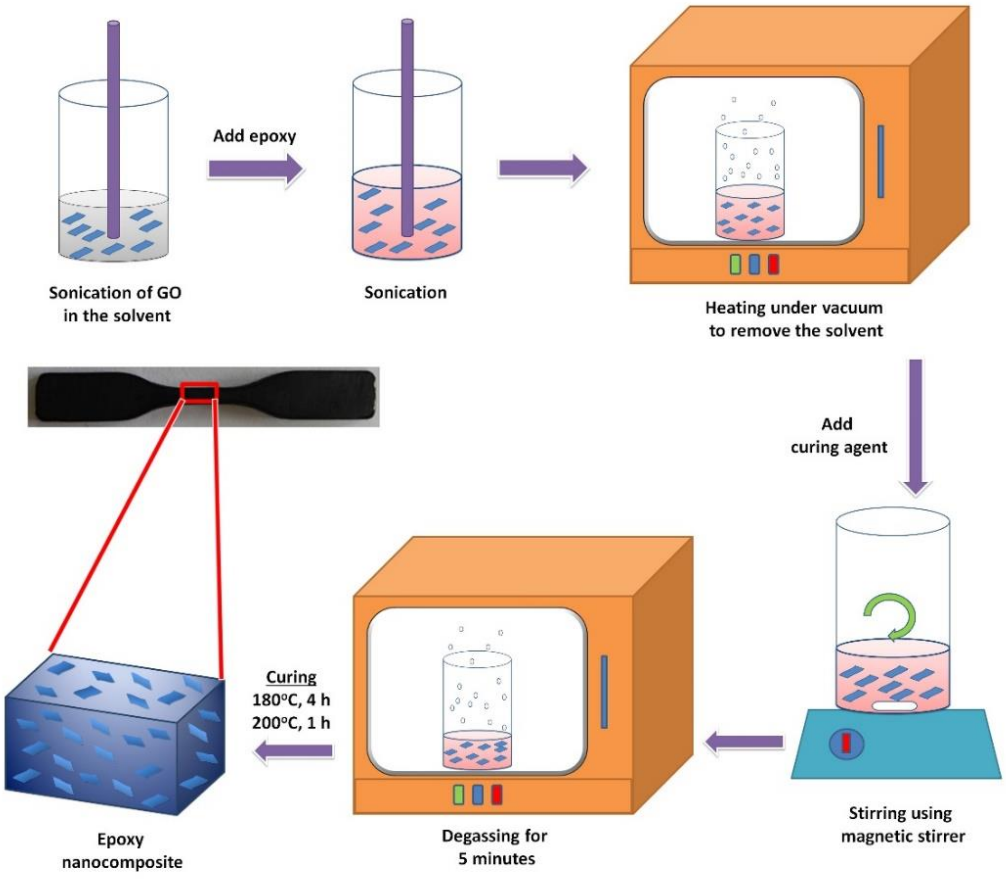


Figure 5.3: Schematic illustration of the preparation process of epoxy nanocomposites

## 5.2.4. Characterization

Fourier transform infrared spectroscopy (FT-IR) analysis was carried out using a Perkin Elmer System series 100 spectrophotometer in a frequency range of 4000–500 $cm^{-1}$ with a spectral resolution of 4 $cm^{-1}$ to identify the functionalization of GO. XPS was carried out with a Kratos Axis Ultra DLD spectrometer, using Al Kα excitation radiation. The high-resolution transmission electron microscopy (HRTEM) was conducted using JEOL JEM-2100 with an acceleration voltage of 200 kV being equipped with an EDX spectrometer. Sliced thin sections of GO/epoxy composites with a thickness of about 60-80 nm, prepared by ultramicrotomy, were used to take the TEM images of the composites. Raman spectra were recorded from 100 to 3000 $cm^{-1}$ on a Raman spectrometer (INVIA, England) with a 514 nm argon ion laser. Thermal stability of nanocomposites was analyzed using a Thermogravimetric analyzer (Q-50, TA Instruments, USA). The samples were heated from ambient to 800 $^{o}$C at a ramp rate of 10$^{o}$ C/ min. Rheological analysis was done using Modular Rheometer (MCR102, Anton Paar, USA), using a 50 mm parallel plate assembly at room temperature. Optical microscopy analysis was carried out with Leica DM1000 LED (Leica Microsystems, Germany) in transmitted light configuration. Dynamic Mechanic Analysis (DMA) was performed on a DMA 8000, operating in the single cantilever mode at an oscillation frequency of 1 Hz. Data was collected from room temperature to 250 $^{o}$C at a scanning rate of 2 $^{o}$C/min. The sample specimens were cut into rectangular bars measuring 50 mm x 5 mm x 2 mm. The fracture surfaces of the samples were investigated using field emission SEM (FE SEM, FEI Quanta FEG200) at an accelerating voltage of 20 kV, and the fracture surfaces were coated with a conductive layer of gold. Tensile tests were performed with dumbbell shaped specimens using an Instron model 5900 tensile tester at a crosshead speed of 1 mm/min as per ASTM standard D638. The results are the average of at least five measurements. Fracture toughness of the sample was measured using UTM (Instron 5900, Instron, USA) at a crosshead speed of 10mm/min (as per ASTM standard

D5045). Single edge notch specimens of 46 mm x 6 mm x 3 mm (span length = 24 mm) were used to measure the fracture toughness of the epoxy nanocomposites.

#### 5.2.4.1. X-Ray Diffraction

The crystal phase of the samples was measured using X-ray diffractometry (PANalytical 3 kW X'pert PRO X-ray diffractometer) using Cu Kα (k= 1.5406 Å) radiation source operating at a voltage of 45 kV and 300 mA of electric current. The scanning was taken from 5 to 80$^{o}$ (2h).

# 5.3. Results and Discussion

## 5.3.1. Characterization of grafting of CTBN and PEI on GOs

#### 5.3.1.1. FTIR spectroscopy

The FTIR spectra of GO, GCTBN and GOPEI were recorded to obtain information about the structural changes originated during the grafting process (Figure 5.4). The characteristic absorption bands of GOs in the FTIR spectrum were observed at 1721 $cm^{-1}$, 1055 $cm^{-1}$, 1587 $cm^{-1}$ and 3446 $cm^{-1}$ corresponding to the C=O stretching vibrations from carbonyl and carboxylic groups, C–O–C stretching from epoxy groups, C=C in aromatic ring and –O−H stretching frequency of hydroxyl groups respectively (Guan et al., 2014). After the grafting with CTBN, the FTIR spectrum of GO is significantly changed, with the appearance of new and more intense peaks. The new characteristic peaks at 965 $cm^{-1}$, 2236 $cm^{-1}$ and 2920 $cm^{-1}$ appearing in the FTIR spectrum of GCTBN, corresponds to the =C−H out of plane bending vibration of 1, 4 trans olefin in CTBN, stretching vibration of C≡N and the stretching vibration of =C−H, respectively (Tripathi and Srivastava, 2007)[24]. Furthermore, the intensity of peak at 1055 $cm^{-1}$ corresponding to C–O–C of epoxy

groups is reduced drastically in the spectrum of GCTBN and the peak corresponding to C=O stretching vibration is broadened (1713-1743 $cm^{-1}$), indicating the formation of O=C−O ester bond due to the chemical reaction of CTBN to GO surface via nucleophilic substitution reaction between the carboxyl groups of CTBN and the epoxy groups of GO. For GOPEI, new peaks were observed at 1643, 2923 and 3422 $cm^{-1}$ which corresponds to IR stretching frequencies of C=O in amide, C-H and N-H respectively. All these results confirm the successful modification of CTBN with GO.

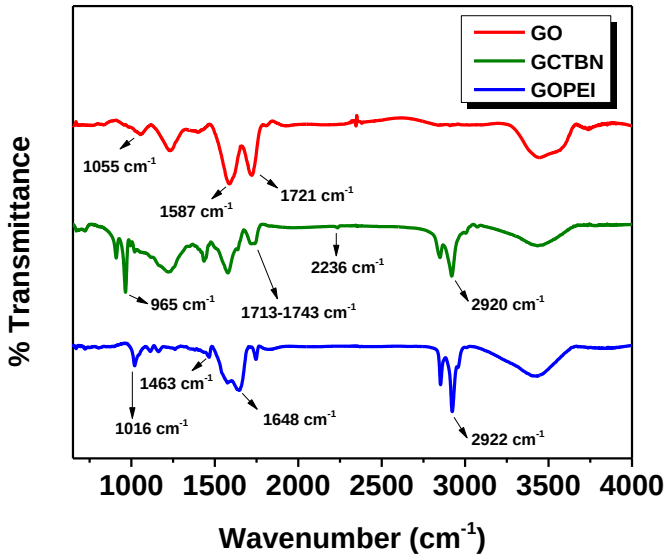


Figure 5.4: FTIR spectra of GO, GCTBN and GOPEI

### 5.3.1.2. XPS spectroscopy

Analysis of the XPS spectra provides clear evidence of the fact that the GOs were chemically modified. The XPS survey spectra of GO, GCTBN and GOPEI is given in Figure 5.5. Compared with GO, the survey of GCTBN and GOPEI shows the presence of N1s, indicating the chemical grafting of polymer chains onto the surface of the GO sheets. The higher resolution C1s spectra of (b) GO, (c) GCTBN and (d) N1s spectra of GCTBN are shown in Figure 5.6. The C1s core level spectra of GOs shows peaks at 284.8 eV (C -C/C=C), 285.9 eV (C -OH), 287.1 eV (C -O -

C/epoxide group), 288.0 eV (C =O), and 289.2 eV (O -C =O), respectively (Ma et al., 2013; Ren et al., 2014). Although the C1s XPS spectrum of the GCTBN (Figure 5.6 (b)) also exhibits the same oxygen functionalities, their peak intensities are much smaller than those in GO indicating partial reduction of GO during the reaction with CTBN. In addition, the area of the peak at 287.1 eV is decreased drastically in the C1s spectrum of GCTBN (Figure 5.6 (b)) indicating that the reaction has happened between the epoxide group of GO and carboxyl groups present in CTBN. An additional peak at 286.4 eV in the C1s high resolution and peak at 399.7 eV in the N1s spectra is arising from the C≡N group in CTBN (Górka et al., 2013). High resolution C1s and N1s core spectra of GOPEI also shows the presence of new peaks at 286.4 eV and 400 eV which corresponds to amide and amine groups present in GOPEI (Figure 5.7 (a) and (b)). These above mentioned XPS results further demonstrates that GO is successfully functionalized by CTBN and PEI molecules, which is in agreement with FTIR results.

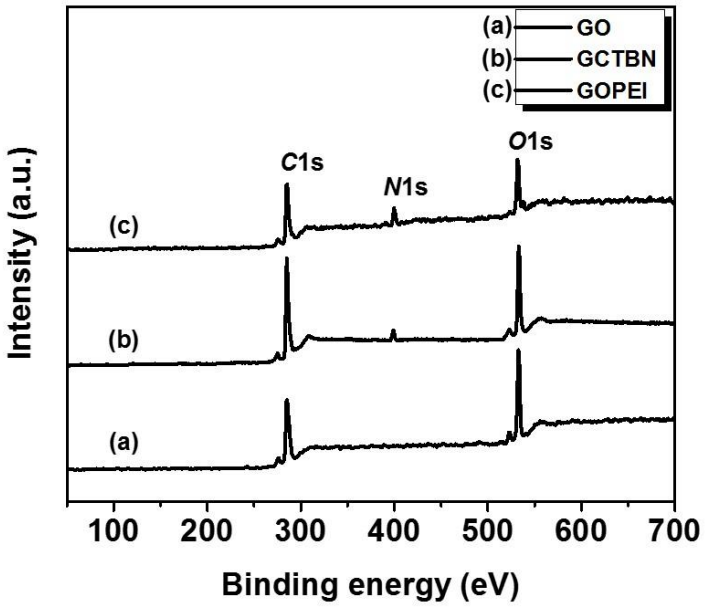


Figure 5.5: XPS survey spectra of (a) GO, (b) GCTBN and (c) GOPEI

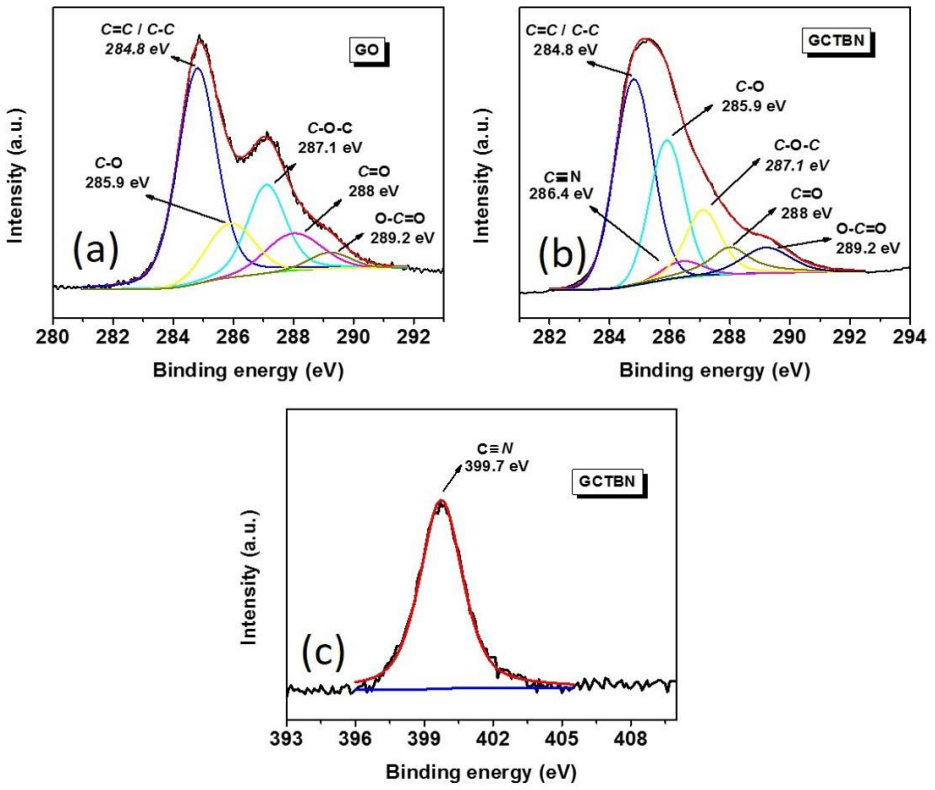


Figure 5.6: High resolution C1s spectra of (a) GO, (b) GCTBN and (c) N1s spectra of GCTBN

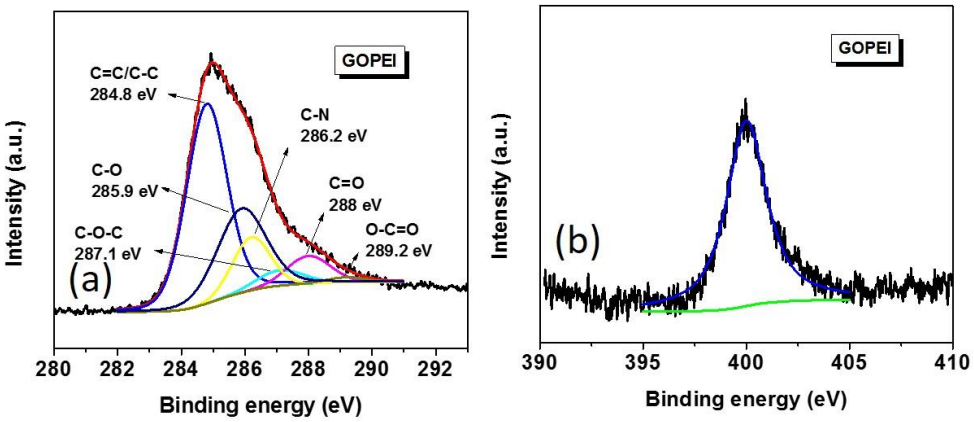


Figure 5.7: (a) High resolution C1s XPS spectra of GOPEI and (b) N1s spectra of GOPEI

### 5.3.1.3. Raman spectroscopy

The Raman spectra of graphite, graphite oxide GCTBN and GOPEI are shown in Figure 5.8. Graphite is usually characterized by two main features, the G band at 1593 $cm^{-1}$ resulting from first order scattering of the in plane vibration of $E_{2g}$ photon of $sp^2$ carbon atoms of graphitic lattice and the D band at 1375 $cm^{-1}$ arising from a breathing mode of κ-point photons of $A_{1g}$ symmetry (Tang et al., 2014). Quantification of the intensity ratio of the D band to G band (i.e., $I_D/I_G$) reveals the extent of defects created by the chemical treatment. The $I_D/I_G$ ratio of graphite is very small (0.05). After the oxidation, the two bands broaden and shift to high frequency accompanied by an increased $I_D/I_G$ value (2.12), indicating the distortion of the bonds and destruction of symmetry due to the reduction in size of the in plane $sp^2$ domains caused by the extensive oxidation. However, the G peak of the GCTBN and GOPEI shifts from 1601 to near 1596 $cm^{-1}$ and 1595 $cm^{-1}$ respectively, getting close to that of natural graphite (1593 $cm^{-1}$) implying restoration of the graphitic $sp^2$ network (Liu et al., 2013). Compared to the as-produced GO, GCTBN and GOPEI sheets show slight increase in the $I_D/I_G$ values (from 2.12 to 2.34 and 2.31 respectively), which further confirms the formation of covalent bonds between the GO and the polymer molecules.

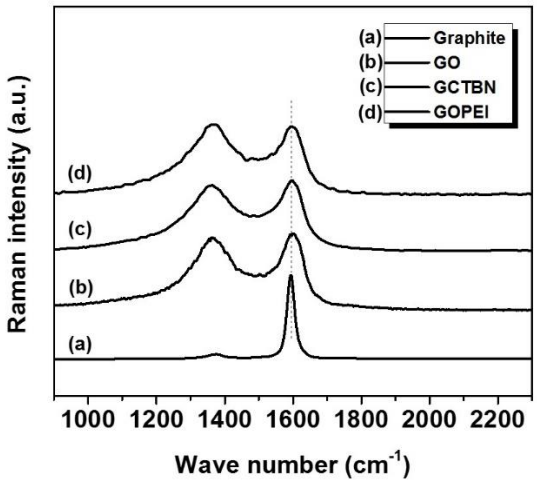


Figure 5.8: Raman spectra of (a) graphite, (b) GO, (c) GCTBN and (d) GOPEI

### 5.3.1.4. XRD Analysis

Figure 5.9 represents the XRD pattern of graphite, GO, GCTBN and GOPEI. Graphite show a characteristic diffraction peak at 26.5$^{o}$ representing the (002) reflection peak corresponding to an interlayer distance of 0.34 nm (Jiang et al., 2014). After the oxidation of graphite, GO shows a diffraction peak at lower diffraction angle at 11.63$^{o}$ degree indicating the increase of interlayer spacing due to presence of oxygen functional group at the surfaces and edges as a result of vigorous oxidation process. XRD pattern of GCTBN and GOPEI shows a weak and broad peak from 11-40 centered at 20.5$^{o}$ and 22.8$^{o}$ respectively, indicating the disappearance of the long-term ordering graphitic structure and the crystalline organization of sheets were affected by the presence of polymers.

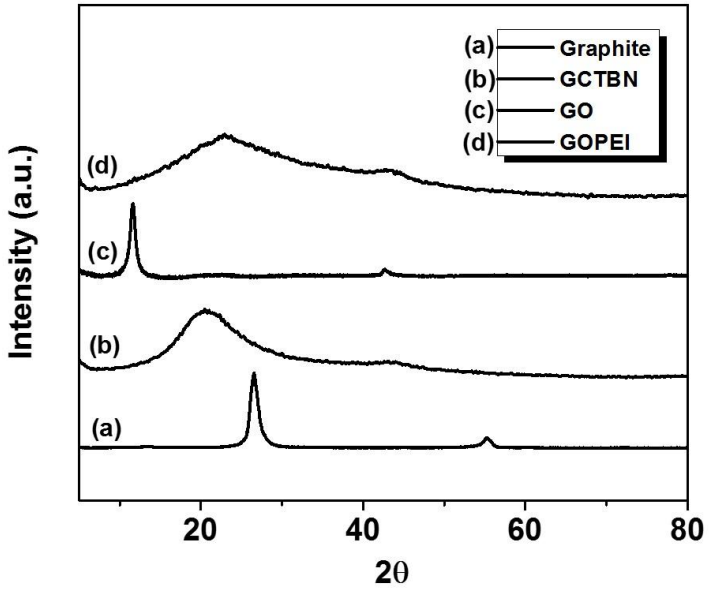


Figure 5.9: XRD of (a) graphite, (b) GCTBN, (c) GO and (d) GOPEI

### 5.3.1.5. TGA Analysis

Thermal gravimetric curves of graphite, GO, GCTBN and GOPEI are shown in Figure 5.10. From the figure, it is understood that GO is highly unstable and has an initial mass loss around 5 %, below 100 $^{o}$C due to the evaporation of absorbed water (Park et al., 2011; Stankovich et al., 2007), and the major weight loss of 40 % around 100–300 $^{o}$C is ascribed to the pyrolysis of the labile oxygen-containing functional groups, yielding CO, $CO_2$ and steam (Paredes et al., 2008). The percent weight of GO further decreased up to 800 $^{o}$C due to the degradation of carbon backbone. The functionalization and reduction of GO improves the thermal stability of the reinforcing filler. This is evident from the fact that for GCTBN, a decomposition of only 4.4 % is observed in the temperature region of 100-300 $^{o}$C. TGA curve of GCTBN shows a major decomposition of 67 % in the temperature range of 300-500 $^{o}$C which could be attributed to the decomposition of CTBN polymer chains that were grafted on the GO sheets. Similarly, GO PEI also exhibits a much higher thermal stability with a mass loss of 10.2 % at 200 $^{o}$C. The decomposition at around 300 $^{o}$C in GO-PEI is ascribed to the decomposition of PEI polymer chains that grafted on graphene sheets.The color change from brown to black and the reduction in intensities of oxygen functional groups in FTIR, XPS and TGA curves indicates the partial reduction of GO after the polymer grafting. This phenomenon of reduction of GOs during functionalization is observed elsewhere (Qian et al., 2014; Tang et al., 2014; Wang et al., 2012; Yuan et al., 2014).

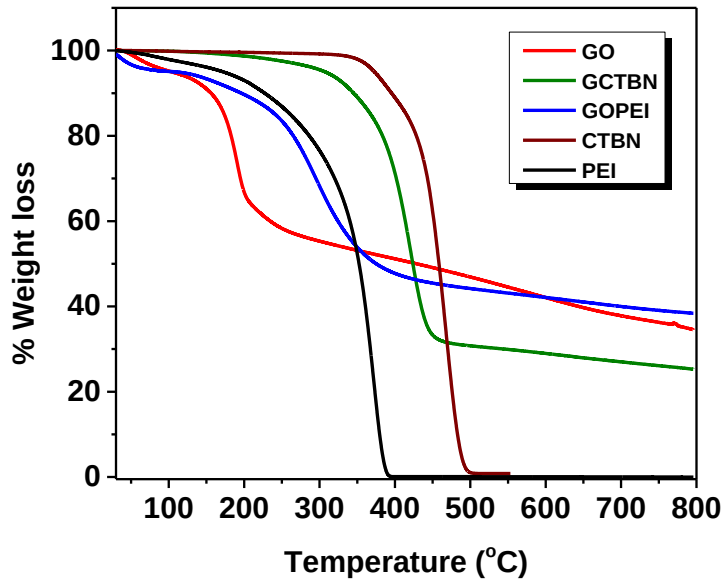


Figure 5.10: TGA curves of GO, GCTBN, GOPEI, CTBN and PEI

### 5.3.1.6. TEM Analysis

The morphology and structure of GO, GCTBN and GOPEI were determined by TEM analysis. The TEM image of the prepared GO sheets shows a thin sheet-like two-dimensional structure with a diameter of several micrometers. GO sheets contain a lot of wrinkles due to the presence of epoxy and hydroxyl functional groups within the graphene sheets (Sengupta et al., 2011). After the polymer functionalization, GCTBN and GOPEI sheets exhibited a rougher and thicker structure and a thin polymer layer seems to be observed surrounding the sheets, as shown in Figure 5.11, suggesting the successful grafting of polymers on GO.

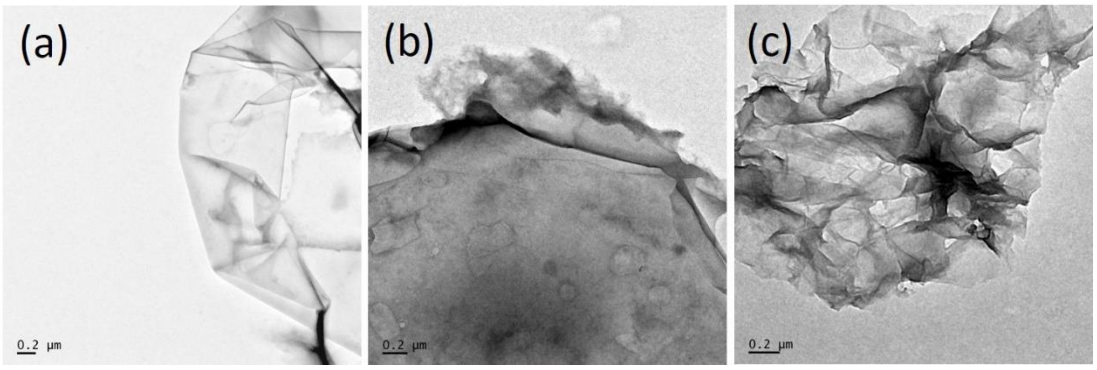


Figure 5.11: TEM images of (a) GO (b) GCTBN and (c) GOPEI

## 5.3.2. Dispersion behavior of nanosuspensions and composites

### 5.3.2.1. Transmission Optical Microscopy (TOM)

TOM micrographs reveal the dispersion of (a) 0.4 wt% GO, (b) 0.4 wt% GCTBN, (c) 0.4 wt% GOPEI, (d) 0.8 wt% GO, (e) 0.8 wt% GCTBN and (f) 0.8 wt% GOPEI in epoxy suspension before curing. TOM micrographs reveal the efficiency of chemical modification in the effective dispersion of GO. Figure 5.12 (a) represents the TOM images of epoxy nano suspension by the addition of 0.4 wt% GO at different magnifications. Small clusters of GO sheets can be seen at higher magnification. This is due to the presence of high functional group density of GO which results in Van der Waals interaction between sheets. The tendency of agglomeration is more at higher concentration of GO and in fact big clusters of GO is visible in Figure 5.12 (b). It can be seen that, after surface modification, the particles are uniformly distributed and show no noticeable degree of agglomeration (Figure 5.12 (c)-(f)).

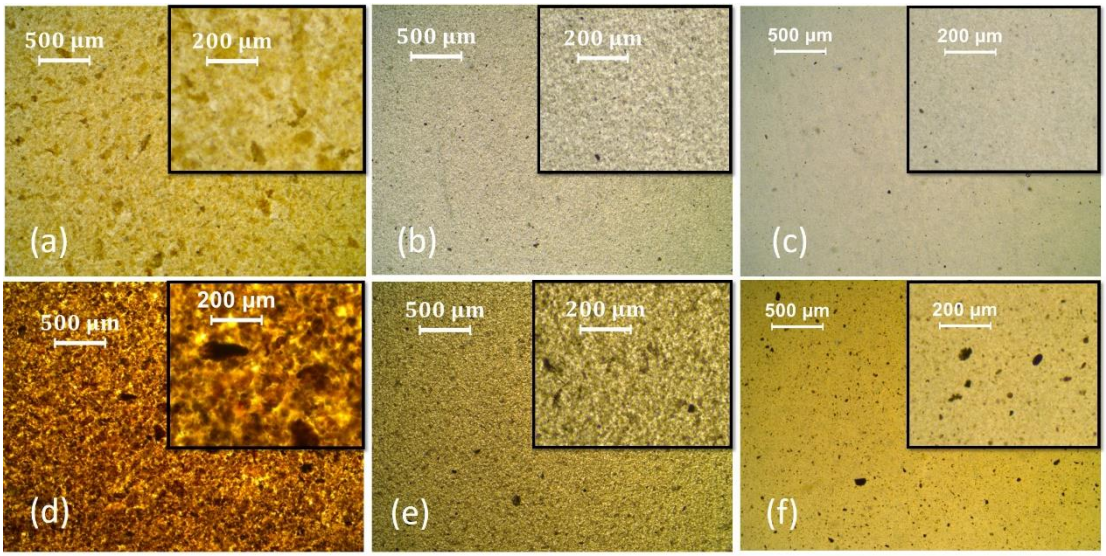


Figure 5.12: TOM images of epoxy nanosuspensions containing (a) 0.4 wt% GO, (b) 0.4 wt% GCTBN, (c) 0.4 wt% GOPEI (d) 0.8 wt% GO (e) 0.8 wt% GCTBN and (f) 0.8 wt% GOPEI. Insets show high magnification images

### 5.3.2.2. Rheology

Figure 5.13 shows the variation of viscosity of GO/epoxy and polymer grafted GO/epoxy nanosuspension with respect to shear rate. Neat epoxy resin showed a near Newtonian behavior whereas addition of GO resulted in a pseudo plastic behavior (viscosity decreases as shear rate increases). For GO/epoxy suspension, a drastic increase in viscosity was observed with increasing GO loading. On the other hand, the viscosity of polymer grafted GO/epoxy suspension is much lower than that of GO/epoxy suspension at low shear rates. This point towards the non-homogenous dispersion of GO in epoxy matrix due to the presence of high functional group density.

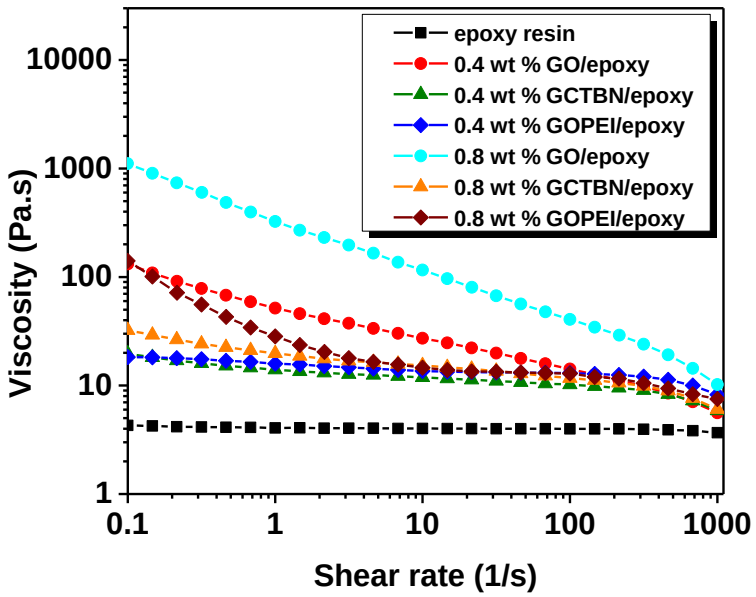


Figure 5.13: Variation of viscosity with shear rate for epoxy nano suspensions of GO, GCTBN and GOPEI

A typical plot between shear rate (log $\gamma$) and shear stress (log $\tau$) is presented in Figure 5.14 for epoxy resin, GO/epoxy and polymer grafted GO/epoxy nanosuspensions. The slope of the plots of shear rate (log $\gamma$) vs shear stress (log $\tau$) provided the pseudo plasticity index (*n).* As seen from data in Table 5.1, the pseudo-plasticity index *n* of the solution decreases by the addition of GOs. On adding pristine GOs, the *n* value shows an abrupt decrease. After chemical modification of GOs, shear thinning behaviour is observed but it is less pronounced; in other words, after chemical modification of GOs, the extent of Newtonian plateau is greater than with the GO epoxy suspension.

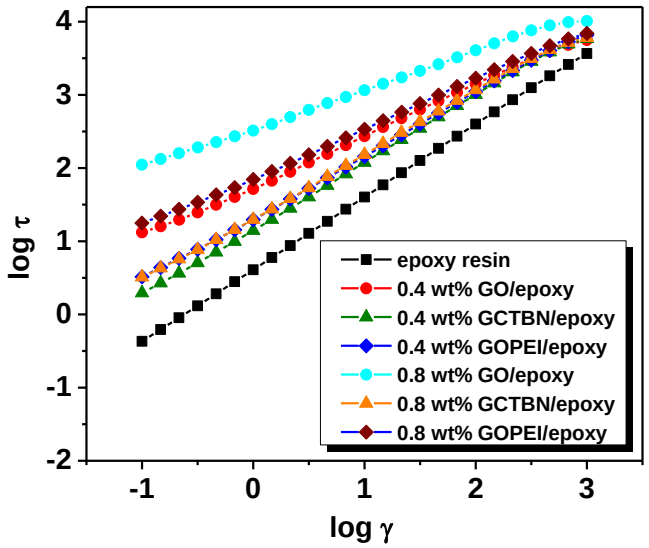


Figure 5.14: Variation of shear stress with shear rate for epoxy nano suspensions of GO, GCTBN and GOPEI

Table 5.1: Rheological data of GO/epoxy nanosuspensions

| **Sample code** | **Viscosity at shear rate 1 $s^{-1}$ (Pa.s)** | **Flow index (n)** |
|---|---|---|
| Epoxy resin | 4.07 | 0.99 |
| 0.4 wt% GO/epoxy | 51.7 | 0.69 |
| 0.4 wt% GCTBN/epoxy | 14.0 | 0.90 |
| 0.4 wt% GOPEI/epoxy | 19.7 | 0.85 |
| 0.8 wt% GO/epoxy | 325.0 | 0.52 |
| 0.8 wt% GCTBN/epoxy | 19.8 | 0.86 |
| 0.8 wt% GOPEI/epoxy | 69.8 | 0.67 |

### 5.3.2.3. TEM micrographs of epoxy composites

TEM images of GO/epoxy GCTBN/epoxy and GOPEI/epoxy composites are shown in Figure 5.15. In the GO/epoxy composite, agglomerates of GO sheets with

over a few microns in lateral size were observed. On the other hand, a significant improvement in exfoliation and dispersion was observed by the grafting of polymers on GO.

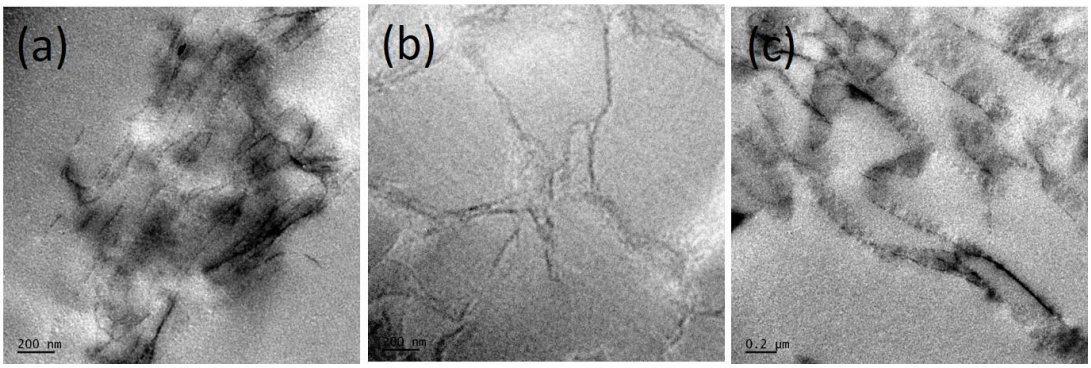


Figure 5.15: TEM images of epoxy nanocomposites containing (a) 0.6 wt% GO (b) 0.6 wt% GCTBN and (c) 0.6 wt% GOPEI

### 5.3.3. Tensile strength of epoxy composites

The tensile properties for neat epoxy and its composites with different filler loadings of GOs, GCTBN and GOPEI are summarized in Figure 5.16 and corresponding values are given in Table 5.2. From the Table, the addition of GOs improved the tensile properties. The tensile strength increases to a maximum of around 22% by the addition of 0.4 wt% GOs. Similarly, the tensile modulus and elongation at break shows a maximum increase of ≈16% and ≈ 36% respectively with the addition of 0.6 wt% GOs. The increase in tensile modulus represent the improved stiffness, on the other hand the increase in elongation at break represent the improved ductility. This means that the modification of epoxy with small amount of GOs (0.4 to 0.6 wt% of GOs) is an ideal way to improve the properties of epoxy systems. In fact this improvement in properties make the GO based composites attractive for many industrial applications.

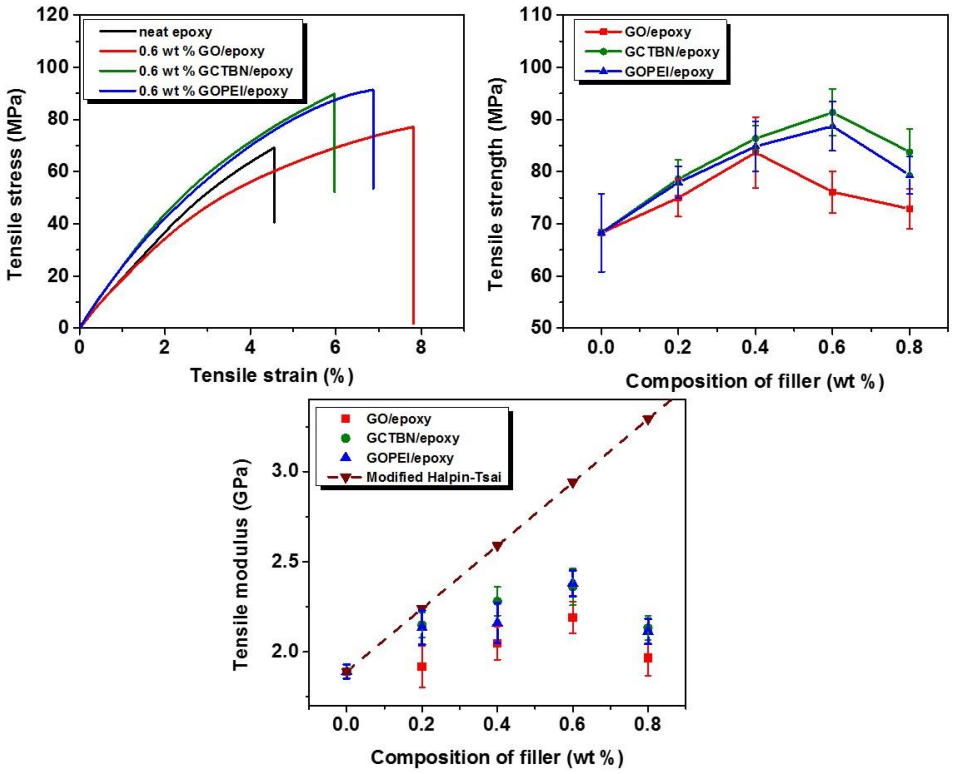


39

Figure 5.16: (a) Representative stress-strain curves (b) tensile strength and (c) tensile modulus of epoxy nanocomposites

Table 5.2: Fracture toughness and tensile properties of epoxy nanocomposites

| SI No | Sample code | $K_{IC}$ (MPa.m$^{1/2}$) | Tensile strength (MPa) | Tensile Modulus (GPa) | Elongation at break (%) |
|---|---|---|---|---|---|
| 1 | Neat epoxy | 0.74 ± 0.02 | 68.4 ± 1.7 | 1.89 ± 0.04 | 5.66 ± 0.63 |
| 2 | 0.2 wt% GO | 0.91 ± 0.10 | 75 ± 3.6 | 1.92 ± 0.11 | 6.01 ± 0.88 |
| 3 | 0.4 wt% GO | 1.46 ± 0.03 | 83.7 ± 6.8 | 2.05 ± 0.09 | 7.23 ± 1.45 |
| 4 | 0.6 wt% GO | 1.21 ± 0.10 | 76.1 ± 3.9 | 2.19 ± 0.09 | 7.69 ± 0.99 |
| 5 | 0.8 wt% GO | 0.98 ± 0.02 | 72.9 ± 3.8 | 1.97 ± 0.10 | 5.58 ± 0.67 |
| 6 | 0.2 wt% GCTBN | 1.09 ± 0.09 | 78.6 ± 3.6 | 2.15 ± 0.07 | 8.27 ± 0.11 |
| 7 | 0.4 wt% GCTBN | 1.58 ± 0.06 | 86.4 ± 2.4 | 2.28 ± 0.08 | 6.05 ± 0.40 |

| | | | | | |
|---|---|---|---|---|---|
| **8** | **0.6 wt% GCTBN** | **1.69 ± 0.07** | **91.4 ± 4.5** | **2.36 ± 0.10** | **6.23 ± 1.27** |
| 9 | 0.8 wt% GCTBN | 0.90 ± 0.03 | 83.8 ± 4.4 | 2.13 ± 0.07 | 6.96 ± 0.88 |
| 10 | 0.2 wt% GOPEI | 1.29 ± 0.02 | 77.9 ± 3.0 | 2.13 ± 0.09 | 7.12 ± 0.65 |
| 11 | 0.4 wt% GOPEI | 1.65 ± 0.02 | 84.9 ± 4.8 | 2.16 ± 0.11 | 6.98 ± 0.47 |
| **12** | **0.6 wt% GOPEI** | **1.98 ± 0.07** | **88.7 ± 4.7** | **2.38 ± 0.07** | **6.47 ± 1.12** |
| 13 | 0.8 wt% GOPEI | 1.55 ± 0.08 | 79.3 ± 3.6 | 2.11 ± 0.07 | 6.01 ± 0.87 |

The composites containing the polymer grafted GOs exhibit better tensile strength, and modulus values than their GO counterparts. For epoxy composite with 0.6 wt% GCTBN, the tensile modulus, and strength increased by ≈ 25% (2.36± 0.16 GPa), and ≈ 34% (91.4 ± 4.3 MPa) respectively with respect to neat epoxy system. Similarly for GOPEI/epoxy composites, an improvement of 26 and 30 % in tensile modulus and strength were observed. The experimental tensile modulus of the GCTBN/epoxy and GOPEI/epoxy composites are found to be comparable to the modulus predicted using the modified Halpin-Tsai modeling. From these results, it is clear that the reinforcing capability of polymer grafted GOs were better than that of GOs. The mechanical properties of the epoxy nanocomposites depend on the proper dispersion of fillers in the polymer matrix along with a good interaction between the reinforcement and the polymer. After grafting of GO with liquid rubbers, the fine dispersion and exfoliation of GCTBN and GOPEI sheets as well as the strong interfacial interaction between GO and epoxy due to the presence of soft polymer at the interface, favors proper stress transfer between the matrix and reinforcing filler and thus result in a significant enhancement in the tensile properties. This is schematically represented in Figure 5.17.

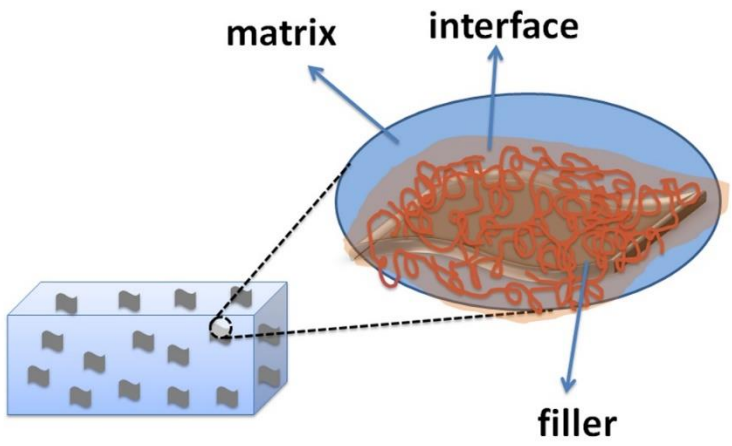


Figure 5.17: Schematic showing the interface between the epoxy matrix and polymer grafted GO filler

### 5.3.4. Fracture toughness of epoxy composites

Fracture toughness ($K_{IC}$) values of neat epoxy, GO, GCTBN and GOPEI epoxy nanocomposites are given in Table 5.2. Addition of GO and polymer grafted GOs into the epoxy matrix resulted in an improvement in fracture toughness (Figure 5.18). By the addition of 0.4 wt% GOs, $K_{IC}$ increased from 0.74 ± 0.02 MPa.m$^{1/2}$ to 1.46 ± 0.03 MPa.m$^{1/2}$ an increase of ≈ 97% improvement. This is followed by a decrease in the value of $K_{IC}$ at higher GO concentrations due to the presence of agglomerates and defects. GCTBN/epoxy composites shows higher fracture toughness values than GO/epoxy nanocomposites with highest fracture toughness of 1.69 ± 0.07 MPam$^{1/2}$ with an improvement of 128% compared to neat epoxy. It is interesting to notice that composite prepared by PEI grafted GO showed the maximum improvement in fracture toughness (166% improvement compared to neat epoxy) at a composition of 0.6 wt%. The functionalization of the GOs with PEI used in these composites created amino groups on the surface of filler which resulted in stronger bonding interactions with the epoxy matrix material and promoted improved dispersion of the particles, both of which contributed to improved fracture toughness.

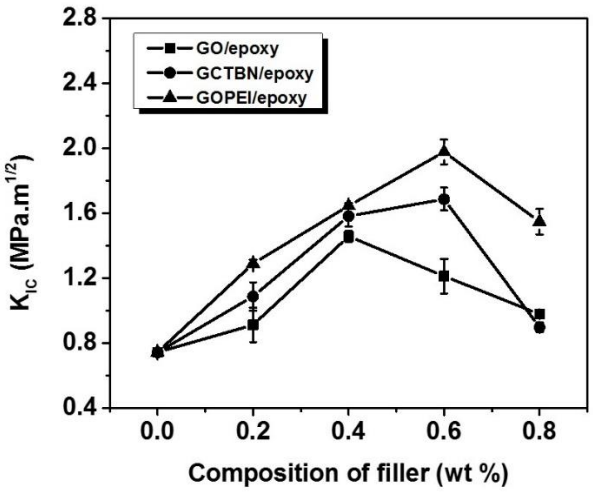


Figure 5.18: Fracture toughness of epoxy nanocomposites containing GO, GCTBN and GOPEI

To evaluate the dispersion and interfacial behavior of the composites, the fracture surface obtained after the fracture toughness test was evaluated using HRSEM (Figure 5.19 and 5.20). Fracture surface of neat epoxy shows smooth mirror like pattern which suggests poor absorption of energy during crack propagation which results in brittle fracture. Considerable difference is noticed between the failure surface of neat epoxy and that of GO/epoxy composite system. The fracture surfaces of the composites became very rough with the inclusion of GOs. These changes are attributed to the crack deflection and pinning created by the addition of the rigid GO sheets. The total fracture surface area of the system is increased as a result of incorporation of GOs resulting in greater energy absorption as compared to that of the unfilled polymer. The SEM image of the epoxy composites containing higher loading of GOs show non-uniform dispersion due to aggregated GOs. Aggregates of GO with size of several microns were observed at the surface of 0.8 wt% GO modified epoxy composite (shown as red circle in Figure 5.20). This indicates the breakdown of filler/matrix interface or in other words represents poor interactions between matrix and particle (Parameswaranpillai et al., 2013). Such aggregates of GO sheets and poor filler/matrix interface would cause stress concentrations during the fracture

process. These stress concentrations may facilitate failure during the fracture test. The fracture surface of polymer grafted GO/epoxy composite reveals a different surface morphology, and is relatively coarser than the composites containing GO. The rougher surfaces signify much more energy absorption. Moreover, SEM micrographs reveal no sheet pull out, which means that graphene surface is fully wet by the epoxy matrix. This indicates that the sheet/matrix interfacial bonding is effectively improved after doing the grafting with liquid rubbers (Naebe et al., 2014). Since functionalized GOs produced a stronger interface with the matrix than GO, polymer grafted GOs were able to carry a higher level of loading upon fracture, as indicated by the excellent fracture features. As in the case of GO/epoxy composites, a higher loading of functionalized GOs in the system resulted in the agglomeration of sheets resulting in a decrease in the $K_{IC}$ values

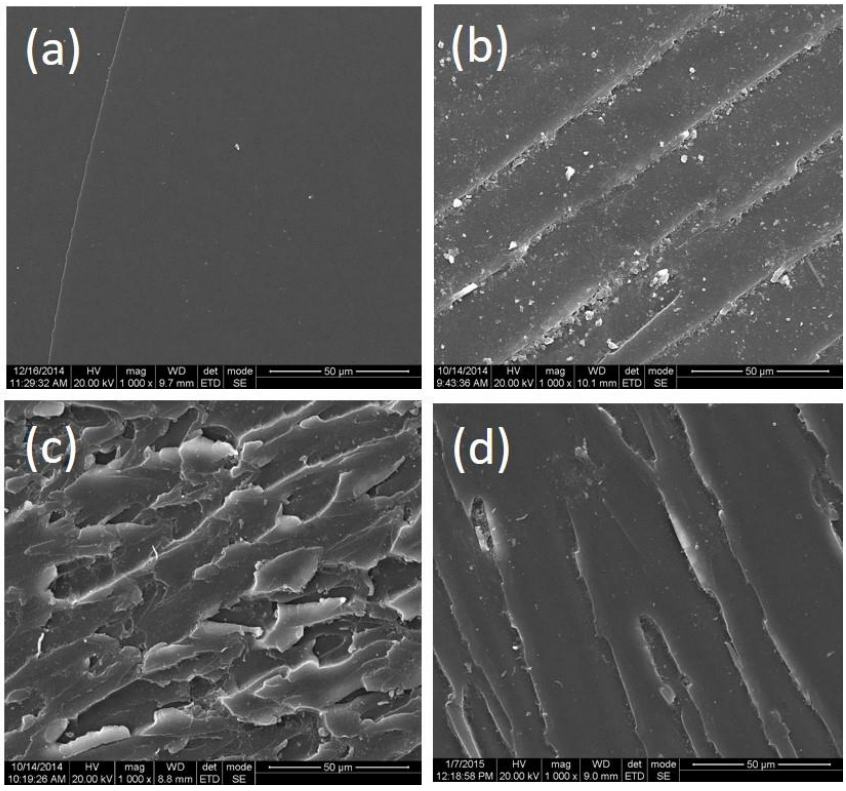


Figure 5.19: FESEM images of fractured surface of sample: (a) neat epoxy (b) 0.6 wt% GO (c) 0.6 wt% GCTBN and (d) 0.6 wt% GOPEI

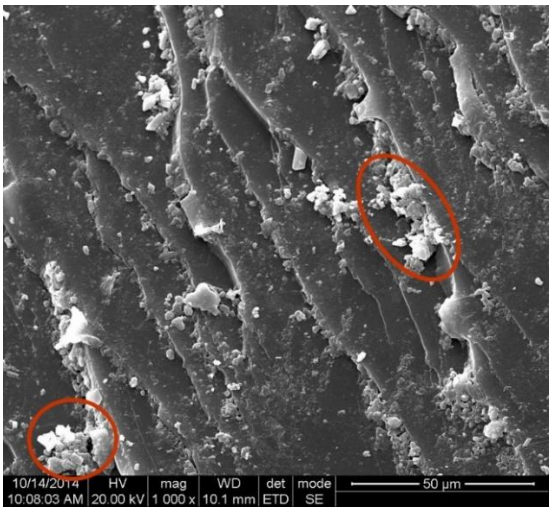


Figure 5.20: FESEM image of fractured surface of epoxy composite containing 0.8 wt% GO

## 5.3.5. Dynamic mechanical analysis

DMA was carried out to understand the viscoelastic behavior over a wide range of temperatures for neat epoxy, GO/epoxy and polymer grafted GO/epoxy. Figure 5.21 shows a comparison of the *G′* of neat epoxy and epoxy with 0.6 wt% of GOs and polymer grafted GOs in the temperature range 30 – 250 $^{o}$C. The storage modulus of neat epoxy system was improved significantly with the incorporation of GO sheets. The storage modulus at the glassy region and rubber region are given in Table 5.3. From the table, the storage modulus of neat epoxy at 30 $^{o}$C is 1995 MPa, while that of GO, GCTBN and GOPEI epoxy composites are 2319, 2476 and 2561 MPa respectively. These values were ≈ 16, 24 and 28 % higher than those obtained for the neat epoxy system. The increased stiffness is due to the high modulus of graphene platelets dispersed in the epoxy matrix. It can be noticed that the storage modulus is maximum for polymer grafted GO/epoxy composites. This is due to the strong interfacial interaction between the filler and matrix after chemical modification with rubber, which reduces the mobility of the local matrix around the sheets. All the composites show two inflection points, one at 60 $^{o}$C, due to lower cross-link density

sites in the epoxy network and the other at the glass transition temperature ($T_g$) of the cross-linked epoxy system at around 200 $^oC$.

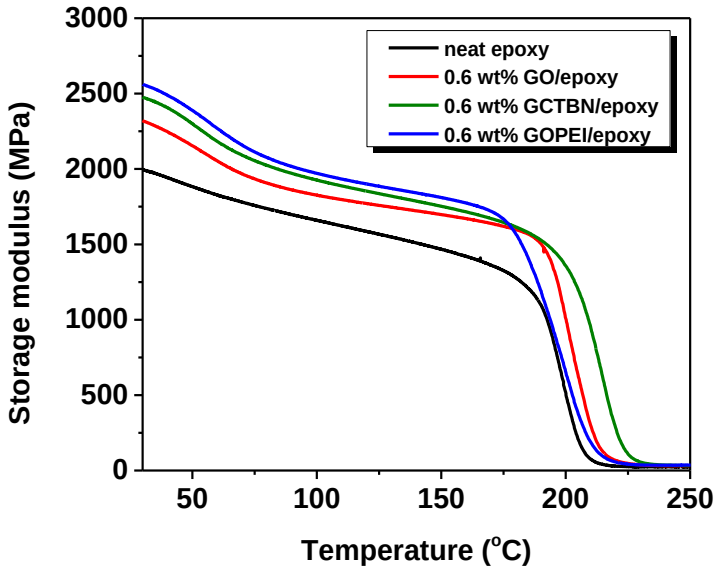


Figure 5.21: Storage modulus versus temperature curves for neat epoxy, 0.6 wt% GO, 0.6 wt% GCTBN and 0.6 wt% GOPEI modified epoxy nanocomposites

Table 5.3: Values of storage modulus (G') at rubbery and glassy region and *Tg* for the prepared epoxy composites

| **Sample code** | ***G'* at 30 $^oC$ (MPa)** | ***G'* at 245 $^oC$ (MPa)** | **$T_g$ ($^oC$)** | **Interaction parameter (B)** | **Constrained region (Cr)** |
|---|---|---|---|---|---|
| Neat epoxy | 1995 | 24.75 | 208.5 | -- | 0 |
| 0.6 wt% GO/ epoxy | 2319 | 31.89 | 214.5 | 0.022 | 0.0040 |
| 0.6 wt% GCTBN/ epoxy | 2476 | 34.72 | 225 | 0.062 | 0.0114 |
| 0.6 wt% GOPEI/ epoxy | 2561 | 35.36 | 214.2 | 0.111 | 0.0202 |

Figure 5.22 shows the temperature dependence of tan $\delta$ of cured neat epoxy and its GO composites. The tan $\delta$ is the ratio of G" to G' and the peaks of tan $\delta$ are often used to determine the $T_g$ of the material. The obtained $T_g$ for the composites are shown in Table 5.3. The $T_g$ of epoxy composites increased with the addition of GO, from 208.5 $^oC$ in the case of pristine resin to 214.5 $^oC$ for the 0.6 wt% GO/epoxy composite, with an increase of 7 $^oC$. On the other hand, the GCTBN/epoxy composite shows the highest $T_g$ (~225 $^oC$), with a remarkable increase of 16.5 $^oC$. This increase in $T_g$ is due to the hindered polymer chain mobility near the filler/matrix interface or surrounding the filler due to chemical bonding.

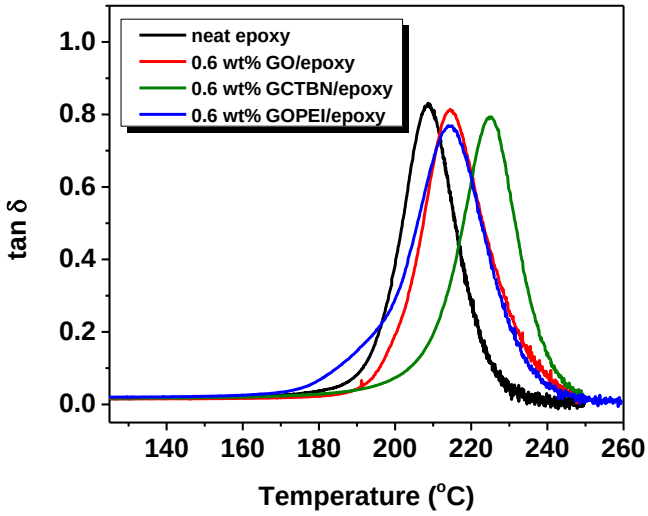


Figure 5.22: Tan delta versus temperature curves for neat epoxy, 0.6 wt% GO, 0.6 wt% GCTBN and 0.6 wt% GOPEI modified epoxy nanocomposite

The height depression in the *tan* $\delta$ peak indicates a reduction in the amount of mobile polymer chains during the glass transition; therefore the height loss in tan $\delta$ peak can be used to determine the volume fraction of the constrained region (polymer chains immobilized by the GO platelets) in epoxy phase in the epoxy nanocomposites. The height depression in the *tan* $\delta$ peak and the increase in $T_g$ is considerably significant for the GO/epoxy and polymer grafted GO/epoxy system. The volume fraction of the constrained region in each sample can be estimated from

the height of the tan $\delta$ peak. In GO/epoxy composites, the GOs have high surface to volume ratio and hence epoxy chains get attached to the GO surface thereby limiting the mobility of the surrounding polymer chains and hence leads to the formation of constrained regions around the nano filler with higher $T_g$. Among the epoxy nanocomposites, the GOPEI/epoxy system exhibits the highest fraction of constrained region. For the GOPEI modified epoxy blends, the sheet/matrix interfacial bonding is effectively improved and therefore more epoxy chains get attached with the GO surface leading to the formation of a higher fraction of constrained regions with highest $T_g$ and height depression in the *tan* $\delta$ peak.

The interfacial interaction between the polymer grafted GOs and epoxy matrix can also be calculated from tan $\delta$ profile (Ziegel and Romanov, 1973). The relationship between tan $\delta$ of the polymer nanocomposites and neat polymer can be evaluated by the following equation.

$$\tan\delta = \frac{\tan\delta_m}{\left(1+1.5B\phi\right)} \tag{5.1}$$

where tan $\delta$ and tan $\delta_m$ are the loss tangent of polymer nanocomposite and neat polymer, respectively; $\phi$ and B represents the volume fraction of the fillers and an interaction parameter respectively. The positive value of B indicates good interaction between the fillers and polymer matrix (Zeng et al., 2014).

The calculated interaction parameter (B) for GO/epoxy, GCTBN/epoxy and GOPEI/epoxy nanocomposites is given in table 5.3. As mentioned above, the positive value of B indicates good interaction between the fillers and polymer matrix. Please note that the interaction parameter for functionalized GO/epoxy nanocomposites is much higher when compared with GO/epoxy system. This is due to the strong interfacial interaction between the filler and matrix after chemical modification with

rubber, which reduces the mobility of the local matrix around the sheets, which led to better modulus and $T_g$.

### 5.3.6. TGA of epoxy composites

Thermal stability of the epoxy composites was traced using TGA. The thermal stability of epoxy composites with 0.6 wt% loading of GO and functionalized GOs were compared with neat epoxy system in Figure 5.23. The thermal stability of epoxy matrix was not affected by the addition of GO. As shown in the figure, the main weight loss for the composites takes place at around 320 $^{o}$C, which is attributed to the degradation of epoxy network. This means that all the composites prepared are very stable and show little degradation below 320 $^{o}$C and therefore can be used for many high temperature applications.

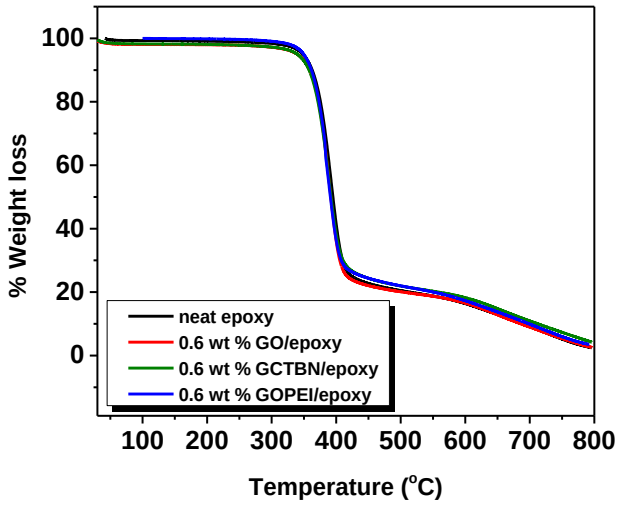


Figure 5.23: TGA and DTG curves of epoxy nanocomposites

## 5.4. Conclusions

Polymer grafted GOs were successfully synthesized. Partial reduction of GO was observed during functionalisation with CTBN and PEI. The prepared GO and

polymer grafted GOs were characterized by FTIR, XPS, Raman spectroscopy, XRD, TEM, TOM and TGA. The studies reveal the grafting of polymers with GO. The thermo-mechanical properties were carefully analyzed using UTM, DMA and TGA. The fracture surface was carefully characterized by SEM. The mechanical properties of the epoxy system show an excellent improvement by the addition of polymer grafted GOs. The surface morphology reveals improved interfacial bonding between the filler/matrix. Therefore, polymer grafted GO/epoxy composites are able to carry higher level of loading during fracture. The viscoelastic properties also show drastic improvement in modulus and $T_g$. This improvement in $T_g$ is due to the hindered polymer chain mobility near the filler/matrix interface. The improvement in modulus and $T_g$ was further confirmed by the quantitative analysis of the constrained region. Furthermore, the TGA studies reveal good thermal stability and depicts that the decomposition temperatures of epoxy composites are above 320 $^{o}$C. In addition, it can be concluded that polymer grafted GOs can be effectively utilized to improve significantly the thermo-mechanical properties of epoxy composites.

# CHAPTER 6

# FABRICATION AND CHARACTERISATION OF $TiO_2$-NANOWIRE BASED EPOXY NANOCOMPOSITES

*$TiO_2$-derived nanowires were prepared by a simple hydrothermal synthesis using commercial $TiO_2$ powder (Aeroxide P25) as starting material. This experimental study was intended to compare the properties of epoxy composites prepared with $TiO_2$(B)-NWs to that with commercial $TiO_2$ nanoparticles. Differences in the mechanical, thermal, and morphological properties of composites prepared with these two materials at different filler loadings were studied. The mechanism that paved way to the enhancement in the fracture toughness of the $TiO_2$(B)-NW/epoxy nanocomposites was evaluated.*

The results of this chapter have been communicated for publication in **Composite Part B: Engineering**

# 6.1. Introduction

Many ways to toughen epoxies have been discussed extensively in the literature, including the use of liquid rubbers (Chikhi et al., 2002; Puglia et al., 2013), thermoplastic (Jyotishkumar et al., 2012; Kim, Chiba and Inoue, 1995) and inorganic particles (Lim et al., 2010; Ragosta et al., 2005), etc. The incorporation of inorganic particulate fillers has also proved to be an effective way of improving the mechanical properties, such as modulus and strength of resin (Adachi et al., 2008). Nano-reinforcements, as opposed to traditional reinforcements, have been shown to improve mechanical and thermal properties at much lower filler loadings (Hsieh et al., 2010; Park et al., 2015; Yang et al., 2009). Due to their extremely high specific surface area, the nanoparticles exhibit high interfacial interactions between the particles and the polymer matrix that primarily leads towards the achievement of novel properties in materials.

Filler geometry of a composite plays a crucial role in determining the mechanical performance of the composites. Effect of particles size and shape on the mechanical properties of composites have been discussed by several authors. Hassanabadi and Rodrigue (2014) investigated the effect of particle characteristics such as size and shape on the reinforcing efficiency of different nanofillers ($CaCO_3$, talc, nano-crystalline cellulose (NCC), multi-walled nanotube and clay) in ethylene vinyl acetate composites. Suraiti et al. (2011) measured flexural properties of nano-sized silver nanoparticle/epoxy nanocomposites and compared them with those of composites with micron sized silver flakes. The correlation between the shape and size of the ceria nanostructures and the mechanical performance of their epoxy composites was investigated by He et al. (2011). Their results demonstrate that epoxy resins made with high aspect ratio ceria nanorods show the highest impact strength, up to 17.27 $kJ/m^2$, which is about four times that of the neat epoxy resin. Alishahi et al. (2013) studied the effect of shape of carbon nanofillers on the mechanical

properties of epoxy nanocomposites. It is noteworthy that while nano diamond and fibrous (carbon nanotube and nanofiber) particles provided better tensile properties, platelet (graphene oxide) nano reinforcements lead to a considerable increase in the fracture toughness of the composites. A few researchers have investigated the effect of aspect ratio of carbon nano tubes on the properties of nanocomposites and it has been found that they can have a substantial effect on both the mechanical and electrical properties. For instance, the effect of aspect ratio of nanotubes on the mechanical properties of nanocomposites was investigated by Martone et al. (2011). Interestingly it was noticed that composites with high aspect ratio MWNTs present higher modulus than those with low aspect ratio MWCNTs at identical filler loading levels. Moreover, the impact behavior of polypropylene (PP) filled with MWCNTs of different lengths was studied by Zhang and Zhang (2007) and they concluded that the longer MWCNTs exhibited higher toughening efficiency than the shorter ones.

$TiO_2$ is extensively used in industry as an additive in plastics, catalysts and catalyst supports, photochemical degradation of toxic chemicals, and so on. Therefore, $TiO_2$/epoxy nanocomposites do have wide applications, particularly in organic photovoltaics, fire retardant composites, and so on (Bittmann et al., 2011; Carballeira and Haupert, 2010; Hamming et al., 2009; Wu et al., 2011). $TiO_2$ has not received much attention as a filler for the enhancement of mechanical performance of polymers. Only a few reports are concerned about the effect of volume fraction and size of $TiO_2$ particle on the mechanical performance of epoxy composites in the literature (Al-Turaif, 2010). $TiO_2$(B)-NWs offer promising advantages towards the improvement of mechanical properties in polymer composites because of their wire structure and high aspect ratio which makes them impart better stress transfer from $TiO_2$ to the matrix during loading. The larger surface area of $TiO_2$(B)-NWs increases the contact area with the polymer matrix maximizing the stress transfer from the polymer to the nanowires. Thus, $TiO_2$(B)-NW/epoxy composite can be expected to exhibit better reinforcement than nano $TiO_2$ powder in polymer composites, due to its high aspect ratio and higher contact surface area.

It is significant to determine the influence of shape on the properties of the composites made with $TiO_2$. Many previous works have been focused on size, distribution of filler and volume fraction of filler, to the best of author's knowledge, not much of an experimental comparison has been made on the effect of shape of $TiO_2$ nanoparticle on the mechanical properties of nanocomposites. The main objective of this chapter is to analyse the mechanical performance and fracture resistance of epoxy-based nanocomposites reinforced with $TiO_2$ of two different shapes including nanowires and nanoparticles. The fracture mechanisms involved in nano-reinforcement and the effect of particle shape on these mechanisms are discussed in detail.

# 6.2. Materials and Methods

## 6.2.1. Materials

$TiO_2$ (Aeroxide P25) was purchased from Sigma Aldrich, Bangalore, India. Sodium hydroxide (NaOH) and hydrochloric acid was purchased from Spectrochem, India. The polymer matrix used in the present study was epoxy resin Lapox ARL-135 DGEBA (epoxy equivalent 187 g/eq) and DDS hardener under the commercial name Lapox K10 and was purchased from Atul India private limited, Gujarat. All the chemicals were used as received without further purification.

## 6.2.2. Preparation of $TiO_2$(B)-NWs

$TiO_2$-derived nanowires ($TiO_2$(B)-NWs) were synthesized by the hydrothermal treatment using commercial $TiO_2$ powder (Aeroxide P25) as starting material. In a typical preparation procedure (Armstrong et al., 2004), 150 mg $TiO_2$ white powders were placed into a Teflon-lined autoclave of 25 mL capacity. Then,

the autoclave was filled with 10 M solution of NaOH up to 80% of the total volume, sealed into a stainless steel tank and maintained at 200 $^{o}$C for 24 h. It was cooled down to room temperature and the obtained sample was sequentially washed with 0.1 M HCl aqueous solution (250 mL) followed by distilled water until pH becomes neutral. It was subsequently dried at 70 $^{o}$C for 12 h in a vacuum oven. Titanate nanowires, obtained by the above-mentioned method, were heated in an air atmosphere at 400 $^{o}$C for 4 h to obtain $TiO_2$(B)-NWs.

### 6.2.3. Preparation of $TiO_2$/epoxy nanocomposites

Epoxy composites with different loadings of $TiO_2$ were prepared by the following procedure. Required amounts of $TiO_2$ (0.2, 0.4, 0.6 and 0.8 wt% with respect to DGEBA) was initially dispersed in a mixture of acetone by sonication for 15 min and then mixed with DGEBA and sonicated again for 15 min to obtain a white suspension. Acetone was evaporated off by heating at 90 $^{o}$C for 2 h. The trace amount of solvent was then removed by keeping in a vacuum oven. It was then added to molten hardener (35 g/100 g DGEBA) and stirred for 10 minutes. It was degassed for 5 min until there was no sign of trapped bubbles. The mixture was poured into a preheated mould and cured for 4 h at 180 $^{o}$C. Post curing was done at 200 $^{o}$C for an hour. The same procedure was followed for the preparation of $TiO_2$(B)-NW/epoxy composite. The flow chart of the preparation of epoxy composites filled with $TiO_2$ is shown in Figure 6.1.

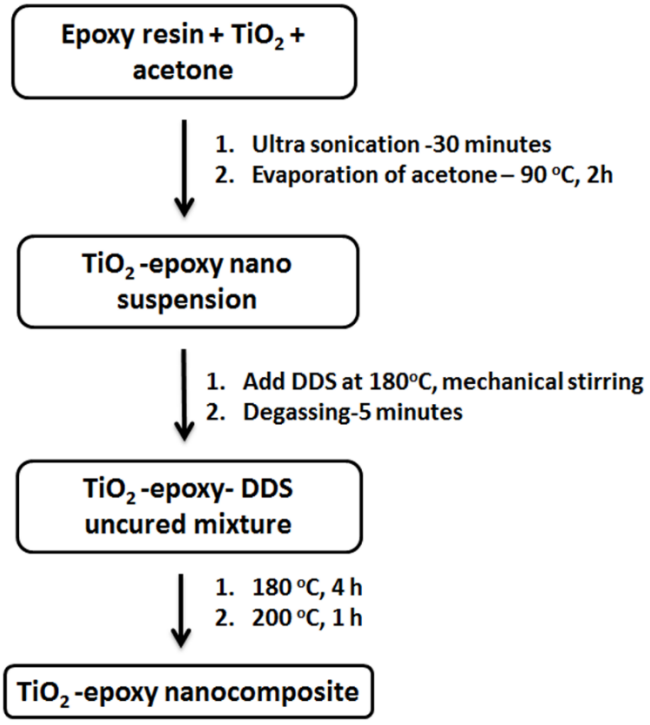


Figure 6.1: Flow chart of the preparation of $TiO_2$/epoxy nanocomposites

## 6.2.4. Characterization

The morphology of $TiO_2$(B)-NWs as well as the fracture surfaces of the composite samples were investigated using field emission SEM (FE SEM, FEI Quanta FEG200) at an accelerating voltage of 20 kV, and the fracture surfaces were coated with a conductive layer of gold. The phase identification of the nanowire samples was conducted with powder X-ray diffraction (XRD) using using X-ray diffractometry (PANalytical 3 kW X'pert PRO X-ray diffractometer) using Cu Ka (k= 1.5406 Å) radiation source operating at a voltage of 45 kV and 300 mA of electric current. The data was collected for scattering angles ($2\theta$) ranging from 5 to $70^o$ (2h). The high-resolution transmission electron microscopy (HRTEM) of the samples was performed using JEOL JEM-2100 equipped with an EDX spectrometer with an acceleration voltage of 200 kV. Sliced thin sections of $TiO_2$/epoxy

composites with a thickness of about 60-80 nm, prepared by ultra-microtomy, were used to take the TEM images of the composites. Dynamic Mechanic Analysis (DMA) was performed on a DMA Q800, operating in the single cantilever mode at an oscillation frequency of 1 Hz. Data was collected from room temperature to 250 $^{o}$C at a scanning rate of 2 $^{o}$C/min. The sample specimens were cut into rectangular bars measuring 50 x 5 x 2 $mm^3$. Tensile tests were performed with dumbbell shaped specimens using an Instron model 5969 tensile tester at a crosshead speed of 1 mm/min as per ASTM standard D638. The results are the average of at least five measurements. Fracture toughness of the sample was measured using UTM (Instron 5969, Instron, USA) at a crosshead speed of 10 mm/min (as per ASTM standard D5045). Single edge notch specimens of 46 × 6 × 3 $mm^3$ (span length =24 mm) were used to measure the fracture toughness of the epoxy nanocomposites.

# 6.3. Results and Discussion

## 6.3.1. Characterization of $TiO_2$(B)-NWs

### 6.3.1.1. SEM Analysis

The morphologies of both $TiO_2$ nanoparticle and $TiO_2$(B)-NWs were characterized by scanning electron microscopy, as shown in Figure 6.2. Figure 6.2 (a) shows the HRSEM images of the commercial $TiO_2$ nano particles. Although commercial P-25 $TiO_2$ powder is known to be very fine with a particle size of 25–30 nm (information provided by the manufacturer), SEM analysis of nano $TiO_2$ particles shows particles with clumped distributions. After the hydrothermal treatment followed by heating at 400 $^{o}$C, the as-synthesized $TiO_2$(B)-NWs exhibit wire-like morphology with typical lengths in the range of 3 microns to more than 5 microns and diameter of 50 to 80 nm (Figure 6.2 (b)).

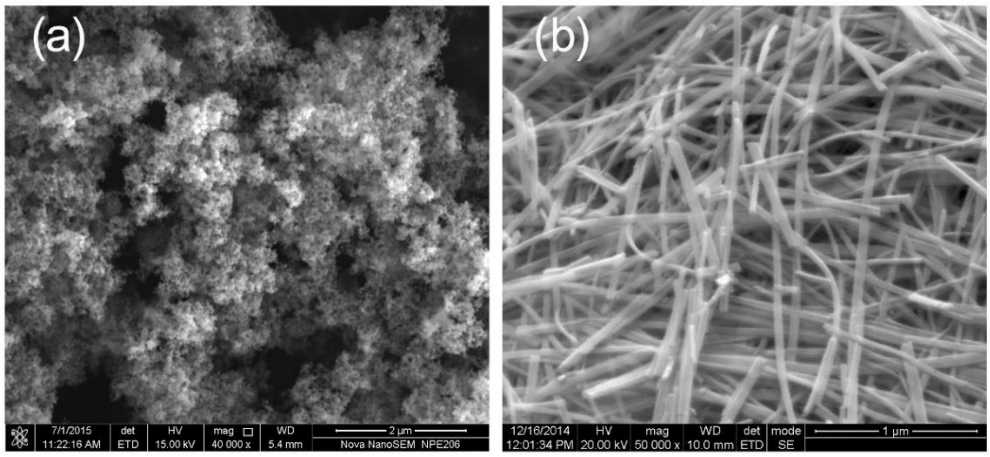


Figure 6.2: HRSEM image of (a) $TiO_2$ nanoparticle and (b) $TiO_2$(B)-NWs

### 6.3.1.2. XRD Analysis

The XRD patterns of $TiO_2$ precursor (Degussa P-25) and the synthesized nanowires are shown in Figure 6.3. The XRD pattern of nanowire obtained after hydrothermal treatment and HCl washing showed a close resemblance to the reported literature (Kolen'ko et al., 2006; Yoshida et al., 2005), indicating hydrogen titanate nanowire structure. After the heat-treatment at a temperature of 400 $^{o}$C, the nanowires were dehydrated and re-crystallized into the metastable form of $TiO_2$(B)-NWs (Armstrong et al., 2004; Tsai and Teng, 2006). At 400 °C, all the peaks shown in the XRD spectrum can be indexed to $TiO_2$(B) phase and is in good agreement with published data (Armstrong et al., 2005; Kolen'ko et al., 2006; Li et al., 2011), indicating that the titanate nanowires are converted into $TiO_2$(B)-NWs.

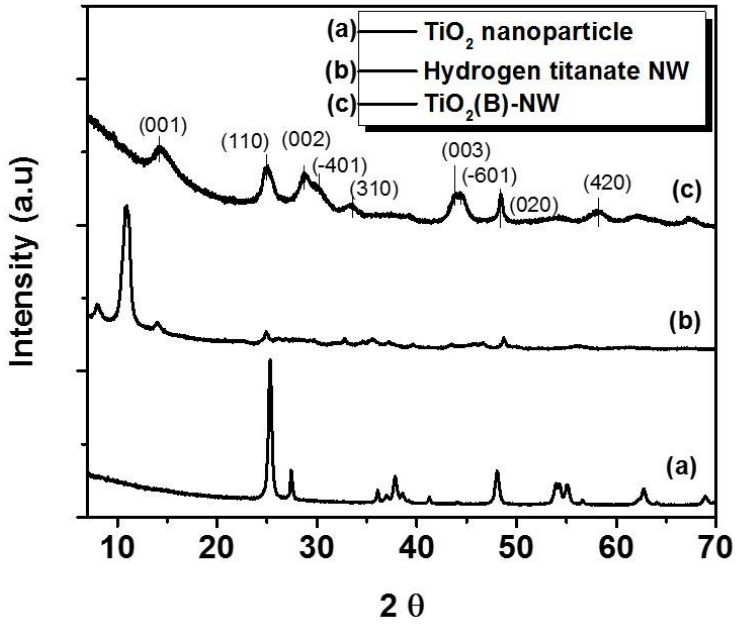


Figure 6.3: XRD image of (a) $TiO_2$ nanoparticles, (b) hydrogen titanate NWs and (c) $TiO_2$(B)-NWs

## 6.3.2. Dispersion behavior of epoxy nanosuspension and composites

### 6.3.2.1. Transmission Optical Microscopy (TOM)

Optical microscopy images can be used effectively to characterize the state of aggregation at the micrometer scale. Optical micrographs at different magnification levels for the dispersion of (a) 0.6 wt% $TiO_2$ and (b) 0.6 wt% $TiO_2$(B)-NWs in epoxy suspension before curing are presented in Figure 6.4. As revealed in Figure 6.4 (a), the $TiO_2$ particles show many agglomerates in the epoxy matrix, which are indicated by the red circles. This is due to the presence of hydroxyl group density on the surface of $TiO_2$ which results in Van der Waals interaction between the particles. On the contrary, it can be seen that in $TiO_2$(B)-NW/epoxy suspension (Figure 6.4 (b)), the nanowires are uniformly distributed and the dispersion of $TiO_2$(B)-NWs in epoxy is relatively better.

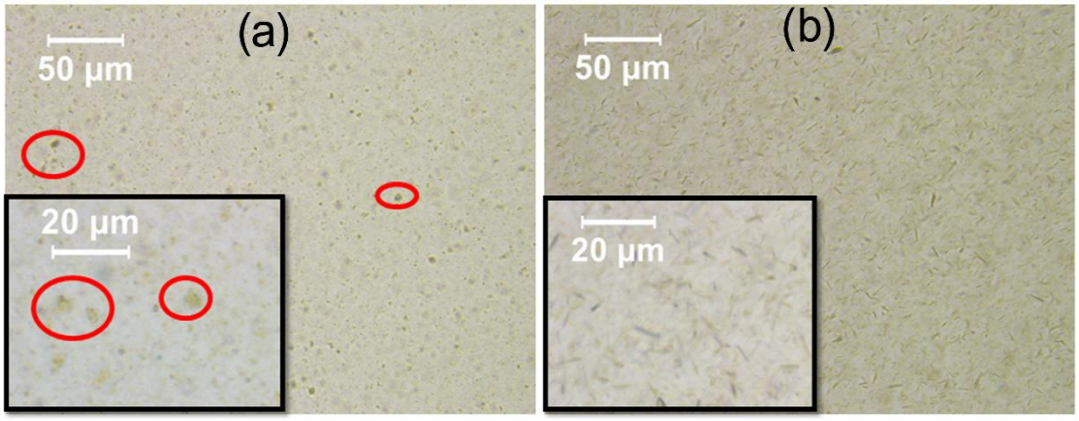


Figure 6.4: TOM images of epoxy nano suspensions containing (a) 0.6 wt% $TiO_2$ and (b) 0.6 wt% $TiO_2$(B)-NWs. Insets show high magnification images

### 6.3.2.2. Rheology

Figure 6.5 shows the variation of viscosity of $TiO_2$/epoxy and $TiO_2$(B)-NW/epoxy nano suspension with respect to shear rate. All the systems showed a near Newtonian behavior. In the case of $TiO_2$/epoxy suspension, no drastic increase in viscosity was observed with increasing $TiO_2$ loading. On the other hand, the viscosity of $TiO_2$(B)-NW/epoxy suspension is lower than that of $TiO_2$/epoxy suspension at low shear rates. This point towards the homogenous dispersion of $TiO_2$(B)-NWs in the epoxy matrix as observed in TOM images.

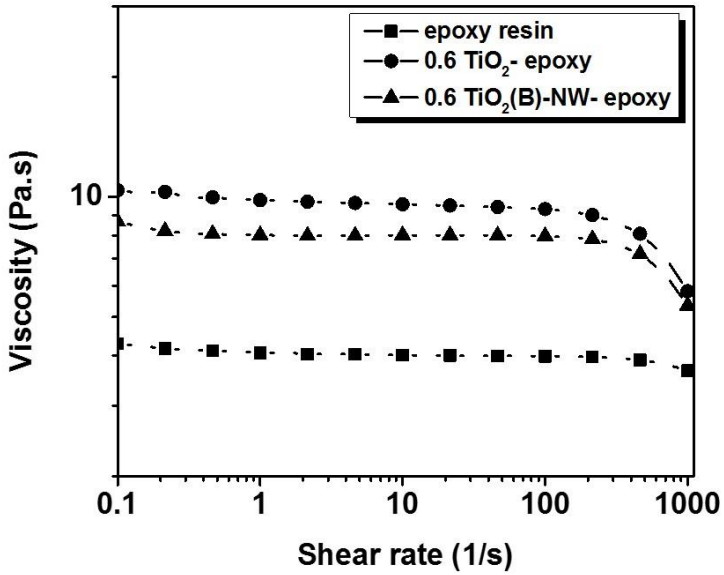


Figure 6.5: Variation of viscosity with shear rate for epoxy nano suspensions of $TiO_2$ and $TiO_2$(B)-NWs

## 6.3.3. Characterization of Epoxy Composites

### 6.3.3.1. TEM micrographs

TEM images of $TiO_2$ modified epoxy and $TiO_2$(B)-NW/epoxy composites are shown in Figure 6.6. In $TiO_2$ modified epoxy composite, agglomerates of $TiO_2$ with over a few microns in lateral size were observed. The micrograph of $TiO_2$(B)-NW/epoxy composite shows the existence of individual $TiO_2$(B)-NWs embedded in the epoxy matrix. A significant improvement in the dispersion was observed by using $TiO_2$ (B)-NWs as fillers instead of nanopowder.

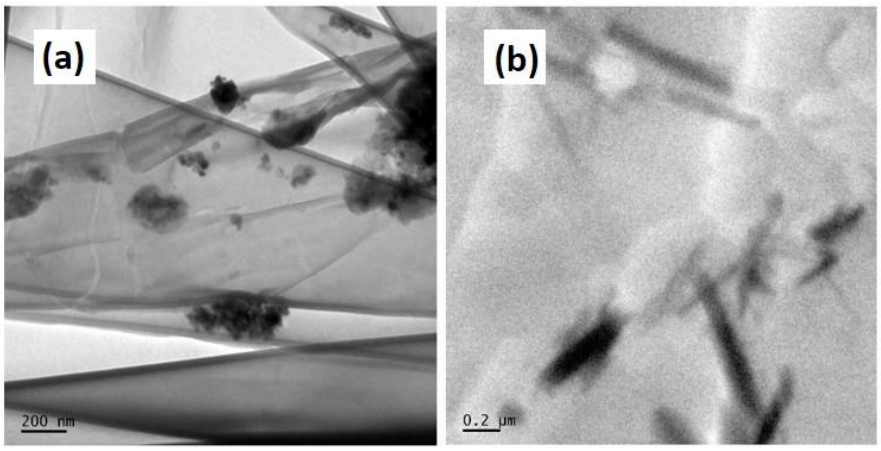


Figure 6.6: TEM image of epoxy nanocomposites containing (a) 0.6 wt% $TiO_2$ and (b) 0.6 wt% $TiO_2$(B)-NWs

### 6.3.3.2. Tensile strength of epoxy nanocomposites

The mechanical properties of the epoxy nanocomposites depend on the volume fraction and aspect ratio of the filler, dispersion of fillers in the polymer matrix and interaction between the filler and the polymers. Effects of the addition of $TiO_2$ and $TiO_2$(B)-NWs as fillers on the tensile strengths of the resultant composites are illustrated in Figure 6.7 and also summarized in Table 6.1. Representative tensile stress versus strain curves are shown in Figure 6.7 (c). $TiO_2$/epoxy composites show limited increases in tensile properties. For epoxy composites with 0.6 wt% $TiO_2$, the tensile modulus and strength increased by 7% (2.02 ± 0.02 GPa) and 13% (77.3 ± 2.6 MPa), respectively. It was clear that the reinforcing capability of $TiO_2$(B)-NWs was much higher than that of $TiO_2$ for all concentrations. The highest increase in tensile modulus is 16% (from 1.89 ± 0.03 to 2.20 ± 0.01 GPa) at $TiO_2$(B)-NW loading of 0.60 wt%. The highest increase in tensile strength is 26% (from 68.4 ± 1.7 to 85.2 ± 3.4 MPa) at $TiO_2$(B)-NW loading of 0.6 wt%. Nevertheless, the tensile strength decreases with further increase of $TiO_2$(B)-NW loading. The decreased tensile strength is probably due to the aggregation of the $TiO_2$(B)-NWs which can result in the concentration of stress at the aggregation points. High aspect ratios, i.e., large surface areas per volume, can lead to higher levels of stress transferability since this

phenomenon is governed by shear mechanisms between matrix and fiber/filler at the interphase, hence increasing the tensile modulus of the composite system (Figure 6.8). This result confirms that the interface is actually allowing the stress to be transferred from the matrix to the reinforcing agent.

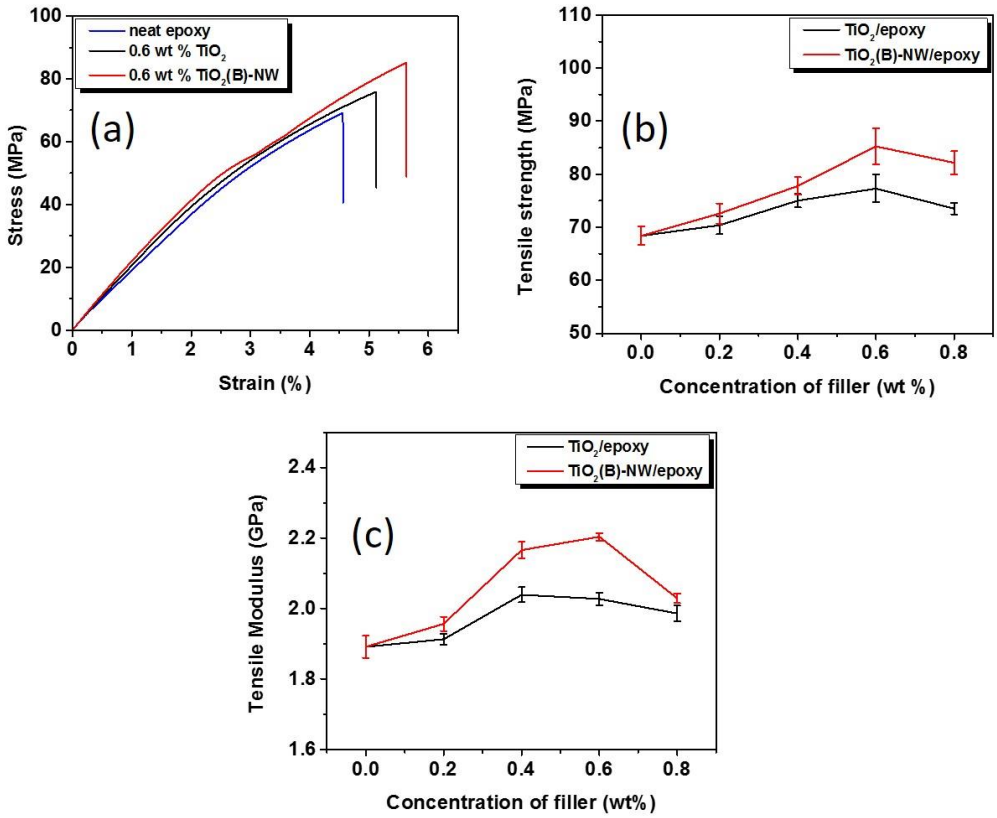


Figure 6.7: (a) Representative stress-strain curves (b) tensile strength and (c) tensile modulus of epoxy nanocomposites containing $TiO_2$ nanoparticles and $TiO_2$(B)-NWs

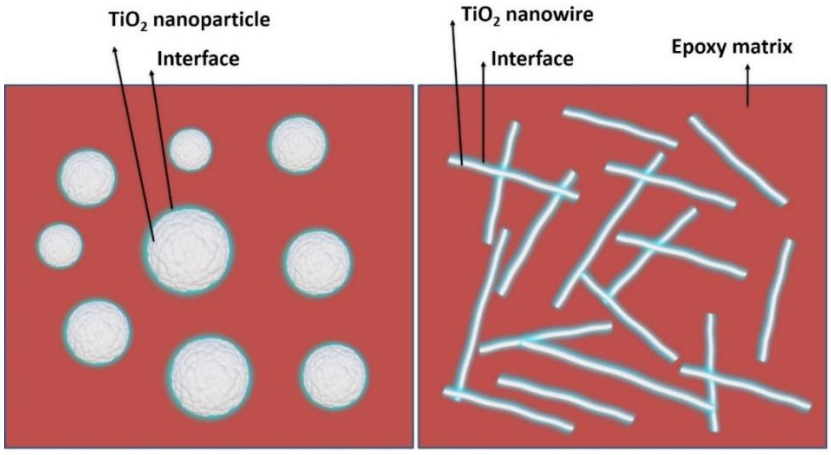


Figure 6.8: Schematic showing the interaction between reinforcing fillers and the epoxy matrix

Table 6.1: Fracture toughness and tensile properties of $TiO_2$/epoxy nanocomposites

| **SI No** | **Sample code** | **$K_{IC}$ (MPa.m$^{1/2}$)** | **Tensile strength (MPa)** | **Tensile Modulus (GPa)** | **Elongation at break (%)** |
|---|---|---|---|---|---|
| 1 | Neat epoxy | 0.74 ± 0.08 | 68.4 ± 1.7 | 1.89 ± 0.03 | 5.66 ± 0.63 |
| 2 | 0.2 wt% $TiO_2$ | 0.88 ± 0.06 | 70.4 ± 1.7 | 1.91 ± 0.01 | 6.24 ± 0.3 |
| 3 | 0.4 wt% $TiO_2$ | 0.96 ± 0.11 | 75.0 ± 1.2 | 2.04 ± 0.02 | 5.7 ± 0.45 |
| 4 | 0.6 wt% $TiO_2$ | 1.03 ± 0.01 | 77.3 ± 2.6 | 2.02 ± 0.02 | 5.55 ± 0.67 |
| 5 | 0.8 wt% $TiO_2$ | 0.93 ± 0.01 | 73.5 ± 1.1 | 1.98 ± 0.02 | 5.24 ± 0.63 |
| 6 | 0.2 wt% $TiO_2$(B)-NW | 1.20 ± 0.17 | 72.6 ± 1.9 | 1.96 ± 0.02 | 6.69 ± 0.31 |
| 7 | 0.4 wt% $TiO_2$(B)-NW | 1.40 ± 0.10 | 77.9 ± 1.6 | 2.17 ± 0.02 | 6.77 ± 0.59 |
| 8 | **0.6 wt% $TiO_2$(B)-NW** | **1.75 ± 0.14** | **85.2 ± 3.4** | **2.20 ± 0.01** | **5.54 ± 0.42** |
| 9 | 0.8 wt% $TiO_2$(B)-NW | 1.02 ± 0.09 | 82.2 ± 2.2 | 2.03 ± 0.01 | 6.39 ± 0.54 |

### 6.3.3.3. Fracture toughness of epoxy nanocomposites

Fracture toughness ($K_{IC}$) values of neat epoxy, $TiO_2$, and $TiO_2$(B)-NW/epoxy nanocomposites are given in Table 6.1. By the addition of 0.6 wt% $TiO_2$, $K_{IC}$ increased from 0.74 ± 0.02 MPa.m$^{1/2}$ to 1.03 ± 0.01 MPa.m$^{1/2}$, an increase of around 39% improvement. During fracture, when the crack growth path reaches the nanoparticles, it deviates from its initial path and propagates along the interface area between the particle and the matrix. Hence, the crack propagates in a longer path and its extension requires higher fracture energy. This improvement in fracture toughness of $TiO_2$ composite was not noteworthy when compared to epoxy composite prepared by 0.6 wt% $TiO_2$(B)-NWs. The highest gains in $K_{IC}$ value (136% improvement compared to neat epoxy) are observed for the $TiO_2$(B)-NW/epoxy composite with 0.6 wt% $TiO_2$(B)-NWs (Figure 6.9). Further loading of $TiO_2$(B)-NWs did not bring about any further advantage. This might be attributed to the poor dispersion of $TiO_2$(B)-NWs at higher concentrations. The increasing trend of $K_{IC}$ for $TiO_2$(B)-NW/epoxy composite indicates the fact that high aspect ratio fillers enhance fracture toughness of the nanocomposites more efficiently than their particulate counterparts.

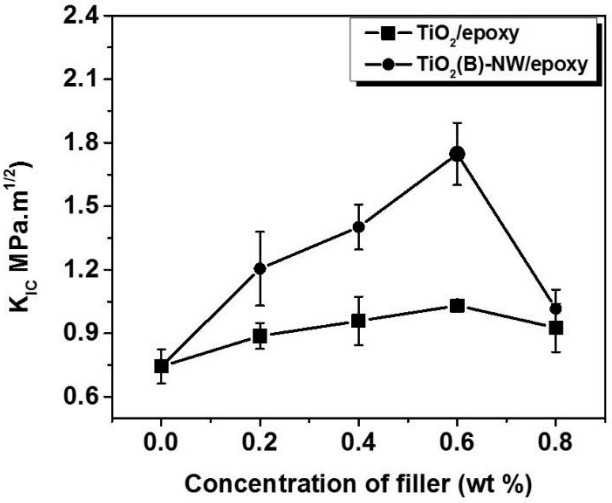


Figure 6.9: Fracture toughness of epoxy nanocomposites of $TiO_2$ nanoparticles and $TiO_2$(B)-NWs

HRSEM observation was employed in order to examine the fracture surfaces of the nanocomposite samples. As shown in Figure 6.10 (a), the neat epoxy shows a smooth glassy fracture surface, which is a clear indication of the brittleness of the sample, with no plastic deformation. The composite containing 0.6 wt% $TiO_2$ exhibits rougher fracture surface with more river-like lines (Figure 6.10 (b)). These changes are mainly attributed to debonding of the rigid $TiO_2$ nanoparticles followed by subsequent plastic void growth of the epoxy polymer (Hsieh et al., 2010). The total fracture surface area of the system is increased as a result of incorporation of $TiO_2$ resulting in greater energy absorption as compared to that of the unfilled polymer. The fracture path becomes more tortuous with $TiO_2$(B)-NW loading and is evident from the change in microstructure (Figure 6.10 (c)).These changes are attributed to the presence of localized shear bands initiated by the stress concentrations around the periphery of the $TiO_2$(B)-NWs. Apart from shear yielding, fracture mechanisms like crack bridging and crack deflection was also observed in the analysis (Figure 6.10 (c) and (d)). These mechanisms are usually observed in nanocomposites containing high aspect ratio fillers like carbon nanotube and graphene (Chandrasekaran et al., 2014; Guan et al., 2014; Prolongo et al., 2011). All these mechanisms contribute to an increase in the total fracture surface area resulting in greater energy absorption compared to the neat epoxy and $TiO_2$/epoxy nanocomposite. A schematic of the possible toughening mechanisms during fracture of $TiO_2$(B)-NW/epoxy nanocomposites is shown in Figure 6.11. Based upon these fratographic analyses, it can be suggested that interfacial properties in polymer composites are to a great extent affected by the shape of the reinforcing agent.

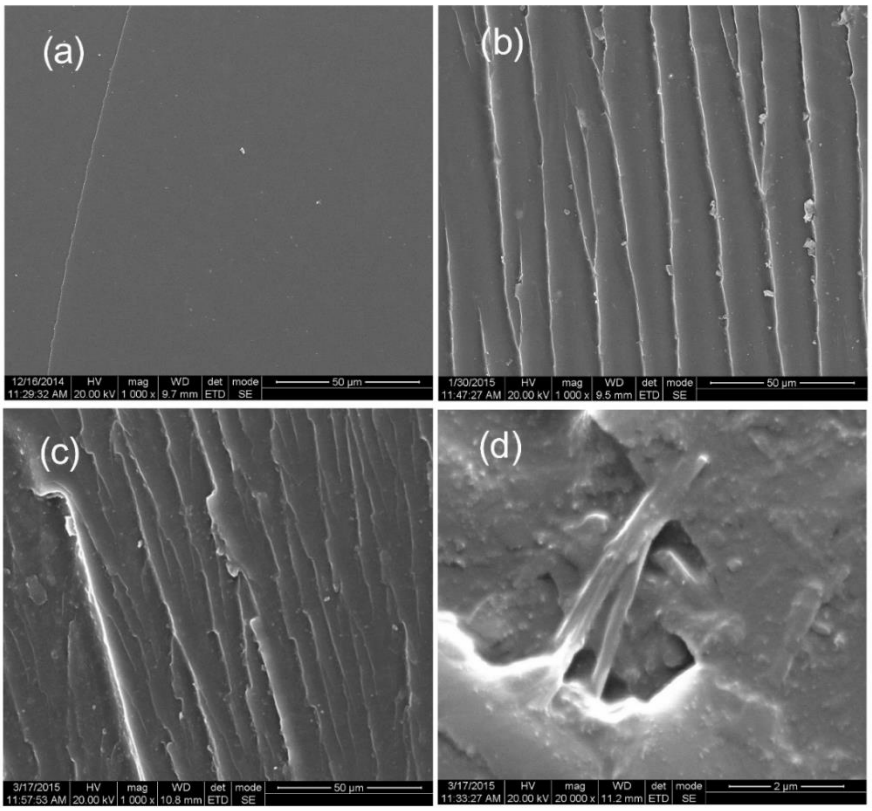


Figure 6.10: FESEM images of fractured surface of sample: (a) neat epoxy (b) 0.6 wt% $TiO_2$ (c) 0.6 wt% $TiO_2$(B)-NWs (d) 0.6 wt% $TiO_2$(B)-NWs at 20000 x magnification

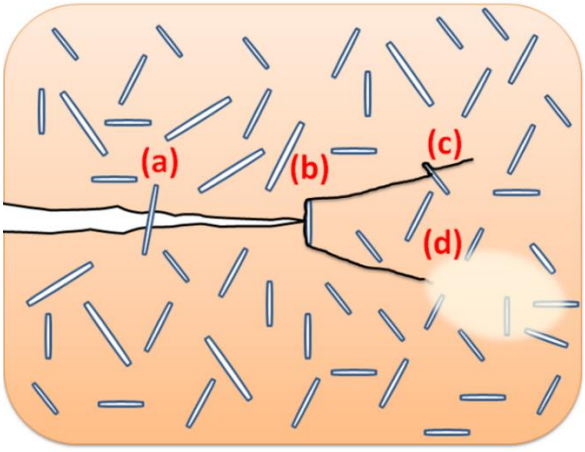


Figure 6.11: Schematic showing the crack propagation of $TiO_2$(B)-NW/epoxy composite during fracture; (a) crack bridging, (b) crack deflection, (c) crack pinning and (d) shear banding

### 6.3.3.4. Dynamic mechanical analysis

Dynamic mechanical analysis (DMA), is considered as a convincing approach to illustrate the interaction between the fillers and matrix. DMA was carried out to understand the viscoelastic behavior over a wide range of temperatures for neat epoxy, $TiO_2$/epoxy and $TiO_2$(B)-NW/epoxy composites. Figure 6.12 shows a comparison of the G′ of neat epoxy and epoxy with 0.6 wt% of $TiO_2$ and $TiO_2$(B)-NWs in the temperature range 30 – 250 $^oC$. No substantial improvement in storage modulus was observed by the addition of 0.6 wt% $TiO_2$. The storage modulus at 30 $^oC$, as shown in Figure 6.12 (a), illustrates an increase of only 2% with addition of 0.6 wt% $TiO_2$ (i.e. from 1.99 to 2.04 GPa). It can be found that adding $TiO_2$(B)-NWs into DGEBA systems lead to a remarkable increase in storage modulus of the composites. About 11% increase in G' is observed at a concentration of 0.6 wt% $TiO_2$(B)-NWs. The enhancement of storage modulus may result from $TiO_2$(B) NW's high aspect ratio, nano level distribution of $TiO_2$(B)-NWs and its strong interaction with DGEBA.

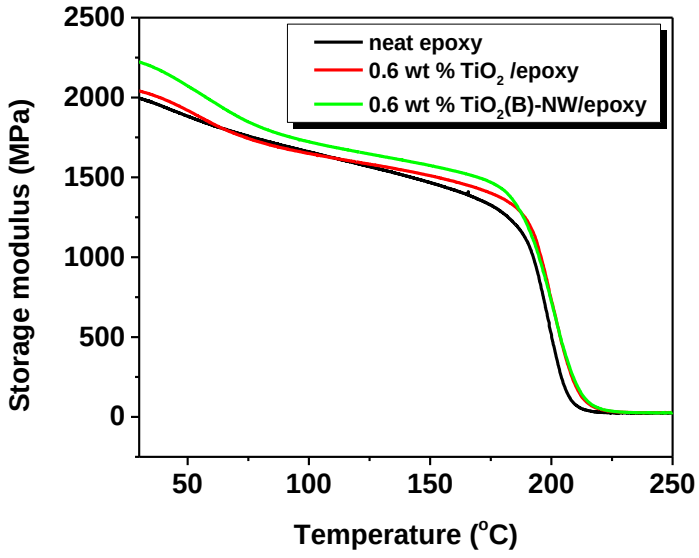


Figure 6.12: Storage modulus versus temperature curves for neat epoxy, 0.6 wt% $TiO_2$/epoxy and 0.6 wt% $TiO_2$(B)-NW/epoxy nanocomposite

Figure 6.13 shows the temperature dependent tan $\delta$ of cured neat epoxy and its $TiO_2$ composites. The tan $\delta$ is the ratio of G" to G' and the tan $\delta$ peaks are often used to determine the $T_g$ of the material. The obtained $T_g$ for the composites are shown in Table 6.2. In this study, a significant reduction of damping (tan $\delta$) was observed in the nanocomposites, together with a strong increment in *Tg* values. These changes in both *Tg* and damping are generally attributed to the existence of a strong filler-matrix interface. It is known that the *Tg* of a polymer composite is substantially related to the mobility of polymer segments or to the free volume fraction in polymer. The mobility of polymer chains near the nanofillers will be restricted which will delay the occurrence of relaxation behavior at the glass transition region, leading to an increase of *Tg*.

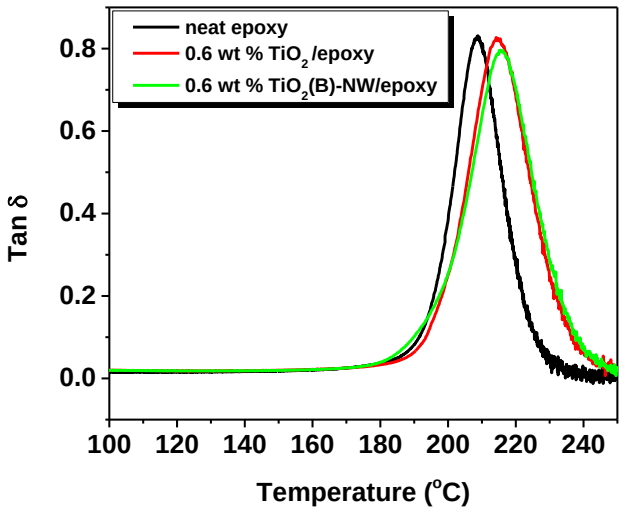


Figure 6.13: Tan delta versus temperature curves for neat epoxy, 0.6 wt% $TiO_2$/epoxy and 0.6 wt% $TiO_2$(B)-NW/epoxy nanocomposite

Since the height depression in tan δ peak has been correlated with the chain mobility, a quantitative estimation of volume fraction of the constrained regions (polymer chains immobilized by the $TiO_2$) in the epoxy phase is done using the height of the tan $\delta$ peak (Rao and Pochan, 2007). The calculated constrained region is given in the Table 6.2. In nanocomposites, the presence of fillers immobilize a

significant amount of the polymer chains during glass transition thereby limiting the mobility of surrounding polymer chains and hence facilitates the formation of constrained regions around the nanofiller with higher $T_g$. Among the epoxy nanocomposites, $TiO_2$(B)-NW/epoxy composite has the highest fraction of constrained region. In the epoxy nanocomposite, it is expected that the $TiO_2$(B) nanowire having high aspect ratio and good filler/matrix interaction may produce more confinement to epoxy polymer than the clumped $TiO_2$ spherical particles. Hence the constrained phase in $TiO_2$(B)-NW/epoxy nanocomposite is much higher than that in $TiO_2$/epoxy nanocomposite which is in turn reflected in the value of $C_r$ (fraction of constrained region) in Table 6.2.

Table 6.2: Values of storage modulus (G') at rubbery and glassy region and *Tg* for the $TiO_2$/epoxy composites

| **Sample code** | ***G'* at 30ºC (MPa)** | ***G'* at 245ºC (MPa)** | **$T_g$ (ºC)** | **Interaction parameter (B)** | **Constrained region (Cr)** |
|---|---|---|---|---|---|
| Neat epoxy | 1995 | 24.75 | 208.5 | | 0 |
| 0.6 wt% $TiO_2$/ epoxy | 2041 | 27.54 | 214.2 | 0.009 | 0.0001 |
| 0.6 wt% $TiO_2$(B)-NW/epoxy | 2222 | 25.95 | 215.5 | 0.069 | 0.0103 |

For further understanding the interaction between the filler and epoxy polymer chains, the interface bonding strength between the $TiO_2$(B)-NWs and epoxy matrix can by indirectly shown by interaction parameter B. The calculated interaction parameter, B for $TiO_2$/epoxy and $TiO_2$(B)-NW/epoxy nanocomposites is given in Table 6.2. The interaction parameter for $TiO_2$(B)-NW/epoxy nanocomposites is much higher when compared with$TiO_2$/epoxy system. The results indicated that the interfacial interaction of $TiO_2$(B)-NW/epoxy was stronger than that of $TiO_2$/epoxy because of the mechanical bonding along with the Van der Waals binding between $TiO_2$(B)-NW and epoxy chains.

### 6.3.3.5. TGA of epoxy nanocomposites

Thermal stability of the epoxy composites was observed using TGA. The thermal stability of epoxy composites with 0.6 wt% loading of $TiO_2$ or $TiO_2$(B)-NWs were compared with neat epoxy system in Figure 6.14. As shown in the figure, no appreciable change is observed in the initial degradation temperature and overall thermal stability of all composites. In the case of composites, a small improvement in char residue from 420-800 $^oC$ is observed due to the presence of inorganic $TiO_2$ fillers.

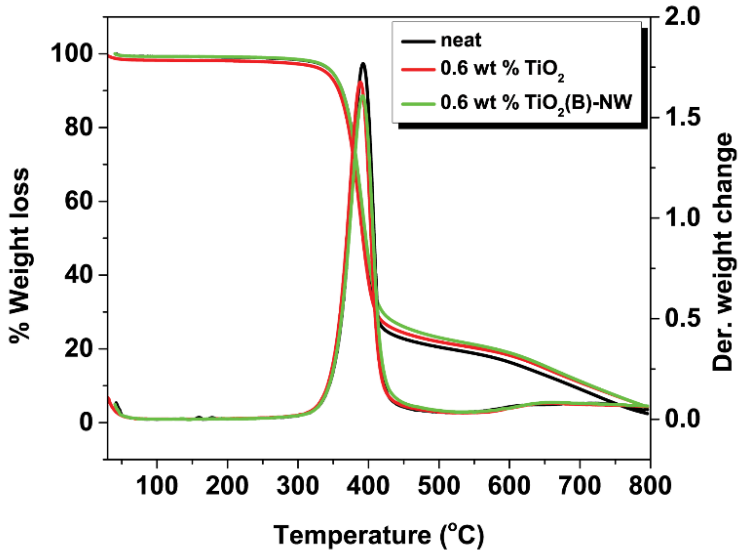


Figure 6.14: TGA and DTG curves of $TiO_2$/epoxy nanocomposites

## 6.4. Conclusions

$TiO_2$(B) nanowires ($TiO_2$(B)-NWs) were synthesized and characterized by XRD, and SEM and the influence of different morphologies of $TiO_2$ nanostructures on the mechanical performance of epoxy nanocomposites were thoroughly investigated. The $TiO_2$(B)-NWs shows the highest mechanical properties and

comparable thermal properties when compared to $TiO_2$ nanoparticle. The optimum properties of this system are attributed to the particle shape or particle dimension that has been described by the aspect ratio wherein the elongated filler shows the highest aspect ratio hence improving the bonding between resin and filler. $TiO_2$/epoxy composite showed little effect on fracture toughness, but $TiO_2$ nanowires increased toughness significantly. The $TiO_2$(B)-NWs incorporated into the epoxy matrix effectively disrupted the development of crack growth and prevented crack propagation. The viscoelastic properties also showed excellent improvement in modulus and $T_g$. This improvement in $T_g$ is due to the hindered polymer chain mobility near the filler/matrix interface. The improvement in $Tg$ was further confirmed by the quantitative analysis of the constrained region and interaction parameter B. TGA analysis indicates that the presence of $TiO_2$ fillers had not deteriorated the thermal stability of the epoxy matrix. To conclude, the introduction of well-dispersed $TiO_2$(B)-NWs into the epoxy matrix has paved way towards the improvement of the mechanical, viscoelastic and thermal performance of the composites which tailors them for an array of industrial as well as high-temperature applications.

# CHAPTER 7

# CONCLUSIONS AND FUTURE WORK

## 7.1. Conclusions

Epoxy based composite materials are being increasingly used as structural components in aerospace and automobile industry due to their excellent mechanical properties, low-weight, and good chemical/corrosion-resistance. However, like other thermoset resins, the crosslinking character of epoxies lead to a highly undesirable property of brittleness with poor resistance to crack initiation and growth. The inherent brittle nature of epoxy resin necessitates toughening for many structural applications. To address this issue, resin formulators have developed technology that permits some thermosets to be toughened by the addition of a second phase. Adding reinforcements such as nano $TiO_2$, nanotubes and graphene has attracted considerable attention as a means to enhance the toughening of epoxy resins. But generally nanoparticles have a tendency for agglomeration because of the weak van der Waals force of attraction. Surface modifications of nanofillers are an effective way to improve interfacial interaction between the nanofillers and the epoxy matrix, which in turn leads to better filler dispersion, and enhanced mechanical performance in the nanocomposites. This thesis investigates the influence of geometry and surface modification of nanofiller on the morphology, mechanical, thermal and viscoelastic properties of the epoxy composite system. Four nanofillers of different geometry, namely POSS, MWCNTs, GOs and nano $TiO_2$ were opted for the current study.

A general introduction about the preparation and applications of epoxy resins is given in chapter 1. A review of the toughening of epoxy with different varieties of

modifiers is also provided in chapter 1. Chapter 2 describes the preparation and cure kinetics studies of a novel organic–inorganic hybrid material by cross linking CTBN with glycidyl POSS. FTIR confirms the successful reaction between carboxyl group of CTBN and epoxide group of POSS. The cure kinetics of CTBN and Glycidyl POSS with and without TPP catalyst was investigated by non-isothermal DSC at different heating rates. The activation energy of POSS-CTBN system with TPP was lower than that of POSS-CTBN without catalyst system, suggesting that the TPP has a catalytic effect on the curing reaction. The dependence of the activation energy on the cure conversion was determined using different isoconversional method and the results showed an increase in activation energy with an increase in the extent of conversion which is due to a restriction in mobility of reactants as the system tends to be more viscous. The curing kinetics could be successfully described with the two-parameter autocatalytic model (Sestak–Berggren equation). Fitting of calculated kinetic parameters (*Ea*, *m*, *n*, and *A*) with measured values obtained good agreement. The activation energy of gelation obtained from rheological studies is comparable with activation energy obtained from DSC study in league with Flory's theory of gelation.

The preparation of a novel hybrid epoxy nanocomposite with glycidyl POSS as nanofiller, CTBN as modifying agent and DGEBA as matrix polymer is described in chapter 3. The reaction between DGEBA, CTBN and glycidyl POSS was carefully monitored and interpreted by using FTIR and DSC. The fracture toughness increases for CTBN/epoxy, POSS/epoxy and POSS-CTBN/epoxy hybrid systems with respect to neat epoxy, but for hybrid composites toughening capability of soft rubber particles is lost by the presence of POSS. FESEM images of the fractured surfaces were examined to understand the toughening mechanism. For POSS-CTBN/epoxy hybrid composites, the size of the rubber particles dispersed in the epoxy matrix dramatically decreases by the addition of POSS. The viscoelastic properties of CTBN/epoxy, POSS/epoxy and POSS-CTBN/epoxy hybrid systems were analyzed using dynamic mechanical analysis. The modulus shows a complex storage modulus

behavior for the POSS/epoxy composites due to the existence of lower and higher crosslink density sites. However, the storage modulus of the epoxy phase decreases with the addition of soft CTBN phase. The $T_g$ corresponding to epoxy rich phase was evident from the dynamic mechanical spectrum. $T_g$ of the epoxy phase decreased linearly as a function of the amount of soft rubber phase. But on the other hand, $T_g$ increased linearly as a function of the amount of POSS, due to its small size and good interaction with epoxy matrix. For hybrid systems the $T_g$ is intermediate between the epoxy/rubber and POSS/epoxy systems. Finally TGA studies were employed to evaluate the thermal stability of the prepared blends and composites.

In chapter 4, polymer grafted MWCNTs have been proposed as an innovative filler for the preparation of epoxy nanocomposites with enhanced thermomechanical properties. The functionalized nanotubes were characterized by FTIR, Raman spectroscopy, TEM and TGA. A systematic study has been conducted to investigate the thermo-mechanical and viscoelastic properties of epoxy nanocomposites prepared by the introduction of polymer functionalized nanotubes into epoxy resin. The study indicates that the polymer functionalisation of nanotube is a good route to achieve higher mechanical properties of the composites. It has been possible to obtain an improvement of ~117% in fracture toughness and 25 % improvement in tensile strength in the CTBN functionalized MWCNT based epoxy composites with only 0.3 wt. % loading. PES grafted MWCNT-epoxy nanocomposite also induces a significant increase in both tensile strength (26 %) and fracture toughness (125 %) of the epoxy matrix. The mechanism of fracture behavior was also studied using SEM, which reveals that crack deflection, pullout of nanotubes, debonding of MWCNTs and bridging mechanism plays an important role in improving the fracture toughness of composites. The surface morphology reveals improved interfacial bonding between the filler/matrix. Therefore, polymer functionalized MWCNT/epoxy composites are able to carry higher level of loading during mechanical testing. The nanocomposites also exhibited an increase in the storage modulus and glass transition temperature compared to those of the neat epoxy resin. This improvement in $T_g$ is due to the

hindered polymer chain mobility near the filler/matrix interface. TGA analysis indicates that the presence of nanotubes has not deteriorated the thermal stability of the epoxy matrix.

In chapter 5, CTBN and PEI were grafted on to GO to prepare GCTBN and GOPEI in order to improve the dispersion and interfacial bonding between GO and epoxy resin in an epoxy/DDS system. GCTBN and GOPEI were characterized by FTIR, XPS, Raman spectroscopy, XRD, TEM, TOM (morphology) and TGA. All these studies reveal the grafting of polymers with GO. The thermal stability of GCTBN was found to improve considerably. TEM micrograph of GCTBN/epoxy and GOPEI/epoxy reveals an excellent dispersion of fillers in epoxy matrix. Fracture toughness (128 %) and tensile strength (30%), improved remarkably for GCTBN modified epoxy matrix. Similarly, a significant improvement in fracture toughness (168 % improvement compared to neat epoxy) and tensile strength (34 % improvement compared to neat epoxy) were observed by the addition of 0.6 wt % GOPEI in epoxy system. SEM micrographs reveal no sheet pull out for GCTBN or GOPEI modified epoxy, due to the complete wetting of these fillers by the epoxy matrix. This confirms effective sheet/matrix interfacial bonding for polymer grafted GO modified epoxy matrix. Moreover, the viscoelastic properties reveal a very high modulus and improved $T_g$ for the GCTBN/epoxy and GOPEI/epoxy when compared with the neat crosslinked epoxy.

The influence of different morphologies of $TiO_2$ nanostructures on the mechanical performance of epoxy nanocomposites were described in chapter 6. $TiO_2$(B) nanowires ($TiO_2$(B)-NWs) were synthesized and characterized by XRD, and SEM. Transmission Optical Micrograph images of $TiO_2$(B)-NW/epoxy nanosuspension reveals an excellent dispersion of $TiO_2$(B)-NWs in the epoxy matrix. Tensile strength (ca 26%), tensile modulus (ca 16%), and fracture toughness (ca 136%) improved remarkably for $TiO_2$(B)-NWs modified epoxy composites. The mechanism that paved way to the enhancement in the fracture toughness of the

$TiO_2$(B)-NW/epoxy nanocomposites was evaluated. SEM micrographs disclose that the phenomena of shear yielding, crack deflection and crack bridging are responsible for the improved fracture toughness of $TiO_2$(B)-NW/epoxy composite. Moreover, the analysis of viscoelastic properties revealed a very high modulus and improved $T_g$ for the $TiO_2$(B)-NW/epoxy composites when compared with neat epoxy owing to better filler/matrix interfacial interaction between $TiO_2$(B)-NWs and epoxy matrix. This was further confirmed by quantitative analysis of the constrained region and by the evaluation of the interaction parameter B. TGA study shows that the thermal stability of composites are not compromised by the incorporation of $TiO_2$ nanofillers.

## 7.2. Future Work

Increasing the fracture resistance without compromising the desirable processing and product characteristics remains a leading challenge in the development of superior thermoset plastic materials. Surface modification of nanofillers with polymer is found to be an excellent route to improve the thermo-mechanical performance of epoxy nanocomposites. This work can be extended to modify the reinforcing nanofillers with different block copolymers (BCP) having better compatibility with epoxy matrix to enhance the thermo-mechanical performance of epoxy system. Self-assembled amphiphilic block copolymers are a new type of toughening agent that has been shown to greatly improve toughness without sacrificing other mechanical properties. It is possible to develop a high performance thermosetting material with combined desirable Tg, modulus and toughness.

Many of the applications of epoxy composites especially in electronic industry require enhanced strength and electrical performance, which can be enabled by adding conductive reinforcing fillers to the epoxy composites. We propose the use of polymer grafted multi-walled carbon nanotubes and graphite oxide prepared by us

can be used as conductive nanofiller to get the required performance at low filler content.

Because of the wide use of commercial, military and scientific electronic devices and communication instruments, electromagnetic interference (EMI) shielding of radio frequency radiation continues to be a serious concern for modern society. Compared with conventional metal-based EMI shielding materials, conducting polymer composites are lightweight, resistant to corrosion, and flexible and offer processing advantages. The high aspect ratio, high conductivity, good mechanical strength and better dispersion of polymer grafted CNTs and GOs make them an excellent option to create conductive composites for high-performance EMI shielding materials at very low filling.

Our research work showed use of $TiO_2$ nanowires as a nanofiller in epoxy resulted in improved mechanical properties compared to $TiO_2$ nanoparticle. We propose the use of titanium carbide (TiC) nanowire instead of $TiO_2$ nanowire in epoxy can result in the enhancement of both mechanical and electric properties of epoxy nanocomposites.

# REFERENCES


1. Adachi, T., Osaki, M., Araki, W., and Kwon, S.-C. (2008). Fracture toughness of nano-and micro-spherical silica-particle-filled epoxy composites. *Acta Materialia, 56*(9): 2101-2109.

2. Akbari, R., Beheshty, M. H., and Shervin, M. (2013). Toughening of dicyandiamide-cured DGEBA-based epoxy resins by CTBN liquid rubber. *Iranian Polymer Journal, 22*(5): 313-324.

3. Alishahi, E., Shadlou, S., Doagou-R, S., and Ayatollahi, M. R. (2013). Effects of Carbon Nanoreinforcements of Different Shapes on the Mechanical Properties of Epoxy-Based Nanocomposites. *Macromolecular Materials and Engineering, 298*(6): 670-678.

4. Al-Turaif, H. A. (2010). Effect of nano $TiO_2$ particle size on mechanical properties of cured epoxy resin. *Progress in Organic Coatings, 69*(3): 241-246.

5. Amdouni, N., Sautereau, H., and Gerard, J. (1992). Epoxy composites based on glass beads. II. Mechanical properties. *Journal of Applied Polymer Science, 46*(10): 1723-1735.

6. Armstrong, A. R., Armstrong, G., Canales, J., and Bruce, P. G. (2004). TiO2-B nanowires. *Angewandte Chemie International Edition, 43*(17): 2286-2288.

7. Armstrong, G., Armstrong, A. R., Canales, J., and Bruce, P. G. (2005). Nanotubes with the TiO 2-B structure. *Chemical communications*(19): 2454-2456.

8. Asif, A. A., John, B., Rao, V. L., and Ninan, K. N. (2010). Surface morphology, thermomechanical and barrier properties of poly(ether sulfone)-toughened epoxy clay ternary nanocomposites. *Polymer International, 59*(7): 986-997.

9. Auad, M. L., Nutt, S. R., Stefani, P. M., and Aranguren, M. I. (2006). Rheological study of the curing kinetics of epoxy–phenol novolac resin. *Journal of Applied Polymer Science, 102*(5): 4430-4439.

10. Ayatollahi, M., Shadlou, S., and Shokrieh, M. (2011). Fracture toughness of epoxy/multi-walled carbon nanotube nano-composites under bending and shear loading conditions. *Materials & Design, 32*(4): 2115-2124.

11. Bahr, J. L., and Tour, J. M. (2001). Highly functionalized carbon nanotubes using in situ generated diazonium compounds. *Chemistry of Materials, 13*(11): 3823-3824.

12. Bai, Y., Yang, P., Zhang, S., Li, Y., and Gu, Y. (2015). Curing kinetics of phenolphthalein–aniline-based benzoxazine investigated by non-isothermal

differential scanning calorimetry. *Journal of Thermal Analysis and Calorimetry, 120*(3): 1755-1764.

13. Balakrishnan, A., and Saha, M. C. (2011). Tensile fracture and thermal conductivity characterization of toughened epoxy/CNT nanocomposites. *Materials Science and Engineering: A, 528*(3): 906-913.

14. Becu, L., Maazouz, A., Sautereau, H., and Gerard, J. (1997). Fracture behavior of epoxy polymers modified with core-shell rubber particles. *Journal of Applied Polymer Science, 65*(12): 2419-2431.

15. Bittmann, B., Haupert, F., and Schlarb, A. K. (2011). Preparation of TiO 2/epoxy nanocomposites by ultrasonic dispersion and their structure property relationship. *Ultrasonics sonochemistry, 18*(1): 120-126.

16. Blackman, B., Kinloch, A., Lee, J. S., Taylor, A., Agarwal, R., Schueneman, G., and Sprenger, S. (2007). The fracture and fatigue behaviour of nano-modified epoxy polymers. *Journal of materials science, 42*(16): 7049-7051.

17. Boumbimba, R. M., Froustey, C., Viot, P., and Gerard, P. (2015). Low velocity impact response and damage of laminate composite glass fibre/epoxy based tri-block copolymer. *Composites Part B: Engineering, 76*: 332-342.

18. Brown, M. E., Dollimore, D., and Galwey, A. K. (1980). *Reactions in the solid state*. Elsevier.

19. Brydson, J. A. (1999). *Plastics materials*. Butterworth-Heinemann.

20. Bucknall, C. B., and Gilbert, A. H. (1989). Toughening tetrafunctional epoxy resins using polyetherimide. *Polymer, 30*(2): 213-217.

21. Callister, W. D., and Rethwisch, D. G. (2007). *Materials science and engineering: an introduction*. Wiley New York.

22. Cano, M., Khan, U., Sainsbury, T., O'Neill, A., Wang, Z., McGovern, I. T., Maser, W. K., Benito, A. M., and Coleman, J. N. (2013). Improving the mechanical properties of graphene oxide based materials by covalent attachment of polymer chains. *Carbon, 52*: 363-371.

23. Carballeira, P., and Haupert, F. (2010). Toughening effects of titanium dioxide nanoparticles on $TiO_2$/epoxy resin nanocomposites. *Polymer Composites, 31*(7): 1241-1246.

24. Carfagna, C., Nicolais, L., Amendola, E., and Filippov, A. (1992). Toughening epoxy resins by liquid crystalline polymers. *Journal of Applied Polymer Science, 44*(8): 1465-1471.

25. Chandrasekaran, S., Sato, N., Tölle, F., Mülhaupt, R., Fiedler, B., and Schulte, K. (2014). Fracture toughness and failure mechanism of graphene based epoxy composites. *Composites Science and Technology, 97*: 90-99.

26. Chaudhary, S., Surekha, P., Kumar, D., Rajagopal, C., and Roy, P. (2015). Amine-functionalized poly (styrene) microspheres as thermoplastic toughener for epoxy resin. *Polymer Composites, 36*(1): 174-183.

27. Chen, J., Kinloch, A., Sprenger, S., and Taylor, A. (2013). The mechanical properties and toughening mechanisms of an epoxy polymer modified with polysiloxane-based core-shell particles. *Polymer, 54*(16): 4276-4289.

28. Chikhi, N., Fellahi, S., and Bakar, M. (2002). Modification of epoxy resin using reactive liquid (ATBN) rubber. *European Polymer Journal, 38*(2): 251-264.

29. Choi, J., Yee, A. F., and Laine, R. M. (2004). Toughening of cubic silsesquioxane epoxy nanocomposites using core-shell rubber particles: a three-component hybrid system. *Macromolecules, 37*(9): 3267-3276.

30. Chonkaew, W., and Sombatsompop, N. (2012). Mechanical and tribological properties of epoxy modified by liquid carboxyl terminated poly (butadiene-co-acrylonitrile) rubber. *Journal of Applied Polymer Science, 125*(1): 361-369.

31. Chung, D. D. (2004). *Composite materials*. Wiley Online Library.

32. Chuayjuljit, S., Soatthiyanon, N., and Potiyaraj, P. (2006). Polymer blends of epoxy resin and epoxidized natural rubber. *Journal of Applied Polymer Science, 102*(1): 452-459.

33. Coleman, J. N., Khan, U., Blau, W. J., and Gun'ko, Y. K. (2006). Small but strong: a review of the mechanical properties of carbon nanotube–polymer composites. *Carbon, 44*(9): 1624-1652.

34. Datsyuk, V., Kalyva, M., Papagelis, K., Parthenios, J., Tasis, D., Siokou, A., Kallitsis, I., and Galiotis, C. (2008). Chemical oxidation of multiwalled carbon nanotubes. *Carbon, 46*(6): 833-840.

35. Daugaard, A. E., Jankova, K., and Hvilsted, S. (2014). Poly (lauryl acrylate) and poly (stearyl acrylate) grafted multiwalled carbon nanotubes for polypropylene composites. *Polymer, 55*(2): 481-487.

36. Davis, D. C., Wilkerson, J. W., Zhu, J., and Hadjiev, V. G. (2011). A strategy for improving mechanical properties of a fiber reinforced epoxy composite using functionalized carbon nanotubes. *Composites Science and Technology, 71*(8): 1089-1097.

37. Dean, J., Lipic, P., Grubbs, R., Cook, R., and Bates, F. (2001). Micellar structure and mechanical properties of block copolymer-modified epoxies. *Journal of Polymer Science Part B: Polymer Physics*, *39*(23): 2996-3010.

38. Dean, J. M., Grubbs, R. B., Saad, W., Cook, R. F., and Bates, F. S. (2003). Mechanical properties of block copolymer vesicle and micelle modified epoxies. *Journal of Polymer Science Part B: Polymer Physics*, *41*(20): 2444-2456.

39. DeCarli, M., Kozielski, K., Tian, W., and Varley, R. (2005). Toughening of a carbon fibre reinforced epoxy anhydride composite using an epoxy terminated hyperbranched modifier. *Composites Science and Technology*, *65*(14): 2156-2166.

40. Deng, S., Zhang, J., Ye, L., and Wu, J. (2008). Toughening epoxies with halloysite nanotubes. *Polymer*, *49*(23): 5119-5127.

41. Deng, Y., and Martin, G. C. (1994). Diffusion and diffusion-controlled kinetics during epoxy-amine cure. *Macromolecules*, *27*(18): 5147-5153.

42. Devasia, R., Reghunadhan Nair, C., and Ninan, K. (2005). Effect of oxalic acid on the rheological properties of dope solution of poly [acrylonitrile-co-(methyl acrylate)-co-(itaconic acid)]. *Polymer international*, *54*(2): 381-385.

43. Dhevi, D. M., Jaisankar, S., and Pathak, M. (2013). Effect of new hyperbranched polyester of varying generations on toughening of epoxy resin through interpenetrating polymer networks using urethane linkages. *European Polymer Journal*, *49*(11): 3561-3572.

44. Di Pasquale, G., Motto, O., Rocca, A., Carter, J., McGrail, P., and Acierno, D. (1997). New high-performance thermoplastic toughened epoxy thermosets. *Polymer*, *38*(17): 4345-4348.

45. Díez-Pascual, A. M., Martínez, G., González-Domínguez, J. M., Ansón, A., Martínez, M. T., and Gómez, M. A. (2010). Grafting of a hydroxylated poly (ether ether ketone) to the surface of single-walled carbon nanotubes. *Journal of Materials Chemistry*, *20*(38): 8285-8296.

46. Dreyer, D. R., Park, S., Bielawski, C. W., and Ruoff, R. S. (2010). The chemistry of graphene oxide. *Chemical Society Reviews*, *39*(1): 228-240.

47. Foix, D., Serra, A., Amparore, L., and Sangermano, M. (2012). Impact resistance enhancement by adding epoxy ended hyperbranched polyester to DGEBA photocured thermosets. *Polymer*, *53*(15): 3084-3088.

48. Francis, B., Rao, V. L., Poel, G. V., Posada, F., Groeninckx, G., Ramaswamy, R., and Thomas, S. (2006a). Cure kinetics, morphological and dynamic mechanical analysis of diglycidyl ether of bisphenol-A epoxy resin modified with hydroxyl terminated poly (ether ether ketone) containing pendent tertiary butyl groups. *Polymer*, *47*(15): 5411-5419.

49. Francis, B., Thomas, S., Thomas, S. P., Ramaswamy, R., and Rao, V. L. (2006b). Diglycidyl ether of bisphenol-A epoxy resin–polyether sulfone/polyether sulfone ether ketone blends: phase morphology, fracture toughness and thermo-mechanical properties. *Colloid and Polymer Science, 285*(1): 83-93.

50. Gam, K., Miyamoto, M., Nishimura, R., and Sue, H. (2003). Fracture behavior of core-shell rubber–modified clay-epoxy nanocomposites. *Polymer Engineering & Science, 43*(10): 1635-1645.

51. Geim, A. K., and Novoselov, K. S. (2007). The rise of graphene. *Nature materials, 6*(3): 183-191.

52. George, N., Chandra, J., Mathiazhagan, A., and Joseph, R. (2015). High performance natural rubber composites with conductive segregated network of multiwalled carbon nanotubes. *Composites Science and Technology, 116*: 33-40.

53. George, S. M., Puglia, D., Kenny, J. M., Causin, V., Parameswaranpillai, J., and Thomas, S. (2013). Morphological and mechanical characterization of nanostructured thermosets from epoxy and styrene-block-butadiene-block-styrene triblock copolymer. *Industrial & Engineering Chemistry Research, 52*(26): 9121-9129.

54. Gerard, P., Boupat, N. P., Fine, T., Gervat, L., and Pascault, J. P. (2007). Toughness properties of lightly crosslinked epoxies using block copolymers. *Macromolecular Symposia* (Vol. 256, pp. 55-64): Wiley Online Library.

55. Giannakopoulos, G., Masania, K., and Taylor, A. (2011). Toughening of epoxy using core–shell particles. *Journal of materials science, 46*(2): 327-338.

56. Gogotsi, Y., and Presser, V. (2013). *Carbon nanomaterials*. CRC Press.

57. Gojny, F. H., and Schulte, K. (2004). Functionalisation effect on the thermo-mechanical behaviour of multi-wall carbon nanotube/epoxy-composites. *Composites Science and Technology, 64*(15): 2303-2308.

58. Gong, S., Zhu, Z., and Meguid, S. (2015). Anisotropic electrical conductivity of polymer composites with aligned carbon nanotubes. *Polymer, 56*: 498-506.

59. Gónzalez-Dominguez, J. M., Gonzalez, M., Anson-Casaos, A., Diez-Pascual, A., Gomez, M., and Martinez, M. (2011). Effect of various aminated single-walled carbon nanotubes on the epoxy cross-linking reactions. *The Journal of Physical Chemistry C, 115*(15): 7238-7248.

60. Goodman, S. H. (1999). Epoxy resins. *Handbook of thermoset plastics*, 193.

61. Górka, J., Mayes, R. T., Baggetto, L., Veith, G. M., and Dai, S. (2013). Sonochemical functionalization of mesoporous carbon for uranium extraction from seawater. *Journal of Materials Chemistry A, 1*(9): 3016-3026.

62. Guan, L.-Z., Wan, Y.-J., Gong, L.-X., Yan, D., Tang, L.-C., Wu, L.-B., Jiang, J.-X., and Lai, G.-Q. (2014). Toward effective and tunable interphases in graphene oxide/epoxy composites by grafting different chain lengths of polyetheramine onto graphene oxide. *Journal of Materials Chemistry A, 2*(36): 15058-15069.

63. Guild, F., and Kinloch, A. (1995). Modelling the properties of rubber-modified epoxy polymers. *Journal of materials science, 30*(7): 1689-1697.

64. Hamming, L. M., Qiao, R., Messersmith, P. B., and Brinson, L. C. (2009). Effects of dispersion and interfacial modification on the macroscale properties of TiO 2 polymer–matrix nanocomposites. *Composites Science and Technology, 69*(11): 1880-1886.

65. Harper, C. A. (2000). *Modern Plastics Handbook: handbook*. McGraw-Hill Professional.

66. Hartmann-Thompson, C. (2011). *Applications of polyhedral oligomeric silsesquioxanes*. Springer Science & Business Media.

67. Hassanabadi, H. M., and Rodrigue, D. (2014). Effect of particle size and shape on the reinforcing efficiency of nanoparticles in polymer nanocomposites. *Macromolecular Materials and Engineering, 299*(10): 1220-1231.

68. Hayashida, K., and Matsuoka, Y. (2015). Electromagnetic interference shielding properties of polymer-grafted carbon nanotube composites with high electrical resistance. *Carbon, 85*: 363-371.

69. He, H., Li, K., Wang, J., Sun, G., Li, Y., and Wang, J. (2011). Study on thermal and mechanical properties of nano-calcium carbonate/epoxy composites. *Materials & Design, 32*(8): 4521-4527.

70. He, X., Zhang, D., Li, H., Fang, J., and Shi, L. (2011). Shape and size effects of ceria nanoparticles on the impact strength of ceria/epoxy resin composites. *Particuology, 9*(1): 80-85.

71. He, Y.-x., Li, Q., Kuila, T., Kim, N. H., Jiang, T., Lau, K.-t., and Lee, J. H. (2013). Micro-crack behavior of carbon fiber reinforced thermoplastic modified epoxy composites for cryogenic applications. *Composites Part B: Engineering, 44*(1): 533-539.

72. Höfflin, F., Könczöl, L., Döll, W., Morawiec, J., and Mülhaupt, R. (2000). Toughening of epoxy resins modified with polyetherester block copolymers: the influence of modifier molecular architecture on mechanical properties. *Journal of Applied Polymer Science, 76*(5): 623-634.

73. Hsieh, T., Kinloch, A., Masania, K., Taylor, A., and Sprenger, S. (2010). The mechanisms and mechanics of the toughening of epoxy polymers modified with silica nanoparticles. *Polymer, 51*(26): 6284-6294.

74. Hsieh, T., Kinloch, A., Taylor, A., and Kinloch, I. (2011). The effect of carbon nanotubes on the fracture toughness and fatigue performance of a thermosetting epoxy polymer. *Journal of materials science, 46*(23): 7525-7535.

75. Hu, H., Hui, K., Hui, K. S., Lee, S., and Zhou, W. (2012). Facile and green method for polystyrene grafted multi-walled carbon nanotubes and their electroresponse. *Colloids and Surfaces A: Physicochemical and Engineering Aspects, 396:* 177-181.

76. Hu, W., Yu, B., Jiang, S.-D., Song, L., Hu, Y., and Wang, B. (2015). Hyper-branched polymer grafting graphene oxide as an effective flame retardant and smoke suppressant for polystyrene. *Journal of hazardous materials, 300*: 58-66.

77. Huang, P., Zheng, S., Huang, J., Guo, Q., and Zhu, W. (1997). Miscibility and mechanical properties of epoxy resin/polysulfone blends. *Polymer, 38*(22): 5565-5571.

78. Hull, D., and Clyne, T. (1996). *An introduction to composite materials*. Cambridge university press.

79. Hummers Jr, W. S., and Offeman, R. E. (1958). Preparation of graphitic oxide. *Journal of the American Chemical Society, 80*(6): 1339-1339.

80. Hussain, M., Nakahira, A., Nishijima, S., and Niihara, K. (1996). Fracture behavior and fracture toughness of particulate filled epoxy composites. *Materials letters, 27*(1): 21-25.

81. Iijima, S. (1991). Helical microtubules of graphitic carbon. *nature, 354*(6348): 56-58.

82. Ilčíková, M., Mrlík, M., Sedláček, T., Chorvát, D., Krupa, I., Šlouf, M., Koynov, K., and Mosnáček, J. (2014). Viscoelastic and photo-actuation studies of composites based on polystyrene-grafted carbon nanotubes and styrene-b-isoprene-b-styrene block copolymer. *Polymer, 55*(1): 211-218.

83. Jakubinek, M. B., Ashrafi, B., Zhang, Y., Martinez-Rubi, Y., Kingston, C. T., Johnston, A., and Simard, B. (2015). Single-walled carbon nanotube–epoxy composites for structural and conductive aerospace adhesives. *Composites Part B: Engineering, 69*: 87-93.

84. Janković, B. (2008). Kinetic analysis of the nonisothermal decomposition of potassium metabisulfite using the model-fitting and isoconversional (model-free) methods. *Chemical Engineering Journal, 139*(1): 128-135.

85. Ji, Q. L., Zhang, M. Q., Rong, M. Z., Wetzel, B., and Friedrich, K. (2004). Tribological properties of surface modified nano-alumina/epoxy composites. *Journal of materials science, 39*(21): 6487-6493.

86. Jia, Q., Zheng, M., Xu, C., and Chen, H. (2006). The mechanical properties and tribological behavior of epoxy resin composites modified by different shape nanofillers. *Polymers for advanced technologies, 17*(3): 168-173.

87. Jiang, T., Kuila, T., Kim, N. H., and Lee, J. H. (2014). Effects of surface-modified silica nanoparticles attached graphene oxide using isocyanate-terminated flexible polymer chains on the mechanical properties of epoxy composites. *Journal of Materials Chemistry A, 2*(27): 10557-10567.

88. Jin, F.-L., and Park, S.-J. (2008). Interfacial toughness properties of trifunctional epoxy resins/calcium carbonate nanocomposites. *Materials Science and Engineering: A, 475*(1): 190-193.

89. Jin, F. L., and Park, S. J. (2006). Thermal properties and toughness performance of hyperbranched-polyimide-modified epoxy resins. *Journal of Polymer Science Part B: Polymer Physics, 44*(23): 3348-3356.

90. Johnsen, B., Kinloch, A., Mohammed, R., Taylor, A., and Sprenger, S. (2007). Toughening mechanisms of nanoparticle-modified epoxy polymers. *Polymer, 48*(2): 530-541.

91. Johnsen, B., Kinloch, A., and Taylor, A. (2005). Toughness of syndiotactic polystyrene/epoxy polymer blends: microstructure and toughening mechanisms. *Polymer, 46*(18): 7352-7369.

92. Jones, A., Watkins, C., White, S., and Sottos, N. (2015). Self-healing thermoplastic-toughened epoxy. *Polymer, 74:* 254-261.

93. Jyotishkumar, P. (2011). "Development of high performance epoxy resin/ engineering thermoplastic blends" Ph.D Thesis, Mahathma Gandhi University, Kottayam, Kerala, India.

94. Jyotishkumar, P., Abraham, E., George, S. M., Elias, E., Pionteck, J., Moldenaers, P., and Thomas, S. (2013). Preparation and properties of MWCNTs/poly(acrylonitrile-styrene-butadiene)/epoxy hybrid composites. *Journal of Applied Polymer Science, 127*(4): 3093-3103.

95. Jyotishkumar, P., Moldenaers, P., George, S. M., and Thomas, S. (2012). Viscoelastic effects in thermoplastic poly (styrene-acrylonitrile)-modified epoxy–DDM system during reaction induced phase separation. *Soft Matter, 8*(28): 7452-7462.

96. Karger-Kocsis, J., and Friedrich, K. (1993). Microstructure-related fracture toughness and fatigue crack growth behaviour in toughened, anhydride-cured epoxy resins. *Composites science and technology, 48*(1-4): 263-272.

97. Kasemsiri, P., Neramittagapong, A., and Chindaprasirt, P. (2015). Curing kinetic, thermal and adhesive properties of epoxy resin cured with cashew nut shell liquid. *Thermochimica Acta, 600*: 20-27.

98. Kawaguchi, T., and Pearson, R. A. (2003). The effect of particle–matrix adhesion on the mechanical behavior of glass filled epoxies. Part 2. A study on fracture toughness. *Polymer, 44*(15): 4239-4247.

99. Kim, B. C., and Park, S. W. (2008). Fracture toughness of the nano-particle reinforced epoxy composite. *Composite structures, 86*(1): 69-77.

100. Kim, B. S., Chiba, T., and Inoue, T. (1995). Morphology development via reaction-induced phase separation in epoxy/poly (ether sulfone) blends: morphology control using poly (ether sulfone) with functional end-groups. *Polymer, 36*(1): 43-47.

101. Kim, D., Cho, K., Kim, J., and Park, C. (1996). Effects of particle size and rubber content on fracture toughness in rubber-modified epoxies. *Polymer Engineering & Science, 36*(6): 755-768.

102. Kim, G. M., Qin, H., Fang, X., Sun, F., and Mather, P. (2003). Hybrid epoxy-based thermosets based on polyhedral oligosilsesquioxane: Cure behavior and toughening mechanisms. *Journal of Polymer Science Part B: Polymer Physics, 41*(24): 3299-3313.

103. Kimoto, M., and Mizutani, K. (1997). Blends of thermoplastic polyimide with epoxy resin: Part II Mechanical studies. *Journal of materials science, 32*(9): 2479-2483.

104. Kinloch, A., Lee, J., Taylor, A., Sprenger, S., Eger, C., and Egan, D. (2003). Toughening structural adhesives via nano-and micro-phase inclusions. *The Journal of Adhesion, 79*(8-9): 867-873.

105. Kinloch, A., Shaw, S., Tod, D., and Hunston, D. (1983). Deformation and fracture behaviour of a rubber-toughened epoxy: 1. Microstructure and fracture studies. *Polymer, 24*(10): 1341-1354.

106. Kissinger, H. E. (1957). Reaction kinetics in differential thermal analysis. *Analytical chemistry, 29*(11): 1702-1706.

107. Kojima, Y., Usuki, A., Kawasumi, M., Okada, A., Fukushima, Y., Kurauchi, T., and Kamigaito, O. (1993). Mechanical properties of nylon 6-clay hybrid. *Journal of Materials Research, 8*(05): 1185-1189.

108. Kolacyak, D., Ihde, J., Merten, C., Hartwig, A., and Lommatzsch, U. (2011). Fast functionalization of multi-walled carbon nanotubes by an atmospheric pressure plasma jet. *Journal of colloid and interface science, 359*(1): 311-317.

109. Kolen'ko, Y. V., Kovnir, K. A., Gavrilov, A. I., Garshev, A. V., Frantti, J., Lebedev, O. I., Churagulov, B. R., Van Tendeloo, G., and Yoshimura, M. (2006). Hydrothermal synthesis and characterization of nanorods of various titanates and titanium dioxide. *The Journal of Physical Chemistry B, 110*(9): 4030-4038.

110. Konnola, R., Joji, J., Parameswaranpillai, J., and Joseph, K. (2015a). Structure and thermo-mechanical properties of CTBN-grafted-GO modified epoxy/DDS composites. *RSC Advances, 5*(76): 61775-61786.

111. Konnola, R., Parameswaranpillai, J., and Joseph, K. (2015b). Mechanical, thermal, and viscoelastic response of novel in situ CTBN/POSS/epoxy hybrid composite system. *Polymer Composites*. DOI: 10.1002/pc.23390.

112. Konnola, R., Nair, C. R., and Joseph, K. (2016). Cross-linking of carboxyl-terminated nitrile rubber with polyhedral oligomeric silsesquioxane. *Journal of Thermal Analysis and Calorimetry*, 123(2): 1479-1489.

113. Koo, J. H. (2006). *Polymer nanocomposites*. McGraw-Hill Professional Pub.

114. Kuang, Y., and Huang, B. (2015). Effects of covalent functionalization on the thermal transport in carbon nanotube/polymer composites: A multi-scale investigation. *Polymer, 56*: 563-571.

115. Kumar, R. M., Sharma, S. K., Kumar, B. M., and Lahiri, D. (2015). Effects of carbon nanotube aspect ratio on strengthening and tribological behavior of ultra high molecular weight polyethylene composite. *Composites Part A: Applied Science and Manufacturing, 76*: 62-72.

116. Kumar, K. S., Nair, C. R., and Ninan, K. (2006). Rheokinetic investigations on the thermal polymerization of benzoxazine monomer. *Thermochimica Acta, 441*(2): 150-155.

117. Kunz-Douglass, S., Beaumont, P. W., and Ashby, M. (1980). A model for the toughness of epoxy-rubber particulate composites. *Journal of materials science, 15*(5): 1109-1123.

118. Kunz, S., Sayre, J., and Assink, R. (1982). Morphology and toughness characterization of epoxy resins modified with amine and carboxyl terminated rubbers. *Polymer, 23*(13): 1897-1906.

119. Kuo, S.-W., and Chang, F.-C. (2011). POSS related polymer nanocomposites. *Progress in Polymer Science, 36*(12): 1649-1696.

120. Ladani, R. B., Wu, S., Kinloch, A. J., Ghorbani, K., Zhang, J., Mouritz, A. P., and Wang, C. H. (2015). Improving the toughness and electrical conductivity of epoxy nanocomposites by using aligned carbon nanofibres. *Composites Science and Technology, 117*: 146-158.

121. Lange, F. (1971a). Fracture Energy and Strength Behavior of a Sodium Borosilicate Glass-Al2O3 Composite System. *Journal of the American Ceramic Society, 54*(12): 614-620.

122. Lange, F., and Radford, K. (1971b). Fracture energy of an epoxy composite system. *Journal of materials science, 6*(9): 1197-1203.

123. Larrañaga, M., Serrano, E., Martin, M. D., Tercjak, A., Kortaberria, G., de la Caba, K., Riccardi, C. C., and Mondragon, I. (2007). Mechanical properties–morphology relationships in nano-/microstructured epoxy matrices modified with PEO–PPO–PEO block copolymers. *Polymer international, 56*(11): 1392-1403.

124. Latha, P., Adhinarayanan, K., and Ramaswamy, R. (1994). Epoxidized hydroxy-terminated polybutadiene—synthesis, characterization and toughening studies. *International journal of adhesion and adhesives, 14*(1): 57-61.

125. Lee, H.-J., San Choi, W., Nguyen, T., Lee, Y. B., and Lee, H. (2011). An easy method for direct metal coordination reaction on unoxidized single-walled carbon nanotubes. *Carbon, 49*(15): 5150-5157.

126. Lee, S., and Kim, S. C. (1997). Morphology and properties of polydimethylsiloxane-modified epoxy resin. *Journal of Applied Polymer Science, 64*(5): 941-955.

127. Lee, K.-Y., Kim, K.-Y., Hwang, I.-R., Choi, Y.-S., and Hong, C.-H. (2010). Thermal, tensile and morphological properties of gamma-ray irradiated epoxy-clay nanocomposites toughened with a liquid rubber. *Polymer Testing, 29*(1): 139-146.

128. Lee, Y.-J., Kuo, S.-W., Huang, C.-F., and Chang, F.-C. (2006). Synthesis and characterization of polybenzoxazine networks nanocomposites containing multifunctional polyhedral oligomeric silsesquioxane (POSS). *Polymer, 47*(12): 4378-4386.

129. Lei, L., Shan, J., Hu, J., Liu, X., Zhao, J., and Tong, Z. (2016). Co-curing effect of imidazole grafting graphene oxide synthesized by one-pot method to reinforce epoxy nanocomposites. *Composites Science and Technology, 128*: 161-168.

130. Levita, G., Marchetti, A., and Butta, E. (1985). Influence of the temperature of cure on the mechanical properties of ATBN/epoxy blends. *Polymer, 26*(7): 1110-1116.

131. Li, B., Hou, W., Sun, J., Jiang, S., Xu, L., Li, G., Memon, M. A., Cao, J., Huang, Y., and Bielawski, C. W. (2015). Tunable functionalization of graphene oxide sheets through surface-initiated cationic polymerization. *Macromolecules, 48*(4): 994-1001.

132. Li, G., Wang, L., Ni, H., and Pittman Jr, C. U. (2001). Polyhedral oligomeric silsesquioxane (POSS) polymers and copolymers: a review. *Journal of Inorganic and Organometallic Polymers, 11*(3): 123-154.

133. Li, J., Wan, W., Zhou, H., Li, J., and Xu, D. (2011). Hydrothermal synthesis of $TiO_2$ (B) nanowires with ultrahigh surface area and their fast charging and discharging properties in Li-ion batteries. *Chemical communications, 47*(12): 3439-3441.

134. Li, S., Cui, C., and Hou, H. (2015a). Synthesis and characterization of amino-terminated hyperbranched polymer and its effect on impact resistance of epoxy resin thermosets. *Colloid and Polymer Science, 293*(9): 2681-2688.

135. Li, S., Zhu, H., Lv, T., Lin, Q., Hou, H., Li, Y., Wu, Q., and Cui, C. (2015b). The effect of amino-terminated hyperbranched polymers on the impact resistance of epoxy resins. *Colloid and Polymer Science*, 1-9.

136. Li, T., Heinzer, M. J., Redline, E. M., Zuo, F., Bates, F. S., and Francis, L. F. (2014). Microstructure and performance of block copolymer modified epoxy coatings. *Progress in Organic Coatings, 77*(7): 1145-1154.

137. Liang, J.-Z. (2010). Predictions of storage modulus of glass bead-filled low-density-polyethylene composites. *Materials Sciences and Applications, 1*(06): 343.

138. Lim, S., Zeng, K., and He, C. (2010). Morphology, tensile and fracture characteristics of epoxy-alumina nanocomposites. *Materials Science and Engineering: A, 527*(21): 5670-5676.

139. Lin, K. F., and Shieh, Y. D. (1998). Core-shell particles designed for toughening the epoxy resins. II. Core-shell-particle-toughened epoxy resins. *Journal of Applied Polymer Science, 70*(12): 2313-2322.

140. Liu, H.-H., Peng, W.-W., Hou, L.-C., Wang, X.-C., and Zhang, X.-X. (2013). The production of a melt-spun functionalized graphene/poly (ε-caprolactam) nanocomposite fiber. *Composites Science and Technology, 81*: 61-68.

141. Liu, J., Thompson, Z. J., Sue, H.-J., Bates, F. S., Hillmyer, M. A., Dettloff, M., Jacob, G., Verghese, N., and Pham, H. (2010). Toughening of epoxies with block copolymer micelles of wormlike morphology. *Macromolecules, 43*(17): 7238-7243.

142. Liu, J. D., Sue, H.-J., Thompson, Z. J., Bates, F. S., Dettloff, M., Jacob, G., Verghese, N., and Pham, H. (2009). Effect of crosslink density on fracture behavior of model epoxies containing block copolymer nanoparticles. *Polymer, 50*(19): 4683-4689.

143. Liu, Q., Ren, W., Zhang, Y., and Zhang, Y.-X. (2011a). Hydrogenated carboxylated nitrile rubber/modified zinc carbonate basic composites with photoluminescence properties. *European Polymer Journal, 47*(5): 1135-1141.

144. Liu, Q., Ren, W., Zhang, Y., and Zhang, Y. (2011b). Curing reactions and properties of organic–inorganic composites from hydrogenated carboxylated nitrile rubber and epoxycyclohexyl polyhedral oligomeric silsesquioxanes. *Polymer International, 60*(3): 422-429.

145. Liu, Q., Ren, W., Zhang, Y., and Zhang, Y. (2012). A study on the curing kinetics of epoxycyclohexyl polyhedral oligomeric silsesquioxanes and hydrogenated

carboxylated nitrile rubber by dynamic differential scanning calorimetry. *Journal of Applied Polymer Science, 123*(5): 3128-3136.

146. Liu, W., Ma, S., Wang, Z., Hu, C., and Tang, C. (2010). Morphologies and mechanical and thermal properties of highly epoxidized polysiloxane toughened epoxy resin composites. *Macromolecular Research, 18*(9): 853-861.

147. Liu, Y. L., Chang, G. P., Hsu, K. Y., and Chang, F. C. (2006). Epoxy/polyhedral oligomeric silsesquioxane nanocomposites from octakis (glycidyldimethylsiloxy) octasilsesquioxane and small-molecule curing agents. *Journal of Polymer Science Part A: Polymer Chemistry, 44*(12): 3825-3835.

148. Loh, K. P., Bao, Q., Ang, P. K., and Yang, J. (2010). The chemistry of graphene. *Journal of Materials Chemistry, 20*(12): 2277-2289.

149. Luo, L., Meng, Y., Qiu, T., and Li, X. (2013). An epoxy-ended hyperbranched polymer as a new modifier for toughening and reinforcing in epoxy resin. *Journal of Applied Polymer Science, 130*(2): 1064-1073.

150. Ma, C., Liu, H.-Y., Du, X., Mach, L., Xu, F., and Mai, Y.-W. (2015). Fracture resistance, thermal and electrical properties of epoxy composites containing aligned carbon nanotubes by low magnetic field. *Composites Science and Technology, 114*: 126-135.

151. Ma, J., Meng, Q., Michelmore, A., Kawashima, N., Izzuddin, Z., Bengtsson, C., and Kuan, H.-C. (2013). Covalently bonded interfaces for polymer/graphene composites. *Journal of Materials Chemistry A, 1*(13): 4255-4264.

152. Ma, S., Liu, W., Gao, N., Yan, Z., and Zhao, Y. (2011). Synthesis and properties of LED-packaging epoxy resin toughened by a novel polysiloxane from hydrolysis and condensation. *Macromolecular Research, 19*(9): 972-979.

153. Ma, S., Liu, W., Hu, C., Wang, Z., and Tang, C. (2010). Toughening of epoxy resin system using a novel dendritic polysiloxane. *Macromolecular Research, 18*(4): 392-398.

154. Malik, P. (2007). Fiber reinforced Composites: Materials. *Manufacturing and Design*.

155. Marcano, D. C., Kosynkin, D. V., Berlin, J. M., Sinitskii, A., Sun, Z., Slesarev, A., Alemany, L. B., Lu, W., and Tour, J. M. (2010). Improved synthesis of graphene oxide. *ACS nano, 4*(8): 4806-4814.

156. Mark, H. F. (2013). *Encyclopedia of polymer science and technology, concise*. John Wiley & Sons.

157. Martinez, I., Martin, M., Eceiza, A., Oyanguren, P., and Mondragon, I. (2000). Phase separation in polysulfone-modified epoxy mixtures. Relationships between curing conditions, morphology and ultimate behavior. *Polymer, 41*(3): 1027-1035.

158. Martinez-Rubi, Y., Ashrafi, B., Guan, J., Kingston, C., Johnston, A., Simard, B., Mirjalili, V., Hubert, P., Deng, L., and Young, R. J. (2011). Toughening of epoxy matrices with reduced single-walled carbon nanotubes. *ACS applied materials & interfaces, 3*(7): 2309-2317.

159. Martone, A., Faiella, G., Antonucci, V., Giordano, M., and Zarrelli, M. (2011). The effect of the aspect ratio of carbon nanotubes on their effective reinforcement modulus in an epoxy matrix. *Composites Science and Technology, 71*(8): 1117-1123.

160. Mathew, V. S., Sinturel, C., George, S. C., and Thomas, S. (2010). Epoxy resin/liquid natural rubber system: secondary phase separation and its impact on mechanical properties. *Journal of materials science, 45*(7): 1769-1781.

161. McGarry, F. (1970). Building design with fibre reinforced materials. *Proceedings of the Royal Society of London A: Mathematical, Physical and Engineering Sciences* (Vol. 319, pp. 59-68): The Royal Society.

162. McGrath, L. M., Parnas, R. S., King, S. H., Schroeder, J. L., Fischer, D. A., and Lenhart, J. L. (2008). Investigation of the thermal, mechanical, and fracture properties of alumina–epoxy composites. *Polymer, 49*(4): 999-1014.

163. Mezzenga, R., Boogh, L., and Månson, J.-A. E. (2001). A review of dendritic hyperbranched polymer as modifiers in epoxy composites. *Composites Science and Technology, 61*(5): 787-795.

164. Miao, X., Meng, Y., and Li, X. (2015). A novel all-purpose epoxy-terminated hyperbranched polyether sulphone toughener for an epoxy/amine system. *Polymer, 60*: 88-95.

165. Mimura, K., Ito, H., and Fujioka, H. (2000). Improvement of thermal and mechanical properties by control of morphologies in PES-modified epoxy resins. *Polymer, 41*(12): 4451-4459.

166. Min, B. G., Hodgkin, J., and Stachurski, Z. (1993a). Reaction mechanisms, microstructure, and fracture properties of thermoplastic polysulfone-modified epoxy resin. *Journal of Applied Polymer Science, 50*(6): 1065-1073.

167. Min, B. G., Stachurski, Z., and Hodgkin, J. (1993b). Microstructural effects and the toughening of thermoplastic modified epoxy resins. *Journal of Applied Polymer Science, 50*(9): 1511-1518.

168. Minfeng, Z., Xudong, S., Huiquan, X., Genzhong, J., Xuewen, J., Baoyi, W., and Chenze, Q. (2008). Investigation of free volume and the interfacial, and toughening behavior for epoxy resin/rubber composites by positron annihilation. *Radiation Physics and Chemistry, 77*(3): 245-251.

169. Miracle, D. B., and Donaldson, S. L. (2001). Introduction to composites. *ASM Hand book of composite materials, 21*.

170. Mishra, K., and Singh, R. P. (2013). Reinforcement of Epoxy Resins with POSS for Enhancing Fracture Toughness at Cryogenic Temperature. *Composite Materials and Joining Technologies for Composites, 7*: pp 179-187.

171. Miyagawa, H., and Drzal, L. T. (2004). The effect of chemical modification on the fracture toughness of montmorillonite clay/epoxy nanocomposites. *Journal of adhesion science and technology, 18*(13): 1571-1588.

172. Moniruzzaman, M., and Winey, K. I. (2006). Polymer nanocomposites containing carbon nanotubes. *Macromolecules, 39*(16): 5194-5205.

173. Montazeri, A., Javadpour, J., Khavandi, A., Tcharkhtchi, A., and Mohajeri, A. (2010). Mechanical properties of multi-walled carbon nanotube/epoxy composites. *Materials & Design, 31*(9): 4202-4208.

174. Mortensen, A. (2006). *Concise encyclopedia of composite materials*. Elsevier.

175. Murias, P., Byczyński, Ł., Maciejewski, H., and Galina, H. (2015). A quantitative approach to dynamic and isothermal curing of an epoxy resin modified with oligomeric siloxanes. *Journal of Thermal Analysis and Calorimetry, 122*(1): 215-226.

176. Naebe, M., Wang, J., Amini, A., Khayyam, H., Hameed, N., Li, L. H., Chen, Y., and Fox, B. (2014). Mechanical property and structure of covalent functionalised graphene/epoxy nanocomposites. *Scientific reports, 4*.

177. Naguib, M., Sangermano, M., Capozzi, L. C., Pospiech, D., Sahre, K., Jehnichen, D., Scheibner, H., and Voit, B. (2015). Non-reactive and reactive block copolymers for toughening of UV-cured epoxy coating. *Progress in Organic Coatings, 85*: 178-188.

178. NEZ, L. N., Taboada, J., Fraga, F., and NEZ, M. (1997). Kinetic Study and Time–Temperature–Transformation Cure Diagram for an Epoxy–Diamine System. *Journal of Applied Polymer Science, 66*: 1377-1388.

179. Nguyen, F. N., and Berg, J. C. (2008). Novel core–shell (dendrimer) epoxy tougheners: Processing and hot–wet performance. *Composites Part A: Applied Science and Manufacturing, 39*(6): 1007-1011.

180. Ozawa, T. (1992). Estimation of activation energy by isoconversion methods. *Thermochimica Acta, 203*: 159-165.

181. Ozturk, A., Kaynak, C., and Tincer, T. (2001). Effects of liquid rubber modification on the behaviour of epoxy resin. *European Polymer Journal, 37*(12): 2353-2363.

182. Pearson, R., and Yee, A. (1989). Toughening mechanisms in elastomer-modified epoxies. *Journal of materials science, 24*(7): 2571-2580.

183. Parameswaranpillai, J., George, A., Pionteck, J., and Thomas, S. (2013). Investigation of cure reaction, rheology, volume shrinkage and thermomechanical properties of nano-$TiO_2$ filled epoxy/DDS composites. *Journal of Polymers, 2013*.

184. Paredes, J., Villar-Rodil, S., Martinez-Alonso, A., and Tascon, J. (2008). Graphene oxide dispersions in organic solvents. *Langmuir, 24*(19): 10560-10564.

185. Park, S., An, J., Potts, J. R., Velamakanni, A., Murali, S., and Ruoff, R. S. (2011). Hydrazine-reduction of graphite-and graphene oxide. *Carbon, 49*(9): 3019-3023.

186. Park, Y. T., Qian, Y., Chan, C., Suh, T., Nejhad, M. G., Macosko, C. W., and Stein, A. (2015). Epoxy toughening with low graphene loading. *Advanced Functional Materials, 25*(4): 575-585.

187. Prolongo, S., Gude, M., and Urena, A. (2011). Improving the flexural and thermomechanical properties of amino-functionalized carbon nanotube/epoxy composites by using a pre-curing treatment. *Composites Science and Technology, 71*(5): 765-771.

188. Puglia, D., Maria, H. J., Kenny, J. M., and Thomas, S. (2013). Clay nanostructure and its localisation in an epoxy/liquid rubber blend. *Rsc Advances, 3*(46): 24634-24643.

189. Qian, J. Y., Pearson, R. A., Dimonie, V. L., and El-Aasser, M. S. (1995). Synthesis and application of core–shell particles as toughening agents for epoxies. *Journal of Applied Polymer Science, 58*(2): 439-448.

190. Qian, X., Song, L., Yu, B., Yang, W., Wang, B., Hu, Y., and Yuen, R. K. (2014). One-pot surface functionalization and reduction of graphene oxide with long-chain molecules: Preparation and its enhancement on the thermal and mechanical properties of polyurea. *Chemical Engineering Journal, 236*: 233-241.

191. Quan, D., and Ivankovic, A. (2015). Effect of core–shell rubber (CSR) nano-particles on mechanical properties and fracture toughness of an epoxy polymer. *Polymer, 66*: 16-28.

192. Rao, C. e. N. e. R., Sood, A. e. K., Subrahmanyam, K. e. S., and Govindaraj, A. (2009). Graphene: The New Two-Dimensional Nanomaterial. *Angewandte Chemie International Edition, 48*(42): 7752-7777.

193. Rao, C. N. R., Müller, A., and Cheetham, A. K. (2006). *The chemistry of nanomaterials: synthesis, properties and applications*. John Wiley & Sons.

194. Rao, Y., and Pochan, J. M. (2007). Mechanics of polymer-clay nanocomposites. *Macromolecules, 40*(2): 290-296.

195. Rafiee, M. A., Rafiee, J., Wang, Z., Song, H., Yu, Z.-Z., and Koratkar, N. (2009). Enhanced mechanical properties of nanocomposites at low graphene content. *ACS nano, 3*(12): 3884-3890.

196. Ragosta, G., Abbate, M., Musto, P., Scarinzi, G., and Mascia, L. (2005). Epoxy-silica particulate nanocomposites: chemical interactions, reinforcement and fracture toughness. *Polymer, 46*(23): 10506-10516.

197. Ramírez, C., Rico, M., Torres, A., Barral, L., López, J., and Montero, B. (2008). Epoxy/POSS organic–inorganic hybrids: ATR-FTIR and DSC studies. *European Polymer Journal, 44*(10): 3035-3045.

198. Ratna, D. (2001). Phase separation in liquid rubber modified epoxy mixture. Relationship between curing conditions, morphology and ultimate behavior. *Polymer, 42*(9): 4209-4218.

199. Ratna, D. (2009). Handbook of Thermoset Resins, iSmithers. *Shawbury, Shrewsbury, Shropshire, United Kingdom*.

200. Ratna, D., Becker, O., Krishnamurthy, R., Simon, G., and Varley, R. (2003). Nanocomposites based on a combination of epoxy resin, hyperbranched epoxy and a layered silicate. *Polymer, 44*(24): 7449-7457.

201. Redline, E. M., Declet-Perez, C., Bates, F. S., and Francis, L. F. (2014). Effect of block copolymer concentration and core composition on toughening epoxies. *Polymer, 55*(16): 4172-4181.

202. Ren, P. G., Wang, H., Huang, H. D., Yan, D. X., and Li, Z. M. (2014). Characterization and performance of dodecyl amine functionalized graphene oxide and dodecyl amine functionalized graphene/high-density polyethylene nanocomposites: A comparative study. *Journal of Applied Polymer Science, 131*(2).

203. Ritzenthaler, S., Court, F., Girard-Reydet, E., Leibler, L., and Pascault, J. (2003). ABC triblock copolymers/epoxy-diamine blends. 2. Parameters controlling the morphologies and properties. *Macromolecules, 36*(1): 118-126.

204. Ruiz-Pérez, L., Royston, G. J., Fairclough, J. P. A., and Ryan, A. J. (2008). Toughening by nanostructure. *Polymer, 49*(21): 4475-4488.

205. Saadati, P., Baharvand, H., Rahimi, A., and Morshedian, J. (2005). Effect of modified liquid rubber on increasing toughness of epoxy resins. *Iranian Polymer Journal, 14*(7): 637-646.

206. Sankaran, S., and Chanda, M. (1990). Chemical toughening of epoxies. II. Mechanical, thermal, and microscopic studies of epoxies toughened with hydroxyl-terminated poly (butadiene-co-acrylonitrile). *Journal of Applied Polymer Science, 39*(8): 1635-1647.

207. Saritha, A. (2012). “Polymer nanocomposites based on chlorobutyl rubber” Ph.D Thesis, Mahathma Gandhi University, Kottayam, Kerala, India.

208. Schadler, L., Giannaris, S., and Ajayan, P. (1998). Load transfer in carbon nanotube epoxy composites. *Applied physics letters, 73*(26): 3842-3844.

209. Sengupta, R., Bhattacharya, M., Bandyopadhyay, S., and Bhowmick, A. K. (2011). A review on the mechanical and electrical properties of graphite and modified graphite reinforced polymer composites. *Progress in polymer science, 36*(5): 638-670.

210. Shi, Q., Wang, L., Yu, H., Jiang, S., Zhao, Z., and Dong, X. (2006). A novel epoxy resin/CaCO3 nanocomposite and its mechanism of toughness improvement. *Macromolecular Materials and Engineering, 291*(1): 53-58.

211. Shukla, S. K., and Srivastava, D. (2006). Blends of modified epoxy resin and carboxyl-terminated polybutadiene. I. *Journal of Applied Polymer Science, 100*(3): 1802-1808.

212. Son, B. T., Trung, N. N., Lim, D.-G., Shin, S., and Bae, J.-Y. (2012). Improvements in thermal, mechanical, and dielectric properties of epoxy resin by chemical modification with a novel amino-terminated liquid-crystalline copoly (ester amide). *Reactive and Functional Polymers, 72*(8): 542-548.

213. Song, K., Zhang, Y., Meng, J., Green, E. C., Tajaddod, N., Li, H., and Minus, M. L. (2013). Structural polymer-based carbon nanotube composite fibers: understanding the processing–structure–performance relationship. *Materials, 6*(6): 2543-2577.

214. Spitalsky, Z., Tasis, D., Papagelis, K., and Galiotis, C. (2010). Carbon nanotube–polymer composites: chemistry, processing, mechanical and electrical properties. *Progress in polymer science, 35*(3): 357-401.

215. Stankovich, S., Dikin, D. A., Dommett, G. H., Kohlhaas, K. M., Zimney, E. J., Stach, E. A., Piner, R. D., Nguyen, S. T., and Ruoff, R. S. (2006). Graphene-based composite materials. *nature, 442*(7100): 282-286.

216. Stankovich, S., Dikin, D. A., Piner, R. D., Kohlhaas, K. A., Kleinhammes, A., Jia, Y., Wu, Y., Nguyen, S. T., and Ruoff, R. S. (2007). Synthesis of graphene-based nanosheets via chemical reduction of exfoliated graphite oxide. *Carbon, 45*(7): 1558-1565.

217. Sue, H.-J., Meitin, E. G., Pickelman, D., and Bott, C. (1996). Fracture mechanisms in rigid core-shell particle modified high performance epoxies. *Colloid and Polymer Science, 274*(4): 342-349.

218. Sultan, J. N., Laible, R., and McGarry, F. J. (1971). Microstructure of two-phase polymers. *Appl Polym Symp,* 16: 127-136.

219. Sultan, J. N., and McGarry, F. J. (1973). Effect of rubber particle size on deformation mechanisms in glassy epoxy. *Polymer Engineering & Science, 13*(1): 29-34.

220. Sumerlin, B. S., Tsarevsky, N. V., Louche, G., Lee, R. Y., and Matyjaszewski, K. (2005). Highly efficient "click" functionalization of poly (3-azidopropyl methacrylate) prepared by ATRP. *Macromolecules, 38*(18): 7540-7545.

221. Sun, L., Warren, G., O'reilly, J., Everett, W., Lee, S., Davis, D., Lagoudas, D., and Sue, H.-J. (2008). Mechanical properties of surface-functionalized SWCNT/epoxy composites. *Carbon, 46*(2): 320-328.

222. Suriati, G., Mariatti, M., and Azizan, A. (2011). Effects of filler shape and size on the properties of silver filled epoxy composite for electronic applications. *Journal of Materials Science: Materials in Electronics, 22*(1): 56-63.

223. Tang, B., Liu, X., Zhao, X., and Zhang, J. (2014). Highly efficient in situ toughening of epoxy thermosets with reactive hyperbranched polyurethane. *Journal of Applied Polymer Science, 131*(16).

224. Tang, G., Jiang, Z.-G., Li, X., Zhang, H.-B., Hong, S., and Yu, Z.-Z. (2014). Electrically conductive rubbery epoxy/diamine-functionalized graphene nanocomposites with improved mechanical properties. *Composites Part B: Engineering, 67*: 564-570.

225. Tasis, D., Tagmatarchis, N., Bianco, A., and Prato, M. (2006). Chemistry of carbon nanotubes. *Chemical reviews, 106*(3): 1105-1136.

226. Thio, Y. S., Wu, J., and Bates, F. S. (2006). Epoxy toughening using low molecular weight poly (hexylene oxide)-poly (ethylene oxide) diblock copolymers. *Macromolecules, 39*(21): 7187-7189.

227. Thitsartarn, W., Fan, X., Sun, Y., Yeo, J. C. C., Yuan, D., and He, C. (2015). Simultaneous enhancement of strength and toughness of epoxy using POSS-Rubber core–shell nanoparticles. *Composites Science and Technology, 118*: 63-71.

228. Thomas, R., Abraham, J., Thomas, P., and Thomas, S. (2004). Influence of carboxyl-terminated (butadiene-co-acrylonitrile) loading on the mechanical and thermal properties of cured epoxy blends. *Journal of Polymer Science Part B: Polymer Physics, 42*(13): 2531-2544.

229. Thomas, R., Durix, S., Sinturel, C., Omonov, T., Goossens, S., Groeninckx, G., Moldenaers, P., and Thomas, S. (2007). Cure kinetics, morphology and miscibility of modified DGEBA-based epoxy resin–Effects of a liquid rubber inclusion. *Polymer, 48*(6): 1695-1710.

230. Thomas, R., Yumei, D., Yuelong, H., Le, Y., Moldenaers, P., Weimin, Y., Czigany, T., and Thomas, S. (2008). Miscibility, morphology, thermal, and mechanical properties of a DGEBA based epoxy resin toughened with a liquid rubber. *Polymer, 49*(1): 278-294.

231. Thompson, Z. J., Hillmyer, M. A., Liu, J., Sue, H.-J., Dettloff, M., and Bates, F. S. (2009). Block copolymer toughened epoxy: role of cross-link density. *Macromolecules, 42*(7): 2333-2335.

232. Thostenson, E. T., Ren, Z., and Chou, T.-W. (2001). Advances in the science and technology of carbon nanotubes and their composites: a review. *Composites Science and Technology, 61*(13): 1899-1912.

233. Tian, X., Geng, Y., Yin, D., Zhang, B., and Zhang, Y. (2011). Studies on the properties of a thermosetting epoxy modified with chain-extended ureas containing hydroxyl-terminated polybutadiene. *Polymer Testing, 30*(1): 16-22.

234. Tripathi, G., and Srivastava, D. (2007). Effect of carboxyl-terminated poly (butadiene-co-acrylonitrile)(CTBN) concentration on thermal and mechanical properties of binary blends of diglycidyl ether of bisphenol-A (DGEBA) epoxy resin. *Materials Science and Engineering: A, 443*(1): 262-269.

235. Tripathi, G., and Srivastava, D. (2008). Studies on the physico-mechanical and thermal characteristics of blends of DGEBA epoxy, 3, 4 epoxy cyclohexylmethyl, 3′, 4′-epoxycylohexane carboxylate and carboxyl terminated butadiene co-acrylonitrile (CTBN). *Materials Science and Engineering: A, 496*(1): 483-493.

236. Tripathi, M., Kumar, D., Rajagopal, C., and Roy, P. K. (2015). Curing kinetics of self-healing epoxy thermosets. *Journal of Thermal Analysis and Calorimetry, 119*(1): 547-555.

237. Tsai, C.-C., and Teng, H. (2006). Structural features of nanotubes synthesized from NaOH treatment on TiO2 with different post-treatments. *Chemistry of Materials, 18*(2): 367-373.

238. Varghese, H., Bhagawan, S., and Thomas, S. (1999). Effects of blend ratio, crosslinking systems and fillers on the morphology, curing behavior, mechanical properties, and failure mode of acrylonitrile butadiene rubber and poly (ethylene-co-vinyl acetate) blends. *Journal of applied polymer science, 71*(14): 2335-2364.

239. Varghese, T., Muthiah, R., David, J., Kurian, A., Athithan, S., Krishnamurthy, V., and Kurup, M. (1989). Studies on Composite Extrudable Propellant with varied Burning Rate Pressure Index'n'. *Defence Science Journal, 39*(1): 1.

240. Vyazovkin, S. (2001). Modification of the integral isoconversional method to account for variation in the activation energy. *Journal of Computational Chemistry, 22*(2): 178-183.

241. Vyazovkin, S., and Wight, C. (1997). Kinetics in solids. *Annual review of physical chemistry, 48*(1): 125-149.

242. Vyazovkin, S., and Wight, C. A. (1999). Model-free and model-fitting approaches to kinetic analysis of isothermal and nonisothermal data. *Thermochimica Acta, 340*: 53-68.

243. Wang, L., Wang, K., Chen, L., Zhang, Y., and He, C. (2006). Preparation, morphology and thermal/mechanical properties of epoxy/nanoclay composite. *Composites Part A: Applied Science and Manufacturing, 37*(11): 1890-1896.

244. Wang, M., Fan, X., Thitsartarn, W., and He, C. (2015a). Rheological and mechanical properties of epoxy/clay nanocomposites with enhanced tensile and fracture toughnesses. *Polymer, 58*: 43-52.

245. Wang, M., Hu, N., Zhou, L., and Yan, C. (2015b). Enhanced interfacial thermal transport across graphene–polymer interfaces by grafting polymer chains. *Carbon, 85*: 414-421.

246. Wang, X., Jin, J., and Song, M. (2013). An investigation of the mechanism of graphene toughening epoxy. *Carbon, 65*: 324-333

247. Wang, X., Song, L., Yang, H., Xing, W., Kandola, B., and Hu, Y. (2012). Simultaneous reduction and surface functionalization of graphene oxide with POSS for reducing fire hazards in epoxy composites. *Journal of Materials Chemistry, 22*(41): 22037-22043.

248. Wang, X., Xing, W., Feng, X., Yu, B., Song, L., and Hu, Y. (2014). Functionalization of graphene with grafted polyphosphamide for flame retardant epoxy composites: synthesis, flammability and mechanism. *Polymer Chemistry, 5*(4): 1145-1154.

249. Wang, Y., Wang, C., Yin, H., Wang, L., Xie, H., and Cheng, R. (2012). Carboxyl-terminated butadiene–acrylonitrile-toughened epoxy/carboxyl-modified carbon nanotube nanocomposites: thermal and mechanical properties. *Express Polym Lett, 6*(9): 719-728.

250. Wetzel, B., Rosso, P., Haupert, F., and Friedrich, K. (2006). Epoxy nanocomposites–fracture and toughening mechanisms. *Engineering fracture mechanics, 73*(16): 2375-2398.

251. Wu, J., Thio, Y. S., and Bates, F. S. (2005). Structure and properties of PBO–PEO diblock copolymer modified epoxy. *Journal of Polymer Science Part B: Polymer Physics, 43*(15): 1950-1965.

252. Wu, S., Lin, T., and Shyu, S. (2000). Cure behavior, morphology, and mechanical properties of the melt blends of epoxy with polyphenylene oxide. *Journal of Applied Polymer Science, 75*(1): 26-34.

253. Wu, Y., Song, L., and Hu, Y. (2011). Fabrication and Characterization of TiO2 Nanotube–Epoxy Nanocomposites. *Industrial & Engineering Chemistry Research, 50*(21): 11988-11995.

254. Xiong, X., Ren, R., Liu, S., Lu, S., and Chen, P. (2014). The curing kinetics and thermal properties of epoxy resins cured by aromatic diamine with hetero-cyclic side chain structure. *Thermochimica Acta, 595*: 22-27.

255. Yahyaie, H., Ebrahimi, M., Tahami, H. V., and Mafi, E. R. (2013). Toughening mechanisms of rubber modified thin film epoxy resins. *Progress in Organic Coatings, 76*(1): 286-292.

256. Yang, K., Gu, M., Guo, Y., Pan, X., and Mu, G. (2009). Effects of carbon nanotube functionalization on the mechanical and thermal properties of epoxy composites. *Carbon, 47*(7): 1723-1737.

257. Yee, A. F., and Pearson, R. A. (1986). Toughening mechanisms in elastomer-modified epoxies. *Journal of materials science, 21*(7): 2462-2474.

258. Yoonessi, M., Lebrón-Colón, M., Scheiman, D., and Meador, M. A. (2014). Carbon Nanotube Epoxy Nanocomposites: The Effects of Interfacial Modifications on the Dynamic Mechanical Properties of the Nanocomposites. *ACS applied materials & interfaces, 6*(19): 16621-16630.

259. Yoshida, R., Suzuki, Y., and Yoshikawa, S. (2005). Syntheses of TiO 2 (B) nanowires and TiO 2 anatase nanowires by hydrothermal and post-heat treatments. *Journal of solid state Chemistry, 178*(7): 2179-2185.

260. Yuan, F.-Y., Zhang, H.-B., Li, X., Ma, H.-L., Li, X.-Z., and Yu, Z.-Z. (2014). In situ chemical reduction and functionalization of graphene oxide for electrically conductive phenol formaldehyde composites. *Carbon, 68*: 653-661.

261. Yun, N. G., Won, Y. G., and Kim, S. C. (2004). Toughening of epoxy composite by dispersing polysulfone particle to form morphology spectrum. *Polymer Bulletin, 52*(5): 365-372.

262. Zabihi, O., Aghaie, M., and Zare, K. (2013). Study on a novel thermoset nanocomposite form DGEBA–cycloaliphatic diamine and metal nanoparticles. *Journal of Thermal Analysis and Calorimetry, 111*(1): 703-710.

263. Zeng, S., Reyes, C., Liu, J., Rodgers, P. A., Wentworth, S. H., and Sun, L. (2014). Facile hydroxylation of halloysite nanotubes for epoxy nanocomposite applications. *Polymer, 55*(25): 6519-6528.

264. Zhao, Y., Chen, Z.-K., Liu, Y., Xiao, H.-M., Feng, Q.-P., and Fu, S.-Y. (2013). Simultaneously enhanced cryogenic tensile strength and fracture toughness of epoxy resins by carboxylic nitrile-butadiene nano-rubber. *Composites Part A: Applied Science and Manufacturing, 55*: 178-187.

265. Zhang, B. L., Tang, G. L., Shi, K. Y., You, Y. C., Du, Z. J., and Huang, J. F. (1999). A study on the properties of epoxy resin toughened by a liquid crystal-type oligomer. *Journal of Applied Polymer Science, 71*(1): 177-184.

266. Zhang, C., Liu, X., Cheng, J., and Zhang, J. (2015). Study on curing kinetics of diglycidyl 1, 2-cyclohexane dicarboxylate epoxy/episulfide resin system with hexahydro-4-methylphthalic anhydride as a curing agent. *Journal of Thermal Analysis and Calorimetry, 120*(3): 1893-1903.

267. Zhang, D., Zhang, J., and Zhang, A. (2014). Morphology Analysis by Microscopy Techniques and Light Scattering. *Micro-and Nanostructured Epoxy/Rubber Blends*: 147-178.

268. Zhang, H., and Zhang, Z. (2007). Impact behaviour of polypropylene filled with multi-walled carbon nanotubes. *European Polymer Journal, 43*(8): 3197-3207.

269. Zhang, Y., He, H., and Gao, C. (2008). Clickable macroinitiator strategy to build amphiphilic polymer brushes on carbon nanotubes. *Macromolecules, 41*(24): 9581-9594.

270. Zhou, H., and Xu, S. (2014). A new method to prepare rubber toughened epoxy with high modulus and high impact strength. *Materials letters, 121*: 238-240.

271. Zhu, Y., Murali, S., Cai, W., Li, X., Suk, J. W., Potts, J. R., and Ruoff, R. S. (2010). Graphene and graphene oxide: synthesis, properties, and applications. *Advanced materials, 22*(35): 3906-3924.

272. Ziegel, K., and Romanov, A. (1973). Modulus reinforcement in elastomer composites. I. Inorganic fillers. *Journal of Applied Polymer Science, 17*(4): 1119-1131.

273. Zilg, C., Thomann, R., Finter, J., and Mülhaupt, R. (2000). The influence of silicate modification and compatibilizers on mechanical properties and morphology of anhydride-cured epoxy nanocomposites. *Macromolecular Materials and Engineering, 280*(1): 41-46.

274. Zlatanic, A., and Dunjic, B. (1999). Rheological study of the copolymerization reaction of acrylate-terminated unsaturated copolyesters with styrene. *Macromolecular Chemistry and Physics, 200*(9): 2048-2058.

275. Zunjarrao, S. C., and Singh, R. P. (2006). Characterization of the fracture behavior of epoxy reinforced with nanometer and micrometer sized aluminum particles. *Composites science and technology, 66*(13): 2296-2305.

# LIST OF PUBLICATIONS BASED ON THE THESIS

## International journals

**1.** Raneesh Konnola, and Kuruvilla Joseph. (2016). Effect of side-wall functionalisation of multi-walled carbon nanotube on the thermo-mechanical properties of epoxy nanocomposites. *RSC Advances*, 6: 23887-23899.

**2.** Raneesh Konnola, Jinu Joji, Jyotishkumar Parameswaran Pillai and Kuruvilla Joseph. (2015). Structure and thermo-mechanical properties of CTBN-grafted-GO modified epoxy/DDS composites. *RSC Advances*, 5: 61775-61786.

**3.** Raneesh Konnola, C.P. Reghunadhan Nair and Kuruvilla Joseph. (2016). Crosslinking of carboxyl terminated nitrile rubber with polyhedral oligomeric silsesquioxane; cure kinetics. *Journal of Thermal Analysis and Calorimetry*, 123(2): 1479-1489.

**4.** Raneesh Konnola, C.P. Reghunadhan Nair and Kuruvilla Joseph. (2016). High strength toughened epoxy nanocomposite based on poly (ether sulfone)-grafted multi-walled carbon nanotube. *Polymers for Advanced Technologies*, 27(1): 82-89.

**5.** Raneesh Konnola, Jyotishkumar Parameswaran Pillai and Kuruvilla Joseph. (2015). Mechanical, thermal, and viscoelastic response of novel in situ CTBN/POSS/epoxy hybrid composite system, *Polymer Composites*, DOI: 10.1002/pc.23390.

**6.** Raneesh Konnola, Srinivasan Sampath, Appukuttan Saritha and Kuruvilla Joseph. Fabrication and characterization of TiO2-nanowire based toughened epoxy nanocomposites. *Composite Part B: Engineering (Under Review)* (**communicated**).

## Conference Journals

1. Raneesh Konnola and Kuruvilla Joseph. (2015). Polymer grafted multi-walled carbon nanotube as a novel toughening agent for epoxy system, *Materials Science Forum*, 830-831: pp 577-580.

# PRESENTATIONS IN CONFERENCES/SEMINARS

## Oral Presentations

1. Raneesh Konnola, and Kuruvilla Joseph. Polymer Grafted Carbon Nanofillers for High Strength Toughened Epoxy Nanocomposite; *INCCOM-13, VSSC Thiruvananthapuram, Nov 14-15 (2014).*

2. Raneesh Konnola and Kuruvilla Joseph. Covalent Integration of Polymers on Carbon Nanofillers for Improving Fracture Toughness of Epoxy nanocomposites; *PCYR'14, NIIST, Thiruvananthapuram, Oct 18 (2014).*

3. Raneesh Konnola and Kuruvilla Joseph. Chemically Modified Carbon Nanofillers as New Toughening Agents for Epoxy Matrix; *NCMST 2014, Indian Institute of Space Science and Technology, Thiruvananthapuram, Jul 28-30 (2014).*

4. Raneesh Konnola and Kuruvilla Joseph. Studies on Thermal Decomposition of poly(acrylonitrile-co-butadiene) – POSS Nanocomposite; *Research Scholar's Day 2013, Indian Institute of Space Science and Technology, Thiruvananthapuram, Dec 16-17 (2013).*

5. Raneesh Konnola and Kuruvilla Joseph. Rheological studies on the curing of poly(acrylonitrile-co-butadiene)- POSS nanocomposite; *PPS Asia/Australia Conference (PPS–2013), IIT Bombay, Dec 4-7 (2013).*

6. Raneesh Konnola and Kuruvilla Joseph. Kinetic Analysis of the Non-isothermal Decomposition of POSS-CTBN nanocomposite; *ICAPM 2013, MG UNIVERSITY, Kottayam, Oct 11-13 (2013).*

7. Raneesh Konnola and Kuruvilla Joseph. Multi-scale Composites-Challenges in Processing and Enhancement in Mechanical Properties; *International Conference on Safety by Design 2013, JCET Ottappalam, Palakkad, Aug 16-17 (2013).*

## Poster Presentations

1. Raneesh Konnola and Kuruvilla Joseph. Enhanced Mechanical Performance of Epoxy Nanocomposites Filled with poly(phenylenesulfone) like Polymer Grafted Multi-walled Carbon Nanotube; *NCCM 2015, NPL Delhi, Jul 26-28 (2015).*

2. Raneesh Konnola and Kuruvilla Joseph. Polymer Grafted Multi-walled Carbon Nanotube as a Novel Toughening Agent for Epoxy System; *ICAMPS, Trivandrum, May 13-15 (2015).*

3. Raneesh Konnola and Kuruvilla Joseph. Effect of Polyhedral Oligomeric Silsesquioxane on the Surface Morphology, Fracture Toughness, Thermal and Mechanical Properties of Nanoclay/Epoxy Nanocomposites; *ICAFM 2014, NIIST Trivandrum, Feb 19-21 (2014).*

4. Raneesh Konnola and Kuruvilla Joseph. Novel Toughened Epoxy Nanocomposite Based on Hydroxyl Terminated poly(ethersulfone) Grafted Multi-walled Carbon Nanotube; *NCMST 2013, Indian Institute of Space Science and Technology, Thiruvananthapuram, Jul 10-12 (2013).*

5. Raneesh Konnola and Kuruvilla Joseph. Cure Kinetics Studies on Carboxyl Terminated poly(acrylonitrile-co-butadiene)-POSS Composites Using Differential Scanning Colorimetry; *FAPS-MACRO 2013, IISc Bangalore, May 15-18 (2013).*

6. Raneesh Konnola and Kuruvilla Joseph. Fracture Toughness Behavior of Rubber Modified POSS Epoxy Nanocomposites; *NANO INDIA 2013, NIIST, Thiruvananthapuram, Feb 19-20 (2013).*

7. Raneesh Konnola and Kuruvilla Joseph. Chemical Modification of Carbon Nanotubes; *Research Scholars' Day, IIST, Thiruvananthapuram, Dec 17-19 (2012).*